SURFACTANT STABILISED GAS MICROCELLS

BY

SHARON BROCKBANK

A thesis submitted in fulfilment of the requirements for the degree of Doctor of Philosophy in the University of Bristol.

Department of Physical Chemistry,
University of Bristol.

January, 1997

DECLARATION

The work described in this thesis was carried out in the Department of Physical Chemistry under the supervision of Professor R.H.Ottewill FRS and Dr J.W. Goodwin. The work is claimed to be original except where otherwise indicated by references in the text.

Sharon Brockbank.

SHARON BROCKBANK

ACKNOWLEDGEMENTS

This project was sponsored by Unilever Research, Colworth Laboratory. I would like to thank everyone who helped me during the many weeks I spent working at Colworth House. I am especially grateful to Jennie Brigham and Dudley Ferdinando who gave so much of their time and were always very helpful, often at very short notice. I am also grateful to Nick Hedges for allowing me to make a second home in the DSC room, and thanks to Sally Lane for teaching me how to use it and for patiently solving all my queries. Thanks also to Dave Underwood for being superb in helping me to make the best use of my time at Colworth. Thanks also to Danny Mayes, Steve Ablett, Arthur Darke and Alan Clarke. Hello to Dave N. and Dave Y., Babs and Eddie, Susie, Martin I. and Ruth, thanks for all your help and encouragement. I would also like to thank Unilever for the financial assistance I have received.

Best wishes to Mike Fitzgerald who worked on his PhD at Reading University during the last four years, on a project parallel to this, about the phase behaviour of sucrose esters.

I would also like to thank Jaap Lucassen for visiting Bristol to discuss the project and for his help in rationalising the problem.

I am very grateful to Prof. Ron Ottewill for his good advice and constructive criticism and for many a long discussion during the last few years. Thanks very much for his help with the thesis. Thanks also to Jean Procter for always being helpful, cheery and supportive and to Jim Goodwin for his good advice and for his thoughtful assistance when it was required. Thanks to Rob Richardson for his help with the X-ray work.

Grateful thanks to Rod Bee for being an excellent industrial advisor without whom the project would neither have started nor finished.

Thanks to Sue, Andrea and Richard for their unfailing support and encouragement.

Last but not least, the biggest thanks go to my family for their constant support and encouragement. Thanks to mum for hours of cutting and pasting, thanks to Darren for his skills with a photocopier and thanks to dad for always setting a high standard.

Sharon.

ABSTRACT

Stable foams were prepared by the aeration of a mixture of Sweetose, a viscous, maltodextrin syrup, water and a sucrose stearate surfactant. These foams contain air bubbles, with diameters between 100nm and 20 μm, dispersed in a continuous matrix. The bubbles remain as discrete spherical cells within the viscous matrix, for up to 1 year after preparation, when stored at 4°C. This level of stability in a foam is highly unusual. When examined by TEM the bubbles had a regularly structured surface, consisting of an array of concave hexagonal and pentagonal domains, between 50 and 100nm across, protruding from the surface of the gas cell into the surrounding matrix. These bubbles, with a structured surface and high stability are referred to as gas microcells.

Mixtures of Sweetose, water and sucrose stearate have been examined before and after, aeration to form gas microcells. The ratio of Sweetose to sucrose stearate in the mixture was varied to investigate the functions of both. The sucrose ester was a commercial blend of sucrose mono-, di- and higher stearates. Different blends of sucrose stearates and sucrose esters containing different alkyl chain lengths were also investigated, in part.

The techniques used were polarising and confocal microscopy, TEM, SEM, DSC, rheology and X-ray and neutron diffraction. The surface tension was measured using the du Nouy ring and spinning-drop techniques, according to the viscosity of the sample. The gas microcells were dispersed in water and the variation in optical density and number concentration, of gas microcells in the dispersion, were measured as a function of time. The disperse phase was varied to examine the effects of dilute salt, Sweetose and sucrose ester solutions, on the relative instability of the microcells when removed from their natural environment.

When the sucrose ester contained both sucrose mono- and di-stearate, the mixture of Sweetose, sucrose stearate and water before aeration contained bilayers of liquid crystalline sucrose ester in a gel phase dispersed in a matrix of Sweetose in water. After aeration, a mixed sucrose stearate monolayer was deposited at the surface of the gas microcells. Bubbles larger than the gas microcells survive the aeration process, so disproportionation causes the gas microcells to shrink, and the sucrose stearate monolayer becomes compressed. The low solubility of liquid crystalline sucrose stearate in Sweetose solutions at room temperature prevents the desorption of the sucrose ester from the microcell surface into the matrix. As a result, the monolayer buckles, forming the structured surface observed by TEM. When the proportion of di- stearate in the sucrose ester blend was less than 30% the regular structure of hexagonal and pentagonal domains observed by TEM was formed. When the proportion of di-stearate was greater than 30% the structuring became progressively less regular.

The compressed monolayer formed a rigid surface around the gas microcell which severely retarded the disproportionation process. The high matrix viscosity kept the rate of drainage and creaming to a minimum. The retardation of these processes, which normally lead to the collapse of a foam, results in the gas microcells having the very high stability observed.

To Mum and Dad

SURFACTANT STABILISED GAS MICROCELLS

CONTENTS

INTRODUCTION

Approximately 10 years ago experiments at Unilever Research, Colworth Laboratory, led to the discovery that small, stable gas bubbles could be manufactured by the aeration of a mixture of viscous maltodextrin syrup, water and a food surfactant[1]. The viscous corn syrup used was called Sweetose and the surfactant was a sucrose ester. They discovered that commercial samples of sucrose stearate formed gas bubbles which were not only very stable, they also had a structured surface when examined by transmission electron microscopy (TEM).

Those bubbles ranged in diameter between 100nm and 20 microns. They were discrete spherical bubbles surrounded by a continuous viscous matrix. The structure observed by TEM was on their inner surface after freeze fracture. It consisted of a regular array of hexagonal and pentagonal concave domains, each between 50 and 100nm across.

Figure 1 is a TEM picture of a foam containing these stable air bubbles after freeze fracture, replication and shadow coating. The freeze fracture of a foam reveals the inner surface of a gas bubble in every instant thus each of the gas bubbles in the figure are concave surfaces.

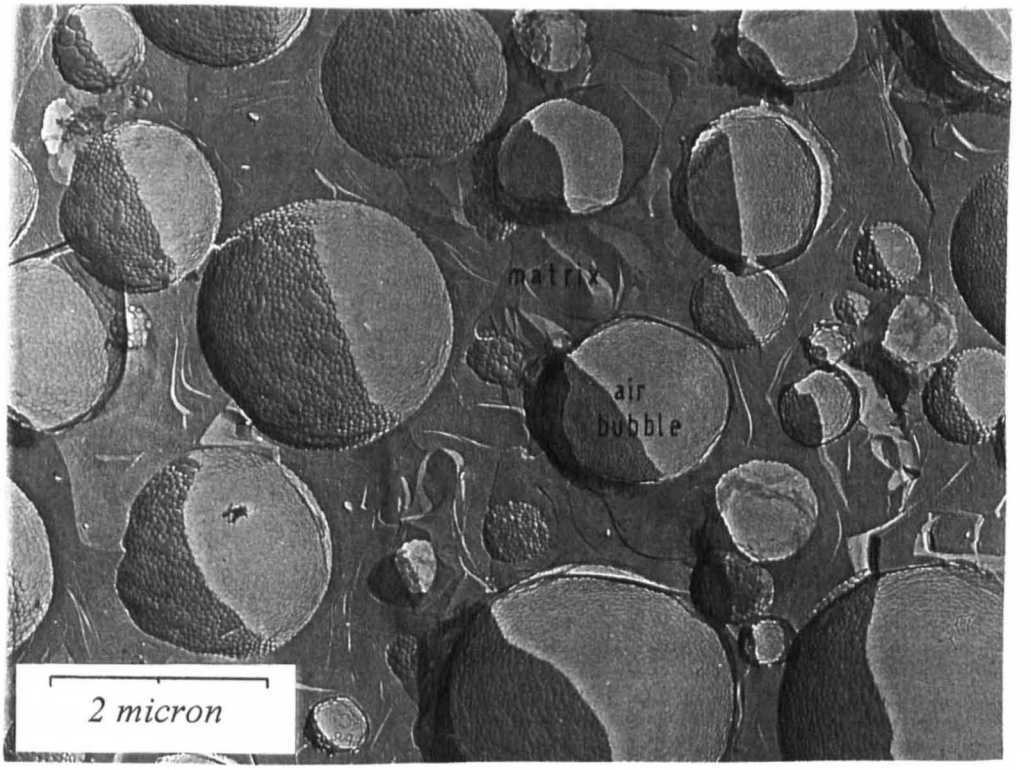

Figure 1

TEM image of a foam containing small stable air bubbles in a continuous matrix, after freeze fracture, replication and low angle shadow coating.

The air bubbles have been shadowed from an angle of 45°, from the right hand side of the picture to the left. Where the shadow coating has entered the bubble hemisphere the surface appears dark. Each bubble appears to be divided into two regions, dark and bright. The area occupied by each is dependent upon the latitude of the fracture section. Those bubbles which have an equal covering of light and dark regions have been fractured at their equator and the diameter observed is close to the true diameter of the bubble. All the bubbles are dark on the same side of their section because they are all concave surfaces and they are all shadowed from the same low angle.

On the surface of each of the bubbles is an array of regular hexagonal and pentagonal domains, separated by some less structured regions. The shadow coating on each of these domains faces the same direction as that on the bubbles themselves, i.e. they appear bright on their right hand edge and dark on the left. This is an indication that each of the domains is a concave surface which protrudes from the surface of the gas cell.

The air bubbles in the foam illustrated above were manufactured by the aeration of 75%w/w Sweetose in water and 2%w/w sucrose ester surfactant. They were observed to remain stable to drainage and disproportionation for up to 1 year if stored in a refrigerator at 4°C. These bubbles are referred to as gas microcells to distinguish them from other bubbles which do not possess this unusually high stability and regularly structured surface.

In general, types of foam resulting from the aeration of a solution of a surfactant, such as SDS in water, vary according to the volume fraction of air they contain. Where the volume fraction of air is very high the bubbles form polyhedral cells separated by thin films of surfactant. Where there is a lower phase volume of gas they can exist as discrete spheres in a continuous liquid. Foams containing gas microcells fall into the second category.

A number of physical changes can occur that lead to the destruction of a foam. These changes are disproportionation, or Ostwald ripening, creaming, drainage and flocculation. Many articles on the factors affecting foam stability have been published[2,3]. The majority of detergent foams have lifetimes of between a few minutes and a few days depending upon the surfactant used and the conditions of storage. Foams containing gas microcells are subject to the same destructive processes as any other surfactant stabilised foam yet the bubbles remain stable for up to 1 year if refrigerated. Disproportionation, creaming and drainage tend to be the most destructive processes. These shall be discussed briefly in terms of the ways in which they might be retarded to increase the stability of the foam.

The effect of disproportionation, creaming and drainage on foam stability

Disproportionation involves the growth of larger bubbles at the expense of smaller ones due to the difference between the Laplace pressure inside them.

The Laplace pressure inside a spherical bubble, $\Delta P = \frac{2 \cdot \gamma}{r}$ where, γ = surface tension

r = bubble radius

Small bubbles have a larger Laplace pressure than large bubbles. The high internal pressure inside a small bubble causes the air in the bubble to diffuse through the disperse phase and into one with a larger radius. This causes the radius of the small bubbles to shrink further and the cycle continues. The smaller the radius of the bubble the faster the rate of disproportionation. The process can be slowed down, or stopped in theory, if certain conditions are satisfied. As the bubble shrinks its surface area decreases and hence the surface excess concentration of surfactant increases, which leads to a decrease in the surface tension of the bubble. If the decreased surface tension balances the effect of the decrease in radius brought about by the shrinking then, according to the Laplace equation, the disproportionation will stop.

This effect is quantified in terms of the surface dilational modulus ε. This is the extent to which the surface excess concentration increases as the bubble surface area decreases. The surface dilational modulus for small soluble molecules tends to be small because they are able to desorb into the bulk phase when the surface area decreases. Large molecules such as proteins are less able to desorb and the surface dilational modulus becomes more appreciable.

If an adsorbed protein forms an insoluble layer on the bubble surface, such as in the case of whipped egg white, the surface dilational modulus can become very large and the disproportionation may be stopped. This can also happen if the surface of the air bubble is fully covered by solid particles or becomes so after a degree of shrinkage. This is the situation that occurs in whipped cream, with the fat globules fully coating the surface of the air bubbles. Whipped foams have also been stabilised by the presence of a gel phase liquid crystal at their surface[4]. Other workers[5,6,7,8] have demonstrated that it is possible to slow the rate of disproportionation in oil-water emulsions by the presence of gel-phase lipid films or with a 'plastic' surface layer such as high molecular weight porphyrins at the surface of the oil droplet.

The other major contributor to the destruction rate of foams is the process of creaming. The natural buoyancy of air bubbles causes them to cream rapidly to the surface. As they cream the liquid film surrounding them becomes thinner and thinner by a process of drainage. The rate at which bubbles cream to the surface is approximated by the Stokes equation,

$$v = 2g \cdot \rho \cdot \frac{r^2}{9\eta}$$

The Stokes equation

where, v = *the velocity of the rising bubble*

g = *the acceleration due to gravity*

ρ = *the density of the liquid*

r = *the radius of the bubble*

g = *the acceleration due to gravity.*

η = *viscosity*

The second power relationship between the radius of the bubble and its rising velocity dictates that smaller bubbles will cream very much slower than large ones. If the liquid is very viscous or has a considerable yield stress then the rising velocity of the bubble will be retarded further. Drainage is the process by which the liquid forming the disperse phase filters to the base of the foam, passing between the air bubbles and thinning the films that separate them. This film thinning eventually leads to film rupture and the gradual collapse of the foam. Increasing the viscosity of the disperse phase can reduce the rate of drainage in the foam.

Gas Microcells

Foams containing gas microcells are made by the aeration of a viscous mixture of 75%w/w Sweetose in water and 2%w/w sucrose ester surfactant. The bubbles contained in these foams are referred to as gas microcells because of their high stability and regular surface structure. This thesis describes in more detail the materials used and the method of preparation of these stable air bubbles.

The aims of the project were to understand why gas microcells have such an unusually high stability and why they possess a regularly structured surface. A further objective was to examine the conditions under which gas microcells remain stable when removed from their natural environment, for example, by dispersion in water.

These objectives were achieved by the use of many different techniques. At the beginning of the project very little was known about the handling characteristics and the limits of stability of the gas microcells within the foam. The process of achieving the above objectives was one of trial and error. None of the techniques described in this thesis were employed for a detailed study of any single aspect. Each has been used to find out the most accessible information about some part of the subject. A separate chapter is devoted to each technique, at the end of which is a short discussion of the results obtained and any tentative conclusions drawn. A full discussion of the results obtained is given in the last chapter with the final conclusions, drawn on the basis of this discussion, presented at the end.

References

[1] Unilever patent. U.S. Patent specification No. 3 480 616.

[2] Ross, S.; 'Interfacial phenomena in apolar media'. Chapter 1, Surf. Sci. series Vol 21. Ed. H.F. Eiche and G.D. Parfitt, Marcel Dekker Inc. NY 1987.

[3] Walstra, P.; 'Overview of emulsion and foam stability'. In: Dickinson E. (ed.) Roy. Soc. Special Pub. 58 p. 242 (1986)

[4] Westerbeek, J.M.M., Prins, A. and Kussendrager, K.; 'The α-gel phase of glycerol lactopalmitate in whipped emulsions', RSC spec. publ. No. 75, Ed Bee, R.D., Richmond, P. and Mingins, J., p364, 1989.

[5] Larsson, K.; Prog. Chem. Fats. other lipids. Vol 16. pp163 - 169. Pergamon Press. 1978. GB.

[6] Jarvis, N.L.; J. Phys Chem. **70**, 3027 (1966)

[7] Bikerman, J.J.; Foams, Springer-Verlag, New York, 1973.

[8] Mannheimer, R.J. and Schechter, R.S., J. Coll. Int. Sci. **32**, 212 (1970).

CHAPTER 1

Surfactant phase behaviour

1.0 SURFACTANT PHASE BEHAVIOUR

1.1 Introduction

Surfactants are molecules which possess both hydrophobic and hydrophilic character due to the substitution of a hydrophilic polar or ionic group into a hydrophobic hydrocarbon chain. This amphiphilic character renders them highly surface active; in both oil and water phases some part of the molecule is in an unfavourable environment. The state of lowest energy for each molecule occurs when it adsorbs at the interface between the two phases. At increased concentration, the surfactant maintains its solubility in the solvent by a process known as micellisation. The single amphiphiles aggregate to form micelles[1], which in aqueous solution consist of an organised group of molecules whose hydrocarbon chains are oriented towards the interior of the micelle leaving the hydrophilic groups in contact with the aqueous medium. The concentration above which micelle formation first occurs is called the critical micelle concentration.

1.2 The Hydrophobic Effect

At room temperature the hydrocarbon chain of a surfactant molecule, in solution as a monomer, occupies a cavity in the water structure. The water molecules at the sides of this cavity have a bonding arrangement that is different from the bulk pattern. The alkyl chain on a single surfactant molecule in solution increases the degree of structuring of the water around the alkyl chain and disrupts the hydrogen bonding network within the water. When the alkyl chains micellise, the cavities previously occupied by the alkyl chains melt, releasing the water molecules that were structured around the alkyl chain and part of the hydrogen bonding network in the water is restored. The combination of these increases the entropy of the water which more than compensates for the decreased randomness of the alkyl chains. This is the driving force for micellisation and is referred to as the Hydrophobic Effect, Tanford[2]. The effect arises from the strong hydrogen bonding network within pure water which must be disrupted or distorted when any solute is dissolved. A polar or ionic solute can form strong bonds to water molecules which compensate for the disruption to the existing network. Non polar groups however cannot compensate and their solution in water is resisted. Beesley et al.[3] and Evans[4] used cationic surfactants to investigate the mechanism of micelle formation in non aqueous solvents. All the solvents were chosen to have high dielectric constants and high cohesive energy densities, similar to water. Those solvents with multiple hydrogen bonding capability, formamide, hydrazine and ethylene glycol, allowed micelle formation, however 3-methyl sydnone, an aprotic solvent, did not. Evans concluded that a solvent capable of forming multiple hydrogen bonds was necessary for amphiphilic self assembly, confirming that the mechanism of micelle formation is based on the hydrophobic effect.

1.3 Micelle Shape

The micelle interior contains the alkyl chains, whose packing density is determined by the combined action of short range intermolecular repulsive forces and long range van-der-Waals attractions. The fluidity of the chains makes the interior of the micelle relatively incompressible, hence the geometry of the chain; its length and volume are also factors which contribute to the shape of the micelle. The area occupied by each head group at the surface is dependant upon a balance of steric, hydration and electrostatic interactions which together contribute a repulsive force between adjacent head groups. It is a combination of these interactions that determine the size and shape of the micelle.

Figure 1.3a is a schematic diagram to illustrate the preferred curvature of the interface for a given packing geometry, based on geometrical considerations.

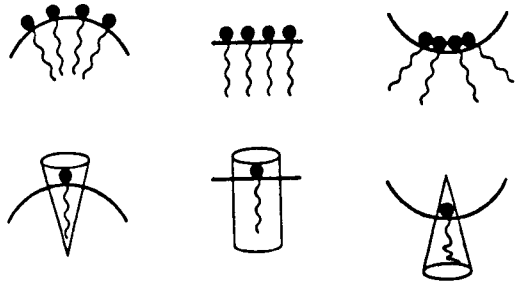

Figure 1.3a

The preferred curvature of an interface for a given packing geometry[5].

Israelachvili et al.[6] derived a set of packing constraints based on the area per head group at the interface and the length and volume of the hydrocarbon chain, to determine whether the amphiphile forms spherical or non-spherical micelles, bilayers or inverted micelles, according to which corresponds to the minimum sized aggregate in which all the surfactant molecules have the minimum free energy. see Figure 1.3b and the description which follows. Further details of these packing parameters are given in the book, 'Intermolecular and Surfaces Forces' by Israelachvili[7].

The packing parameters depend on the optimal area a_o, the volume, v, of the hydrocarbon chains and the maximum effective length that the chains can assume, this is called the critical chain length, l_c. Tanford[2] derived the following expressions for the length, l_c, and volume, v, of a hydrocarbon chain with n carbon atoms;

$$l_c \leq l_{max} \approx (0.154 + 0.1265n) \text{ (nm)}$$

$$v \approx (27.4 + 26.9n) \times 10^{-3} \text{ (nm}^3\text{)}$$

where, l_{max} is the fully extended length of the hydrocarbon chain, as it would be in the crystalline solid form.

Schematic model of a cross section through a spherical micelle,
revealing a geometric model of a single surfactant molecule at the interface

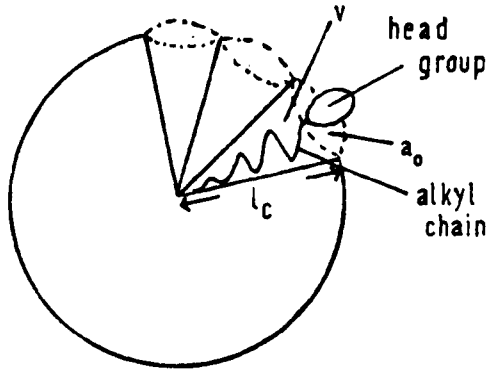

a_o - area per head group at the interface

l_c - critical length of the hydrocarbon chain, beyond which it can no longer be considered as fluid.

v - volume of the hydrocarbon chain

M - aggregation number

Figure 1.3b

The radius of a spherical micelle cannot be greater than a specific critical length l_c of the hydrocarbon chain, therefore for a spherical micelle consisting of M molecules with dimensions as described above:-

$$M = \frac{4 \cdot \pi \cdot r^2}{a_0} = \frac{4 \cdot \pi \cdot r^3}{3 \cdot v} \quad \text{thus} \quad r = \frac{3 \cdot v}{a_0}$$

Hence the packing consideration $r \leq l_c$ is satisfied if $\frac{v}{a_0 \cdot l_c} \leq \frac{1}{3}$.

The same packing considerations were considered to govern the formation of other geometry's. The following structures are formed according to the packing consideration satisfied by the individual surfactant molecules.

1. *spheres* $\quad \frac{v}{a_0 \cdot l_c} < \frac{1}{3}$

2. *non spherical* $\quad \frac{1}{3} < \frac{v}{a_0 \cdot l_c} < \frac{1}{2}$ (between ellipsoids and cylinders)

3. *vesicles or bilayers* $\quad \frac{1}{2} < \frac{v}{a_0 \cdot l_c} < 1$

4. *inverted micelles* $\quad 1 < \frac{v}{a_0 \cdot l_c}$

Changes in the environment, such as dilution or added electrolyte can affect the balance of intermolecular forces, altering a_0 and v and hence the preferred packing of the alkyl chains.

In liquids, surfactant association produces a variety of structures according to physical interaction forces; at high enough concentration surfactants form lyotropic liquid crystals or mesophases. These are close packed assemblies of surfactant molecules whose geometry varies with surfactant concentration and molecular structure.

1.4 Lyotropic liquid crystals

As surfactant concentration is increased other factors begin to affect the packing characteristics. As the number of micellar aggregates increase, repulsion between the micelles will tend to space them out. With still further increased surfactant concentration the free energy can be minimised by changing the packing geometry, e.g. from spherical units to an array of packed cylindrical units or bilayers, depending on the preferred shape of the micelle. The energy required to change the surface curvature is more than offset by changing to a geometry where the average separation of adjacent micellar surfaces is greater. Various liquid crystal phases exist[8], they are named according to the shape of the aggregates they contain; a cubic array of spherical micelles is known as a cubic phase, a hexagonal array of long cylindrical micelles is a hexagonal phase and where the aggregates are arranged as a series of parallel bilayers the phase is called lamellar. The individual amphiphiles within the aggregates are in a state of dynamic equilibrium, in-plane lateral diffusion of the molecules can occur quickly along the surface of the aggregate but 'flip-flop' diffusion through to the opposite side of the aggregate is slow due to the difficulty of passing the polar head group through the hydrocarbon phase. The following are a brief description of some of the lyotropic liquid crystalline phases formed by surfactants.

Cubic Phase, I_1 and I_2

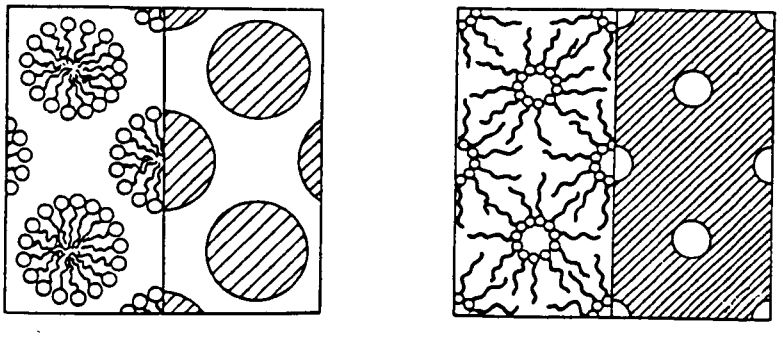

(a) (b)

Face centred cubic packing, (a) spherical micelles, I_1, (b) reversed micelles, I_2

Figure 1.4a[9]

Cubic phases are thought to consist of an array of close packed globular aggregates arranged in a body-centred cubic lattice. Their optical isotropy makes them invisible by

polarising microscopy however they do show a cubic array when viewed by low angle X-ray diffraction. I_1 and I_2 phases are usually located between dilute micellar and hexagonal phases. Alternative cubic phases, known as V_1 and V_2, are located between hexagonal H_1 and lamellar L_α phases at higher concentrations of surfactant. These consist of larger aggregates which form continuous networks either water or oil continuous or in some cases bicontinuous. Cubic phases are usually very viscous because there are no shear planes within the structure to allow the layers of surfactant aggregates to move relative to each other.

Hexagonal Phase, H_1.

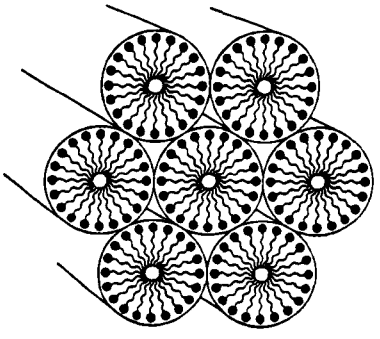

Figure 1.4b[5]

When examined by polarising microscope this phase displays a characteristic fan-like texture[10]. Low angle X-ray diffraction produces a series of spots which can be indexed on the basis of a 2-d hexagonal lattice. The structure comprises a hexagonally packed array of cylindrical aggregates. Hexagonal phases are very viscous despite containing typically 30-60% water by weight, although they are less viscous than cubic phases. Their cylindrical structure allows free movement along their length but shearing in a perpendicular direction is energetically unfavourable.

Reversed hexagonal phase, H_2, is a hydrocarbon continuous structure, with water-filled cylindrical aggregates. By the nature of this phase all the space between adjacent cylinders must be filled with hydrocarbon, dictating that the separation between each cylinder is smaller than that found in the H_1 phase. As a consequence of this H_2 phases are much less common than H_1 phases.

Lamellar Phase, L_{α}.[5]

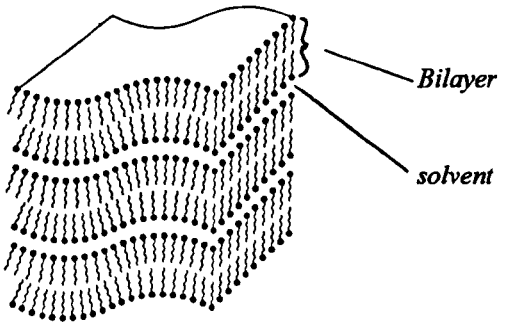

Figure 1.4c

When examined by polarised light, lamellar liquid crystal phases show a characteristic mosaic texture[8]. Low angle X-ray data show spacings with the repeat unit of a back-to-back bilayer of surfactant molecules with their alkyl groups in contact. The alkyl groups, between the layers of hydrophilic head groups, are thought to be in a disordered or fluid arrangement. The basic lamellar phase consists of flexible bi-molecular sheets arranged in large stacks parallel to one another and separated by a solvent[11]. The surfactant bi-layer thickness tends to be 10-30% less than two 'all trans' surfactant chains while the thickness of water layers varies according to composition. The ease with which parallel layers can slide over each other during shear accounts for the low viscosity of lamellar phase compared to hexagonal phase.

Technically these bilayers can accommodate an unlimited number of amphiphile molecules without changing the available surface area per molecule, which is itself essentially independent of the length of the hydrocarbon chains, but if the packing parameter $v/(a_0 l_c)$ is slightly less than unity then the bilayers will bend. As a consequence, closed bilayers form in which the hydrocarbon chains are no longer in contact with the solvent. This closed bilayer is referred to as a vesicle. Where multi-bilayer closed structures are formed these are called liposomes.

Amphiphiles with a single alkyl chain will very rarely form bilayers or vesicles since an approximately two-fold reduction in surface area per head group is required. If the amphiphile has two alkyl chains then the situation is reversed, the surface area per head group becomes twice as large as the surface area per hydrocarbon chain and thus a more planar arrangement will be favoured. Tanford[2] argued that the optimal value of the area per head group for micelles formed with two-chain amphiphiles would be smaller than that for a single chain, for amphiphiles with comparable head groups and similar chain lengths, because the free energy gain on micellisation for a two-chain amphiphile is much larger than that for one with a single chain. Thus the bilayer arrangement should be the optimal form for two-chain amphiphiles because globular or cylindrical micelles would have too

large a surface area. These two chain amphiphiles tend to self-assemble into bilayers directly at the cmc rather than forming a dilute micellar phase. Those lipids in which the difference between hydrocarbon chain volume and head group size is very large tend to form inverted micelles.

1.5 Hydrocarbon chain melting transition

The alkyl chains within a surfactant micelle are generally regarded as being disordered, in effect a small volume of liquid hydrocarbon constrained by the micelle surface. Pure hydrocarbons have a melting point at which temperature the chains undergo an order to disorder transition, this is observed as a solid to liquid melting process. This melting transition can also occur in the hydrocarbon region within a bilayer. This was discussed by Tanford[2] on the basis of the thermodynamic data for phospholipids of Phillips et al.[12] The chain melting transition temperature of the hydrocarbon chains within a liquid crystal tend to be higher than that in the bulk hydrocarbon because when this melting process occurs it is accompanied by a loosening of the order between the head groups[11]. The mobility of the chains within a liquid crystal bilayer is slightly less than that within the chains of a pure hydrocarbon because the region of the alkyl chain near the point of attachment of the head group is more restricted than the region close to the free ends of the chain.

1.6 Gel Phases

When a lamellar phase, L_α, is cooled to below the chain melting temperature of its amphiphiles a phase change can occur that leads to the formation of a metastable gel phase. The characteristic feature of a gel phase is that the alkyl chains are crystalline while liquid-like solvent still exists between the bilayers, thus the head groups remain hydrated. When alkyl chains crystallise, they have a cross-sectional area of approximately 20Å^2 per hydrocarbon chain, with the chains perpendicular to the surface. This imposes certain packing conditions on the bilayer and mismatches between the cross sectional area of the head group and that of the hydrocarbon chain can result in the formation of several types of gel phase structure. If the area of the head groups matches that of the chains then the L_β phase will form, if there is a slight mismatch then the tilted or rippled structures L_β' or P_β' will form, or more unusually the chains may even interdigitate forming a layer with the thickness of the length of a single alkyl chain. These are illustrated in Figure 1.6a.

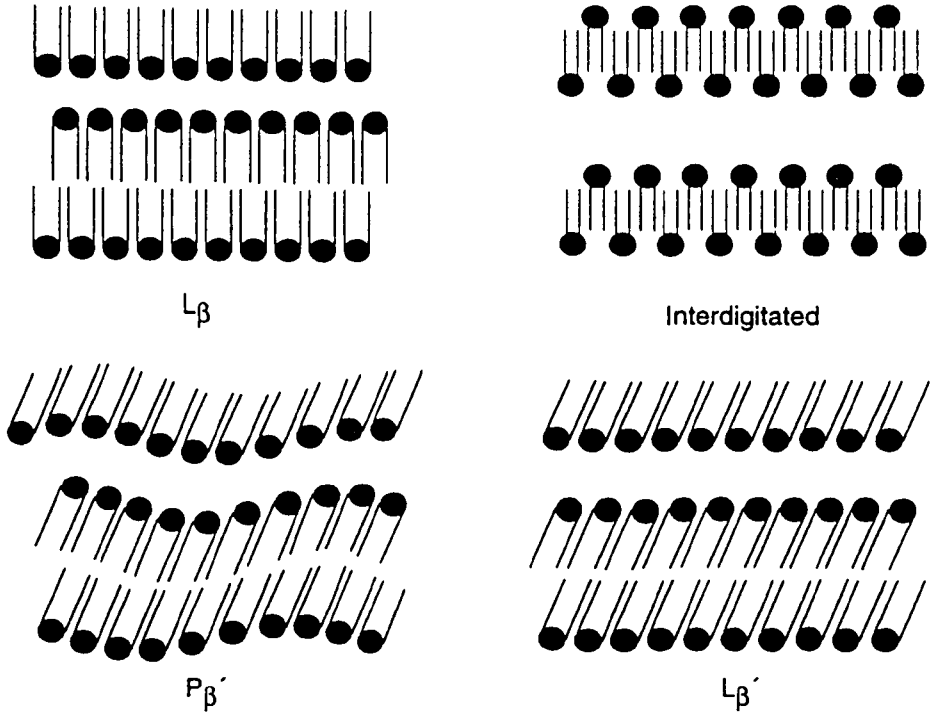

Figure 1.6a

Gel phases in bilayers of two-chain amphiphiles[13]

The formation of liquid crystals by surfactants, their packing characteristics and the existence of a chain melting transition will be referred to in later Chapters, with regard to the behaviour of sucrose ester surfactants.

1.7 References

[1] McBain, J.W.; Trans. Faraday Soc., **9**, 99, (1913)

[2] Tanford, C.; "The Hydrophobic Effect - Formation of Micelles and Biological Membranes", Wiley, (1973)

[3] Beesley, A.H., Evans, D.F. and Laughlin, R.G.; J. Phys. Chem., **92**, 791, (1988)

[4] Evans, D.F.; Langmuir, **4**, 3, (1988)

[5] Clint, J.H.; "Surfactant aggregation", publ. Blackie, 1992.

[6] Israelachvili, J.N., Mitchell, D.J. and Ninham, B.W.; J. Chem. Soc., Faraday Trans I, **72**, 1525, (1976)

[7] Israelachvili, J.N.; "Intermolecular and Surface Forces", Academic Press, London. 1985.

[8] Tiddy, G.J.T.; Physics Reports, **57**, 1, (1980)

[9] Ekwall et al., Liquid crystals 2, ed. G.H. Brown, Gordon and Breach Science publishers Ltd., 1969.

[10] Rosevear, F.B.; J. Amer. Oil Chem. Soc., **31**, 628, (1954)

[11] Luzzati et al.; Disc. of Faraday Soc., **25**, 43, (1958)

[12] Phillips, M.C., Williams, R.M. and Chapman, D.; Chem. Phys. Lipids, **3**, 234, (1969)

[13] 'The Colloidal Domain', D. Fennell Evans and Hakan Wennerstrom, VCH Publ., New York.

CHAPTER 2

Materials, and preparation of gas microcells

2.0 MATERIALS, AND PREPARATION OF GAS MICROCELLS

2.1 Introduction

This thesis describes the manufacture of small, stable air bubbles, referred to as gas microcells, by the aeration of a mixture of Sweetose, sucrose ester surfactant and water. Information about the Sweetose and sucrose ester used and the method for the preparation of gas microcells is given in this chapter.

2.2 Materials

2.2.1 Sweetose

Sweetose 240 is a bright, colourless, viscous maltodextrin corn syrup containing approximately 80% solids by weight. It is a solution of oligosaccharides containing mostly low molecular weight sugars.

The distribution of glucose units, in the oligosaccharides that constitute Sweetose, is shown in the following table.

Table 2.2.1a

%G1	%G2	%G3	%G4	%G5	%G6	%G7	%G8	%G9
29.9	34.9	5.1	1.8	2.7	2.6	1.9	1.0	0.5

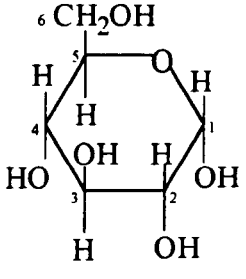

Figure 2.2.1a

A molecule of α-d-Glucopyranose, described here as 1 glucose unit.

Properties of Sweetose

Viscosity at 30°C	22 kg m^{-1} s^{-1}
Density at 20°C	1.3 g cm^{-3}
Sugar Spectrum,	36% Dextrose
(D.S. Basis)	33% Maltose
	8% Maltotriose
	23% Higher Sugars

Sodium	220 ppm#
Potassium	1.2 ppm#
Calcium	2.1 ppm#
Magnesium	0.2 ppm#
Chloride	6.7 ppm#
Sulphate	150 ppm#
Sulphated Ash	Less than 0.4%
Nitrate	0.3 ppm#
Phosphate	<0.1 ppm#

Sweetose Specification

Dry Solids	81.0 - 83.0%
Dextrose Equivalent	61.0 - 64.0
Refractive Index (at 20°C)	1.4952 - 1.5005
Sulphur Dioxide	250 - 400 mg kg^{-1}
Lead	0.5 mg kg^{-1} maximum
Arsenic	0.5 mg kg^{-1} maximum
Copper	0.5 mg kg^{-1} maximum
Iron	<0.1 ppm#
Aluminium	<0.5 ppm#

Data supplied by Unilever Research Ltd, Colworth House Laboratories.

Sweetose 240 is supplied by Tunnel Refineries, Thames Bank House, Tunnel Avenue, Greenwich, London SE10 OPA. Tel. 0181 858 3271

2.2.2 Ryoto Sucrose Ester

These are commercially available surfactants derived from sucrose and long chain carboxylic acid molecules. All sucrose esters employed in this study are cream coloured powdered solids, except where mentioned, all were supplied by Mitsubishi-Kasei Foods Corporation, and supplied under the brand name Ryoto. The sucrose esters supplied for use in this work were analysed by the technique of gel permeation chromatography by D. Mayes at Unilever Research, Colworth Laboratory[1].

Sucrose esters are named by Ryoto, according to the following pattern; S1670 records a sucrose ester in which approximately 70% of all the alkyl chains are stearate which has HLB of 16. The HLB values quoted are those specified by Ryoto and have not been calculated for this work. By the same pattern S170 contains approximately 70% stearate derivatives and has an HLB of 1, B1570 contains approximately 70% behenate derivatives and has an HLB of 15. This is illustrated in Tables 2.2.2 b&c.

Table 2.2.2b

Sucrose ester constituents

Sample ID.	% Mono	% Di	% Tri	% Tri/Higher	% F.F.A.$	% Unknown
S1670 stearate	76.9	20.5	2.7	-	-	-
S1570 stearate	70.2	25.0	4.7	-	-	-
S1170 stearate	52.0	35.8	12.1	-	-	-
S770 stearate	29.1	39.5	24.3	7.1	-	-
S270 stearate	10.9	13.8	-	64.8	4.0	6.4
S170 stearate	-	-	-	96.6	3.4	-
S070 stearate	-	-	-	94.6	5.4	-
P1570 palmitate - C_{16}	65.9	28.2	5.9	-	-	-
B1570 behenate - C_{22}	66.5	26.3	6.7	-	-	0.4
#mono-stearate	98.6	1.0	-	-	-	0.4
#di-stearate	-	40.4	-	54.9	4.7	-
C_8 caprylate	99.5	-	-	-	-	0.5
C_{10} caprate	99.4	-	-	-	-	0.6
C_{12} laurate	99.4	-	-	-	-	0.6
*C_{16} palmitate	97.8	2.2	-	-	-	0.0

$ F.F.A. - for further analysis

Samples obtained from Unilever Research, Vlaardigan Laboratory and used as received.

* Sample prepared by Michael Fitzgerald[2] used as received.

Table 2.2.2 c

Fatty acid chain length

Sample	Fatty Acid Chain Length (% of total fatty acids)													
	8:0	10:0	12:0	14:0	15:0	16:0	18:0	18:1	18:2	18:3	20:0	22:0	24:0	Tot. Trace
S1670	-	-	0.1	1.5	0.2	25.2	69.6	0.2	-	-	1.5	0.4	-	1.3
S1570	-	-	0.2	1.7	0.3	25.8	68.8	0.3	0.1	-	1.3	0.3	-	1.2
S1170	-	-	0.2	1.7	0.2	26.5	68.4	0.3	0.1	-	1.5	0.4	-	0.7
S770	-	-	0.2	1.4	0.2	26.8	68.2	0.3	0.1	-	1.6	0.5	-	0.7
S270	-	-	0.1	1.1	0.2	27.1	68.8	0.2	-	-	1.4	0.3	-	0.8
S170	-	-	0.1	1.2	0.1	26.2	69.5	0.2	-	-	1.5	0.4	-	0.8
S070	-	-	0.1	1.3	0.2	26.9	68.7	0.2	-	-	1.5	0.4	-	0.7
P1570	-	-	0.1	1.2	0.3	79.8	17.5	0.2	-	-	0.2	-	-	0.7
B1570	-	-	-	0.3	-	0.5	1.8	0.3	0.1	-	10.1	85.1	1.6	0.2
#mono-	0.1	-	0.4	1.8	0.3	27.3	67.3	0.3	-	-	1.2	-	-	1.3
#di-	-	-	0.0	1.3	0.0	23.0	73.7	0.4	0.0	-	1.5	-	-	0.1
C_8	95.7	-	1.2	-	-	1.2	-	0.8	-	-	-	-	-	1.1
C_{10}	-	97.8	0.5	-	-	0.6	0.3	0.4	-	-	-	-	-	0.5
C_{12}	0.3	0.3	90.2	0.8	-	1.5	1.6	0.9	0.2	3.5	-	-	-	0.8
*C_{16}	-	-	-	0.2	-	98.8	0.6	0.2	-	-	-	-	-	0.3

Samples obtained from Unilever Research, Vlaardigan Laboratory and used as received.

* Sample prepared by Michael Fitzgerald[2] used as received.

Further properties of sucrose ester S1670

Melting point 49 - 56°C

Decomposition point 237°C

Molecular weight: mono-stearate 636, di-stearate 917, tri-stearate 1197, Av mol. wt. 720.

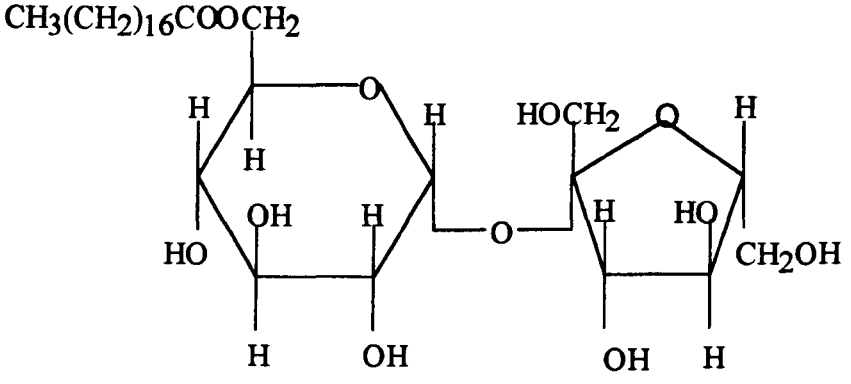

Sucrose Monostearate

Ryoto sucrose esters supplied by Mitsubishi - Kasei Foods Corporation, Ichikawa Building, 13 - 3 Ginza 5 - Chome, Chuo - Ku, Tokyo, Japan.

2.3 Preparation of gas microcells

Mixtures of Sweetose, sucrose ester and water were aerated for two hours in a rotary mixer. The resultant foam was found to contain many small, stable bubbles of approximately 2 micron diameter which are referred to as gas microcells. 75%w/w Sweetose in water and 2%w/w sucrose ester in the sample, was treated as a standard recipe for the consistent production of gas microcells. The ratio of Sweetose to sucrose ester in the mixture was then varied according to the experimental requirements.

This thesis describes the various techniques that have been used to examine the mixture of Sweetose, sucrose ester and water before and after aeration. After aeration the mixture contains gas microcells unless stated otherwise in the text. The mixture before aeration is referred to as a non-aerated mixture. Both aerated and non-aerated mixtures were prepared according to the following procedure.

Procedure

The proportions of Sweetose, sucrose ester and water in the mixtures were divided according to weight. The usual sample weight prepared was 500g. The required weight fractions of Sweetose and sucrose ester were calculated and the total weight was made up with water. For instance in 500g a mixture of 75%w/w Sweetose and 2%w/w sucrose ester would contain 375g of Sweetose, 10g of sucrose ester and 115g of water.

The sucrose ester was dissolved by repeated heating to 80°C with the required water until no solid crystals were visible. The sucrose esters used had a very low solubility in water at room temperature, but formed a gel after heating and cooling. The Sweetose was then heated to 70°C and both constituents were combined. A microwave oven was used for the heating process in both cases.

In the preparation of gas microcells, the mixture was cooled until it ceased steaming and was then aerated for two hours using a Hobart N50 mixer with a paddle stirrer at Speed 2, 324 rpm. The warm mixture reaches room temperature during the aeration process.

In the preparation of a non-aerated sample the hot mixture was stirred for up to 4 hours at 70°C, using a magnetic heater/stirrer, after which time stirring ceased and the mixture was allowed to cool. This process prevented the separation of the Sweetose from the sucrose ester and produced a heterogeneous mixture, without the incorporation of air bubbles.

The practice of aerating a Sweetose-sucrose ester mixture, before cooling was complete, was assumed to have negligible effect on the production of gas microcells. Examination, by TEM, of a cold non-aerated mixture which was subsequently aerated revealed this to be the case. This is discussed further in Chapter 5.

2.4 References

[1] Mayes, D.; 'Gel permeation chromatography of sucrose esters', Unilever Research, Colworth Laboratory, internal report, 1996.

[2] Fitzgerald, M.; PhD Thesis, University of Reading, 1996.

CHAPTER 3

Optical microscopy

3.0 OPTICAL MICROSCOPY

Samples of aqueous sucrose ester, S1670 and non-aerated mixtures of Sweetose and sucrose ester were examined using a polarising optical microscope. S1670 contains a blend of sucrose stearates, with the proportion 77% mono- to 20% di- to 3% tri- ester.

3.1 Sucrose ester S1670 crystals

Pure sucrose ester crystals are insoluble in cold water. These crystals were placed on a microscope slide, contacted with a drop of water and heated until the surfactant and water in the microscope image began to mix, this occurred at approximately 60°C. The sample was cooled to room temperature before photographing.

A variety of optical textures were observed across a range of surfactant concentrations between dilute on the lower LHS and concentrated on the upper RHS, Figure 3.1a.

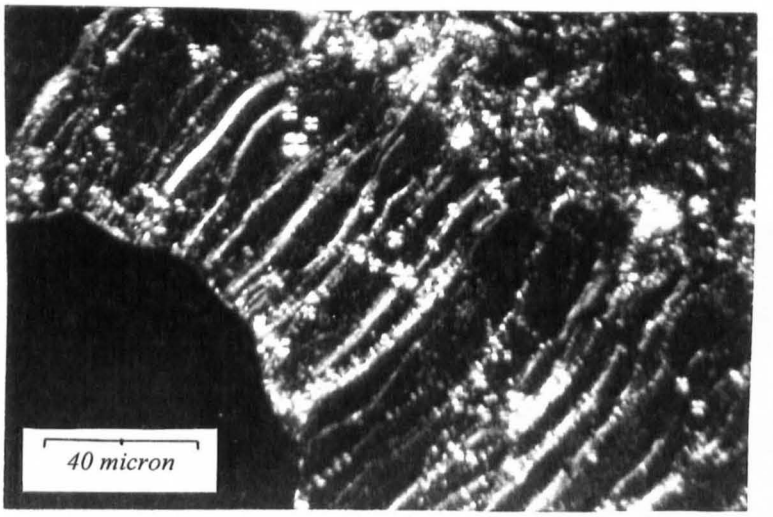

Figure 3.1a

Sucrose ester crystals after contacting with water, melting and cooling to room temperature. Examination under polarised light reveals an isotropic region at dilute concentration (lower LHS), with oily streaks and Maltese crosses in the centre and a mixed behaviour at high surfactant concentration (upper RHS).

Rosevear[1] examined many different surfactant phases under polarised light and published his observations on the optical textures exhibited by the various phases. The micrograph shown in Figure 3.1a shows a number of features similar to those attributed by Rosevear to different surfactant phases, the dark isotropic region on the lower left of the figure resembles a dilute micellar or a cubic phase, the oily streaks and Maltese crosses in the centre are indicative of a hexagonal or lamellar phase and the grain-like texture on the upper right is indicative of mixed surfactant phases. A brief discussion of surfactant phases was given in Chapter 1.

3.2 Aqueous solutions of sucrose ester

Aqueous solutions of sucrose ester, S1670, were prepared by heating the sucrose ester to 60°C with the required amount of water and gently stirring until no crystalline material remained. At concentrations of sucrose ester above 10%w/w the mixture formed a gel rather than an aqueous solution.

Examination of samples with a sucrose ester concentration greater than 20%w/w, using polarised light, revealed regions of anisotropy although no regular surfactant phases, as described by Rosevear[1], were observed. Solutions of less than 20% w/w S1670 concentration were isotropic. The regions of anisotropy had a feather-like appearance and a linear arrangement, possibly due to shearing during preparation or transfer onto the slide. Samples with sucrose ester concentration up to 40%w/w were examined, no recognisable features were observed and the anisotropic regions with a feather-like appearance increased in number. Figure 3.2a illustrates the anisotropic regions in 10%w/w sucrose ester. The sample was slowly heated whilst under observation, at approximately 45°C the contrast of the bright anisotropic regions against the dark background decreased and the sample became more isotropic, Figure 3.2b.

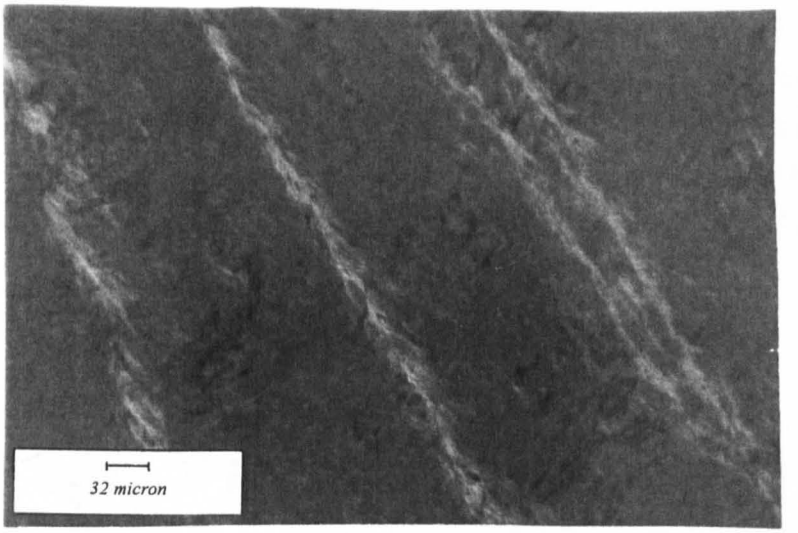

Figure 3.2a

20% w/w sucrose ester, S1670, under polarised light, showing feather-like regions of anisotropy.

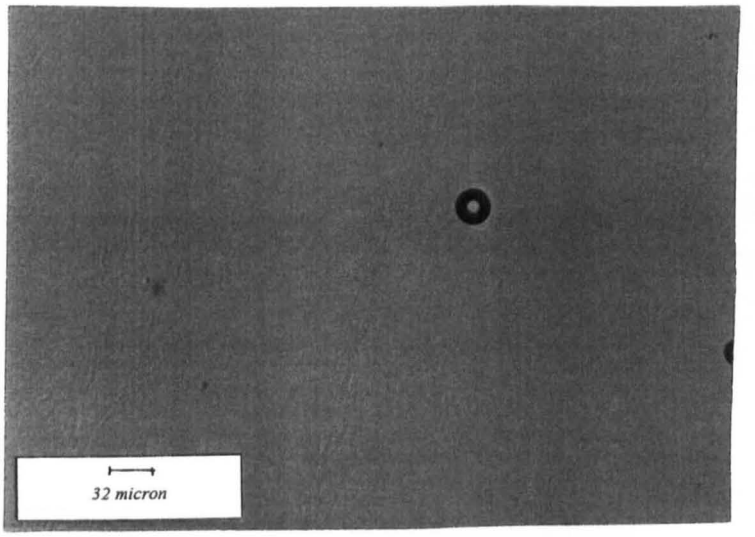

Figure 3.2b

20% w/w sucrose ester, S1670, above 45°C. The bright anisotropic regions seen in Figure 3.2a are less distinct.

3.3 Non-aerated mixtures of Sweetose and sucrose ester

Non-aerated mixtures of Sweetose and sucrose ester, S1670, examined using polarised light were also found to contain optically anisotropic regions, whose number increased with sucrose ester concentration, at constant Sweetose concentration. Figures 3.3 a, b & c illustrate 75% Sweetose with 0.5%, 1% and 2% S1670 respectively. The air bubbles seen in the illustrations are a consequence of the sample preparation and are not gas microcells.

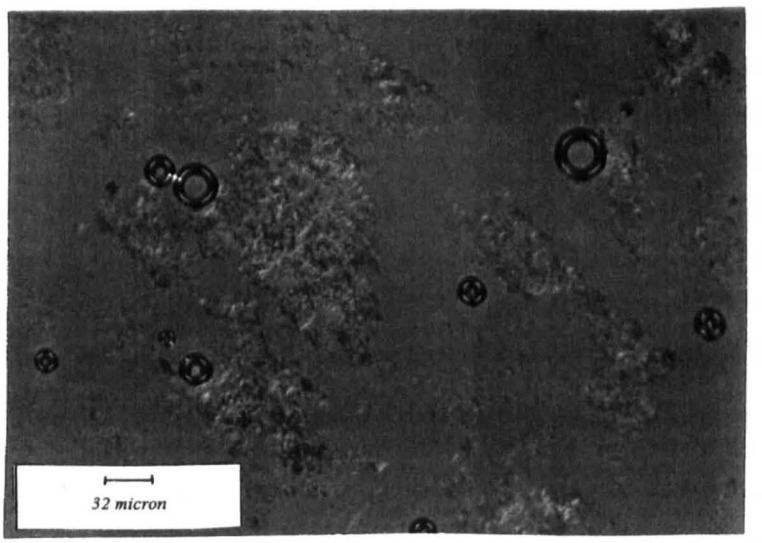

Figure 3.3a

75% Sweetose 0.5% sucrose ester, S1670

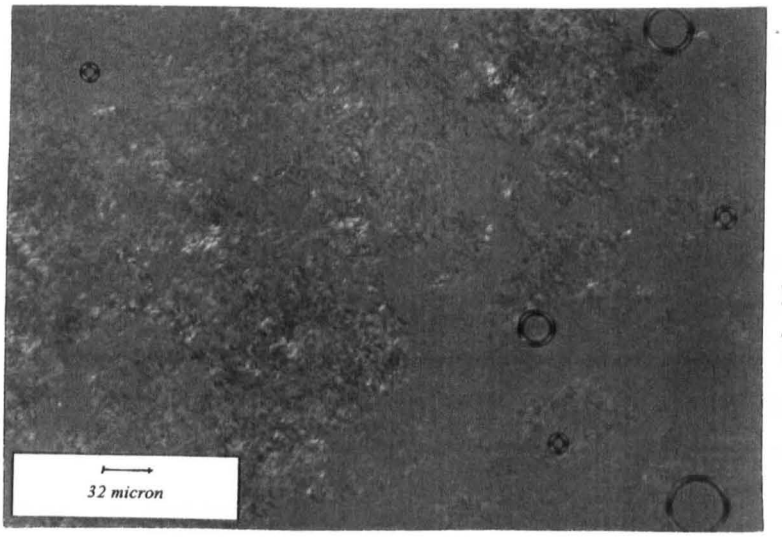

Figure 3.3b
75% Sweetose 1% S1670

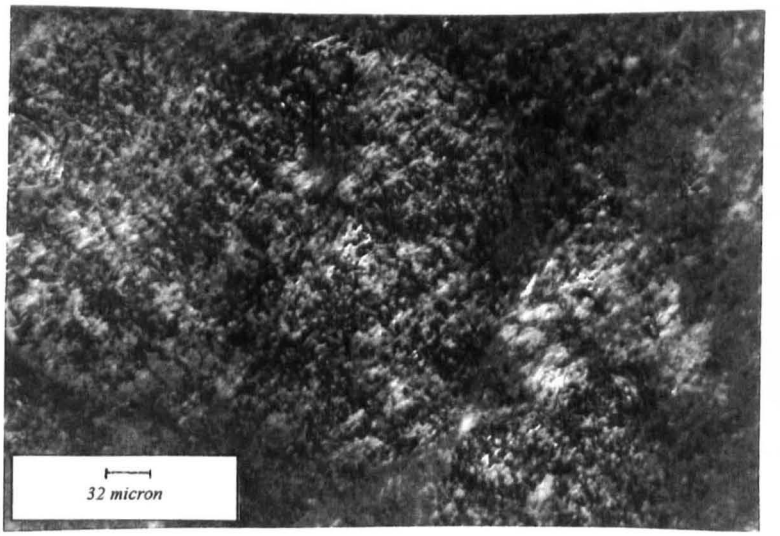

Figure 3.3c
75% Sweetose 2% S1670

Samples of aqueous S1670 were observed to be optically anisotropic at concentrations greater than 20%w/w. When the solvent was 75% Sweetose, a sample of S1670 was partially anisotropic at only 0.5%w/w. When the S1670 concentration was increased to 2%w/w the anisotropic regions became more numerous. The formation of discrete regions with anisotropic character rather than a homogeneous sample is indicative of the formation of two separate phases, one of which is anisotropic. Samples appear anisotropic when they have more than one index of refraction, depending upon the angle from which they are viewed. In the case of sucrose ester this criteria may be satisfied by both crystal and liquid crystalline phases.

In very high dilution aqueous solutions of S1670 are isotropic, as the concentration is increased to 20%w/w the sucrose ester begins to phase separate either in the form of hydrated crystals or liquid crystals. 0.5%w/w sucrose ester phase separates to a greater extent in 75%w/w Sweetose than it does in water.

3.4 Sucrose esters containing different ratios of mono- to higher- esters

Non-aerated mixtures of 75%w/w Sweetose, 2%w/w sucrose ester and water were prepared, using commercially available sucrose esters which contain different proportions of mono- to di- and higher esters, a bar chart to illustrate composition appears below, Figure 3.4a. When viewed using polarised light all samples were anisotropic, however, as the proportion of di- and higher esters in the blend increased their appearance changed, from discrete bundles of plate-like structures, in S1670, through a uniform granular texture, to spheres with a layered surface on a granular background in S270. The Figures 3.4 b-g illustrate S1670, S1570, S1170, S770 and S270 respectively,

Mono-, di- and higher ester composition of sucrose esters

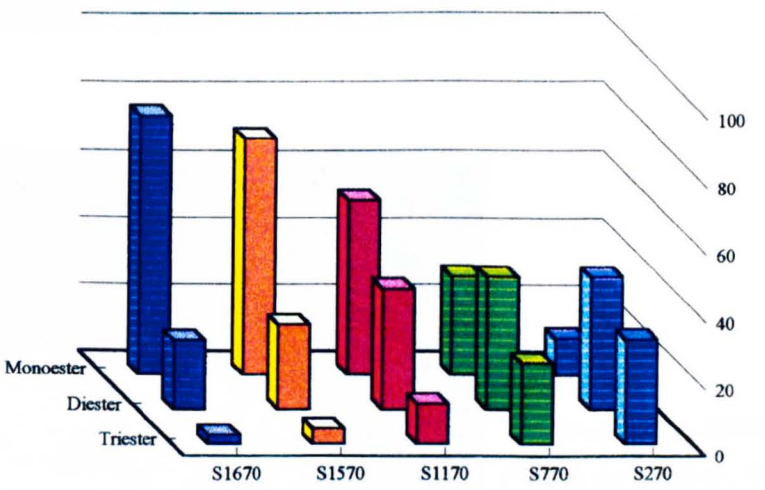

Figure 3.4a

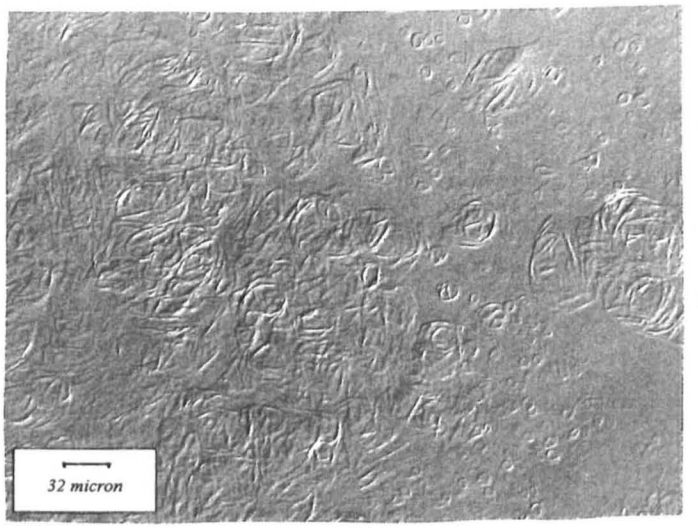

Figure 3.4b

75% Sweetose 2% S1670

(77% mono-, 20% di-, 3% tri- ester)

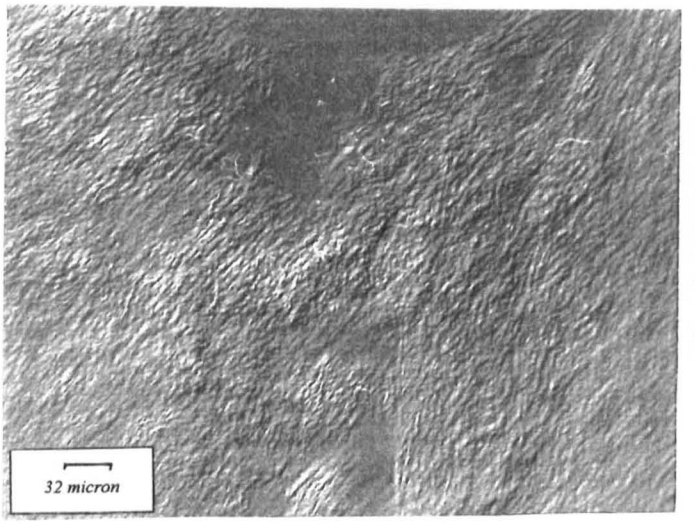

Figure 3.4c

75% Sweetose 2% S1570

(70% mono-, 25% di-, 5% tri- ester)

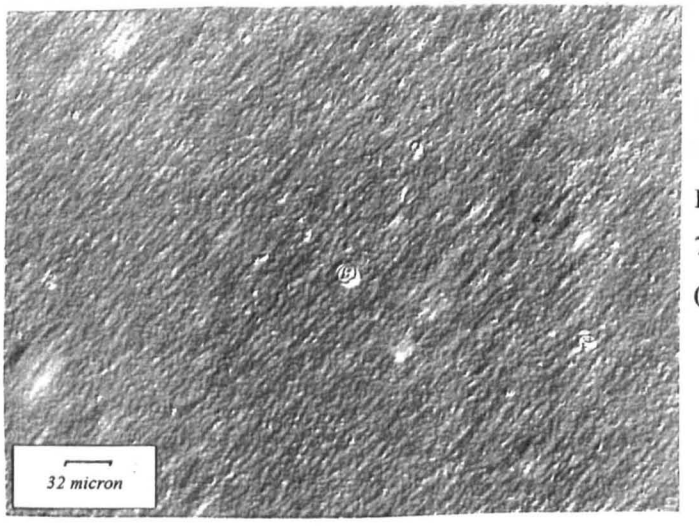

Figure 3.4d

75% Sweetose 2% S1170

(52% mono-, 36% di-, 12% tri- ester)

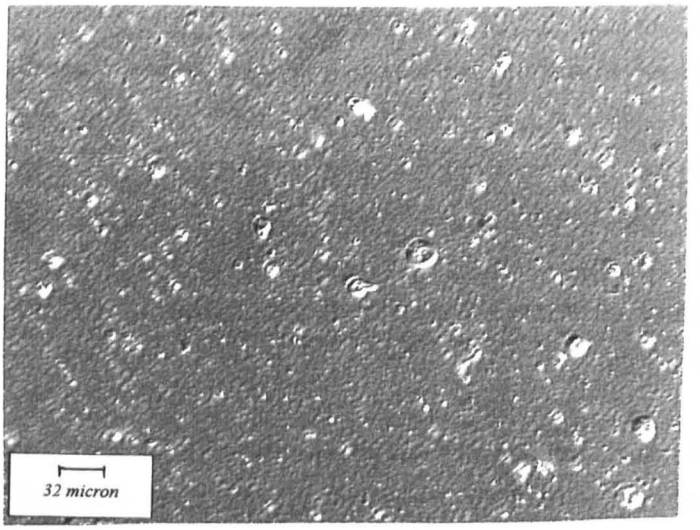

Figure 3.4e
75% Sweetose 2% S770
(29% mono-, 40% di-, 31% poly-)

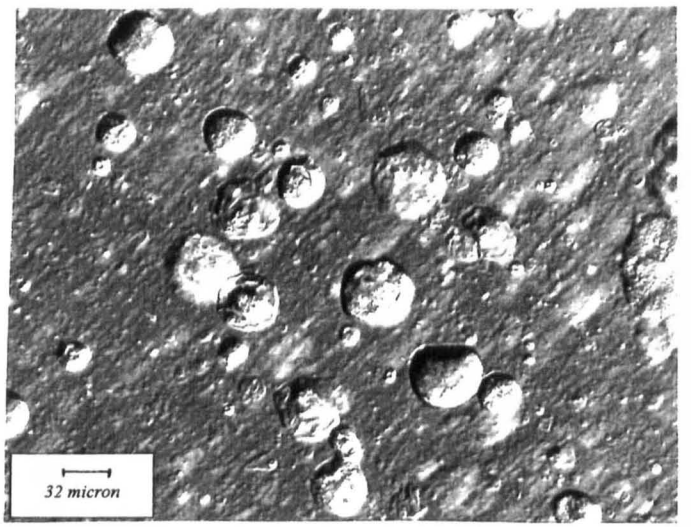

Figure 3.4f
75% Sweetose 2% S270
(11% mono-, 14% di-, 65% tri-/higher)

In mixtures of 75% Sweetose and 2% sucrose ester the appearance of the anisotropic regions varied with the blend of esters it contained. In S1670, with the highest proportion of mono-stearate, the surfactant aggregates had a fairly linear appearance whilst S270, with the highest proportion of di- and higher stearates formed multilayered spheres. Similar spherical globules have been observed in other surfactant systems and are known as vesicles.

3.5 Stirring a non-aerated mixture of Sweetose and sucrose ester to trap air bubbles.

A 75% Sweetose 2% sucrose ester, S1670, (and water) non-aerated mixture was manually stirred, with the removal of successive aliquots for examination under polarised light. In the above examples non-aerated mixtures were seen to contain anisotropic material, thought to be liquid crystalline sucrose ester, as shown in Figure 3.5a. The appearance of this material was altered by stirring; after initial agitation much of the structure was obliterated, Figure 3.5b. After further stirring the gas phase volume had increased such that the matrix surrounding the bubbles was no longer visible, Figure 3.5c. Figure 3.5d illustrates an area of the sample where the heterogeneous material was observed to coat the upper surface of the trapped air bubbles.

A possible explanation for these observations, subject to further investigation, is that the liquid crystals are sheared and become deposited on the gas cell surface. As the number of cells increases the thickness of the layer on each one is reduced until eventually all gas cells are covered by a layer of sucrose ester.

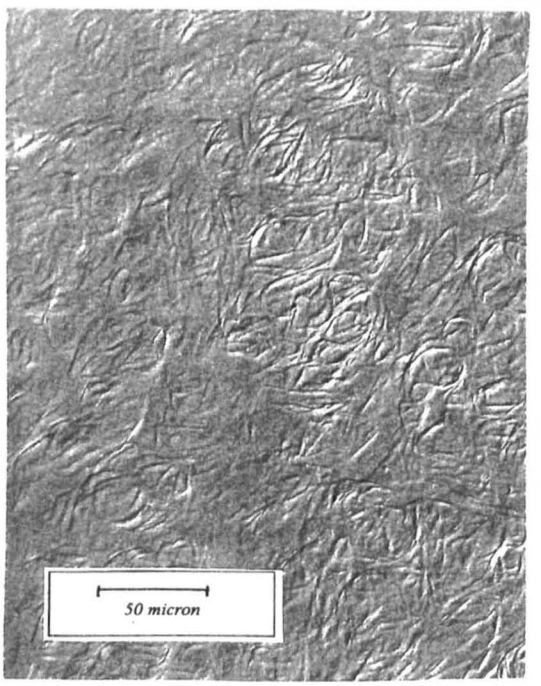

Figure 3.5a

Non-aerated 75% Sweetose 2% sucrose ester.

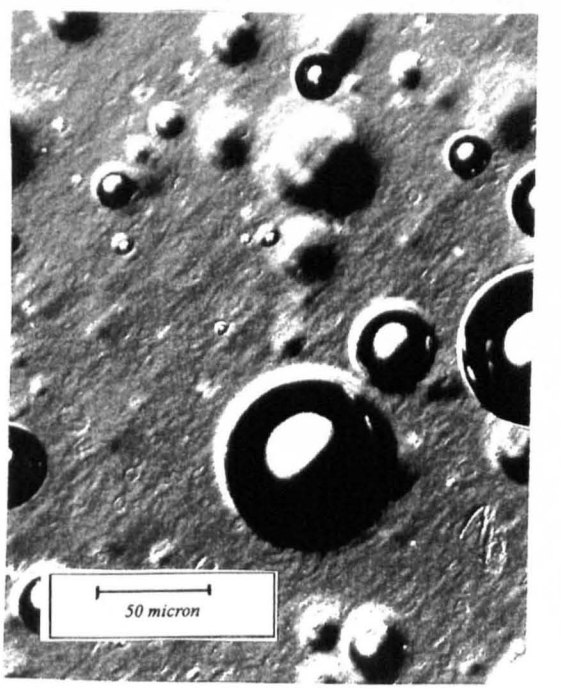

Figure 3.5b

Partially aerated 75% Sweetose 2% sucrose ester.

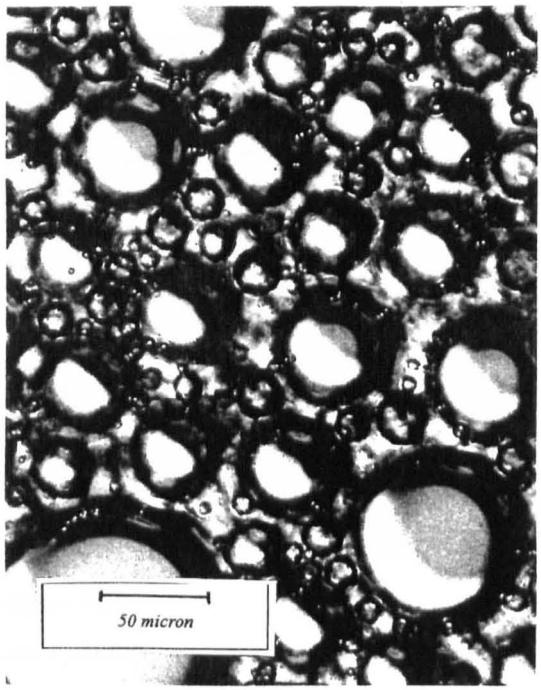

Figure 3.5c

Further aeration of 75% Sweetose 2% sucrose ester.

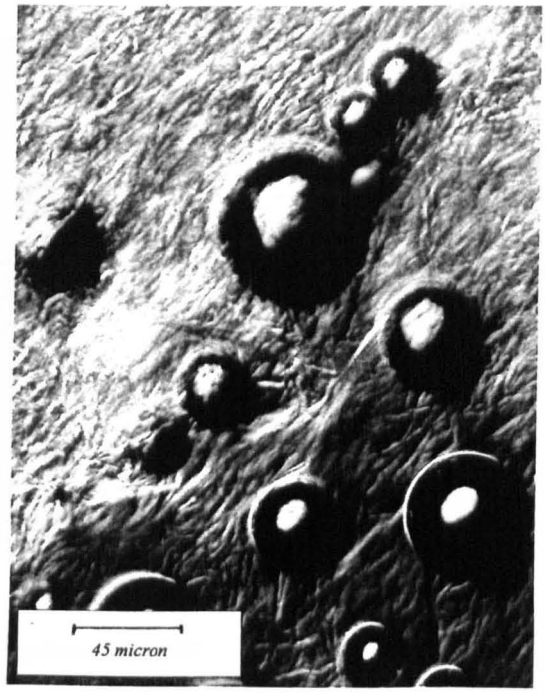

Figure 3.5d

Partially aerated 75% Sweetose 2% sucrose ester, gas cells coated by liquid crystalline sucrose ester.

A tentative conclusion is that in the 2 hour aeration process for the preparation of gas microcells, each gas microcell is being coated by a layer of sucrose ester.

3.6 Gas microcells contacted with a drop of water

Gas microcells were prepared using 75% Sweetose and 2% sucrose ester S1670 by the standard method, as described in Chapter 2. A sample of these microcells was smeared onto a glass microscope slide and irrigated with water to initiate disproportionation. On immediate contact with water the gas cell diameter increased to approximately 1 micron; after this some cells continued to expand, however most remained small. In Figure 3.6a both large and small cells are clearly visible.

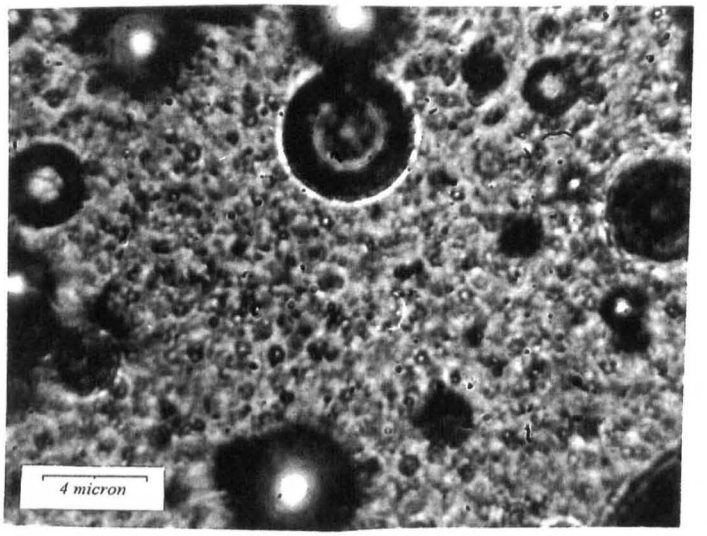

Figure 3.6a

Gas microcells of 75% Sweetose 2% sucrose ester after irrigation with water.

3.7 Dispersions of gas microcells

75% Sweetose 2% S1670 gas microcells were dispersed in water, dilute Sweetose solution or dilute salt solution, to an arbitrary number concentration and an aliquot of this dispersion was immediately sealed between a microscope slide and a coverslip using nail varnish. Time-lapse video was used to record any changes in gas cell size or number with time. The dispersion was deemed to have remained stable as long as the gas microcells existed as discrete units. In water the dispersion was observed for 18 hours during which time limited flocculation occurred. The following Figures 3.7 a-s clearly illustrate how the stability of the dispersion is affected by changes in solution concentration or temperature.

Figures 3.7 a & b show a region of the dispersion in water after 5 minutes and 16 hours respectively.

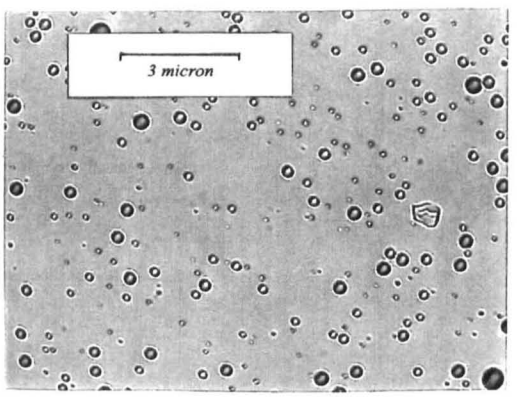

Figure 3.7a

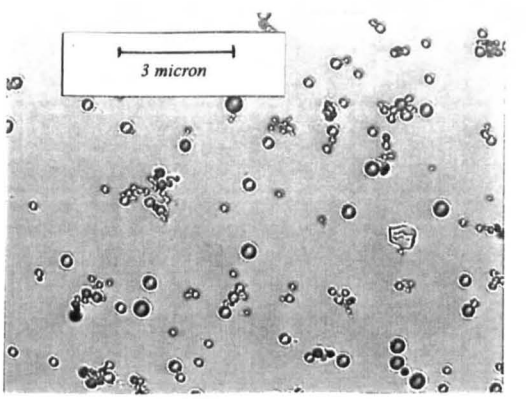

Figure 3.7b

Figures 3.7 c&d illustrate the dispersion of gas microcells in water after 16 hours at progressively lower magnification. Large gas bubbles, approximately 15 micron diameter, were also seen in the sample, (not illustrated).

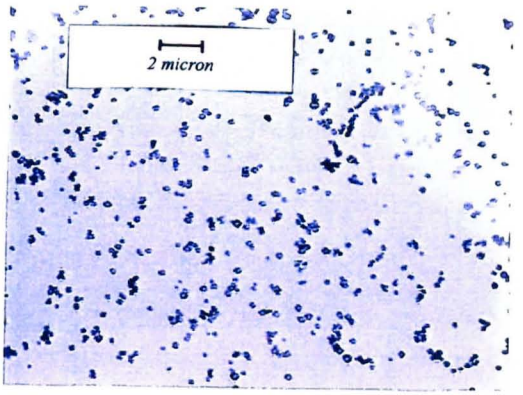

Figure 3.7c

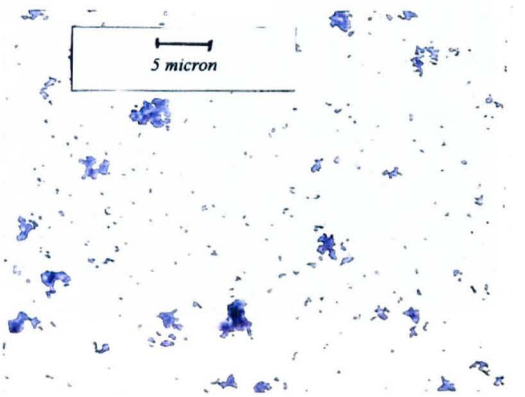

Figure 3.7d

Figures 3.7 e&f illustrate a dispersion of gas microcells in water at 40°C at 5 minutes and 2 hours. It is apparent that after 2 hours at this temperature the cells had flocculated.

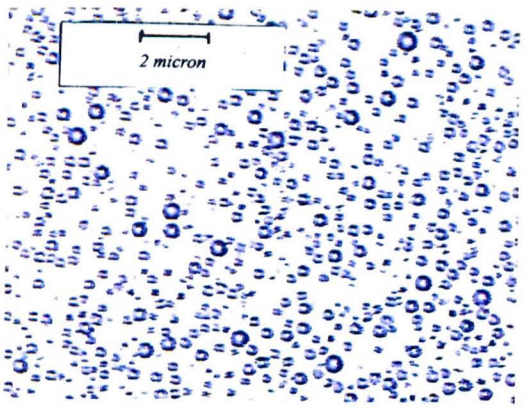

Figure 3.7e

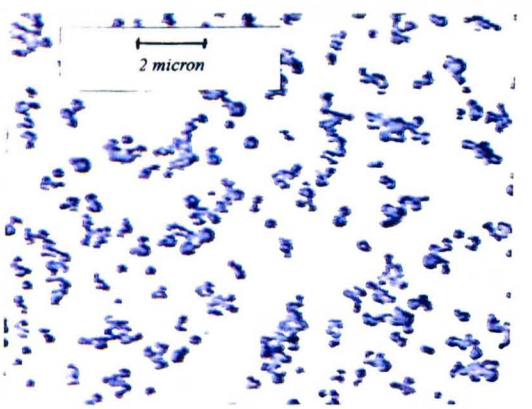

Figure 3.7f

Figures 3.9 g&h illustrate gas microcells dispersed in 10^{-3}mol dm^{-3} KCl, initially and after 15 hours.

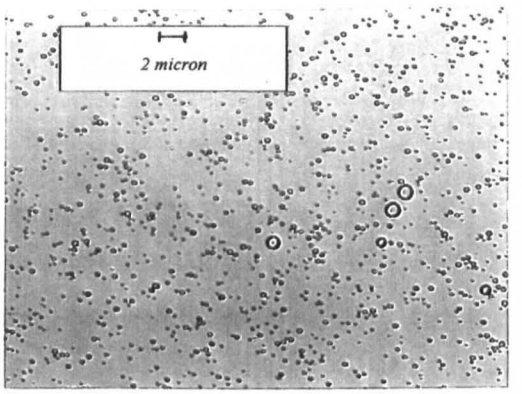

Figure 3.7g

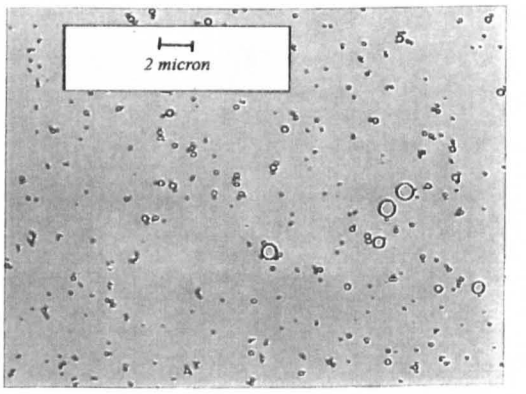

Figure 3.7h

The dispersion of microcells underwent only very limited flocculation in 10^{-3} mol dm^{-3} KCl, with the cells gathering in small groups of only three or four. The following illustrations show the effect of increasing the salt concentration further.

Figures 3.7 i&j illustrate gas microcells dispersed in 10^{-1}mol dm^{-3} KCl initially and after 30 minutes. The gas cells were seen to flocculate within minutes of contact with salt, after which no further change occurred.

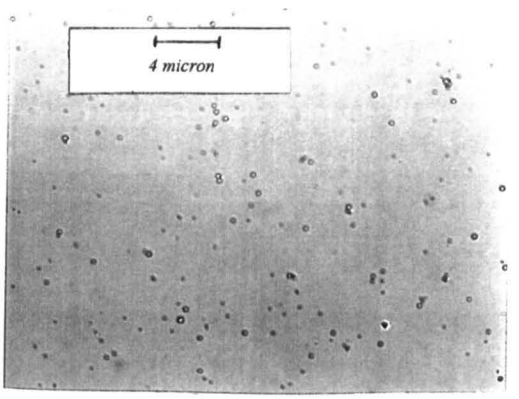

Figure 3.7i

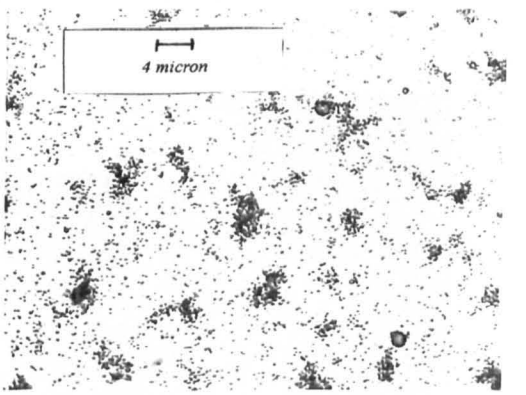

Figure 3.7j

This flocculation of a gas microcell dispersion after 30 minutes in a solution of 10^{-1}mol dm^{-3} KCl, at high magnification, Figure 3.7k.

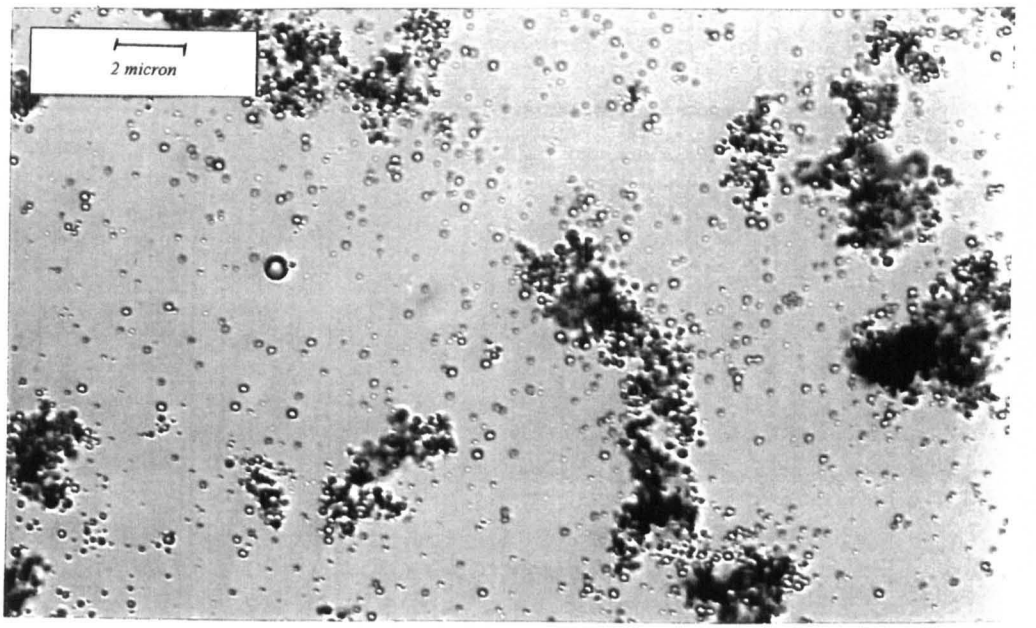

Figure 3.7k

The stability of the following dispersions of gas microcells was monitored by taking photographs at regular intervals of time up to 30 minutes rather than by the use of time-lapse video.

Figures 3.7 l&m illustrate gas microcells, made from 75% Sweetose and 2% sucrose ester S1670, dispersed in a solution of 2%w/w sucrose ester S1670 in water at different magnifications. The microcells had flocculated within 10 minutes.

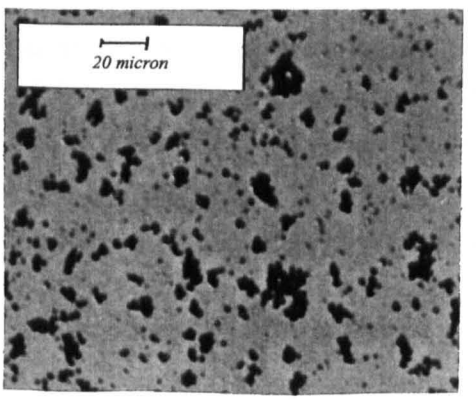

Figure 3.7l

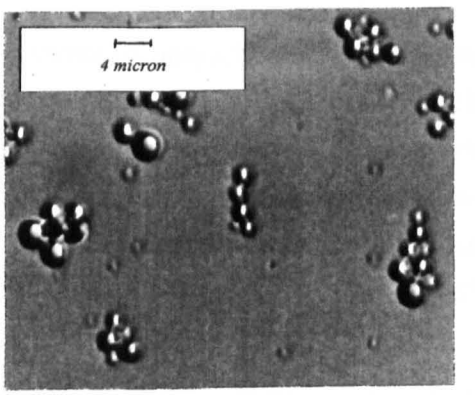

Figure 3.7m

Figures 3.7 n&o illustrate 75/2 gas microcells dispersed in a mixture of 10% w/w Sweetose and 2%w/w sucrose ester S1670 in water , at different magnifications. The gas microcells remained stable during the observation time of 1 hour.

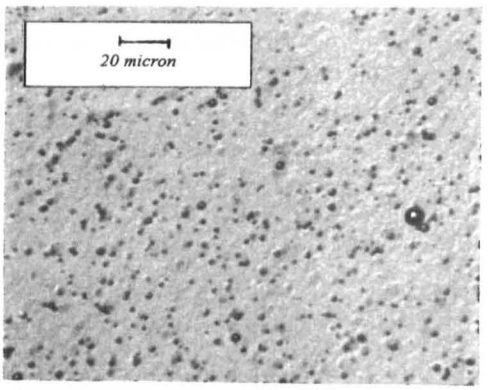

Figure 3.7n

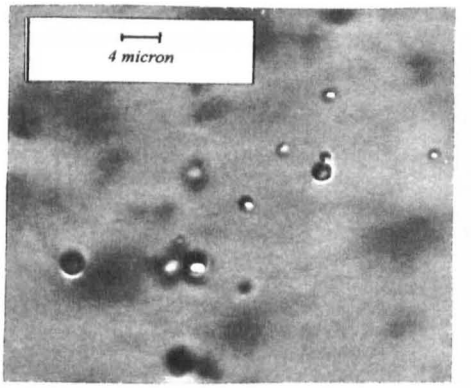

Figure 3.7o

Rapid flocculation was observed between microcells dispersed in a solution of 2%w/w sucrose ester in water but when the micelles were dispersed in a mixture of 10%w/w Sweetose and 2%w/w sucrose ester in water, no flocculation was observed. It was apparent that the presence of a low concentration of Sweetose had a stabilising effect on the dispersed microcells.

When gas microcells were dispersed in dilute aqueous solution they undergo changes that lead to their instability. The observed flocculation in KCl was attributed to the reduction in the extent of the electrostatic repulsive forces at the microcell surface, or colloid flocculation. The instability in water and dilute Sweetose and sucrose ester was attributed to the gradual dissolution of the sucrose ester, from the surface of the gas microcell, into the aqueous phase because of the large concentration gradient.

Gas microcells were also dispersed in viscous mixtures of non-aerated 75%w/w Sweetose and 2%w/w sucrose ester, and 75%w/w Sweetose solution. In both cases no changes were observed in the stability of the gas microcells during 30 minutes observation time. When the microcells were dispersed in viscous liquids no Brownian motion was observed, this was not the case when diluted with mixtures of aqueous viscosity. No change in microcell diameter was observed between either solvent. Dispersion in neat or 75%w/w Sweetose was found to be the most appropriate way to lower the concentration of gas microcells in an aerated foam without noticeably altering their character or behaviour and without adding unnecessary liquid crystalline sucrose ester material to the sample.

Figures 3.7 p&q illustrate gas microcells dispersed in a non-aerated mixture of 75%w/w Sweetose 2%w/w sucrose ester, S1670, (and water). No change was observed during the 30 minutes observation time.

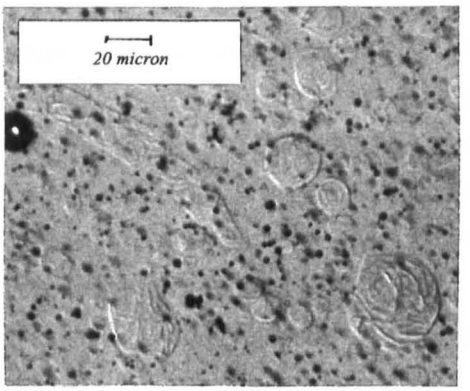

Figure 3.7p

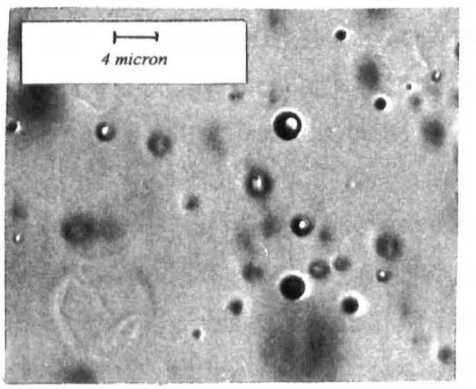

Figure 3.7q

Figures 3.7 r&s illustrate gas microcells dispersed in 75%w/w Sweetose in water at different magnifications. No change was observed during the 30 minutes observation time.

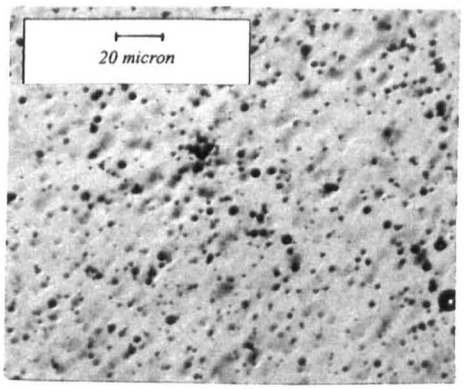

Figure 3.7r

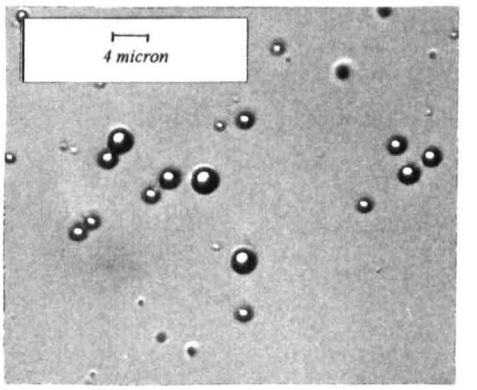

Figure 3.7s

In summary, the gas microcells have been shown to have a finite lifetime, after dilution into aqueous solution, which is dependant upon electrolyte concentration and temperature. On initial dilution a shift in the equilibrium occurred, due to the sudden reduction in viscosity, after which the gas microcells appeared to remain stable. Aqueous dispersions were

examined using time-lapse microscopy, the microcell dispersions were sealed between a microscope slide and coverslip prior to observation; after 15 hours a portion of the microcells had flocculated, however the average diameter appeared to remain constant. Storing an identical dispersion at 40°C caused flocculation to occur more rapidly. The electrolyte concentration was varied between 10^{-3}mol dm^{-3} KCl and 10^{-1}mol dm^{-3} KCl. At 10^{-3}mol dm^{-3} KCl the sample behaved in a similar way to that in water, with limited flocculation occurring slowly. At 10^{-1}mol dm^{-3} KCl the microcells flocculated rapidly, within 5 minutes. 10^{-2}mol dm^{-3} KCl showed intermediate behaviour which was thought to be due to the reduction of the electrical double layer surrounding the microcells..

When gas microcells were dispersed in Sweetose, a more viscous liquid, they were more stable. There appeared to be no difference in stability when the microcells were dispersed in a 75%w/w Sweetose and 2%w/w S1670 mixture or in 75%w/w Sweetose alone. In each case the discrete microcells were clearly resolved by this technique. Microcells dispersed in 2% (aq) S1670 were seen to flocculate within 10 minutes, however dispersions in 10% Sweetose / 2% S1670 were stable for the observation time of 1 hour. Measurements of the change in the optical density of the aqueous dispersions with time reflect a similar pattern of stability to salt and dilute Sweetose concentration, these are described in Chapter 14.

3.8 Reference

[1] Rosevear, F.B.; (1954) J. Am. Oil Chem. Soc., **31**, 628.

CHAPTER 4

X-ray and neutron diffraction

4.0 X-RAY AND NEUTRON DIFFRACTION

4.1 Theory

Optical evidence had indicated the possible presence of a lamellar liquid crystal phase. It was anticipated that such a system should therefore contain bimolecular layers of surfactant species with a well defined spacing. X-ray and neutron diffraction were used to investigate this.

Neutron and electron beams are diffracted by the neutrons or electrons respectively within the atoms in the outer regions of the sample under test. The diffracted wave arises as a result of the interference between the incidental waves after incidence. If the waves start at a common source then their relative phase depends on their path length. When the diffracted waves are in phase then their intensity is enhanced and a peak occurs. The condition for constructive interference is satisfied when the path-length difference is equal to an integral number of wavelengths. Thus if the wavelength of the incident beam and the angle of incidence are known, the position of a peak will correspond to a particular spacing within the sample, as described by the Bragg equation, illustrated schematically below.

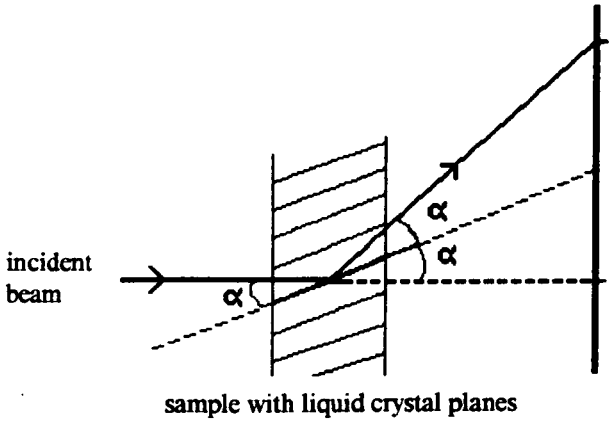

Bragg Equation

$$n\lambda = 2d \sin(\theta/2)$$

where,

n = peak order.

λ = wavelength of the incident beam.

d = repeat distance or layer spacing.

α = incident angle = θ / 2

Figure 4.1a

For small angle scattering the diffraction is described as a function of the scattering vector, Q, where,

$$Q = \frac{4\pi}{\lambda} \cdot \sin(\theta/2)$$

and by substitution into the Bragg equation, the layer spacing, $d = \frac{2\pi}{Q}$.

Thus from the Q value of the peak it is possible to determine the corresponding repeat distance d.

4.2 Results

X-ray diffraction was used to detect any structure contained within a 75% Sweetose 2% sucrose ester, S1670 non-aerated mixture. A 75% Sweetose solution was used as a background and later subtracted. Using X-rays with a wavelength of 1.54Å a diffuse peak was seen to occur at a Q spacing of $0.154 Å^{-1}$ which corresponds to a layer spacing of 40.9Å, Figure 4.2a. The peak was attributed to a crystalline or liquid crystalline phase present within the sample. The intensity of the peak observed was very low and consequently the background appears to be very noisy.

Previous work, had shown that small increases in sucrose ester concentration did not significantly alter the phase behaviour of the mixture. A 75% Sweetose 4% sucrose ester mixture containing deuterated water was prepared for analysis by neutron diffraction. The measurement was carried out by Professor R.H. Ottewill using the small angle scattering diffractometer D22 at the Institute Laue Langevin, Grenoble. Using the detector at a distance of 1.5m and a wavelength of 8Å a single peak was observed at a Q spacing of $0.138 Å^{-1}$, corresponding to a repeat distance of 45.5Å. Figures 4.2 b&c illustrate the diffraction ring observed and the corresponding peak.

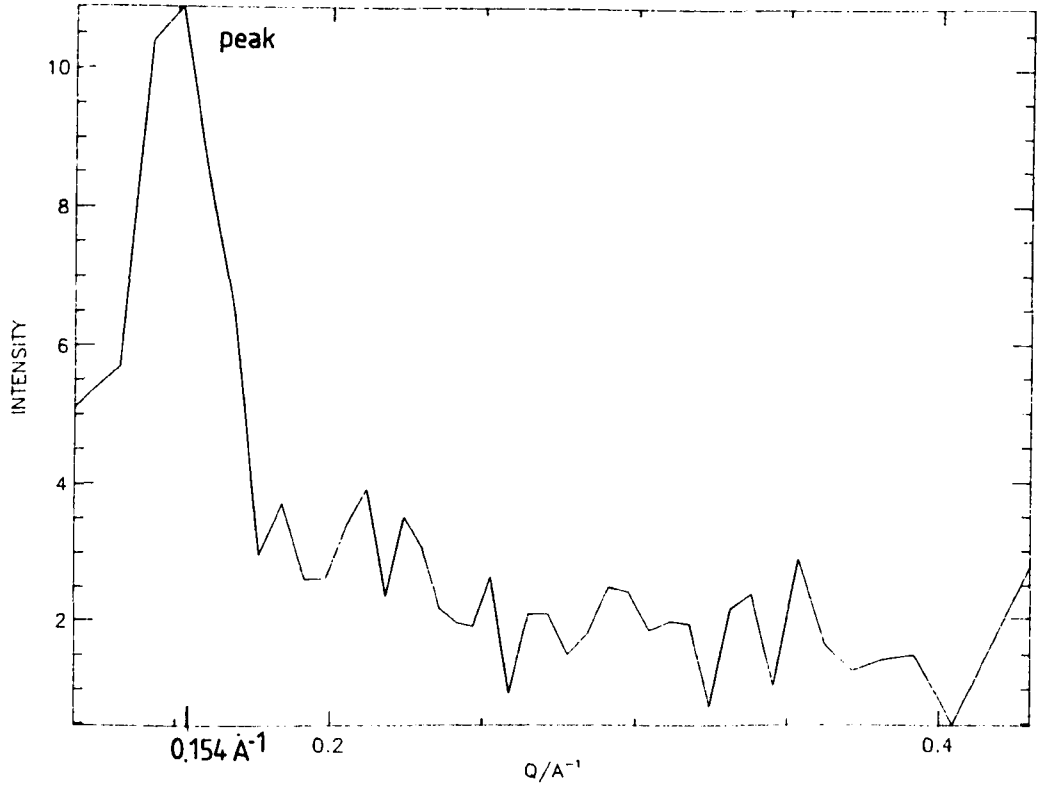

Figure 4.2a

X-ray diffraction spectrum of non-aerated 75% Sweetose 2% sucrose ester, S1670, with a peak at a Q spacing of $0.154 Å^{-1}$.

Figure 4.2b

Neutron diffraction ring corresponding to a peak at Q = 0.138 $\mathring{A}^{-1}$, for a non-aerated sample of 75% Sweetose 4% sucrose ester S1670 containing deuterated water.

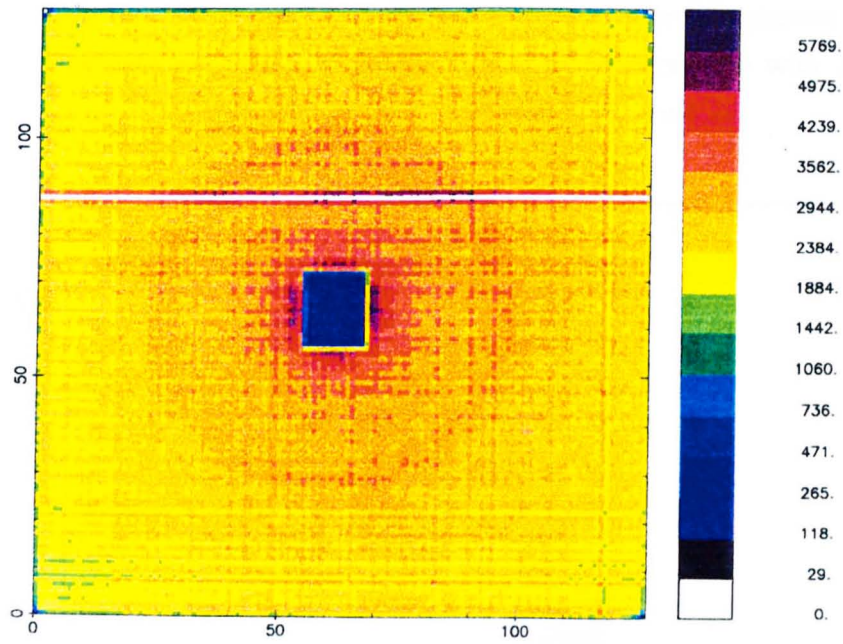

Figure 4.2c

Neutron diffraction spectrum of non-aerated 75% Sweetose 4% sucrose ester S1670 containing deuterated water, with a peak at Q = 0.138 $\mathring{A}^{-1}$.

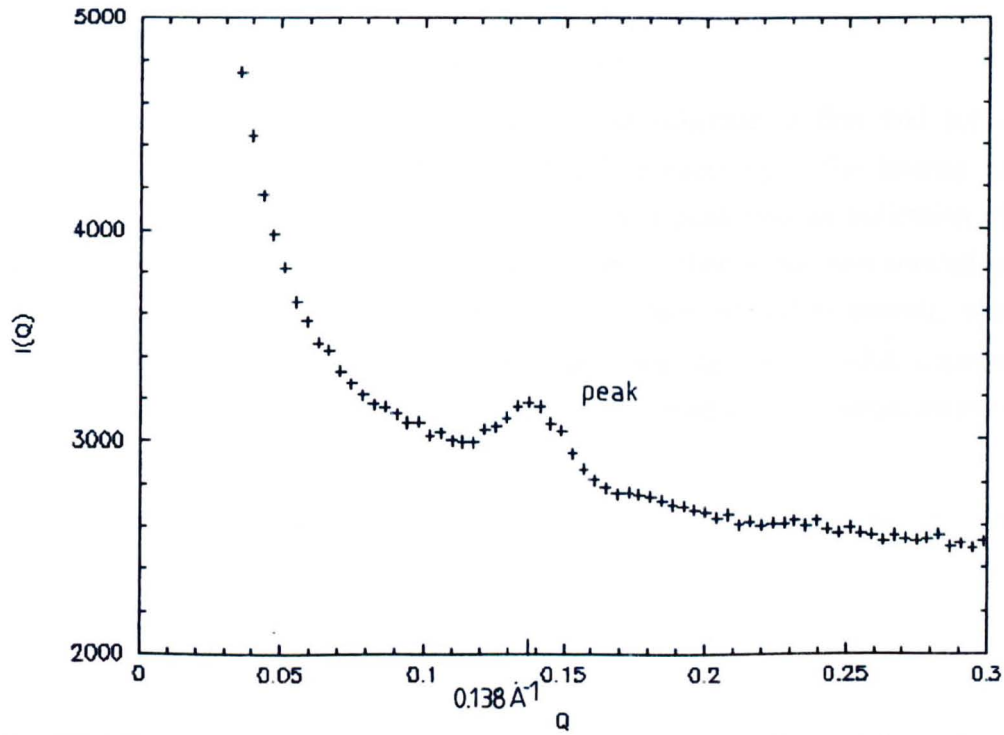

The techniques of X-ray and neutron diffraction on the non-aerated mixture both demonstrated the existence of a structure with an average repeat distance of 43Å despite the apparently low sucrose ester concentration. The diffraction pattern was a ring which indicated a bilayer arrangement of either crystalline or liquid crystalline sucrose ester molecules. In both X-ray and neutron diffraction the intensity of the peak observed was small and the peak was not sharp. A crystalline sample of sucrose behenate was used to compare the diffraction peak from a sample known to be crystalline with that from the non-aerated mixture. The diffraction peak is illustrated in Figure 4.2d.

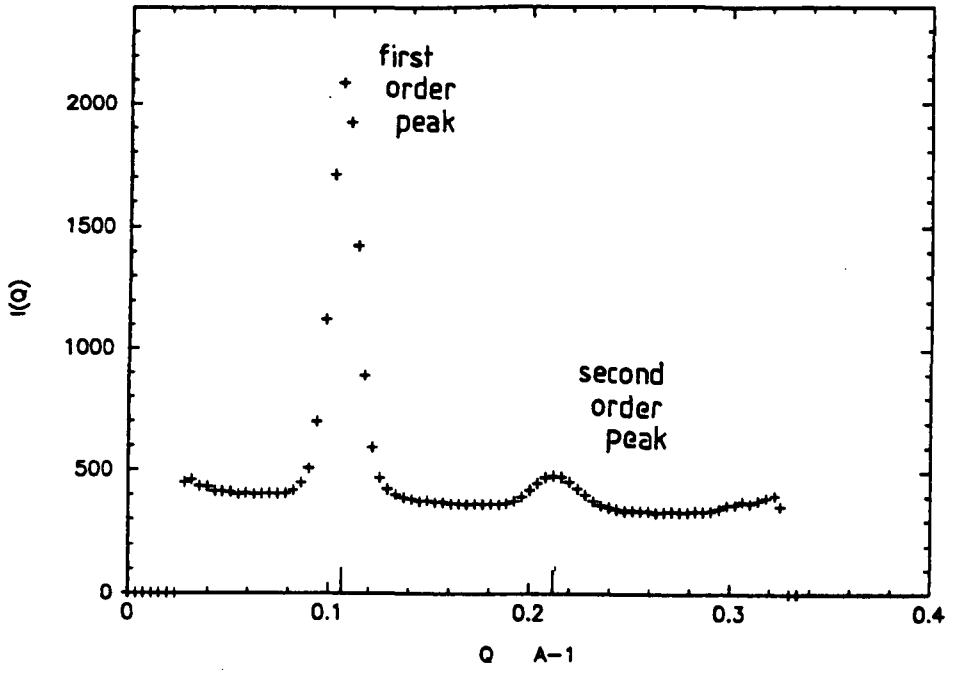

Figure 4.2d

Neutron diffraction spectrum for crystalline sucrose behenate.

Two peaks were observed for crystalline sucrose behenate, a first and second order diffraction at Q spacings of 0.105 and 0.21Å^{-1} respectively. The intense first order diffraction peak together with a smaller second order peak was an indication of a much higher degree of ordering within the crystalline sample than in the non-aerated sample, in which the first order diffraction was the only peak observed and its intensity was 5 times smaller than that of the crystalline sample. The repeat distance of 43Å observed in the non-aerated mixture was thus attributed to the presence of a bilayer arrangement of liquid crystalline sucrose ester.

The conclusion drawn from the X-ray and neutron scattering experiments was that in non-aerated mixtures of 75% Sweetose and 2% sucrose ester S1670, the sucrose ester is present in the form of liquid crystalline bilayers.

CHAPTER 5

Transmission electron microscopy

5.0 TRANSMISSION ELECTRON MICROSCOPY

5.1 Sample Preparation for TEM

A small amount of the sample (approx. 1-2 mm) was placed on a 1cm aluminium disc and nitrogen slushed. The sample was then transferred, under liquid nitrogen, into the Cressington CFE-50 freeze fracture unit where it was fractured at -177°C. A replica was produced using uni-directional 45° tungsten-tantalum and coated with carbon at 90°. Replicas were floated off in distilled water, cleaned overnight in chromic acid and then rinsed in two changes of distilled water. The replicas were then picked up on 400 mesh gold grids and examined in a Jeol 100CXII Transmission Microscope. The replication and imaging work was done by J. Brigham at Unilever Research, Colworth Laboratory.

5.2 Non-aerated 75% Sweetose 2% sucrose ester

The use of replication and shadowing gives 3-dimensional information about the structure of the fracture surface. Figures 5.2a and b illustrate the freeze fracture surface of a non-aerated mixture of 75%w/w Sweetose and 2%w/w sucrose ester. The figures show stratified regions with a layer thickness of approximately 10nm.

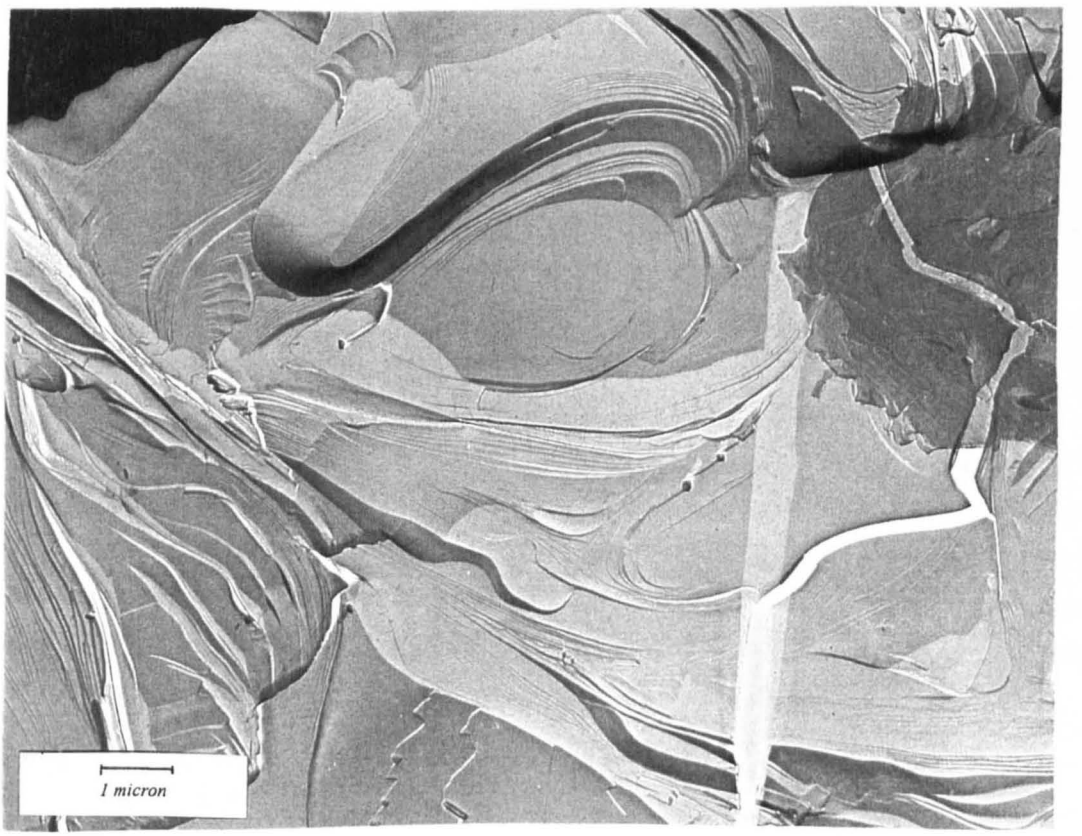

Figure 5.2a

Replica of a non-aerated 75% Sweetose 2% sucrose ester S1670 after freeze fracture

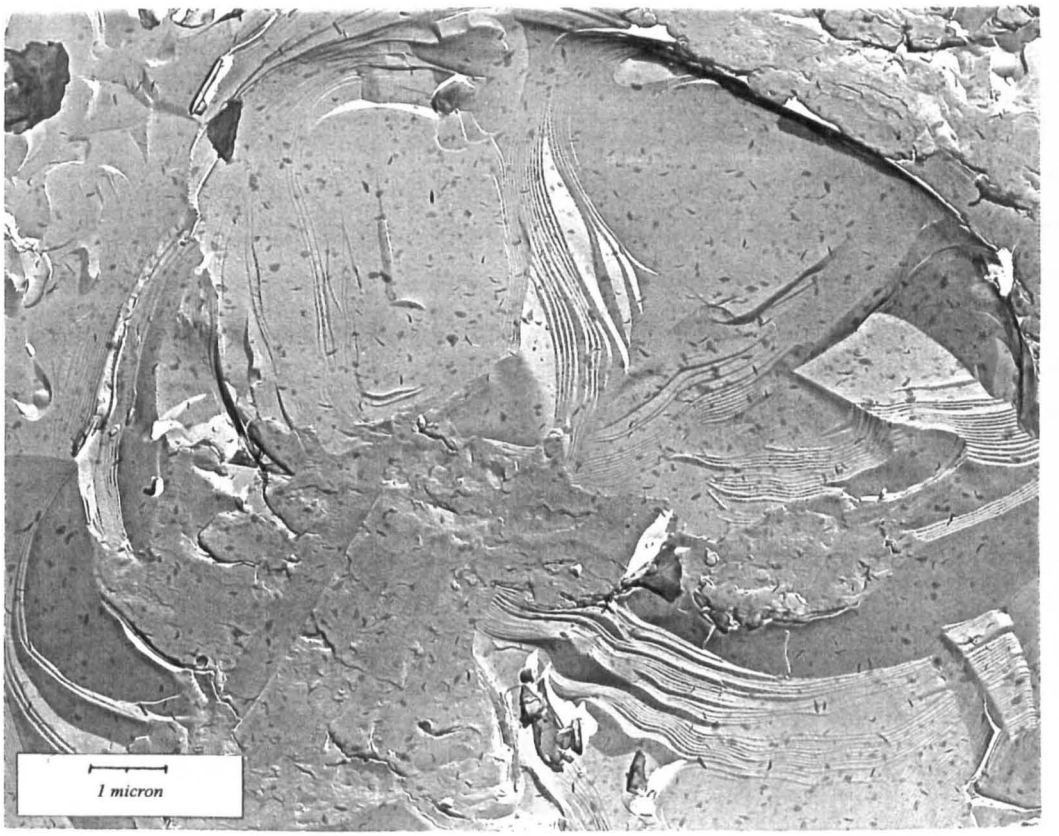

Figure 5.2b

Replica of a non-aerated 75% Sweetose 2% sucrose ester S1670 after freeze fracture.

(The random, dark speckles on this micrograph are an artefact produced during the carbon coating process and are not present in Figure 5.2a.)

In the preparation of non-aerated mixtures, the solutions were stirred for up to 4 hours, to prevent separation of the sucrose ester and Sweetose components. The stirring process dispersed regions of sucrose ester within the Sweetose matrix but complete mixing does not occur and the sample remains two phase, hence the layering is not uniformly spread throughout the sample.

The X-ray and neutron diffraction data shown in Chapter 4 indicate that non-aerated mixtures contain bilayers of liquid crystalline sucrose ester and the anisotropy observed under polarised light supports this. M. Fitzgerald[1] observed that aqueous solutions of S1670 form bilayer aggregates at high concentration. Other workers[2] have observed similar striations after the freeze fracture of a lamellar phase. The appearance of regular striations in a replica of non-aerated 75% Sweetose 2% sucrose ester S1670 is attributed to the formation of bilayers of sucrose ester within a Sweetose matrix.

5.3 Gas Microcells

The use of replication and shadowing gave 3-dimensional information about the gas microcell surface. Gas microcells are hollow and fracturing revealed information about the inner surface in every instant, Figure 5.3a. Shadowing these hollows from a low angle gave greater depth to the surface, unfortunately it was not possible to measure the diameter of the gas cell without complex calculations unless it was fractured at its equator. The extent of shadowing across each gas cell gives some indication of the latitude of the section. The majority of gas microcells in each sample display the domain structures as described, however, there are anomalies in almost every case. Each sample has been discussed on its own merit and the structure formed by the majority of gas cells has been taken to be representative. This is based on direct observation on many replicas, although in most cases only one photograph of each is shown in this report.

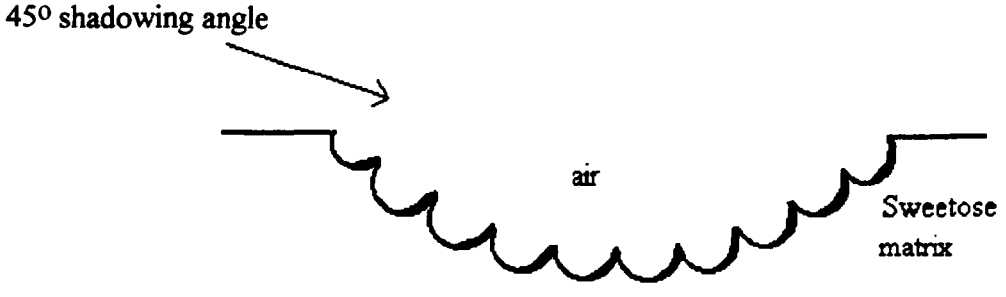

Figure 5.3a

Cross-section through a gas microcell surface

A range of samples was prepared for examination, covering variables such as Sweetose concentration, and sucrose ester type and concentration. Single investigations, including the foam after drainage, overnight storage of the non-aerated mixture, gas microcells after centrifuging and small volume sample preparation are also illustrated.

5.4 A standard dispersion of gas microcells - 75% Sweetose 2% S1670 sucrose ester

Figure 5.4a illustrates an aerated sample of 75%w/w Sweetose 2%w/w sucrose ester S1670, containing a number of gas microcells between approximately 2 and 20 μm diameter. Figure 5.4b illustrates the surface of a single gas microcell at higher magnification. At this magnification regularly packed hexagonal and pentagonal domains approximately 50 to 100nm across are visible. The direction of shadow across each of these domains matches that across each gas microcell as a whole. This indicates that the domains protrude from the surface of each cell and into the matrix.

Figure 5.4a

Replica of gas microcells within a 75% Sweetose 2% sucrose ester S1670 foam

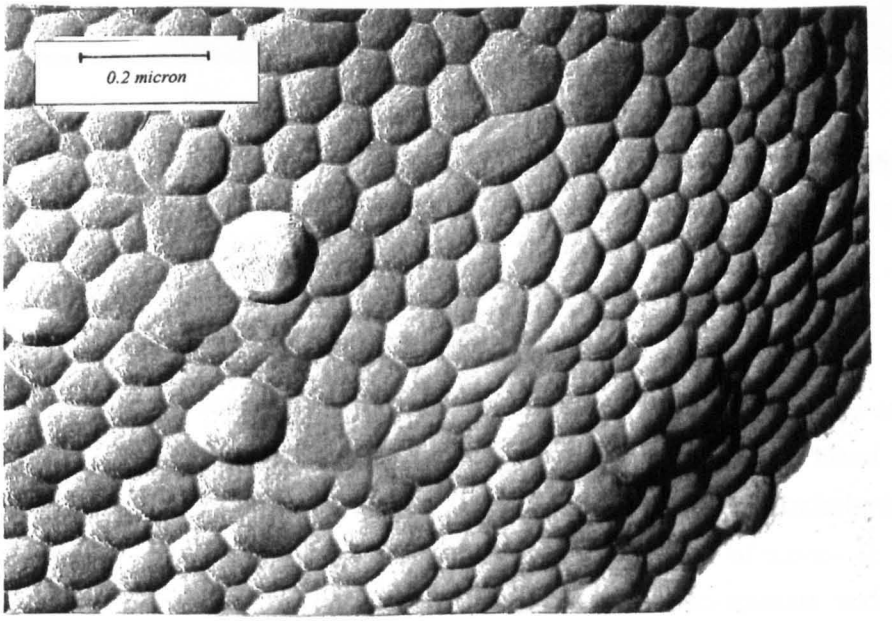

Figure 5.4b

Inner surface of a gas microcell, showing hexagonal and pentagonal domains, between 50 and 100 nm across, protruding from the surface.

Figure 5.4c is a freeze fracture through a gas microcell from a 75%w/w Sweetose 2%w/w sucrose ester S1670 foam. The edge of the cell is cleanly fractured and shows clearly the domains protruding into the matrix. It also illustrates that there are no layers or other structures extending from the microcell surface, which would indicate multilayers of sucrose ester at the microcell surface. Figure 5.4d is a section of the surface of a very large gas microcell from a 30%w/w Sweetose 2%w/w sucrose ester S1670 foam. The surface appears planar because of the large microcell diameter. The figure illustrates the highly regular packing between adjacent hexagonal and pentagonal domains on the microcell surface.

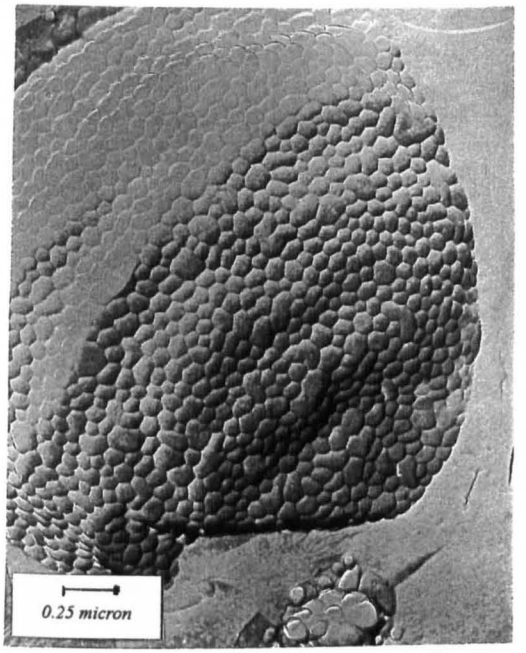

Figure 5.4c
Gas microcell with domains protruding from its surface and a sharp edge, with no indication of multilayers.

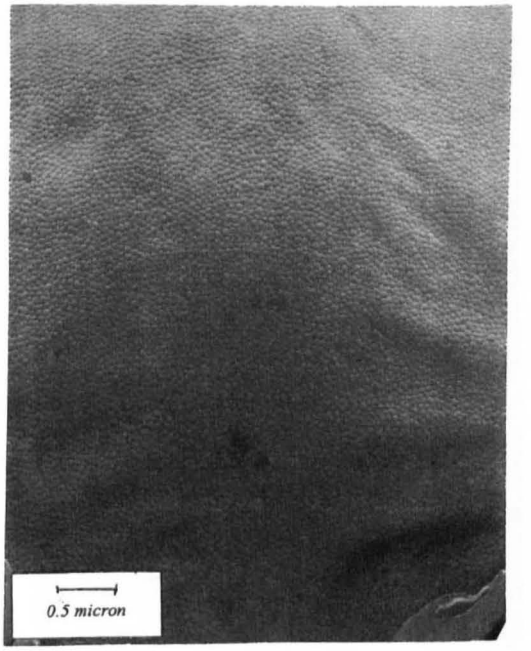

Figure 5.4d
Large gas microcell with highly regular hexagonal and pentagonal surface domain structure.

5.5 Ratio of mono- to di- stearate within the sucrose ester

Gas microcells have been produced by aerating 75%w/w Sweetose and 2%w/w sucrose ester. The sucrose ester surfactants used in this study are a blend of mono-, di- and higher- esters. The exact composition of the commercial surfactants used is given in Chapter 2. In order to investigate the effect of the ratio of mono- to di- ester contained within the sucrose ester, pure samples of sucrose mono-stearate and sucrose di-stearate were combined at ratios of 100:0, 90:10 and 70:30.

A slightly modified method of preparation was used for these samples due to the limited availability of pure sucrose mono- and di- ester. For comparison, an aerated sample of S1670 (containing 77% mono-, 20% di- and 3% tri- ester) was also produced by this method.

Figure 5.5a illustrates the S1670 gas microcells, all with structured domains, of approximate diameter 50nm, the microcells were less numerous and less spherical than those from a standard preparation, probably due to incomplete aeration and mechanical damage. Stratified regions are visible within the matrix, which resemble those seen in a non aerated mixture (Figure 5.2a), this is further evidence of incomplete aeration.

Figure 5.5a
Gas microcells prepared with S1670,
77% mono-, 20% di-, 3% tri- ester

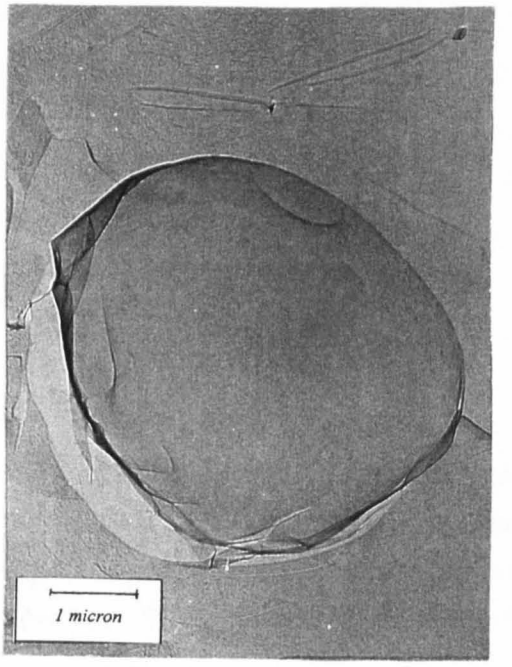

Figure 5.5b
Gas microcells prepared with
100% sucrose mono-stearate

The gas microcells containing only 100% mono-stearate, Figure 5.5b, were not observed to contain structured domains at their surface. Those with 90% mono-stearate and 10% di-stearate displayed a very regular hexagonal and pentagonal surface structure, with domains measuring approximately 100nm in diameter, Figure 5.5c. Gas microcells with 70% mono- and 30% di- stearate also displayed regular hexagonal and pentagonal domains whose diameter was approximately 50nm, Figure 5.5d. The precise geometry of the domains is thought to be controlled by the blend of the sucrose ester used and the reason for the formation of larger domains in the case of 90% mono- 10% di- ester will be discussed later.

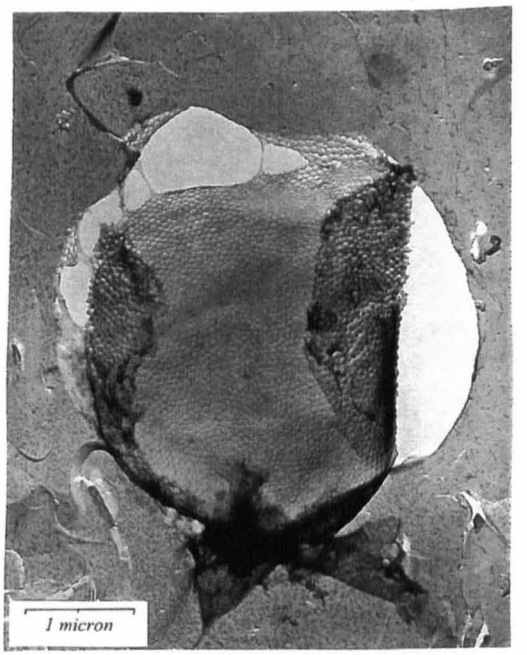

Figure 5.5c
Gas microcells prepared with
70% mono- 30% di-stearate

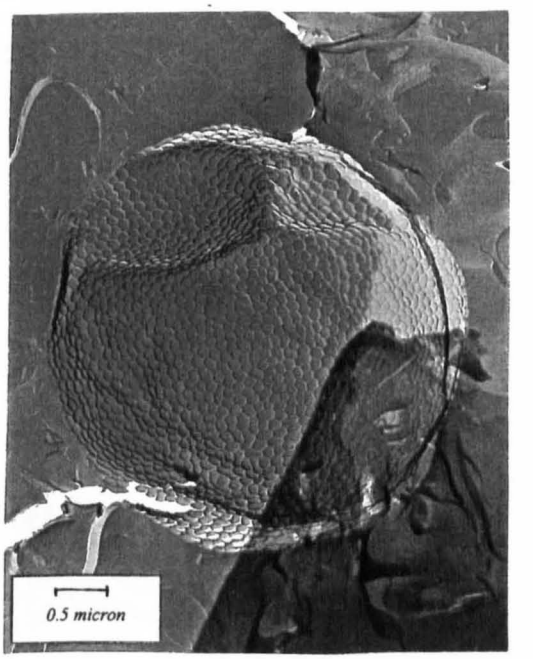

Figure 5.5d
Gas microcells prepared with
90% mono- 10% di- stearate

5.6 Commercial sucrose esters, S1570, S1170, S770 and S270

Gas microcells were produced by the standard method using the commercial sucrose esters S1570, S1170, S770 and S270. These are commercial mixed sucrose stearate surfactants in which the ratio of mono- to poly- esters contained decreases with the sample number. i.e. S1570 contains 70% mono-, 25% di- and 5% tri- stearate whereas S270 contains 11% mono-, 14% di-, 65% tri-/poly- esters and 10% unknowns, thus the lower the sample number the more hydrophobic its character. These analyses were carried out by D. Mayes at Unilever Research[3] using gel-permeation chromatography. Further details are given in Chapter 2.

Figures 5.6 a-d illustrate the surface structuring of the resulting gas microcells. As the hydrophobic proportion of the mixture increases the domains become less regular and their surface curvature decreases, until in S270 no surface domains were observed. Figures 5.6 e-h illustrate the same samples at lower magnification. From these it is possible to make qualitative statements about the number of cells per unit area, or total gas phase volume. S1570 and S1170 appear to have a lower gas phase volume than S770 but greater than S270. The average diameter per cross section appears to be smaller in S770 than the rest. An investigation of gas phase volume during aeration was made, the results are described later, Chapter 11.

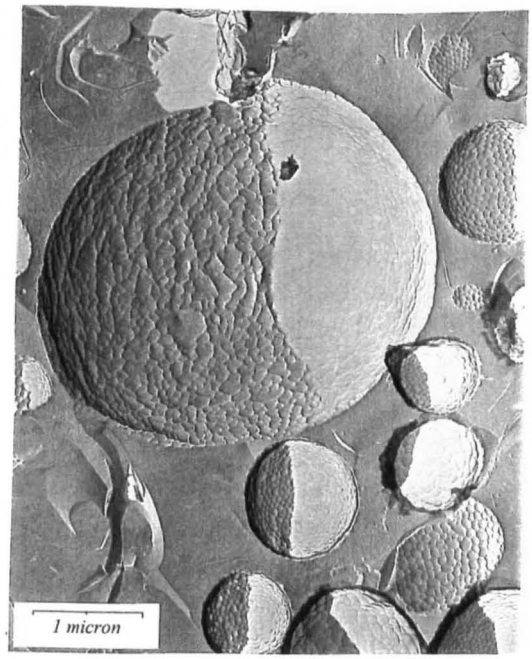

Figure 5.6a

Gas microcells prepared with S1570

70% mono-, 25% di-, 5% tri-

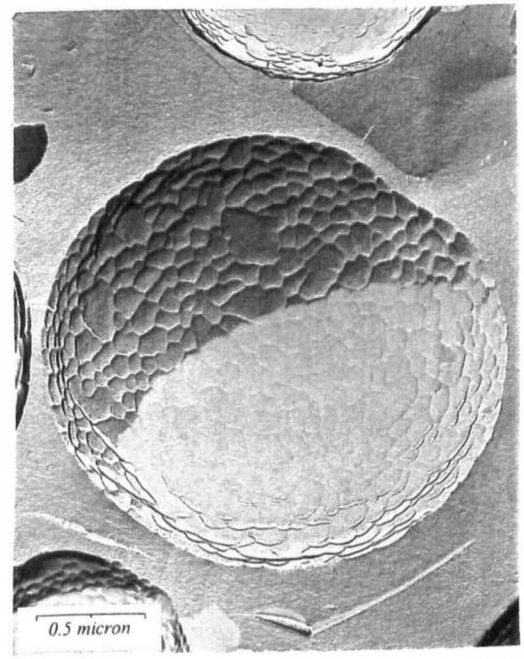

Figure 5.6b

Gas microcells prepared with S1170

52% mono-, 36% di-, 12% tri-

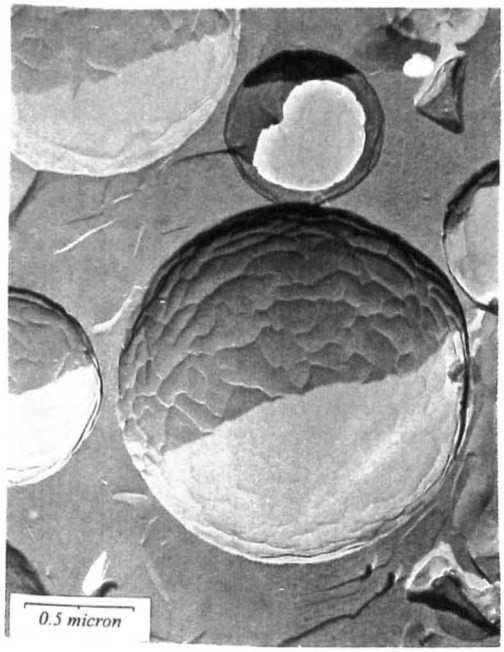

Figure 5.6c

Gas microcells prepared with S770

29% mono-, 40% di-, 31% tri-/higher-

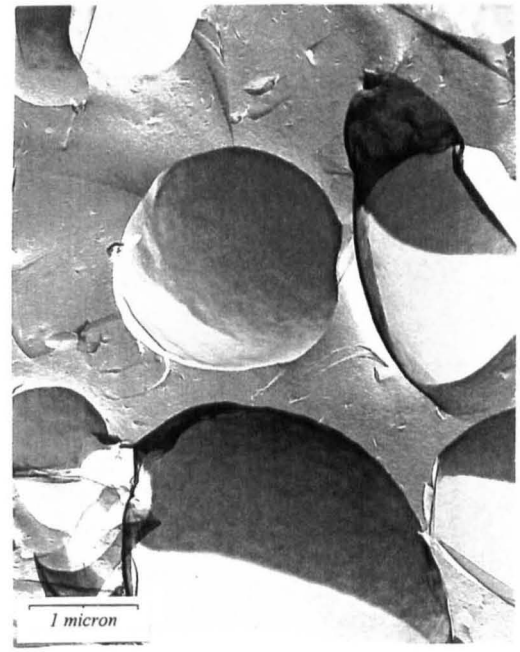

Figure 5.6d

Gas microcells prepared with S270

11% mono-, 14% di-, 65% tri-/higher-

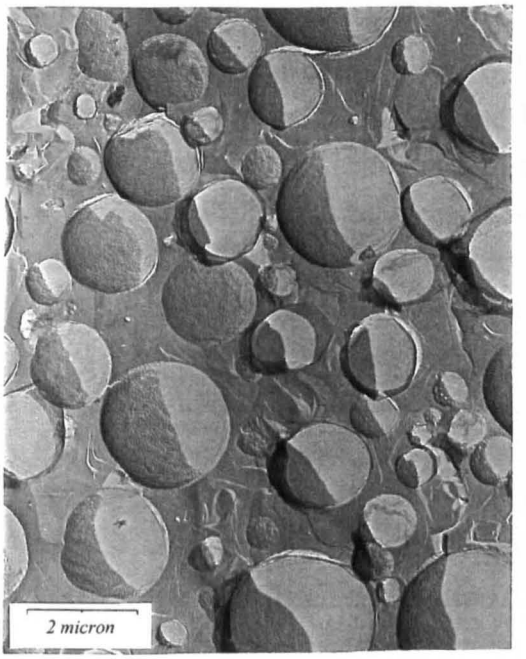

Figure 5.6e

Gas microcells prepared with S1570

70% mono-, 25% di-, 5% tri-

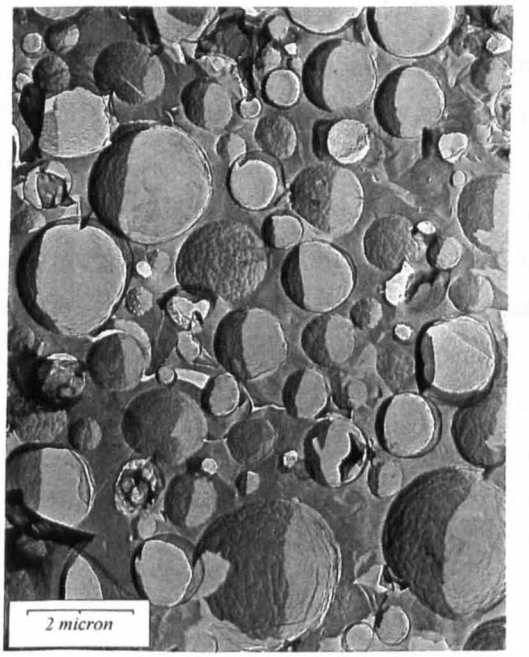

Figure 5.6f

Gas microcells prepared with S1170

52% mono-, 36% di-, 12% tri-

Figure 5.6g

Gas microcells prepared with S770

29% mono-, 40% di-, 31% tri-/higher-

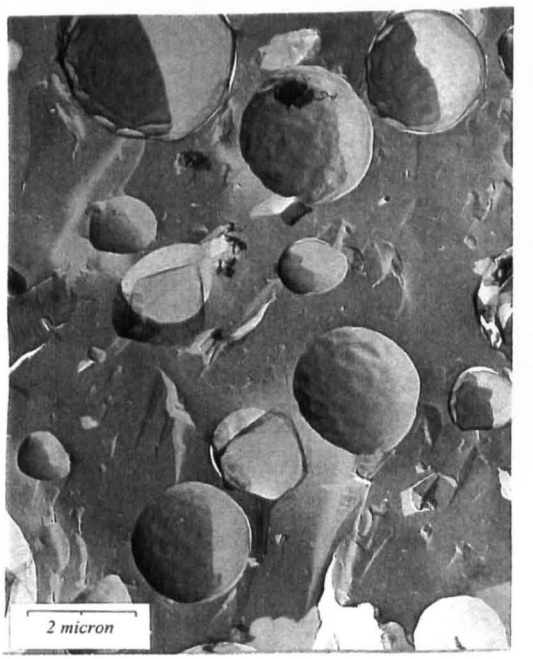

Figure 5.6h

Gas microcells prepared with S270

11% mono-, 14% di-, 65% tri-/higher-

5.7 Altering the alkyl chain length

Gas microcells containing 75%w/w Sweetose and 2%w/w sucrose ester were prepared using the sucrose esters B1570 and P1570. B1570 is sucrose behenate, C_{22}, P1570 is sucrose palmitate, C_{16}, both contain approximately the same ratio of mono- to di- to tri-ester, being 66:27:7. Both samples were observed to form stable foams, B1570 less so than P1570. The gas microcells from these preparations are illustrated in Figures 5.7 a & b, those in P1570 resemble very closely those of S1670 but those of B1570 appear more fluid. It was expected that the longer alkyl chains in the B1570 gas microcells would produce a more rigid surface because according to Tanford[4] the chain melting temperature for long chain hydrocarbons increases with chain length. The head group of the amphiphile has an effect on the chain melting transition, however in this case both have a sucrose head group so any differences are likely to be due to chain length. This was discussed in more detail in Chapter 1.

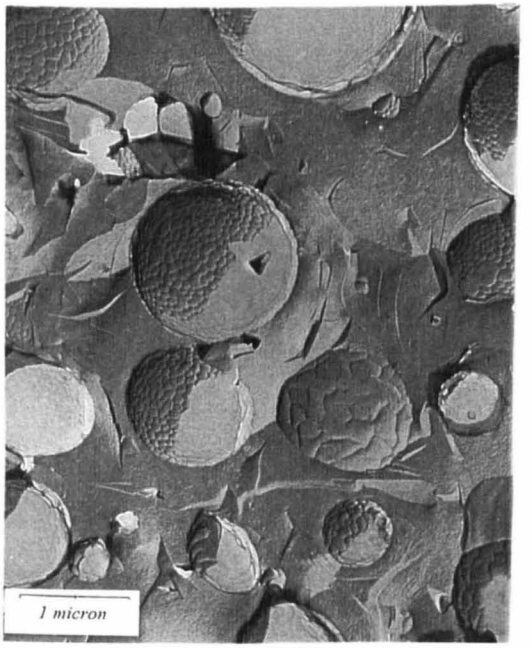

Figure 5.7a
Gas microcells prepared with P1570, sucrose palmitate, C_{16}

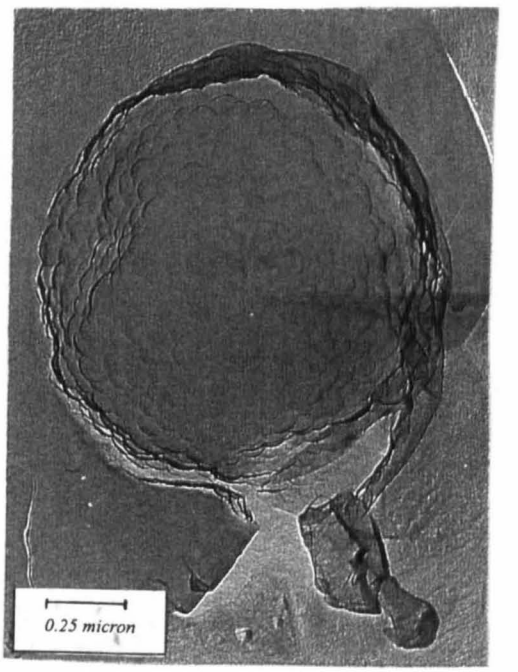

Figure 5.7b
Gas microcells prepared with B1570, sucrose behenate, C_{22}

Mixtures of 75% Sweetose with 2% sucrose caprylate C_8, caprate C_{10} and laurate C_{12}, were prepared. The phase behaviour of these sucrose esters in 75% Sweetose was not studied however it was noted that they appeared isotropic when viewed with polarised light. This was attributed to the presence of a dilute micellar phase. In the absence of a

liquid crystalline phase the formation of gas microcells was not expected and this was verified by experimentation.

5.8 2% sucrose ester S1670, minimum Sweetose

In Chapter 11, the phase volume of air incorporated during whipping is discussed. The minimum Sweetose concentration which would successfully aerate to form a foam was found to be 30%w/w. The resulting foam was observed to contain a portion of gas cells visible with the naked eye and to have a low viscosity relative to a standard prep containing 75%w/w Sweetose, the foam was also observed to undergo partial drainage over 48 hours. Figure 5.8a illustrates a gas microcell from a 30% Sweetose 2% sucrose ester S1670 foam. Structured domains are visible on the surface of the cell, which is large and has been sectioned very close to its base, hence its planar appearance. Direct observation of many replicas indicated that the gas cells had structured surfaces, however the average gas cell diameter was large when compared with a 75% Sweetose 2% S1670 foam.

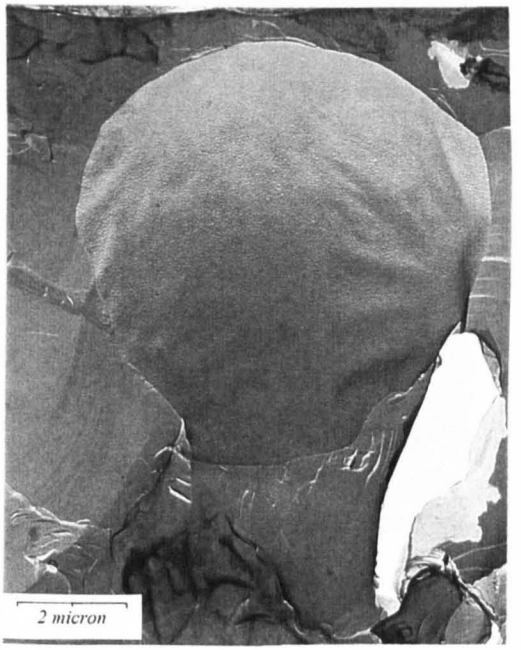

Figure 5.8a

Gas microcells prepared with 30% Sweetose 2% sucrose ester S1670

A low Sweetose concentration was thought to cause three major effects; firstly, an increase in the water concentration, reducing the extent of the phase separation of the sucrose ester and thus the amount of lamellar phase available to coat the microcell surface. Gas bubbles which were not coated with sucrose ester were not expected to remain stable. Secondly, a low matrix viscosity which was less efficient in comminuting the gas cells

during preparation and finally this low viscosity also allowed the larger cells to cream to the surface.

5.9 75% Sweetose minimum sucrose ester S1670

Measurements of the gas phase volume during aeration, to be discussed in Chapter 11, determined the minimum concentration of sucrose ester S1670 required for aeration, in 75% Sweetose, to be 0.2%w/w. Gas microcells were prepared from mixtures of 75% Sweetose and 0.2 and 0.3%w/w sucrose ester S1670, Figures 5.9 a & b, in both cases the gas microcells have structured surfaces.

Direct observation of a number of replicas indicated that, whilst the gas cells possessed structured domains, the average gas cell diameter was larger than that observed with a standard preparation and the number per unit volume was low.

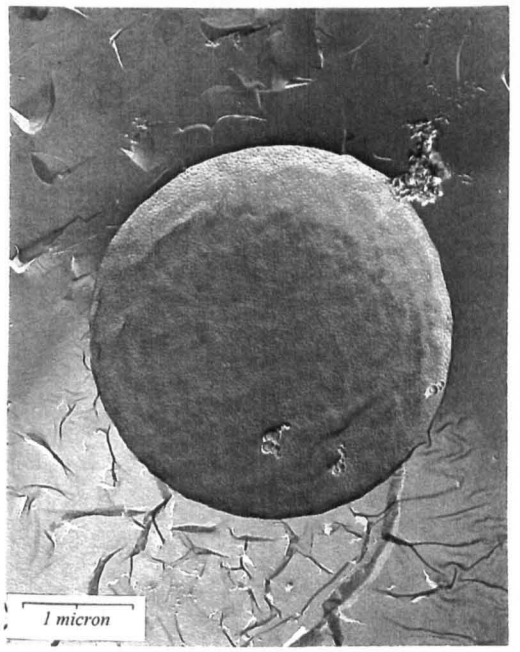

Figure 5.9a
Gas microcells prepared with
75% Sweetose 0.2% sucrose ester S1670

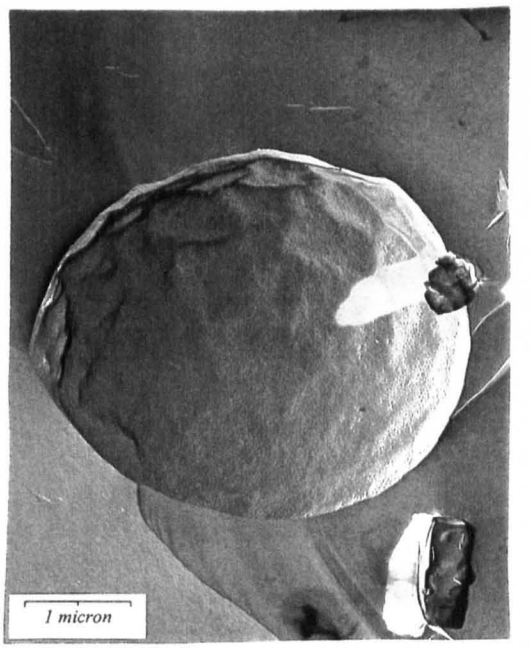

Figure 5.9b
Gas microcells prepared with
75% Sweetose 0.3% sucrose ester S1670

The large size and small number of gas cells was due to the low sucrose ester concentration, limiting the amount of lamellar phase which is available to coat the gas microcell surface. The observation that gas microcells with a domained surface structure were formed at sucrose ester concentrations as low as 0.2%w/w in 75%w/w Sweetose was in agreement with the measurements of gas phase volume at low sucrose ester concentration, discussed in Chapter 11.

5.10 Gas microcells prepared from a cold non-aerated mixture

In the standard preparation of gas microcells, the mixture is prepared hot and allowed to cool to room temperature during aeration. A non-aerated mixture of 75%w/w Sweetose 2%w/w sucrose ester S1670 was prepared by the standard procedure and stored at 5°C for 24 hours. This mixture was then warmed slowly to room temperature and aerated for two hours in the usual manner. Figure 5.10a illustrates the gas microcells prepared by this route. The gas microcells were observed to possess structured domains however their surfaces were wrinkled and less spherical than before.

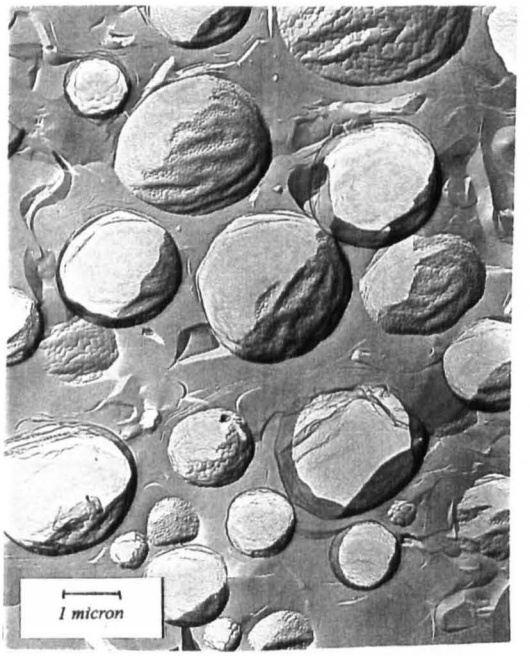

Figure 5.10a

Gas microcells prepared with 75% Sweetose 2% sucrose ester S1670 cold, non-aerated mixture

The undulating surface was thought to be due to the increased rigidity of the surface because the hydrocarbon chains of the sucrose ester were below their chain melting temperature. In a standard preparation the mixture is heated, melting the chains and making the surface more fluid. The mixture is aerated before the chains have had time to cool and condense thus the surface of the bubbles are spherical. The cold non-aerated sample was stored at 4°C overnight, during which time the chains can order themselves and form a more rigid bilayer. When this more rigid structure was aerated the layers did not form a perfectly spherical surface.

5.11 Aerating for 6 minutes at 750 rpm

During a standard preparation, aerating at 324 rpm, the phase volume of gas was found to peak at 80% after 40 minutes. When the same mixture was aerated at 750 rpm the gas phase volume reached 80% after only 6 minutes, these results are discussed further in Chapter 11. Figure 5.11a illustrates the gas microcells after 6 minutes aeration at 750 rpm. Whereas the standard gas microcells were spheres with a structured surface, the gas microcells produced by more vigorous aeration were not smooth, their surface undulated periodically, in addition to having structured domains, this was thought to be due to mechanical damage.

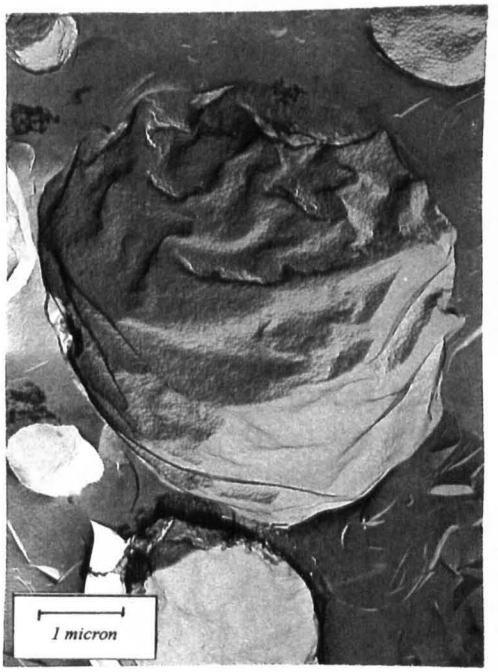

Figure 5.11a
Gas microcells after aeration at
750 rpm for 6 minutes.

5.12 Centrifuging gas microcells at 18,000 rpm for 60 minutes

75%w/w Sweetose 2%w/w S1670 gas microcells were centrifuged for 1 hour at 18,000 rpm to concentrate the gas microcells at the surface of their viscous matrix. Care was taken not to over-centrifuge the samples as this tended to drive the gas cells through the surface of the matrix, resulting in a fine white solid 'ghost' structure with interlinking cells, resembling a sponge-like mould, illustrated later in Chapter 7.

Figures 5.12a-c, illustrate the resultant closely packed gas microcells at a range of magnifications. The gas cells were deformed by this packing but none were observed to

aggregate, all retained their surface structuring. Figures 5.12b and c illustrate the region between two closely packed gas microcells at high magnification, proving that no aggregation occurred. The closest distance of approach between the surface of the two microcells in Figure 5.12c is approximately 10nm.

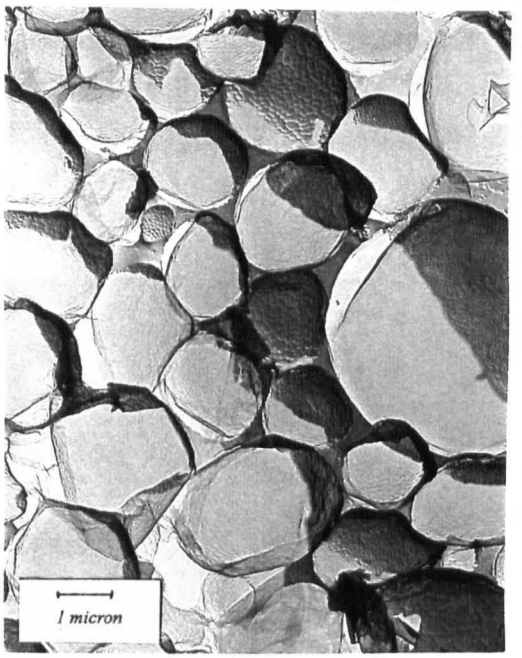

Figure 5.12a

Gas microcells after centrifuging

at 18,000 rpm for 60 minutes.

Figure 5.12b

Gas microcells after centrifuging

at 18,000 rpm for 60 minutes.

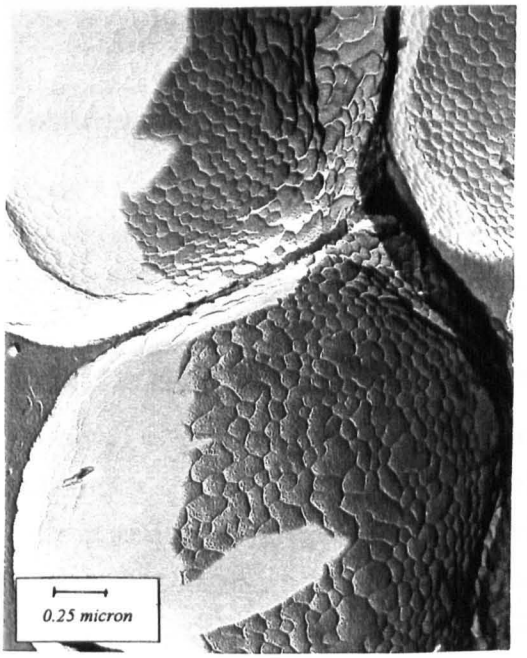

Figure 5.12c

Gas microcells after centrifuging

at 18,000 rpm for 60 minutes.

5.13 Partial drainage at room temperature

When a standard gas microcell preparation was allowed to stand at 25°C for 6 months, partial drainage occurred. A sample of the remaining foam layer was removed for analysis. The layer consisted of white particulate matter in a clear viscous liquid. Figures 5.13 a & b illustrate a sample of this viscous liquid containing fractions of particulate matter which resemble small aggregates by TEM. When the Sweetose matrix surrounding the gas cell drains it was thought that the gas cell surface begins to desiccate, the head groups crystallise and these structures are the remains of the sucrose ester layer surrounding each microcell.

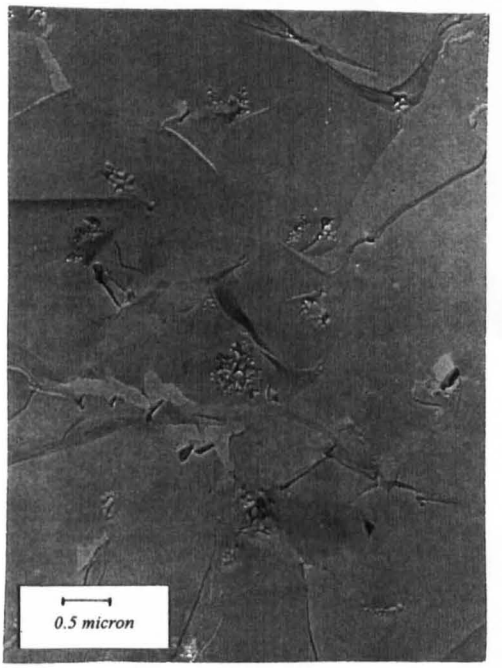

Figure 5.13a
Remains of gas microcell foam layer,
after draining for 6 months at room temperature.

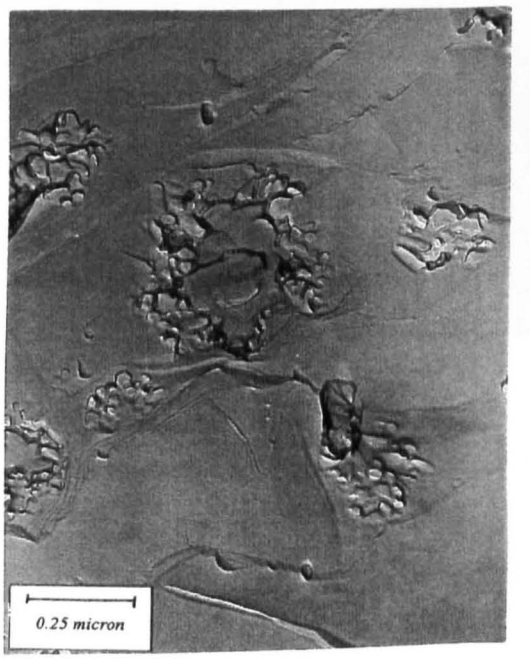

Figure 5.13b
Remains of gas microcell foam layer after draining.
High magnification.

5.14 Large gas bubbles in a gas microcell foam

Observation of all samples of gas microcells at low magnification revealed that, where structuring occurred on the gas microcells, the very large gas bubbles in the sample had smooth surfaces. Examples of this behaviour are shown in Figures 5.14 a, b & c.
During aeration and for a short time thereafter a limited amount of disproportionation[5] takes place until the system reaches equilibrium. Disproportionation is a process by which the small gas cells shrink in favour of the large gas cells due to the Laplace pressure difference inside them. In a foam sample the gas microcells constitute the small diameter bubbles and the lamellar phase sucrose ester on their surface is compressed causing it to buckle, forming the characteristic surface structure. When the sucrose ester layer can no

longer be compressed a limiting diameter is reached and disproportionation ceases. During this process the large cells expand, the lamellar phase sucrose ester at their surface is not compressed and they appear to have smooth surfaces when viewed by TEM.

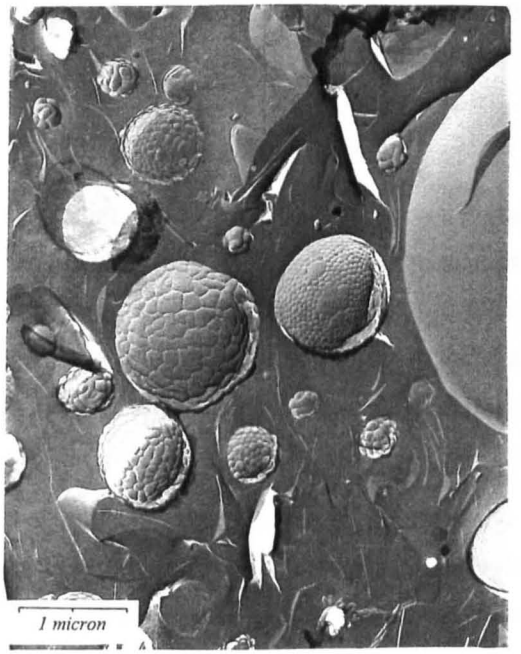

Figure 5.14a

Large gas bubbles with no surface structure,
75% Sweetose 2% sucrose ester P1570.

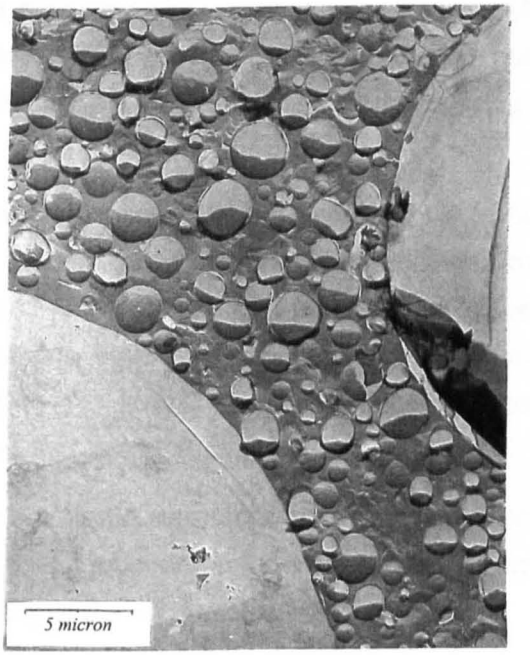

Figure 5.14b

Large gas bubble with no surface structure,
75% Sweetose 2% sucrose ester S1570.

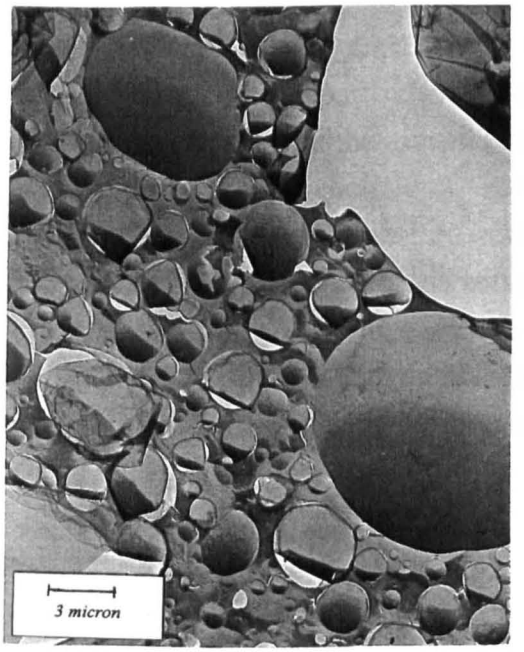

Figure 5.14c

Large gas bubbles with no surface structure,
75% Sweetose 2% sucrose ester S1670.

TEM on non-aerated mixtures confirmed the existence of sucrose ester in liquid crystalline form and gave strong indication that it was arranged in bilayers. Fracturing gas microcells revealed information about the topography of their inner surface. The structure was seen to vary between regular geodesic domes and a near smooth surface, depending upon the ratio of mono- to di- ester within the sucrose ester, i.e. gas cells prepared using pure sucrose monostearate appeared to have smooth surfaces whereas those prepared using a blend had structured surfaces.

Gas microcells produced using a minimum Sweetose concentration were very large but they possessed a regularly structured surface. The number of observed gas cells was low compared to a standard preparation which uses 75% Sweetose. Gas microcells produced with a minimum of sucrose ester were also found to have structured surfaces and a low number concentration. Both were attributed to the limited supply of lamellar phase sucrose ester available to coat the gas microcells.

If the gas microcells are surrounded by a layer of liquid crystalline sucrose ester as the results suggest, then the addition of cholesterol to the mixture ought to change the surface structure observed, by disrupting the close packing of the alkyl chains.

5.15 The addition of cholesterol

Cholesterol is known to affect the properties of membranes by arranging itself at the interface and disrupting the packing of the alkyl chains.

Joint work, with M. Fitzgerald, on the effect of cholesterol on the domain structure of these gas microcells is reported here. Samples of 75% Sweetose 2% S1670 were prepared in the standard way with the exception that the 2%w/w sucrose ester was made up with different proportions of cholesterol. Ratios of 5%, 15% and 30% cholesterol were used. The resultant foams were examined in the usual way. Figures 5.15 a-c illustrate the gas microcell surface structure. It can be seen that at 5% cholesterol, the gas microcells no longer possess their distinctive surface structure however they do have some visible surface texture. At 15% the gas cells have smooth surfaces, at 30% the surface is once again textured however no regular structure was observed.

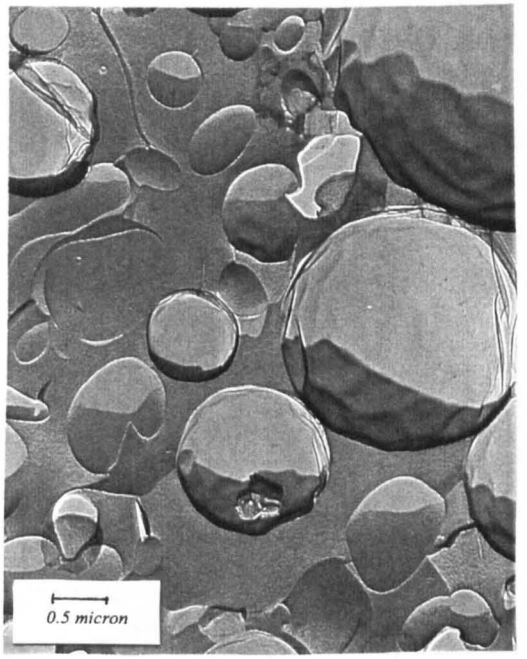

Figure 5.15a

75% Sweetose 2% sucrose ester S1670
gas microcells, containing 5% cholesterol

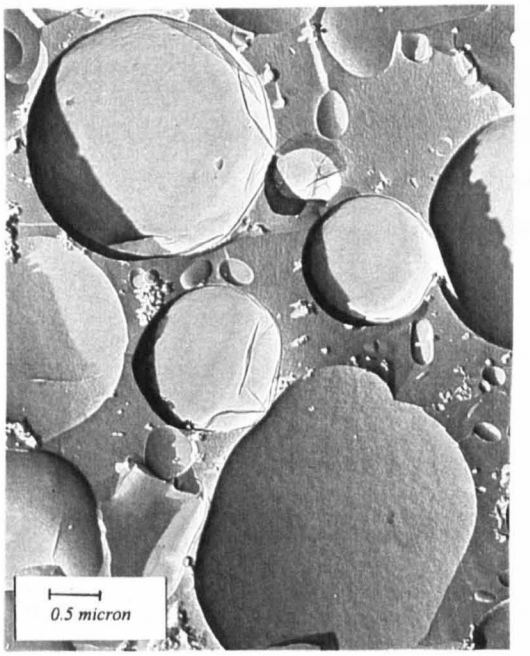

Figure 5.15b

75% Sweetose 2% sucrose ester S1670
gas microcells, containing 15% cholesterol

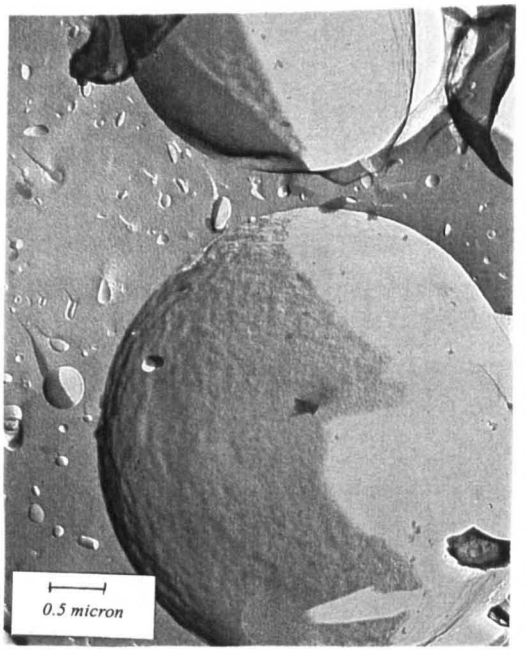

Figure 5.15c

75% Sweetose 2% sucrose ester S1670
gas microcells, containing 30% cholesterol

When cholesterol is added to biological membranes such as phospholipid, it resides at the interface between the alkyl chains and disrupts their close packing. It was anticipated that if the cells were surrounded by a monolayer or bilayer then cholesterol molecules would migrate to the surface and disrupt the packing of the alkyl chains and its effect on the domain structure would be observed. At 5% cholesterol, the curvature of each domain was reduced so drastically that the surface was virtually smooth. Figure 5.15d illustrates the packing of cholesterol molecules between the alkyl chains in a bilayer.

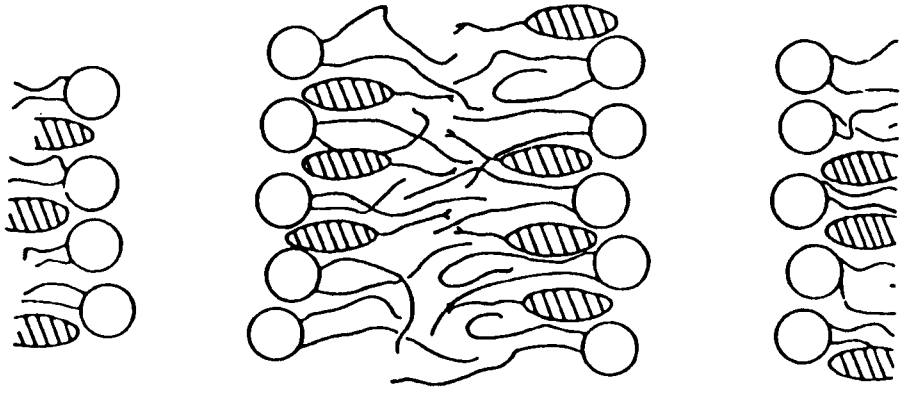

Figure 5.15d

Schematic diagram of the location of cholesterol in a phospholipid bilayer.
Taken from Rand and Luzzati[6]

The addition of cholesterol thus disrupted the packing of the chains at the interface and destroyed the regular geodesic domain structure. Centrifuging for 60 minutes at 18,000 rpm did not flocculate or destroy the gas cells and particulate matter was observed in the remains of a foam after drainage. These observations support the theory that the microcells have a monolayer or bilayer of liquid crystal at their surface.

5.16 References

1 Fitzgerald, M.; PhD Thesis, University of Reading, 1996.

2 Goodman et al.; Proc. Roy. Soc., **312**, 243, 1969.

3 Mayes. D. Internal Unilever Research Report, 1996.

4 Tanford, C.; "The Hydrophobic Effect", p. 43, publ. Wiley, 1973.

5 Ostwald, Wo.; Z. Phys. Chem. (Leipzig), **34**, 295, (1907).

6 Rand, R.P. and Luzzati, V.; Biophys. J., **8**, 125, (1968)

CHAPTER 6

Differential scanning calorimetry

6.0 DIFFERENTIAL SCANNING CALORIMETRY

6.1 Introduction

Non-aerated mixtures of Sweetose and sucrose ester were described in the previous chapters as being heterogeneous, this was thought to be due to the presence of liquid crystalline sucrose ester but it may also be due to insoluble crystals of sucrose ester. This heterogeneous material appeared to melt when heated above 50°C. Observation of non-aerated mixtures of Sweetose and sucrose ester at 20°C, by freeze fracture TEM revealed the mixture to contain bilayers of lamellar phase sucrose ester, the existence of which was confirmed by X-ray and neutron diffraction.

DSC was used to investigate the phase behaviour of these mixtures and their components between 20 and 80°C. Anhydrous crystalline sucrose esters were found to display phase transitions at the same temperature and with the same enthalpy as sucrose esters in aqueous solution and in mixtures with Sweetose. The phase transition observed in all samples was attributed to the hydrocarbon chain melting transition, as described in Chapter 1, rather than the true melting point of the sucrose ester crystal because of the low temperature (50°C), the observance of bilayer formation in mixtures with Sweetose, and the observed dependence of transition temperature on hydrocarbon chain length.

Mixtures of Sweetose and sucrose ester before and after aeration have been examined by various techniques throughout this thesis. In a standard 75% Sweetose 2% sucrose ester, S1670, non-aerated mixture there is liquid crystalline sucrose ester, TEM and optical microscopy revealed that the proliferation of this material is changed by the ratio of Sweetose to sucrose ester in the mixture and also by the nature of the sucrose ester itself. DSC measurements on a standard non-aerated mixture revealed a single melting peak at 48°C and a cooling peak at 40°C. Samples were prepared with, for example, different ratios of Sweetose to sucrose ester, and the effect on the phase change was noted. Many different samples have been studied, using both aerated and non-aerated mixtures, to gain an understanding of the importance of this phase change to the formation of gas microcells and also to try and establish the importance of the ratio of mono- to higher esters within the sucrose ester.

For reference, the following table, 6.1a, (reproduced from Chapter 2) describes the mono- and higher ester components of all the sucrose esters which have been investigated. Figure 6.1a illustrates the information for the commercial sucrose stearates, for clarity, all ester components with more than two alkyl chains have been counted as tri-esters.

Table 6.1a

Sucrose ester constituents

Sample ID.	% Mono	% Di	% Tri	% Tri/Higher	% F.F.A.$	% Unknown
S1670 stearate	76.9	20.5	2.7	-	-	-
S1570 stearate	70.2	25.0	4.7	-	-	-
S1170 stearate	52.0	35.8	12.1	-	-	-
S770 stearate	29.1	39.5	24.3	7.1	-	-
S270 stearate	10.9	13.8	-	64.8	4.0	6.4
S170 stearate	-	-	-	96.6	3.4	-
S070 stearate	-	-	-	94.6	5.4	-
P1570 palmitate - C_{16}	65.9	28.2	5.9	-	-	-
B1570 behenate - C_{22}	66.5	26.3	6.7	-	-	0.4
mono-stearate	98.6	1.0	-	-	-	0.4
di-stearate	-	40.4	-	54.9	4.7	-
C_8 caprylate	99.5	-	-	-	-	0.5
C_{10} caprate	99.4	-	-	-	-	0.6
C_{12} laurate	99.4	-	-	-	-	0.6
C_{16} palmitate	97.8	2.2	-	-	-	0.0

$ - F.F.A. - for further analysis

Figure 6.1a

The ratio of mono- to di- and higher esters within the commercial sucrose esters.

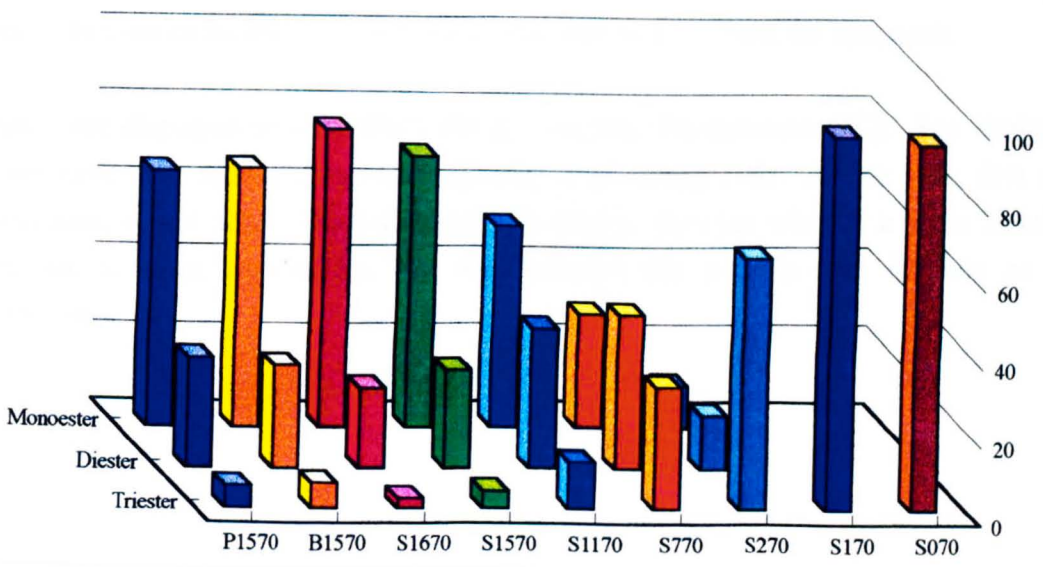

In addition to the above, samples of the light and dense fractions of a non-aerated mixture after separation by centrifugation, and a foam which had been allowed to drain by standing at room temperature for 6 months, were also examined. The fractions of these last two samples were also analysed for sucrose ester content using gel permeation chromatography, details are given in the text. In a further investigation, cholesterol was added to a mixture of 75% Sweetose and 2% sucrose ester, at different concentrations in order to observe any effects on the phase transition. The DSC measurements on pure sucrose esters and non-aerated mixtures of Sweetose and sucrose ester are described first. Measurements on all aerated samples are presented later.

6.2 Experimental

All DSC measurements were carried out at Unilever Research, Colworth House Laboratory, using a Perkin Elmer 7 Series Thermal Analysis System. A known mass of sample was sealed in an aluminium pan immediately before the run commenced. An empty aluminium pan was sealed to act as a reference. The temperature of the calorimeter was varied according to the run conditions, the energy which must be applied to or removed from the sample, to maintain its temperature equal to that of the reference, was recorded in the form of peaks or troughs according to whether the transition was endo- or exo-thermic. The peaks or troughs indicate a phase boundary and the temperature at which this occurred was recorded on the chart.

Except where indicated in the trace, the run conditions were as follows; the sample and pan were brought to equilibrium at 20°C, heated from 20°C to 80°C at 10°C per minute, held at 80°C for 1 minute, cooled to 20°C at 10°C per minute and then held at 20°C for 1 minute; in most cases the run was immediately repeated to check for hysteresis.

Results are displayed as Heat Flow (W g^{-1}) against Temperature (°C). For clarity the curves have been spaced along the ordinate, in ascending order of first heat, first cool, repeat heat, repeat cool. This technique was used to discover whether a phase transition occurred, at what temperature and also whether the process was for one or two components.

6.3 Crystalline samples of sucrose ester, as received

Pure anhydrous crystalline samples of sucrose ester were analysed to determine whether their observed phase behaviour depends on the blend of esters contained in the sample. DSC traces are displayed in Figures 6.3a-e.

Figure 6.3a illustrates the phase transitions occurring in crystals of sucrose mono-stearate, and Figure 6.3b illustrates the information for sucrose di-stearate. These are the components of many of the commercial sucrose esters used in this work. Sucrose mono-stearate crystals melt at 41°C and freeze at 30°C, whereas sucrose di-stearate crystals melt at a higher temperature, nearer to 62°C, and re-crystallise at 54°C.

In each figure the four traces describe the melting and freezing transitions. In each sample the run was repeated to check for hysterisis so there are two melting and two freezing curves. In all the following DSC traces the data are arranged according to the pattern in Figures 6.3a and 6.3b. The melting curves, or endothermic transitions appear as peaks in the trace, whereas the freezing or exo-thermic transitions appear as troughs. The first and repeat runs are spaced along the ordinate in the order first heat, first cool, repeat heat and cool. This information is given on the graph in these examples.

Figure 6.3a sucrose mono-stearate crystals ——— melting point 41°C

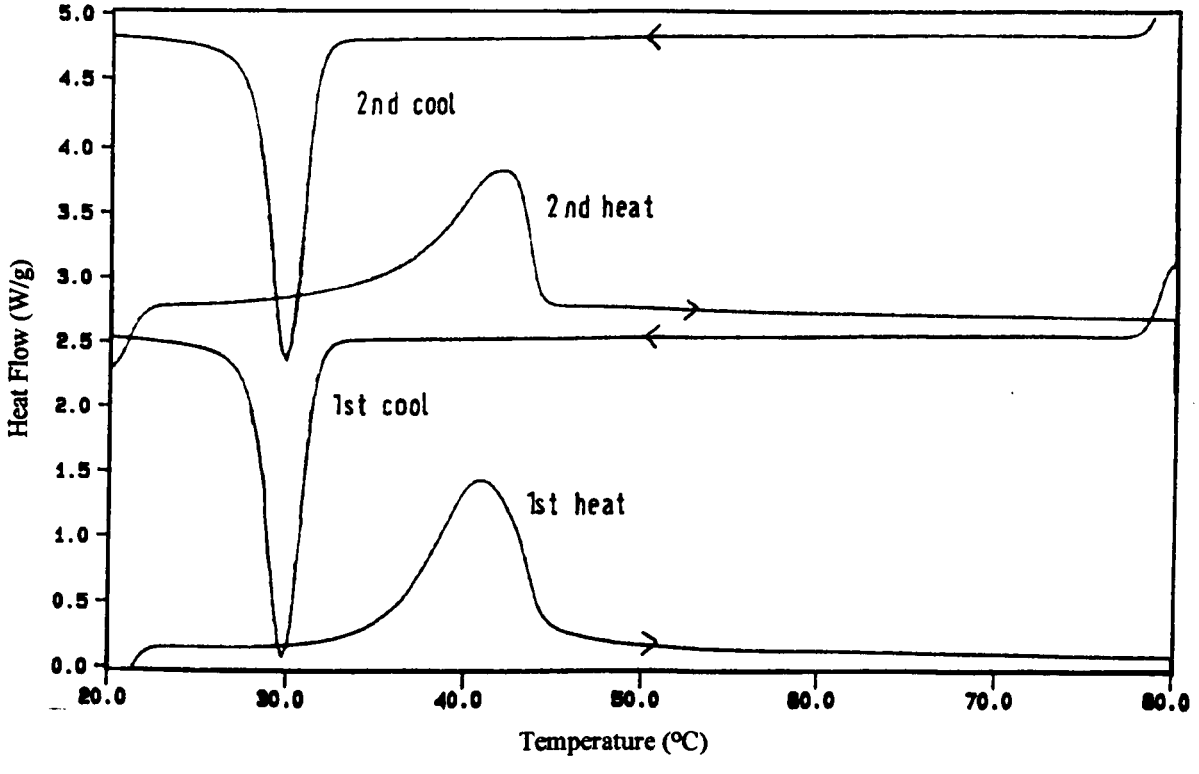

The Figures are diagrams of the heat flow (W g^{-1}) against temperature(°C) for each sample. The scale on the y-axis is purely relative, that is a comparison of the peak area can be made but the exact value at which the tip of the peak occurs on the y-axis is not

meaningful. The values on the temperature scale are real. The enthalpy of the transition is equal to the peak area, this was calculated automatically by the calorimeter used.

Figure 6.3b sucrose di-stearate crystals ——— melting point 62°C

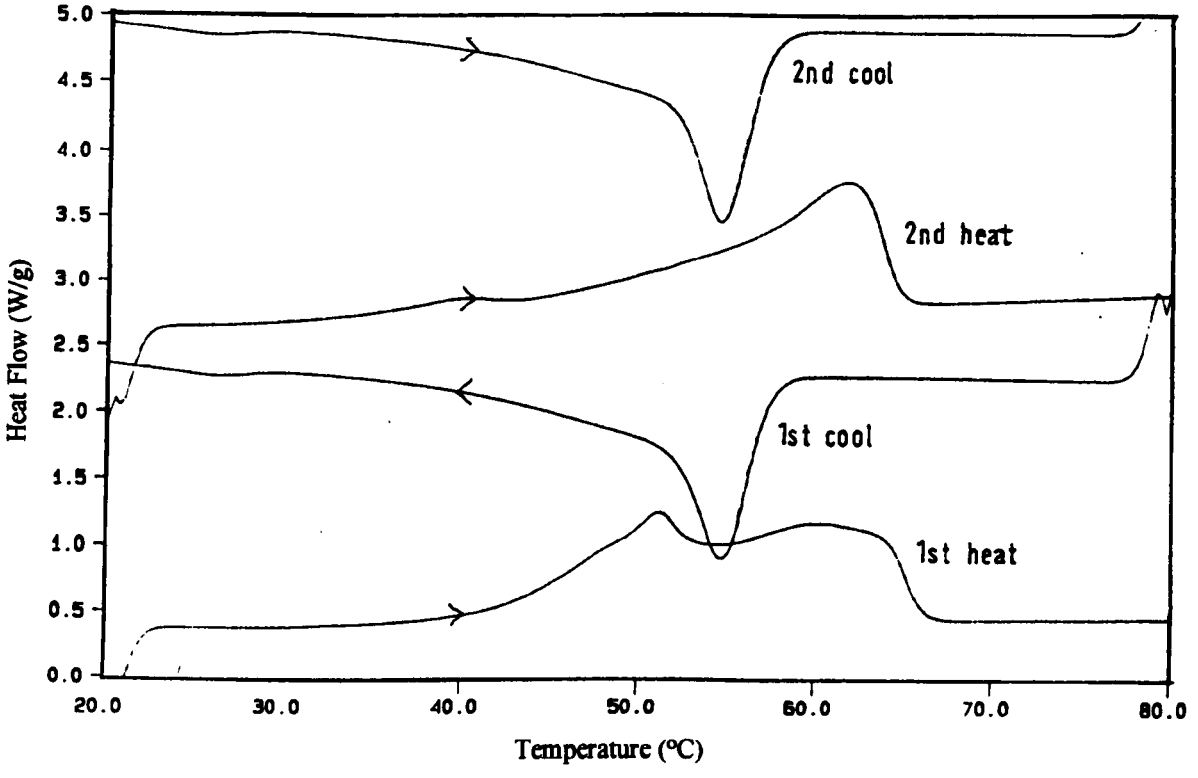

The difference in the melting and freezing behaviour of the mono- and di-stearates described in the above examples forms the basis for the study of the commercial mixtures of sucrose esters which are necessary for the preparation of gas microcells.

The difference in the phase transition according to the ratio of constituent esters is apparent in the traces of the commercial mixtures. Figures 6.3b-f illustrate the phase transitions of those commercial samples, whose exact composition is given in Table 6.1a. A useful generalisation is that the lower the number following the 'S' in the sample name, e.g. S770, the lower the proportion of mono-stearate in the sample and hence the more hydrophobic it is.

Figure 6.3c

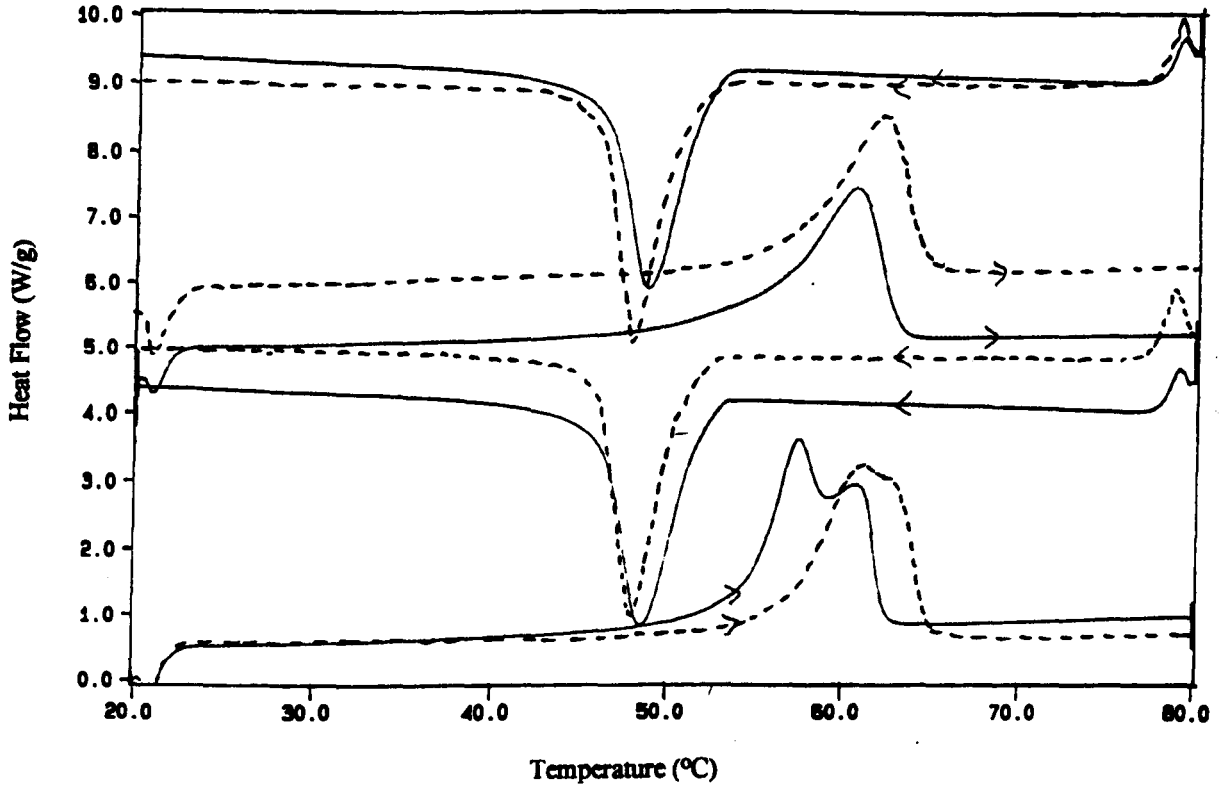

Figure 6.3d

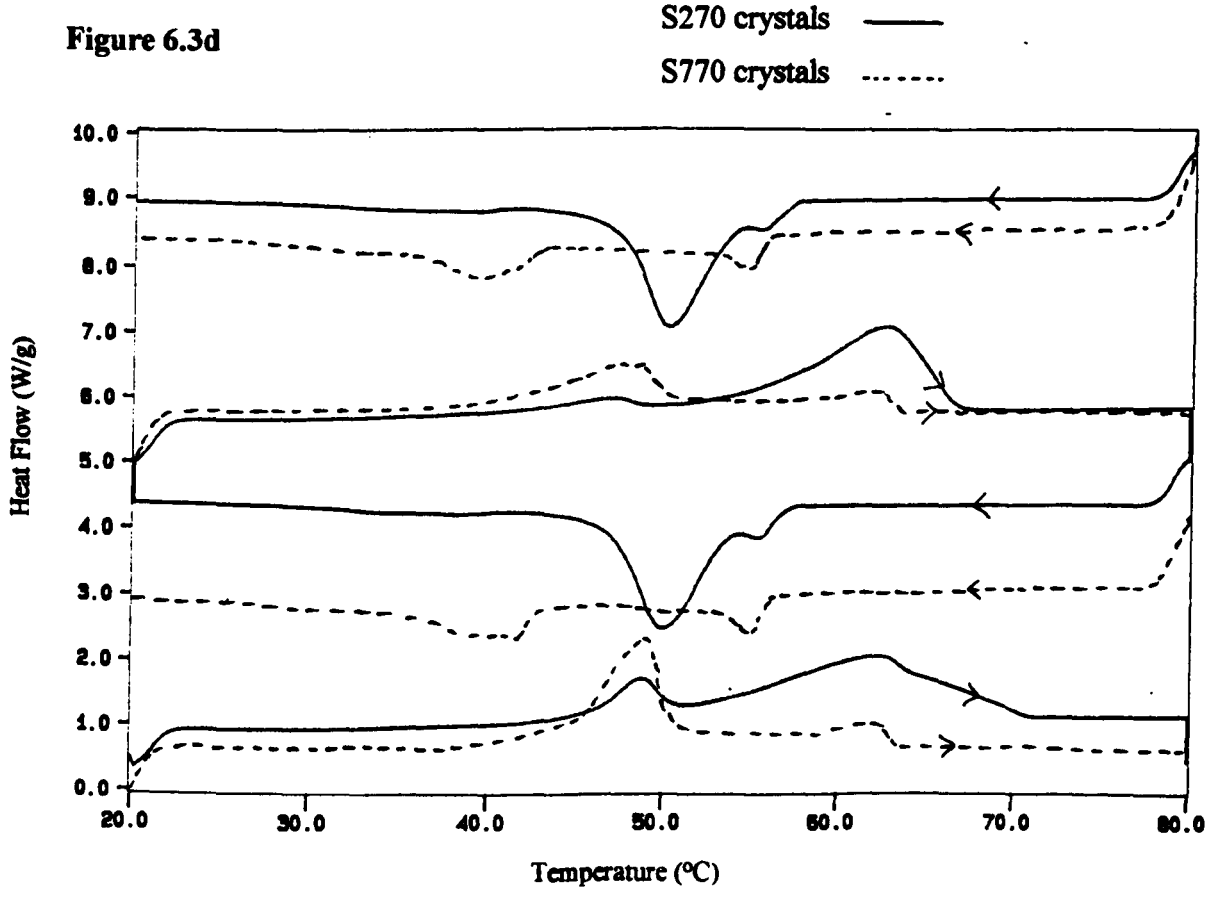

Figure 6.3e

S1170 crystals .....

S1570 crystals ——

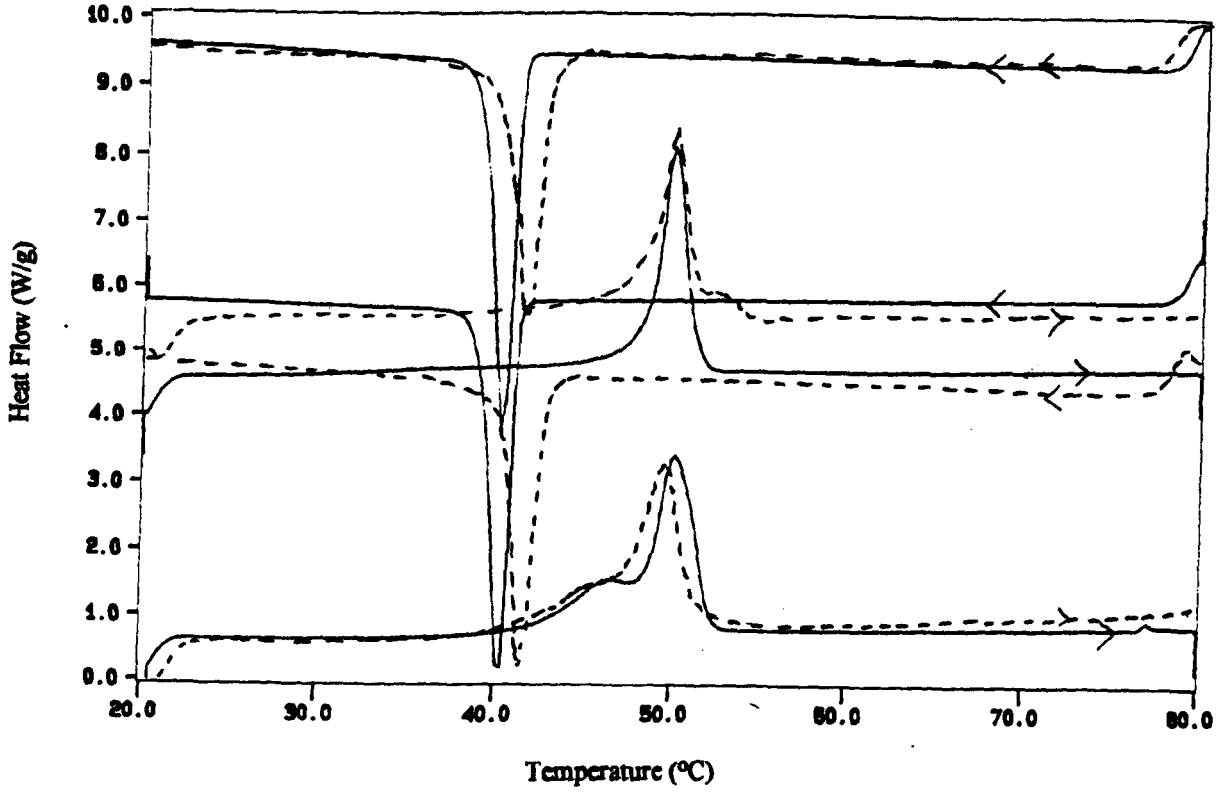

Figure 6.3f

S1670 crystals ——

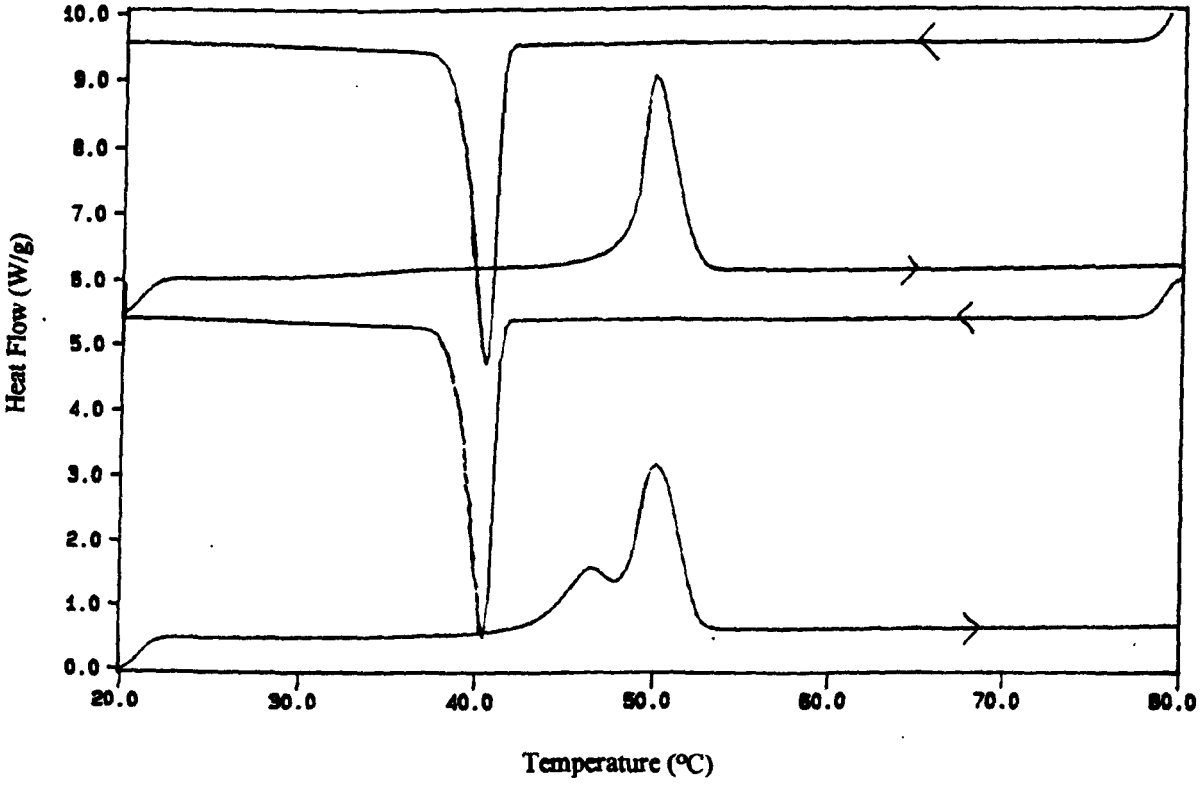

In summary, pure mono-stearate melts at 41°C and pure di-stearate melts at 62°C. The commercial mixed sucrose stearates all melt at intermediate temperatures. Sucrose stearates with a total proportion of di- and higher esters greater than 50% were characterised by an endothermic peak at 62°C corresponding to the di- and higher esters. Those which also contained a mono- stearate component had a second endothermic peak at 50°C. Sucrose stearates with a proportion of mono- stearate greater than 50% which also contained a di- stearate component were characterised by an endothermic peak at 50°C with a shoulder at 46°C, this shoulder increased in size with the proportion of mono-stearate in the sample. The peaks at 50°C and 46°C were observed in all samples which contained mixtures of mono- and di- stearates but was not attributable to either component directly and might therefore be due to the presence of mixed crystals.

In order to present the data more clearly the enthalpy and temperature data for the first endothermic transition in all of the crystalline samples containing mono-stearate or di-stearate or any mixture of the two is illustrated in the following Figure, 6.3h. The exact composition of each of the commercial sucrose ester samples was given in Figure 6.1a, but for the purpose of illustration the samples have been assumed to be a mixture of mono- and di- stearate only, any higher ester portion has been included in the percentage of di-ester. For reference, Figure 6.3g illustrates the composition of mono- to di- ester within the samples. Figure 6.3h shows the enthalpy and temperature of the first endothermic transition in each of the sample as a function of the percentage of mono- ester. 0% mono-stearate corresponds to 100% di-stearate. Some samples had two endothermic transitions, where this was the case the data for both peaks are plotted as peak one and peak two on the graph. The first endothermic transition was chosen for analysis because the samples were known to be at equilibrium before the first melting occured. The freezing transition was thought to be less accurate because the transition temperature was dependant on the rate of cooling, with the possibility for the occurance of supercooling if this was too fast.

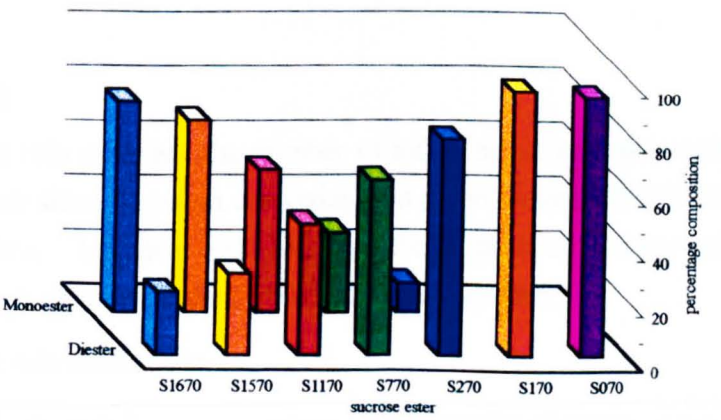

Figure 6.3g

The ratio of mono- to higher esters contained within the commercial sucrose esters.

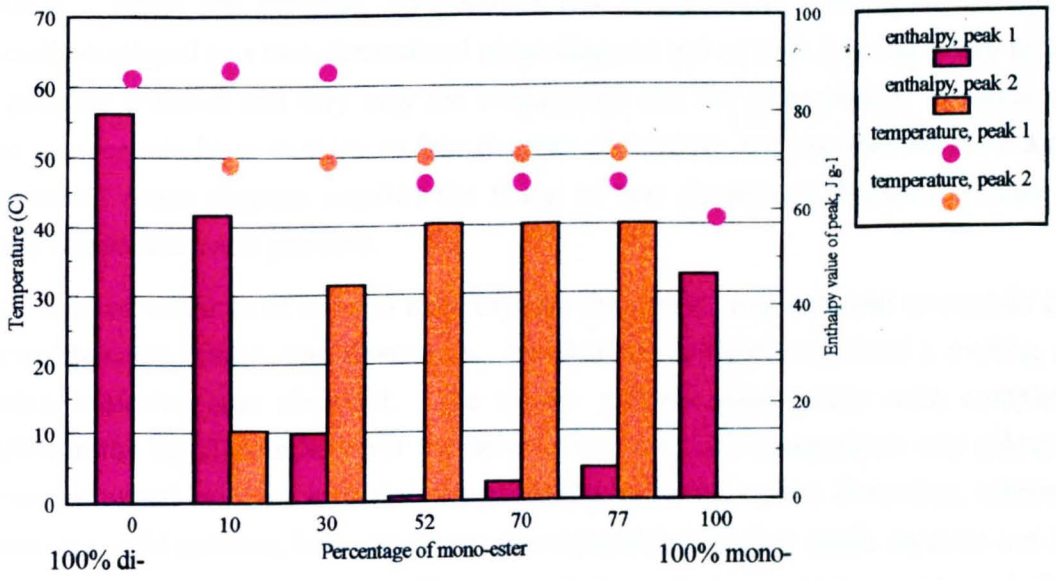

Figure 6.3h

The enthalpy and temperature of the first endothermic transition observed in the crystalline samples of sucrose esters containing mono- and di- stearate.

The observation of two melting points at high concentrations of di-stearate points to the formation of a mixture of solid mono-stearate in solid di-stearate (50°C) together with pure solid di-stearate (62°C). At approximately equal ratio of mono- to di- stearate the mixed solution of solid mono- in solid di-stearate (50°C) predominates but as further mono- is added a second solid solution of di- stearate in mono-stearate is formed which freezes at 46°C.

The following section describes the types of solid-liquid phase behaviour which could be exhibited by the mixed crystals of mono- and di- stearate.

6.4 The Phase Rule

The Gibbs phase rule describes the number of independent intensive variables, or degrees of freedom, which affect a system consisting of a given number of components in a certain number of phases. Intensive variables are those such as temperature, pressure and composition which are independent of the size of the system.

The Gibbs phase rule states that;

$$f = c - p + 2$$

where, f = *the number of degrees of freedom*

c = *the number of components*

p = *the number of phases*

In a two component system, according to the phase rule, there are three degrees of freedom. These are pressure, temperature and composition. Phase information is generally displayed as a two-dimensional phase diagram and as such it is customary to hold the pressure constant and vary only the temperature and the composition. Systems with three components have as many as four degrees of freedom and representation on a two dimensional phase diagram requires the fixing of two degrees of freedom. These are usually temperature and pressure.

In the case of mixtures of sucrose ester crystals the system was assumed to contain only two components, mono- and di-stearate. In all of the samples examined a melting and freezing transition was observed. The mono- and di- components were completely miscible in the liquid state however the behaviour of the solid components was unknown. The experimental evidence indicated the possibility of mixed crystal formation, otherwise known as a solid solution, however it was also a possible that they might separate out into the pure components on freezing. The types of phase diagram which would result from both types of freezing behaviour are discussed below.

A schematic phase diagram of a mixture whose components are completely miscible when melted but which separate into their pure components on freezing, is shown in Figure 6.4a.

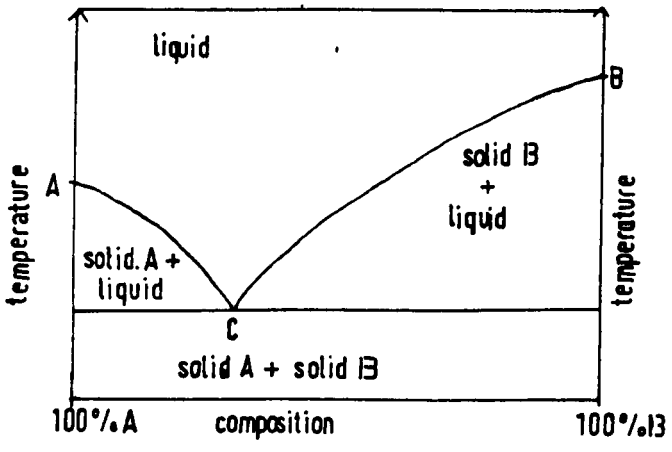

Figure 6.4a

In this diagram the freezing point of each component is reduced by the presence of the other, to a point where the liquid is in equilibrium with both the pure solids, known as the eutectic point, C. This is the lowest temperature at which the liquid mixture can exist at the specified pressure. A full description of phase diagrams of this type are given by Glasstone[1].

The freezing point of mixtures of mono- and di- stearate remained constant across the range of proportions of mono- to di- stearate and was not observed to decrease. For this

reason it was concluded that the mixtures of mono- and di- stearates do not separate into their pure solid components on freezing.

When the components form a miscible liquid it is possible for the freezing point of one component to be raised by the addition of another. A schematic phase diagram to illustrate this behaviour is shown in Figure 6.4b.

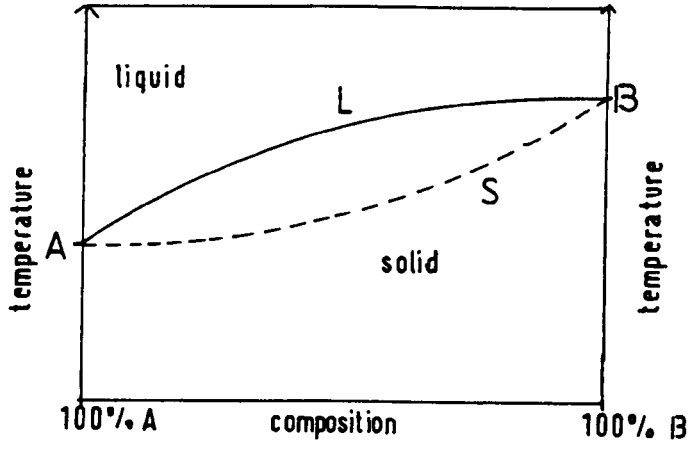

Figure 6.4b

A schematic phase diagram to illustrate the behaviour of mixtures that form a continuous series of solid solutions below the freezing point of the mixture.

In the diagram above the upper curve (L) or liquidus curve represents the composition of the liquid phase which is in equilibrium with the solid whose composition is given by the lower or solidus curve (S). A full explanation of this behaviour and examples in which the freezing point curve has a maximum and minimum are given by Glasstone[1].

When the two components do not form a continuous series of mixed crystals that is, one solid component A can only dissolve a finite amount of the other solid component B, after which further addition of B will not alter its composition, but rather a second solid phase consisting of A in B forms, then the phase diagram of the mixture will be slightly different from that in Figure 6.4b.

Figure 6.4c illustrates this behaviour for mixtures whose freezing point lies between that of each pure component.

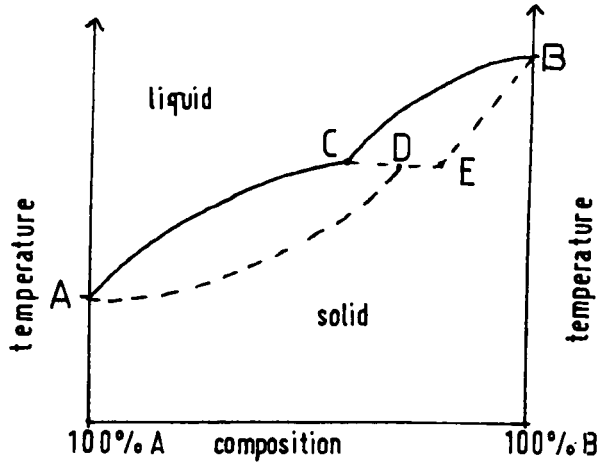

Figure 6.4c.

A schematic phase diagram to illustrate the behaviour of mixtures that form a discontinuous series of mixed crystals below their freezing point.

The addition of B to A raises the melting point of A. At low concentrations of B in A the concentration of B in the mixed crystal, as indicated by the dotted line, is greater than in the solution. At low concentrations of A in B, the melting point of B is lowered, again the concentration of B in the mixed crystal is greater than in the solution. At the temperature of the line CDE, the liquid of composition C is in equilibrium with the mixed crystals of composition D and E. The point C represents an invariant point, that is, there is only one degree of freedom, i.e. pressure. This point is known as a peritectic point. The phase behaviour described in this figure was deemed to have the closest resemblance to the phase behaviour indicated by the enthalpy and temperature of transition data in Figure 6.3g. Using the limited data contained in that Figure, a phase diagram to help interpret the phase behaviour is drawn below, Figure 6.4d.

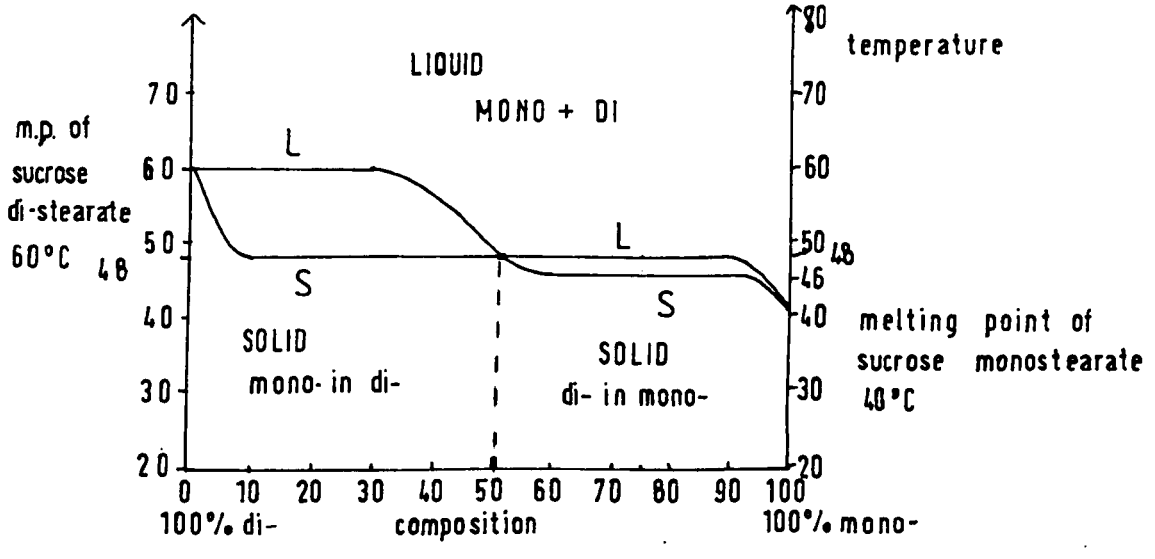

Figure 6.4d

Phase diagram of mixed crystalline sucrose esters containing mono- and di- stearate, based on the first endothermic transition observed by DSC.

The phase diagram above was based on the limited data obtained from the DSC analysis of a small number of samples. The object of the exercise was to determine the mixing behaviour of mixed mono- and di- esters in order to apply this information to the behaviour of non-aerated mixtures of Sweetose and sucrose ester and the gas microcells which result from the aeration of the mixture. If the objective had been to determine the complete phase diagram for all compositions of mixed mono- and di-stearates by this technique then further measurement on samples at very low di-stearate concentration and at 50% mono-stearate concentration would have been more informative. Therefore the data in Figure 6.4d has to be considered as provisional.

6.5 Sucrose esters with different alkyl chain lengths

B1570 crystals, C_{22}, melt at 73°C and freeze at 66°C, whereas P1570 crystals, C_{16}, melt at 44°C and freeze at 33°C, see Figure 6.5a. Compare this with S1570, C_{18}, which melted at 50°C and froze at 40°C. In B1570 and P1570 the ratio of mono-/di-/tri- ester is 66/27/6, in S1570 it is 70/25/5, only a negligible difference. The change in phase transition temperature is thus more likely to be due to the difference in alkyl chain length. When amphiphiles are packed closely together and the hydrocarbon chains are beneath their chain melting transition, the portion of the hydrocarbon chain in the vicinity of the head group will be less ordered than the rest of the chain because of the spacing effect of a large head group. In amphiphiles with a long alkyl chain the ordered region will be longer than in those with a short chain. A more ordered chain will melt at a higher temperature and have a higher enthalpy of transition, thus explaining the observations above.

Figure 6.5a

B1570 crystals ——

P1570 crystals ------

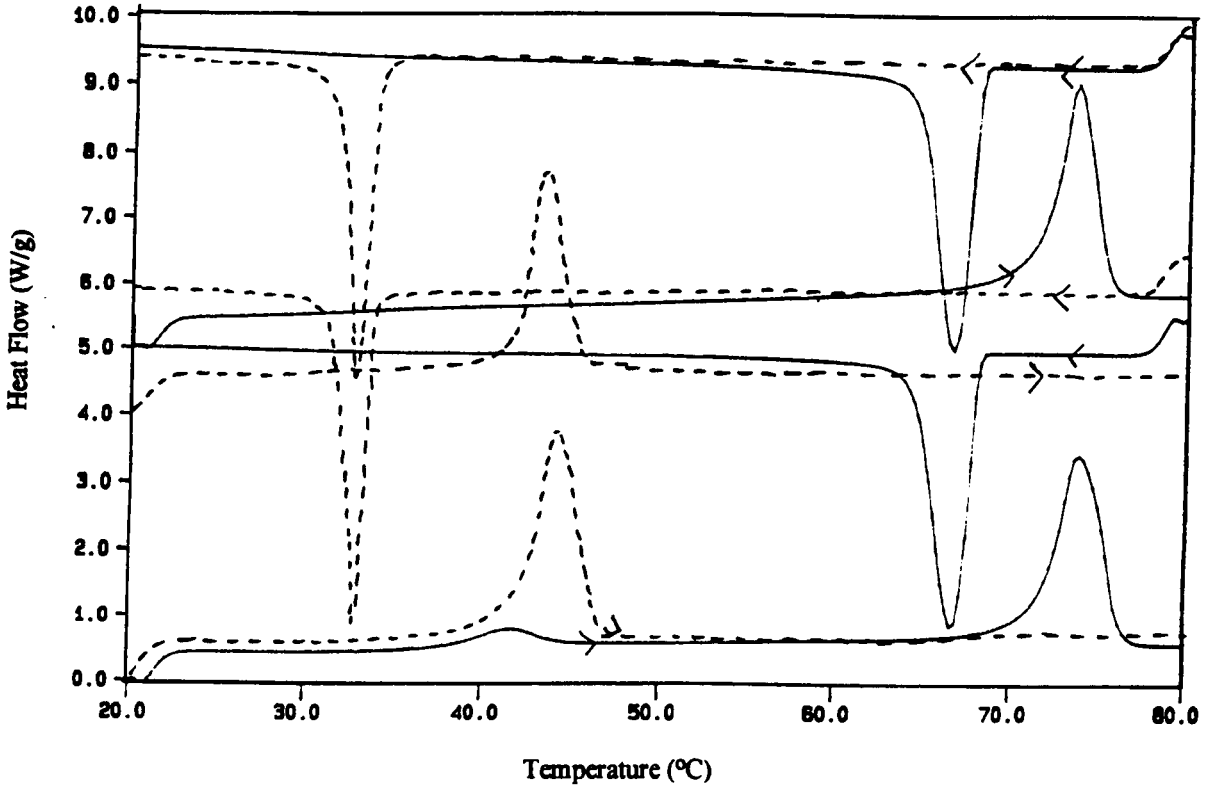

The table below describes the DSC data for all the crystalline samples presented, in the form of number of peaks observed, temperature (°C) and ΔH value (J g^{-1}).

Table 6.5a

Crystalline sucrose esters

Crystal	No. of Peaks		1st heat run		rpt. heat run		1st cool run		rpt. cool run	
sample	*heat*	*cool*	*temp*	*ΔH*	*temp*	*ΔH*	*temp*	*ΔH*	*temp*	*ΔH*
S070	1+	1	57.47	95.18	60.56	82.39	48.57	-84.47	48.80	-85.49
S170	1(+)	1	61.15	88.01	62.23	72.07	48.21	-77.42	48.06	-76.90
S270	2	1+	48.82	14.55	47.02	5.23	50.05	-60.53	50.23	-60.10
			62.24	59.52	62.42	61.41	-	-	-	-
S770	2	2	49.20	44.73	47.33	32.35	55.08	-14.42	54.95	-15.59
			61.94	14.05	61.77	12.48	41.67	-31.20	39.68	-30.79
S1170	1(+)	1	49.72	57.33	50.03	45.89	41.73	-45.14	41.72	-47.83
			46.01	1.21						
S1570	1+	1	50.12	57.30	49.84	45.26	40.31	-47.49	40.29	-48.70
			46.00	3.80						
S1670	2	1	50.13	57.36	49.88	50.28	40.41	-49.60	40.42	-49.55
			46.0	6.51	-	-	-	-	-	-
P1570	1	1	44.24	57.99	43.45	45.06	32.98	-45.67	32.96	-46.23
B1570	1	1	73.86	63.46	-	-	66.65	-62.93	66.58	-62.90
			41.61	8.30	-	-	-	-	-	-
mono-C18	1	1	40.90	46.68	41.95	39.45	29.78	-37.07	29.80	-37.28
di-C18	1+	1	51.19	80.31	61.64	51.08	54.73	-57.57	54.54	-57.56

6.6 20 % w/w sucrose ester in water, in the absence of Sweetose

In the production of gas microcells 2% w/w sucrose esters are aerated in a 75%w/w Sweetose in water solution. Microscopy results in Chapter 2 suggested that the 75%w/w Sweetose concentration caused the sucrose ester to phase separate, forming the lamellar phase described in Chapters 3 and 4. Microscopy was also used in Chapter 2 to examine solutions of sucrose ester in water without Sweetose. At concentrations greater than 20% w/w the sucrose esters in water contained optically anisotropic regions which had a similar appearance to the anisotropic regions observed in non-aerated mixtures of 75% w/w Sweetose and 2% w/w sucrose ester.

Fitzgerald[2] studied the phase behaviour of sucrose ester S1670 in water using the techniques of polarising microscopy, X-ray diffraction and rheological measurement. He observed a temperature dependence, at 48°C, across the whole range of sucrose ester, S1670, concentrations. The aggregate structures favoured by the packing geometry, as calculated by Fitzgerald, were planar bi-layers, with the alkyl chains within the bi-layers ordered below 48°C and fluid above this temperature. Since the optical appearance of the 2% w/w sucrose ester in 75%w/w Sweetose and that of 20% w/w sucrose ester in water were very similar and both formed bilayer aggregates, it was suggested that the sucrose ester in the two samples might be in a lamellar phase, one with Sweetose between the bilayers and one with water.

On this basis, 20% w/w sucrose ester in water samples were prepared and examined by DSC in the hope that the results could be related to the behaviour of sucrose ester in Sweetose or at the very least the behaviour of hydrated crystals of sucrose ester in a lamellar phase. 20% w/w sucrose ester in water samples were prepared by repeatedly heating the required mass of sucrose ester and water to 70°C and stirring until the sucrose ester was fully dissolved after which the mixture was cooled to room temperature where it formed a gel. Samples were prepared using those sucrose esters which were water soluble, this did not include pure sucrose di-ester, S170 or S070.

DSC traces are displayed in Figures 6.6a-h

Figure 6.6a

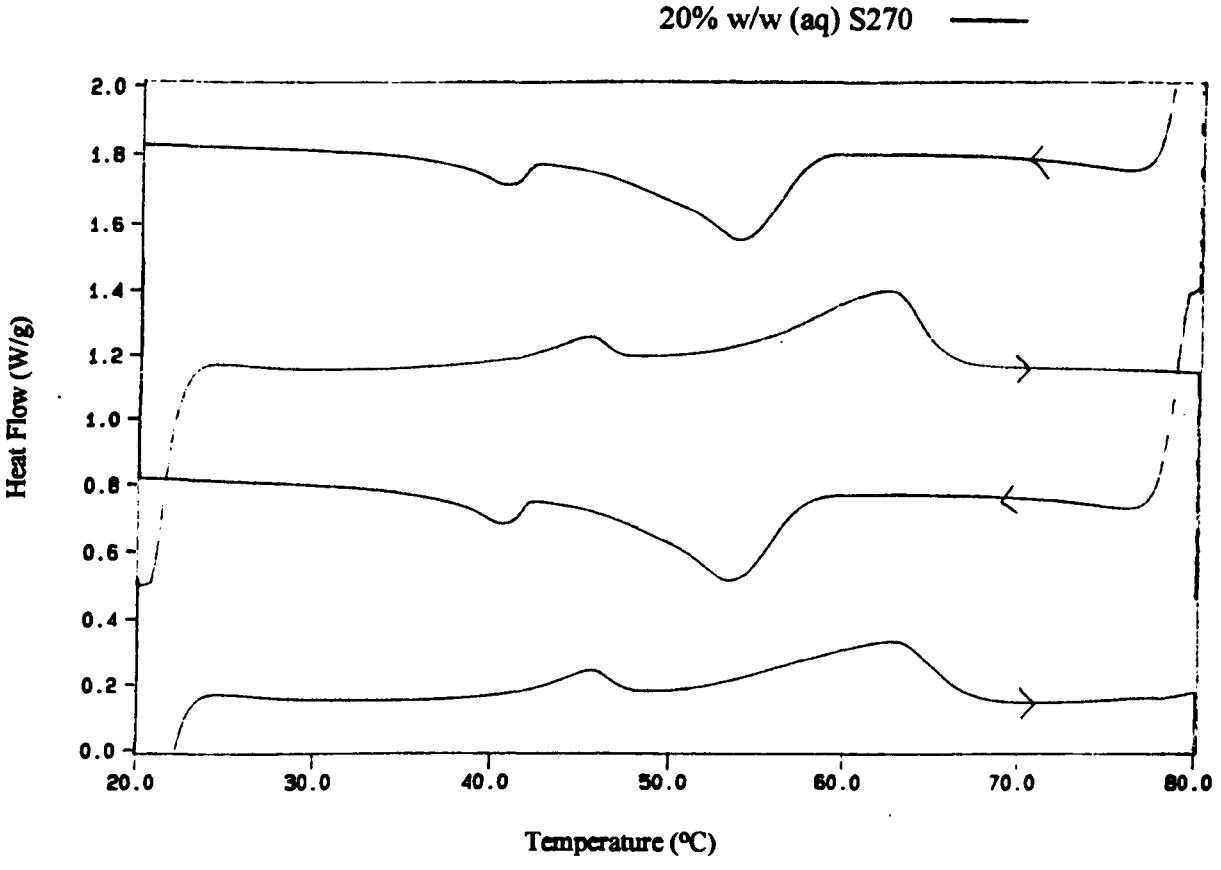

Figure 6.6b

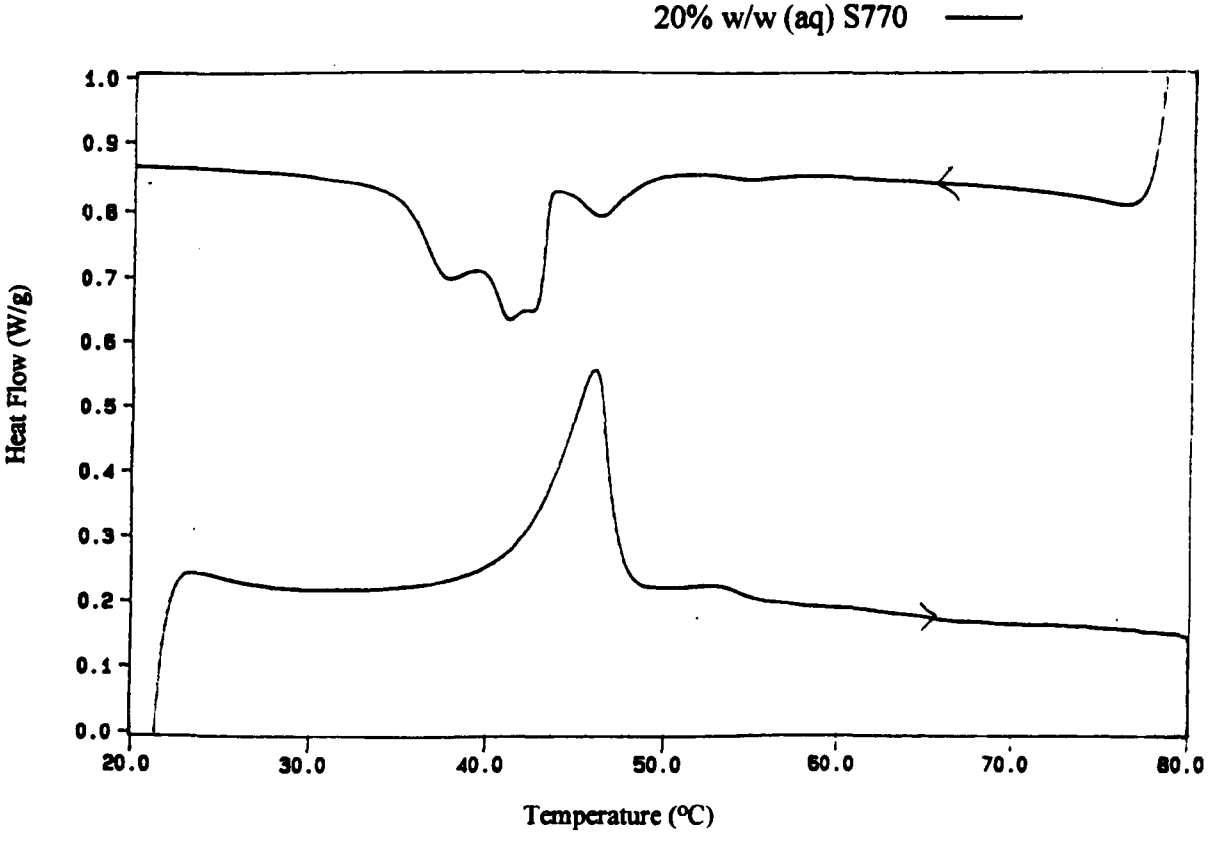

Figure 6.6c

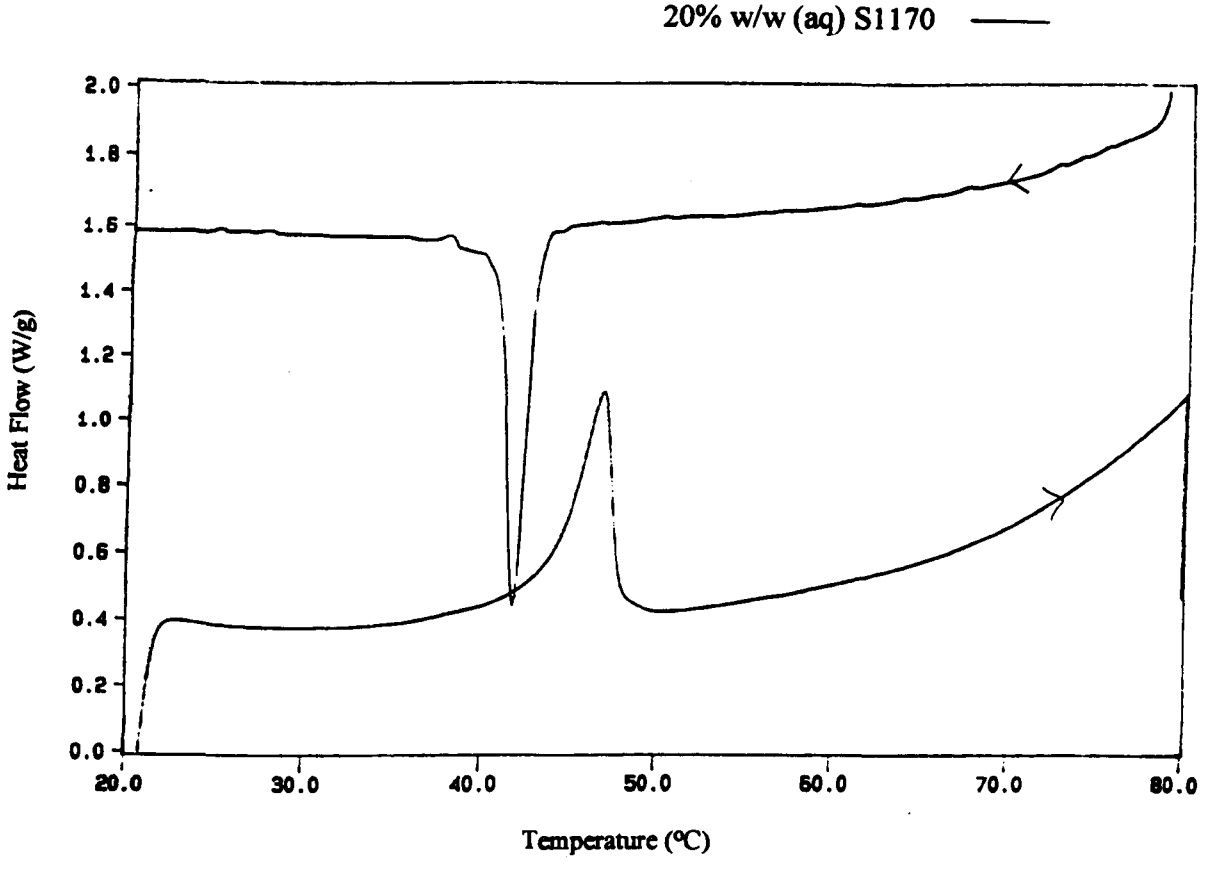

Figure 6.6d

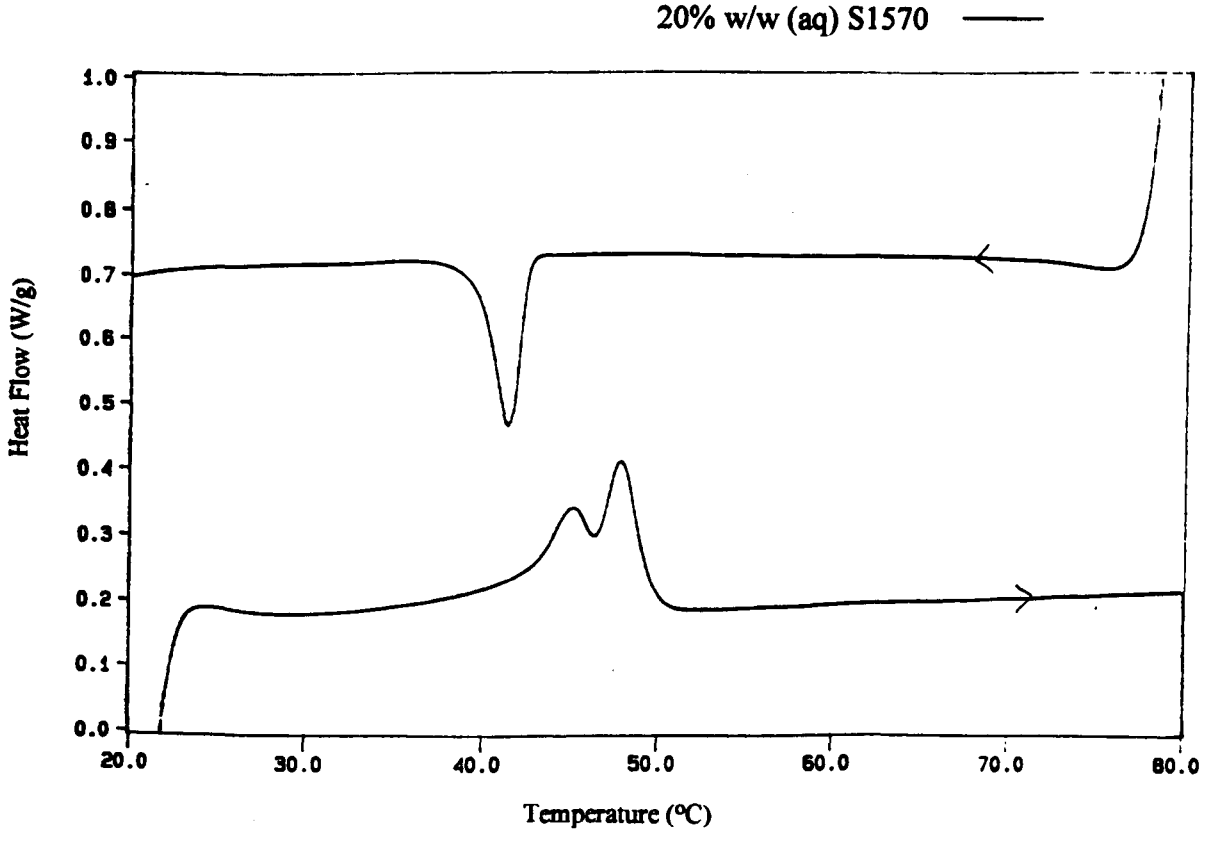

Figure 6.6e 20% w/w (aq) S1670 ——

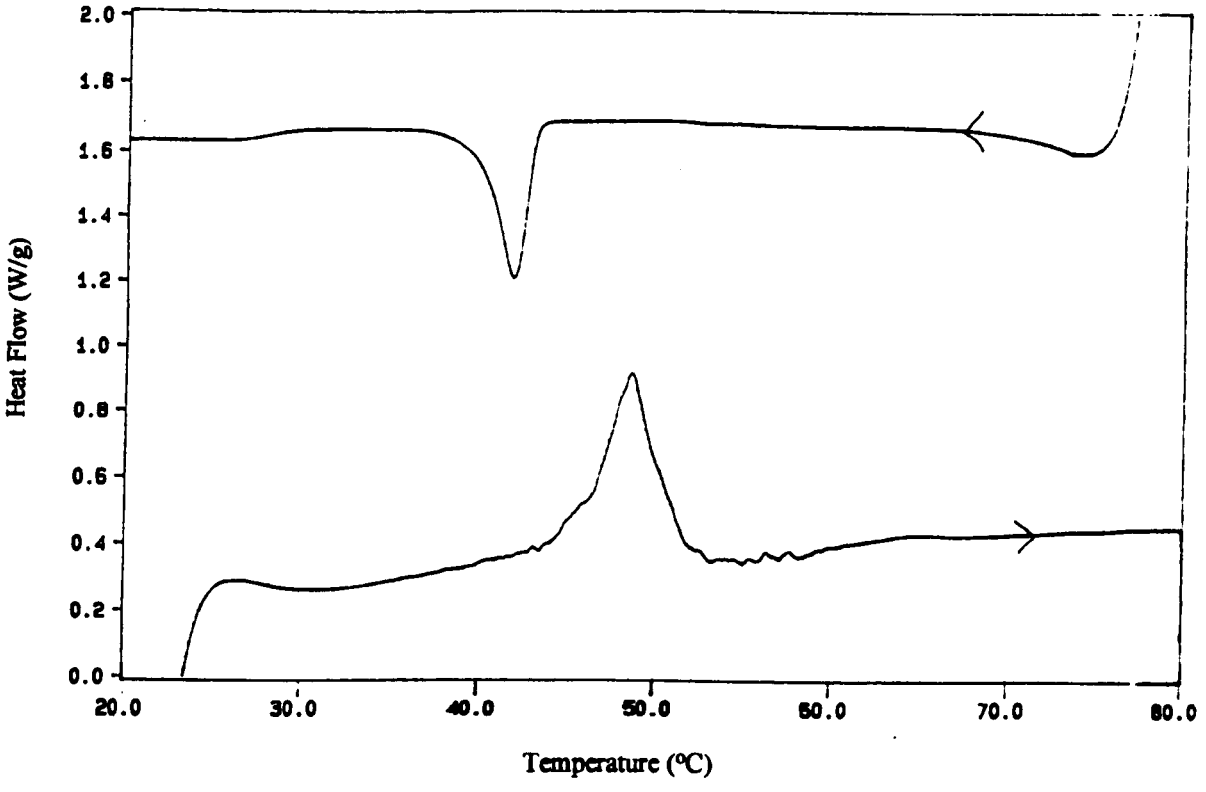

The above figures illustrate that the phase behaviour of the commercial sucrose stearates was similar to that of their crystalline equivalents; the transition temperatures observed were only marginally different and the enthalpy of the transitions were also comparable. The heat flow shown on the graphs was per gram of sample, which contained 0.2g of sucrose ester. When the data were normalised to the value per gram of sucrose ester in the sample, a factor of 50, the enthalpy value was very close to that of the crystalline solids. e.g. the ΔH value of the endothermic peak observed on melting 20% w/w S1170 was 58.10 J g^{-1}, that of crystalline S1170 was 57.33 J g^{-1}.

20% w/w S270 displayed similar behaviour to S270 crystals, with two phase transitions on both heating and cooling, however the exothermic peaks occured at 40 and 53°C in 20% w/w and at 50 and 55°C in the crystals. 20% w/w S770 had two endothermic peaks, at 46 and 53°C and three exothermic peaks between 37 and 46°C.

20% w/w S1170 was little changed from the behaviour of crystalline S1170, with slight differences in the proximity of the melting and freezing temperature and the sharpness of the endothermic peak. 20% w/w S1570 was similarly little changed from the behaviour seen in the crystalline sample, again the endothermic peak was better defined.

20% w/w S1670 displayed a single stage melting and freezing process, contrary to the two stage melting observed in the initial heating of S1670 crystals.

Pure sucrose mono-stearate, Figure 6.6f, was totally soluble in water and no phase transition was observed between 20 and 80°C. For interest, the sample was cooled from 30°C to -30°C, a sharp freezing point was observed at -20°C, a large depression in the freezing point of water. On warming a broad peak was observed at 0°C.

Figure 6.6f

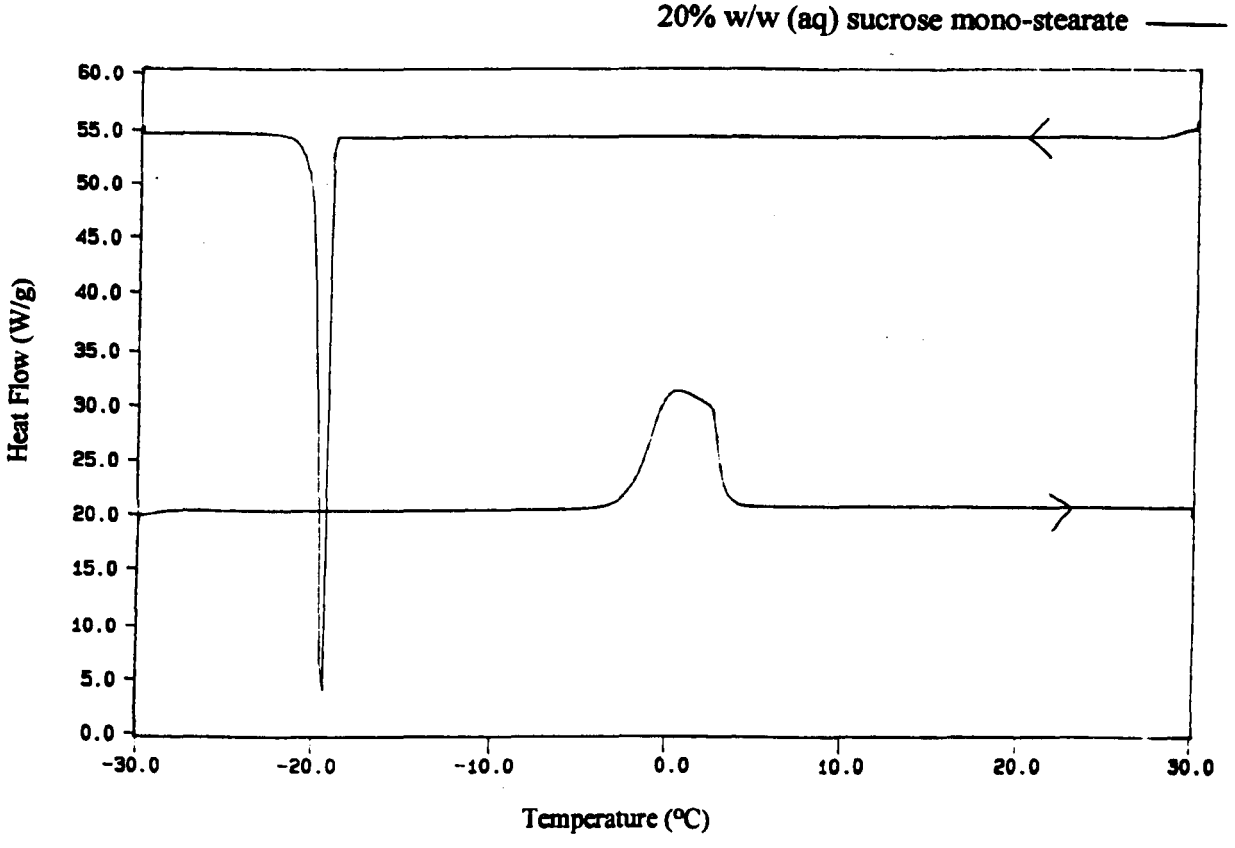

Figure 6.6g illustrates a graph of the enthalpy and temperature of the first endothermic transition of the commercial sucrose stearates as a function of their mono-stearate composition. Any higher ester fraction they contained was included in the di-stearate fraction Pure sucrose mono-stearate was not included in the diagram because it had no phase transitions between 20 and 80°C, indicating that it was either soluble in water and present as a micellar dispersion or it was a liquid crystal above its chain melting temperature and its hydrocarbon chains were fluid in that temperature range. If the hydrocarbon chains were indeed fluid then it was expected that a freezing transition during which the chains crystallise would have been observed before the freezing of the water itself. Since the only transition observed was the much depressed freezing of water the sucrose mono-stearate was taken to be soluble in water at a concentration of 20% w/w.

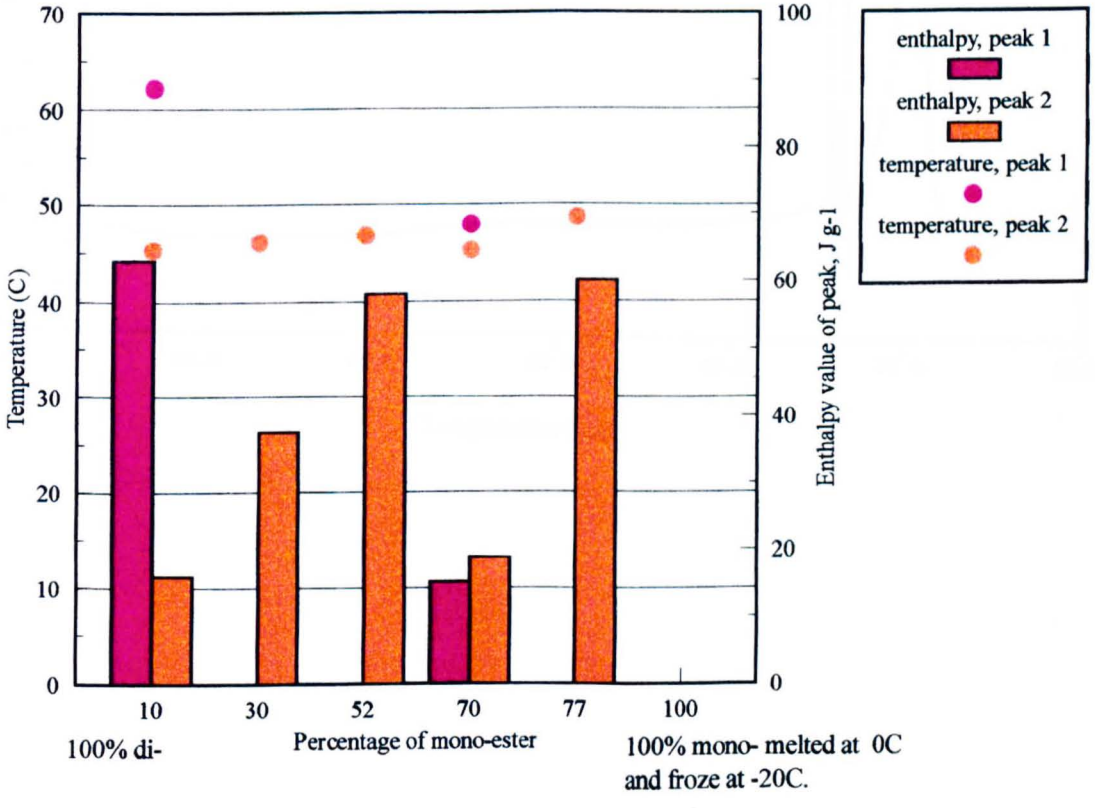

Figure 6.6g

The enthalpy and temperature of transition for the first endothermic peak for 20%w/w sucrose esters in water as a function of mono-stearate composition.

20%w/w B1570 and P1570 melt and freeze in the same temperature range as their crystalline derivatives, however the magnitude of the B1570 transition was much greater than the P1570 transition when previously they had been identical. The DSC measurements on 20%w/w B1570 and 20%w/w P1570 are illustrated in Figures 6.6h & i respectively.

Figure 6.6h

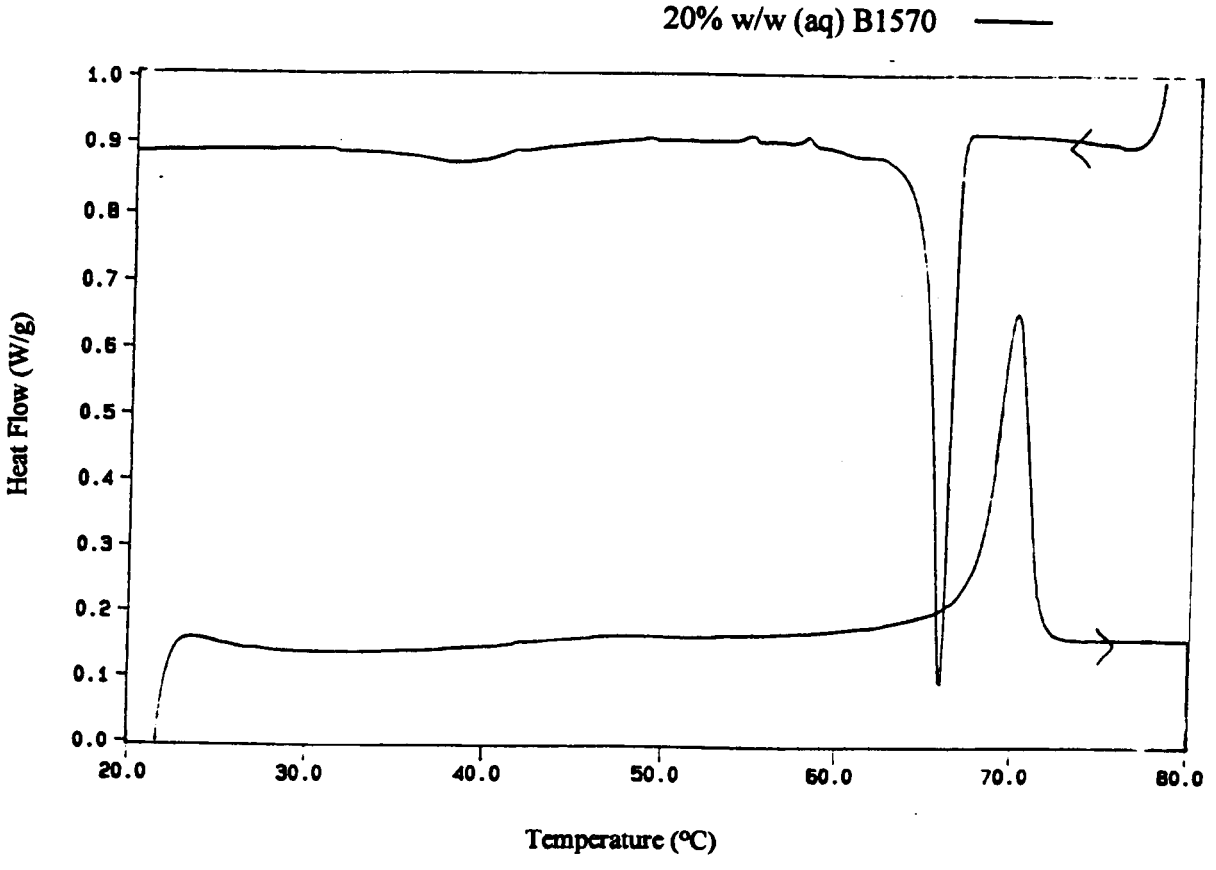

Figure 6.6i

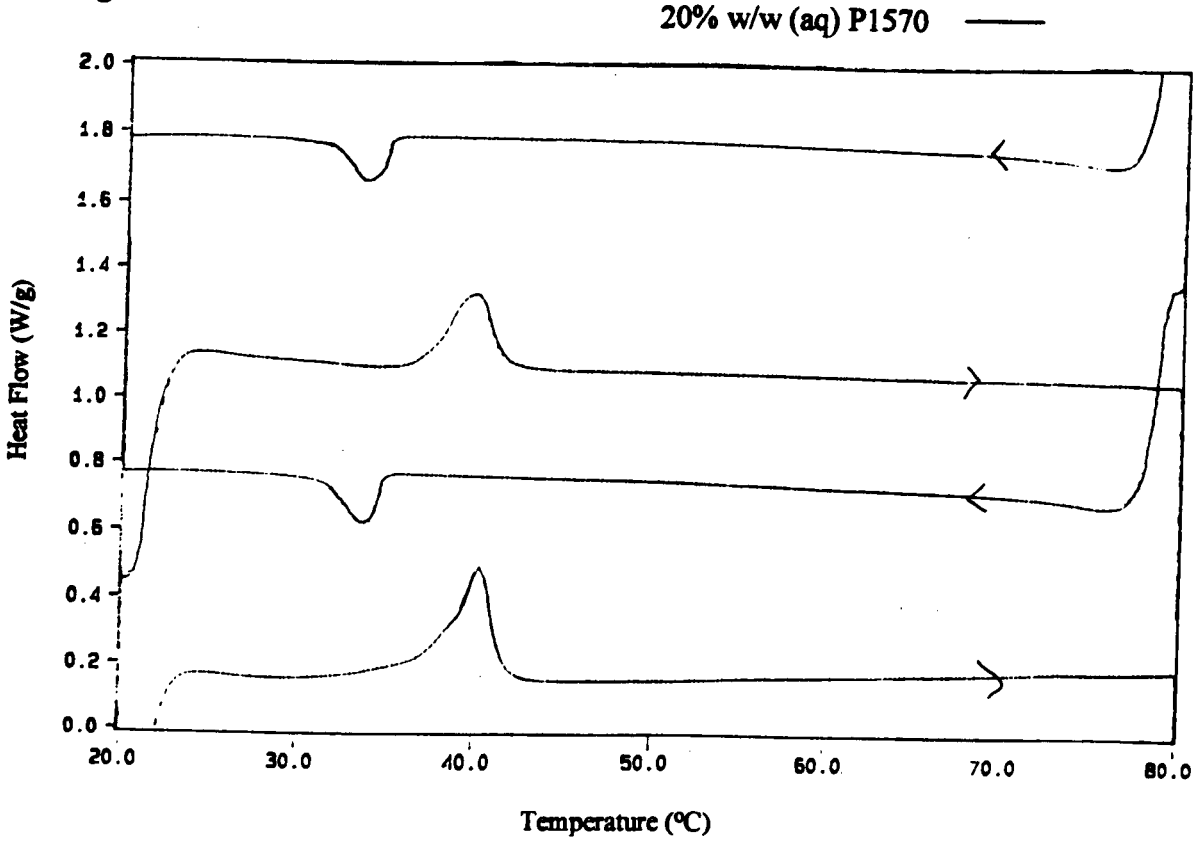

Table 6.6a describes the data in the form of number of peaks observed, temperature (°C) and ΔH value (J g^{-1}sucrose ester in the sample).

Table 6.6a

20 % w/w (aq) sucrose esters

20 % w/w	No. of Peaks		1st heat run		rpt heat run		1st cool run		rpt cool run	
sample	*heat*	*cool*	*temp*	*ΔH*	*temp*	*ΔH*	*temp*	*ΔH*	*temp*	*ΔH*
S270	2	2	-	-	45.23	16.05	40.63	-14.65	40.65	-10.15
			62.73	56.05	62.17	63.00	53.45	-58.35	53.75	-58.25
S770	2	3	46.03	37.45	-	-	46.28	-5.9	-	-
			53.0	not meas	-	-	41.22	-29.85	-	-
			-	-	-	-	37.85	-15.95	-	-
S1170	1	1	46.77	58.10	-	-	41.79	-50.60	-	-
S1570	2	1	45.16	18.75	-	-	41.36	-15.4	-	-
			47.85	15.2	-	-	-	-	-	-
S1670	1	1	48.58	60.05	-	-	41.80	-31.8	-	-
P1570	1	1	40.26	31.75	39.80	20.49	33.64	-10.65	33.53	-10.3
B1570	1	1	70.0	38.05	-	-	65.84	-36.3	-	-
mono-C18	1	1	0.53	1280.1	-	-	-19.47	-1096.5	-	-

7 Variable Sweetose / 2% w/w sucrose ester

Non-aerated mixtures of Sweetose and 2%w/w sucrose ester S1670 were prepared with different concentrations of Sweetose, to examine any changes in the phase transition behaviour. The concentration of sucrose ester S1670 was a constant 2%w/w sample throughout. In Chapter 6 confocal microscopy was used to examine the effect of Sweetose concentration on the appearance of the liquid crystalline sucrose ester. The quantity of optically anisotropic liquid crystalline sucrose ester observed at 2% w/w concentration sucrose ester in the sample increased with Sweetose concentration. In Chapter 3 the same anisotropic liquid crystalline sucrose ester material was observed in a sample containing 75% Sweetose but only 0.5% sucrose ester, whereas samples of 0.5% w/w sucrose ester in water were optically isotropic. It was assumed that these changes were due to the interaction between Sweetose and water, perhaps causing an increase in the water structure, resulting in the phase separation of the sucrose ester at high Sweetose concentration. When examined by DSC, pure Sweetose did not display phase transitions between 20 and 80°C, Figure 6.7a, and thus any changes observed were attributed to the effect of the Sweetose on the sucrose ester itself.

Figure 6.7a

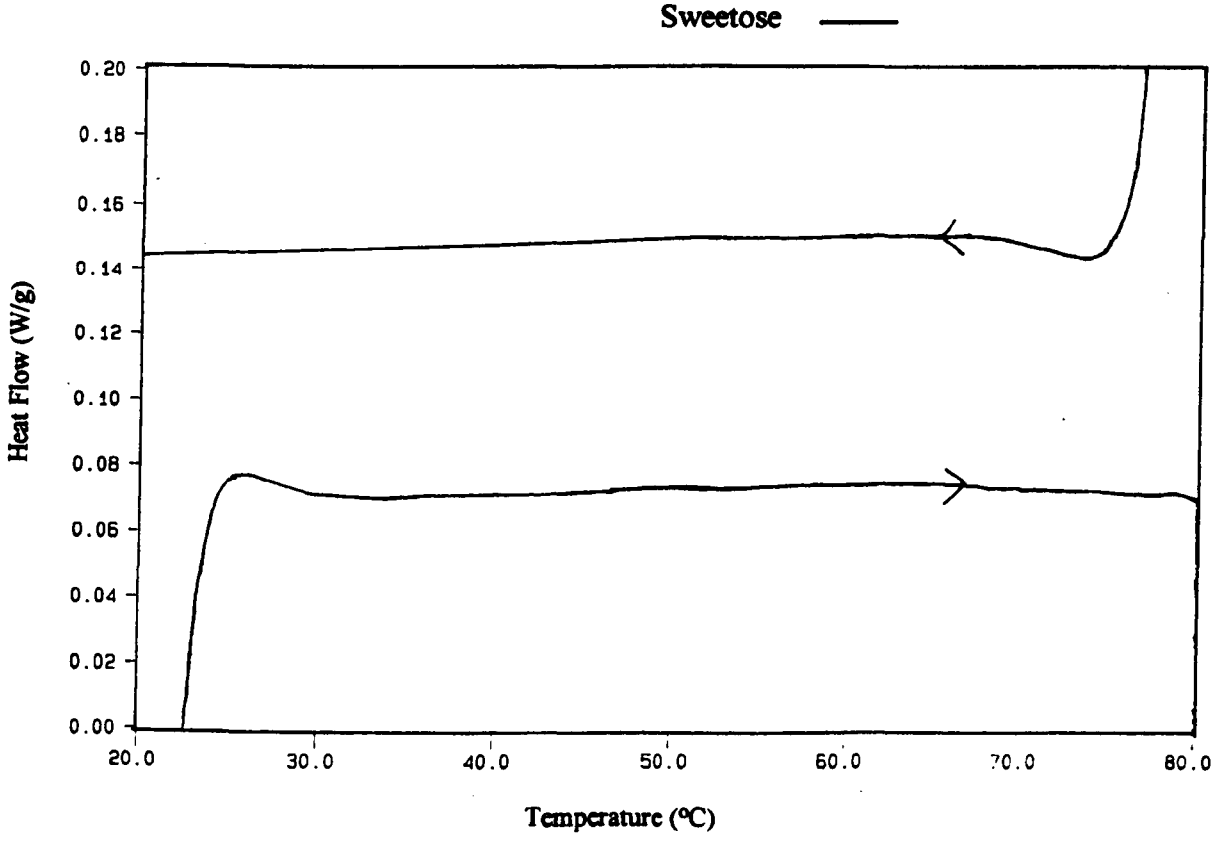

The DSC traces of the non-aerated samples containing 2%w/w sucrose ester in the sample and a variable %w/w Sweetose are displayed in Figures 6.7b-e.

All samples contained 2% w/w S1670 and were prepared by the method described in Chapter 2. The remaining sample weight was made up with water. At low concentrations of Sweetose only an endothermic peak was observed within the time-scale of the experiment, however, above 30% Sweetose both endo- and exo- thermic transitions were observed, melting at 48°C and freezing at 40°C, as recorded previously with S1670. The transition temperatures remained constant but the enthalpy of transition was found to increase with Sweetose concentration.

In Chapter 6 it was observed that the quantity of liquid crystalline sucrose ester observed by confocal microscopy increased with an increase in the Sweetose concentration, for a constant concentration of sucrose ester. The observation that the melting enthalpy of transition observed by DSC also increases with sucrose ester concentration was attributed to the increase in the quantity of sucrose ester within the sample which is present in liquid crystalline form. Further discussion of the effect of Sweetose on the water structure and the reasons for these observations appears in Chapter 14.

Figure 6.7b

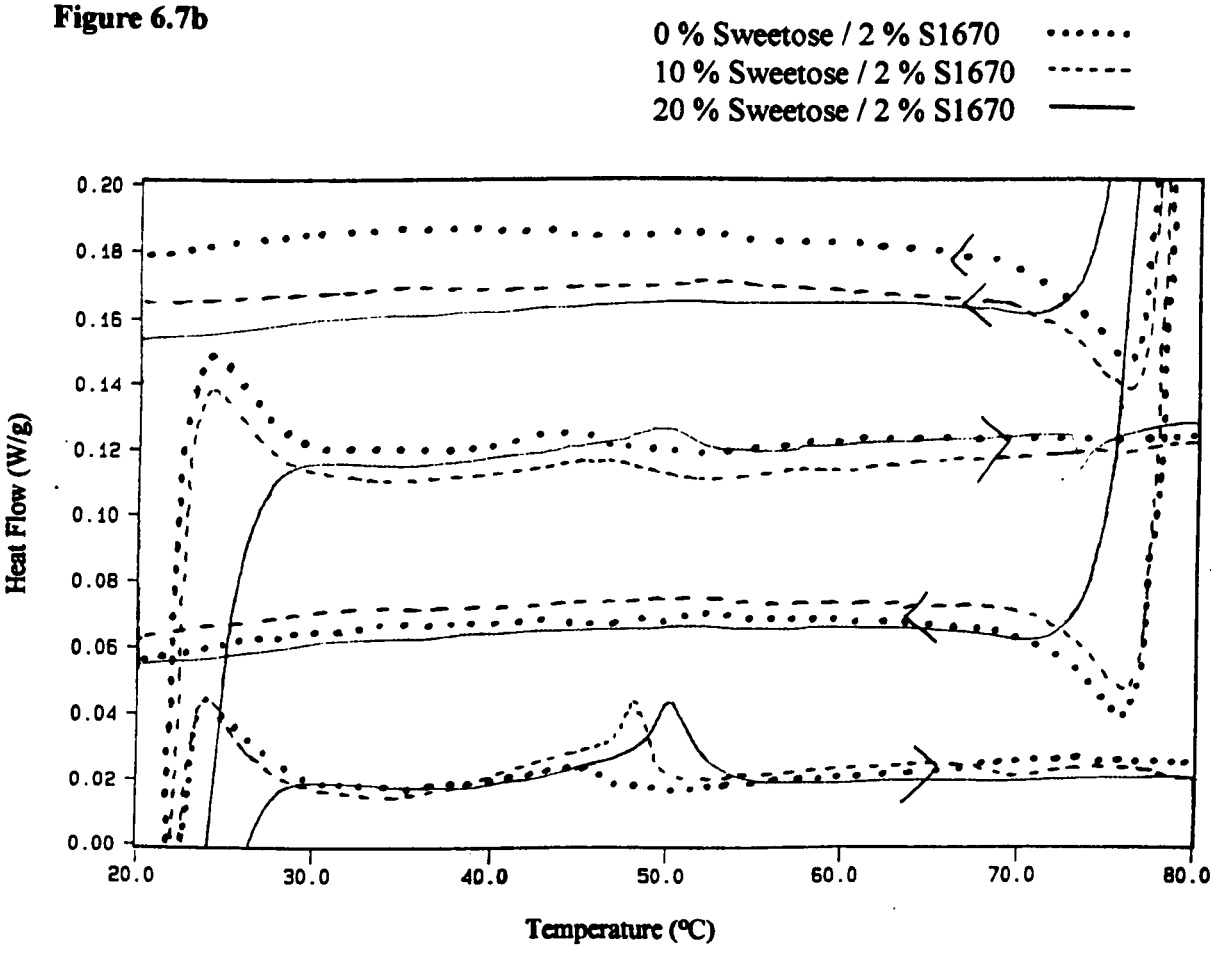

Figure 6.7c

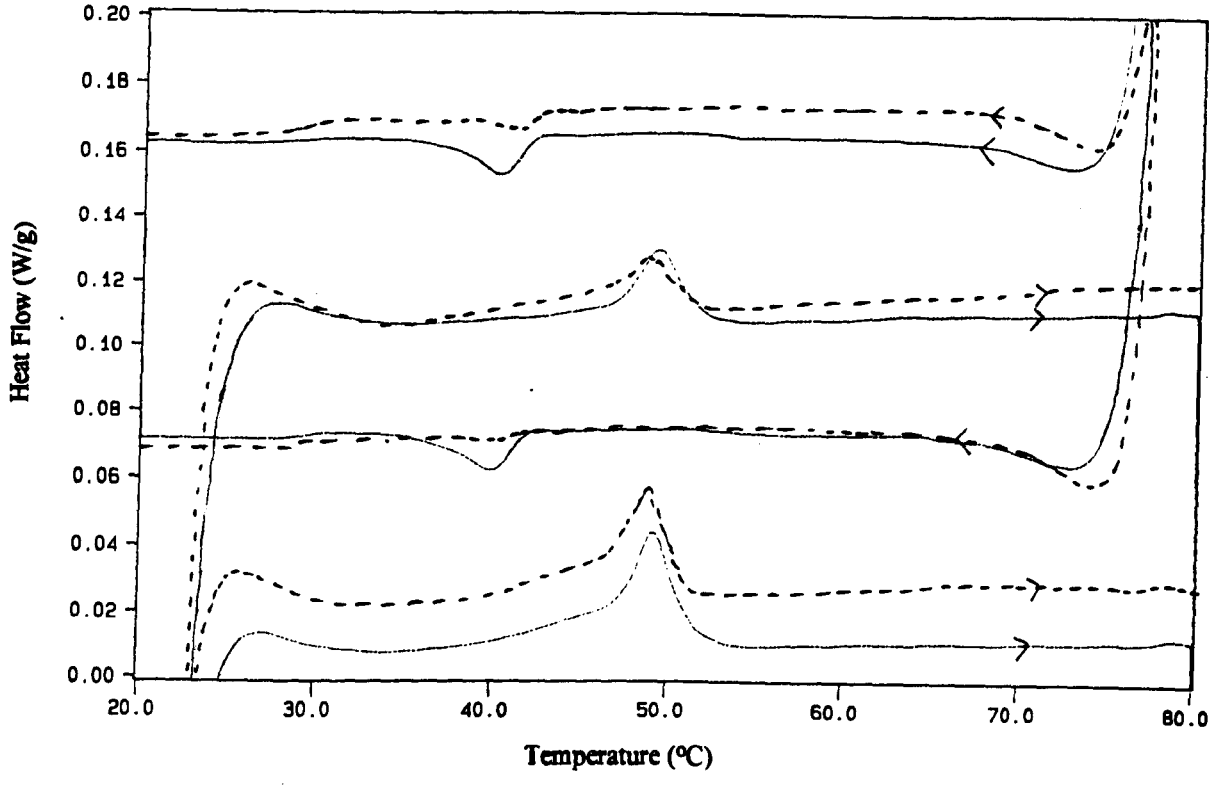

Figure 6.7d

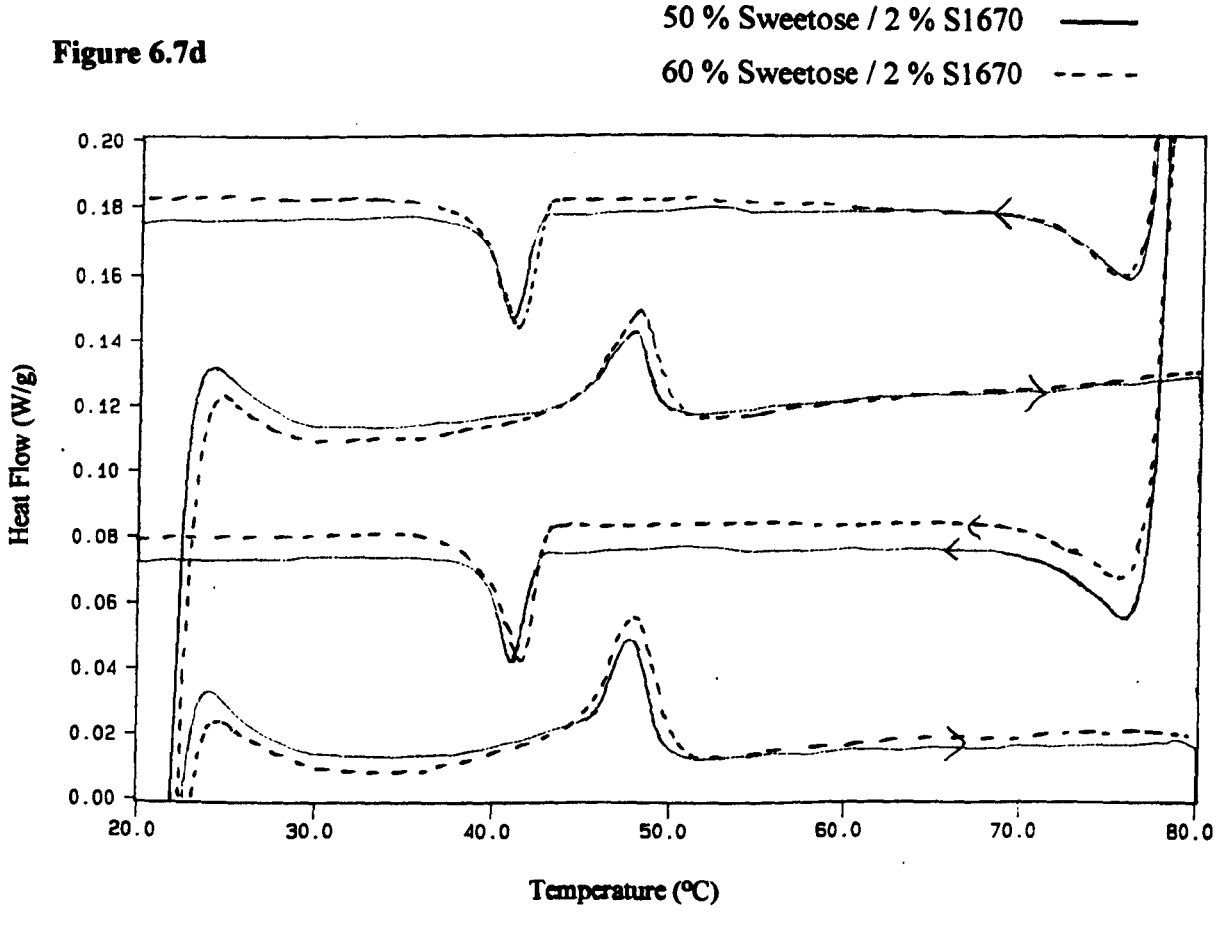

Figure 6.7e

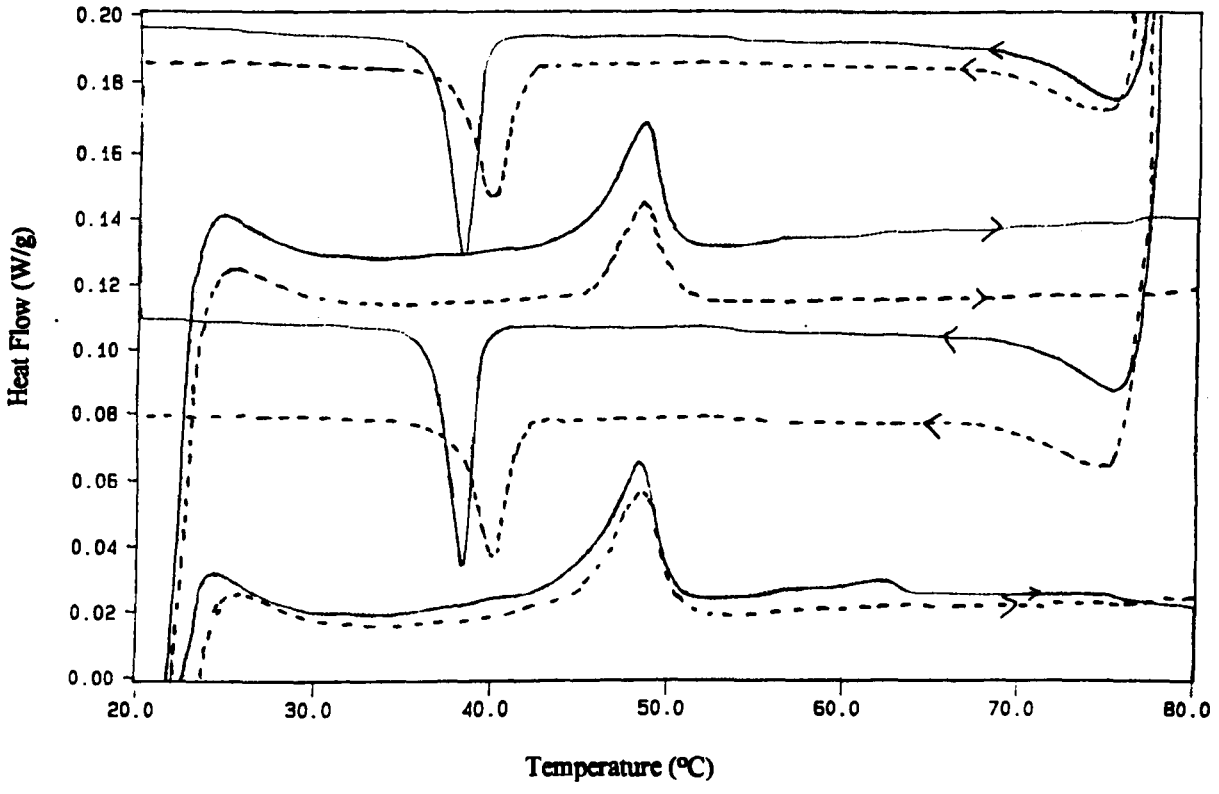
70 % Sweetose / 2 % S1670
80 % Sweetose / 2 % S1670
Heat Flow (W/g)
0.20
0.18
0.16
0.14
0.12
0.10
0.08
0.06
0.04
0.02
0.00
20.0
30.0
40.0
50.0
60.0
70.0
80.0
Temperature (°C)

The enthalpy and temperature of the first endothermic transition for the mixtures containing variable quantities of Sweetose and 2%w/w sucrose ester are illustrated in Figure 6.7f. All samples contained 2% w/w sucrose ester S1670, the difference was solely due to the increased concentration of Sweetose. The endothermic transition temperature remained constant whilst the enthalpy increased with the amount of Sweetose. The enthalpy was normalised to the value per gram of sucrose ester rather than per gram of sample, a factor of 50.

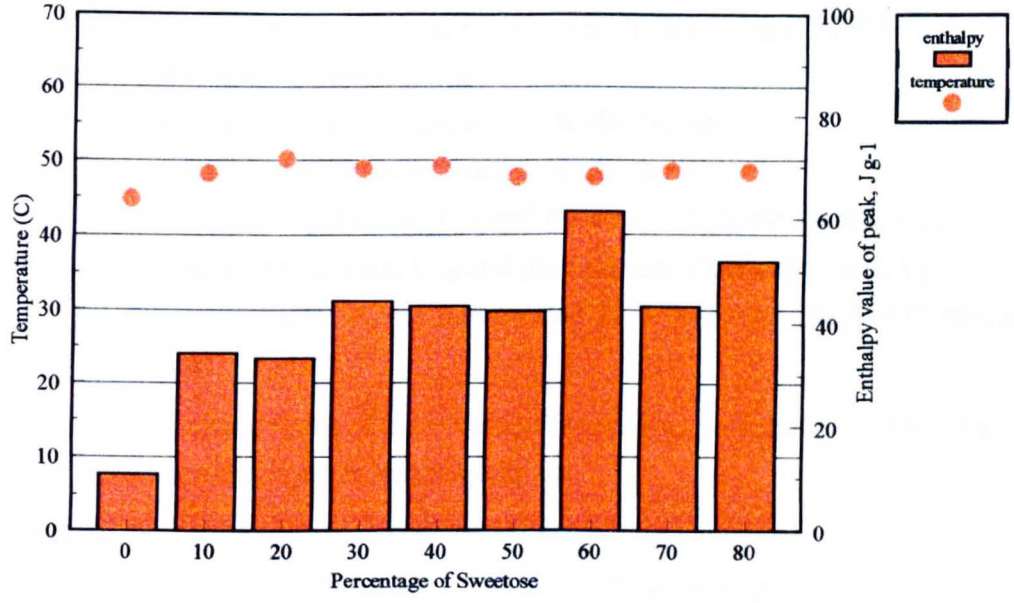

Figure 6.7f

The enthalpy and temperature of the first endothermic transition in samples of 2% w/w sucrose ester mixed with variable concentrations of Sweetose (%w/w).

The table below describes the data in the form of number of peaks observed, temperature (^{o}C) and ΔH value (J g^{-1} sucrose ester in the sample).

Table 6.7a

X % w/w Sweetose / 2 % w/w S1670

SW / S1670	No. of Peaks		1st heat run		rpt heat run		1st cool run		rpt cool run	
sample	*heat*	*cool*	*temp*	*ΔH*	*temp*	*ΔH*	*temp*	*ΔH*	*temp*	*ΔH*
0 / 2	1	0	44.84	11.0	43.30	6.5	-	-	-	-
10 / 2	1	0	48.16	34.5	46.59	15.0	-	-	-	-
20 / 2	1	0	50.15	33.5	49.28	15.0	-	-	-	-
30 / 2	1	1	48.87	44.5	48.77	26.0	-	-	40.70	-1.9
40 / 2	1	1	49.21	43.5	49.24	27.0	39.85	-13.0	40.11	-12.0
50 / 2	1	1	47.77	42.5	47.88	28.0	41.10	-20.5	40.97	-21.5
60 / 2	1	1	47.73	61.5	48.14	42.5	41.47	-31.0	41.35	-30.5
70 / 2	1	1	48.53	43.5	48.70	27.0	40.14	-29.5	39.96	-29.5
80 / 2	1	1	48.42	52.0	48.42	39.5	38.26	-37.0	38.23	-37.5

6.8 75 % w/w Sweetose / 2 % w/w sucrose ester

Non-aerated mixtures of 75%w/w Sweetose with 2%w/w sucrose ester were prepared by heating the sucrose ester with the required amount of water until it was dissolved and combining the solution with the required quantity of Sweetose at 70°C. The mixture was stirred on a magnetic heater stirrer for 4 hours at 70°C. This procedure is more fully described in Chapter 2.

The sucrose esters used were;

- The commercial sucrose esters, S1670 to S270, B1570 and P1570
- pure sucrose mono-stearate, C_{18}
- a 90:10 mixture of pure sucrose mono- to di- stearate
- a 70:30 mixture of pure sucrose mono- to di- stearate
- pure sucrose mono-palmitate, C_{16} and pure sucrose mono-laurate, C_{12}
- pure sucrose mono-caprate, C_{10} and pure sucrose mono-caprylate, C_8
- light and dense fractions of a non-aerated 75% Sweetose 2% S1670 mixture after centrifuging.

The ester composition of each of these sucrose esters was presented in Table 6.1a.
The DSC traces are displayed in Figures 6.8a-h.

Figure 6.8a

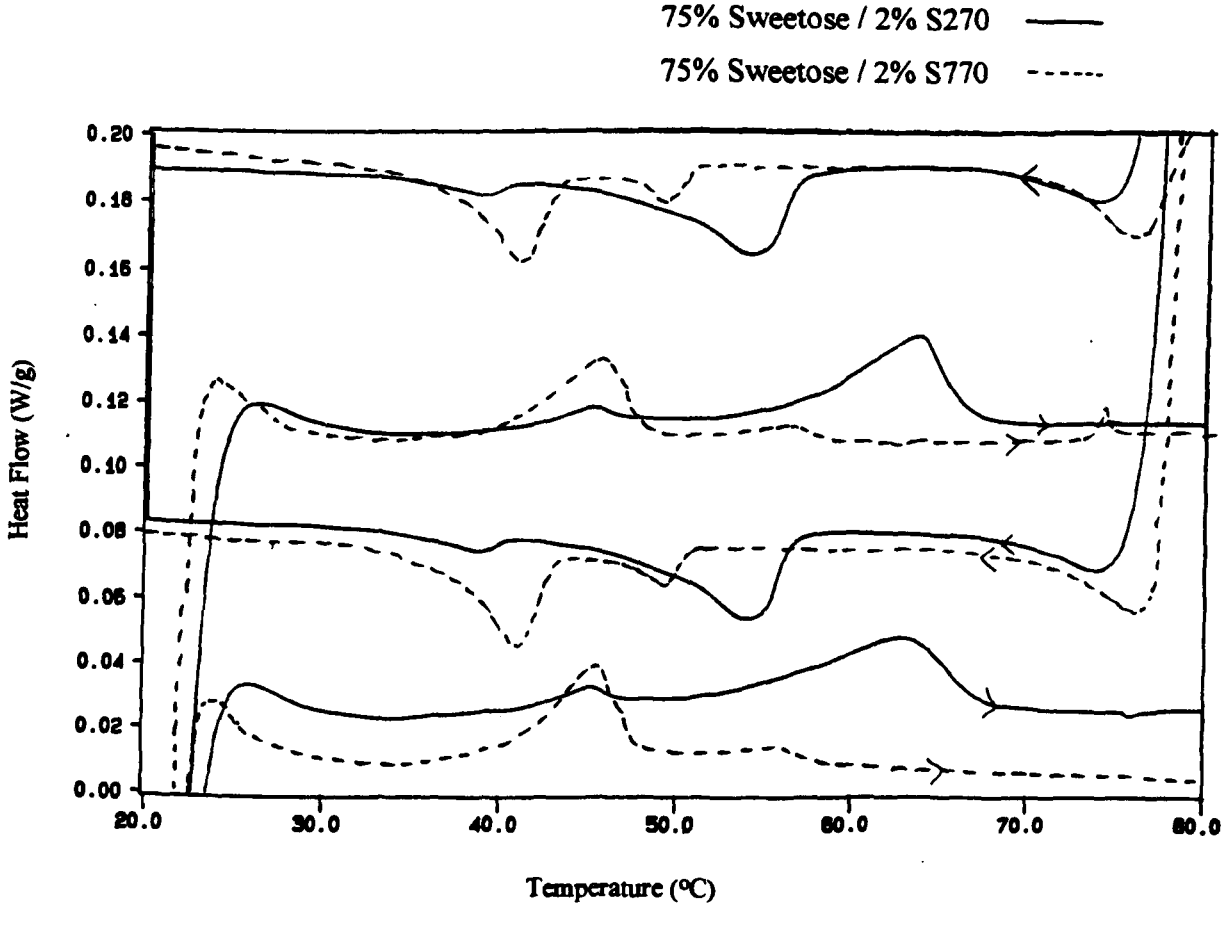

Figure 6.8b

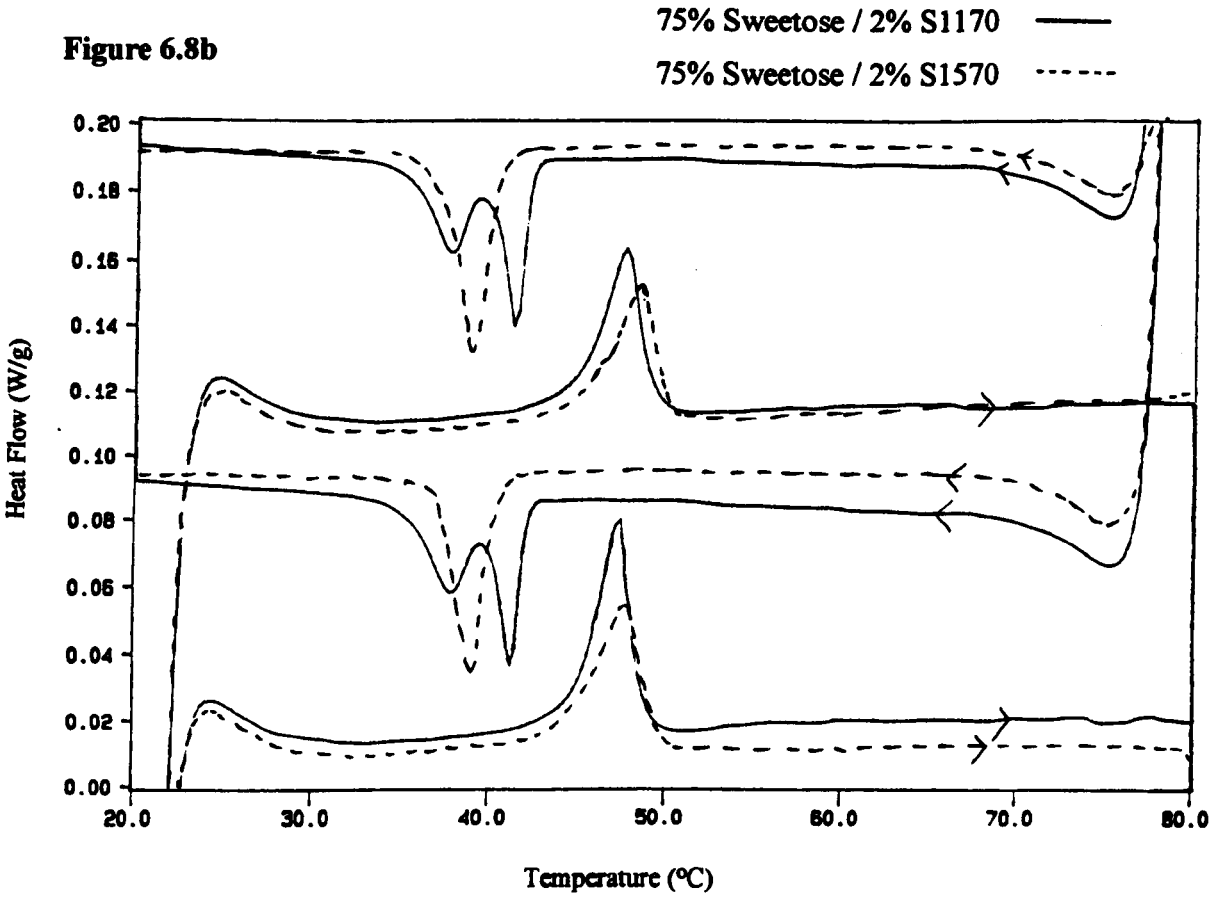

Figure 6.8c

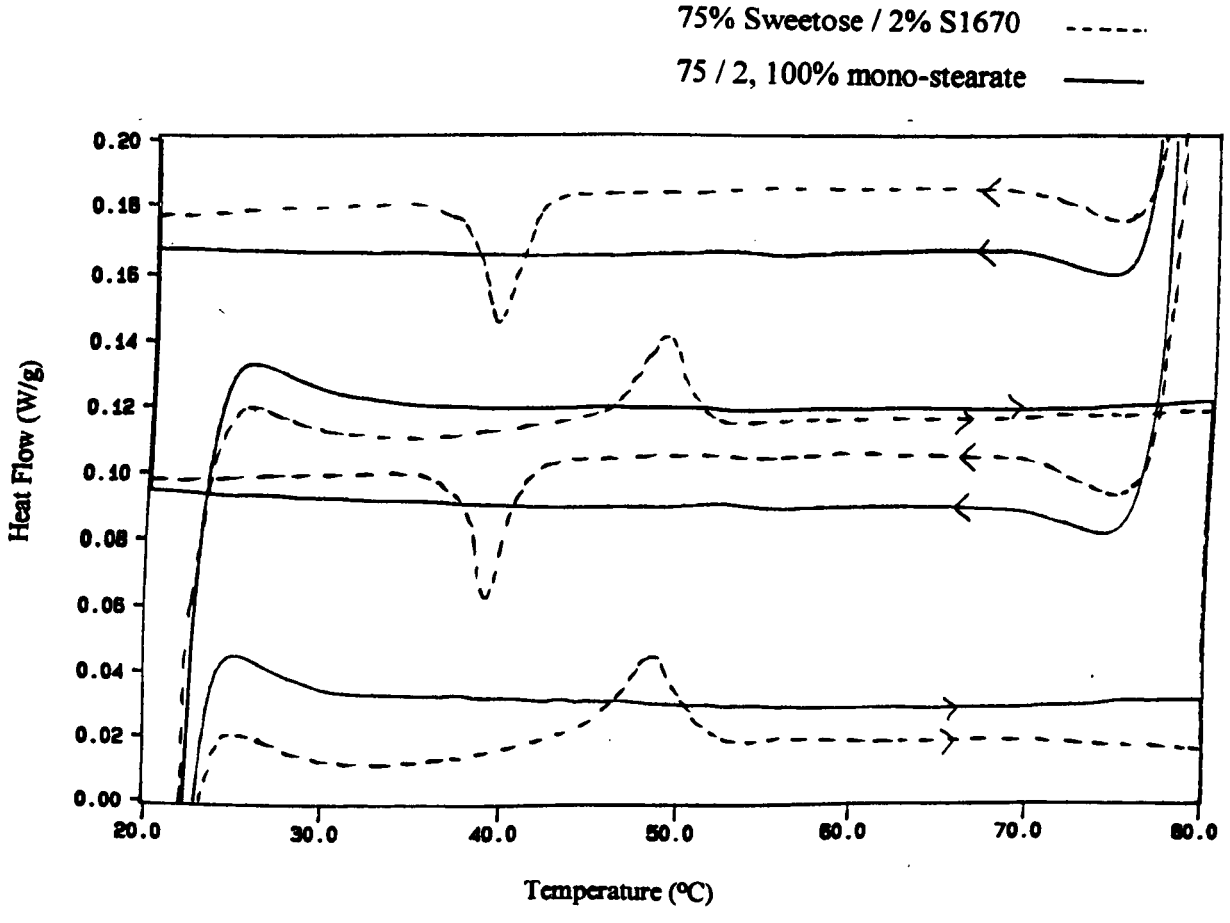

Figure 6.8d

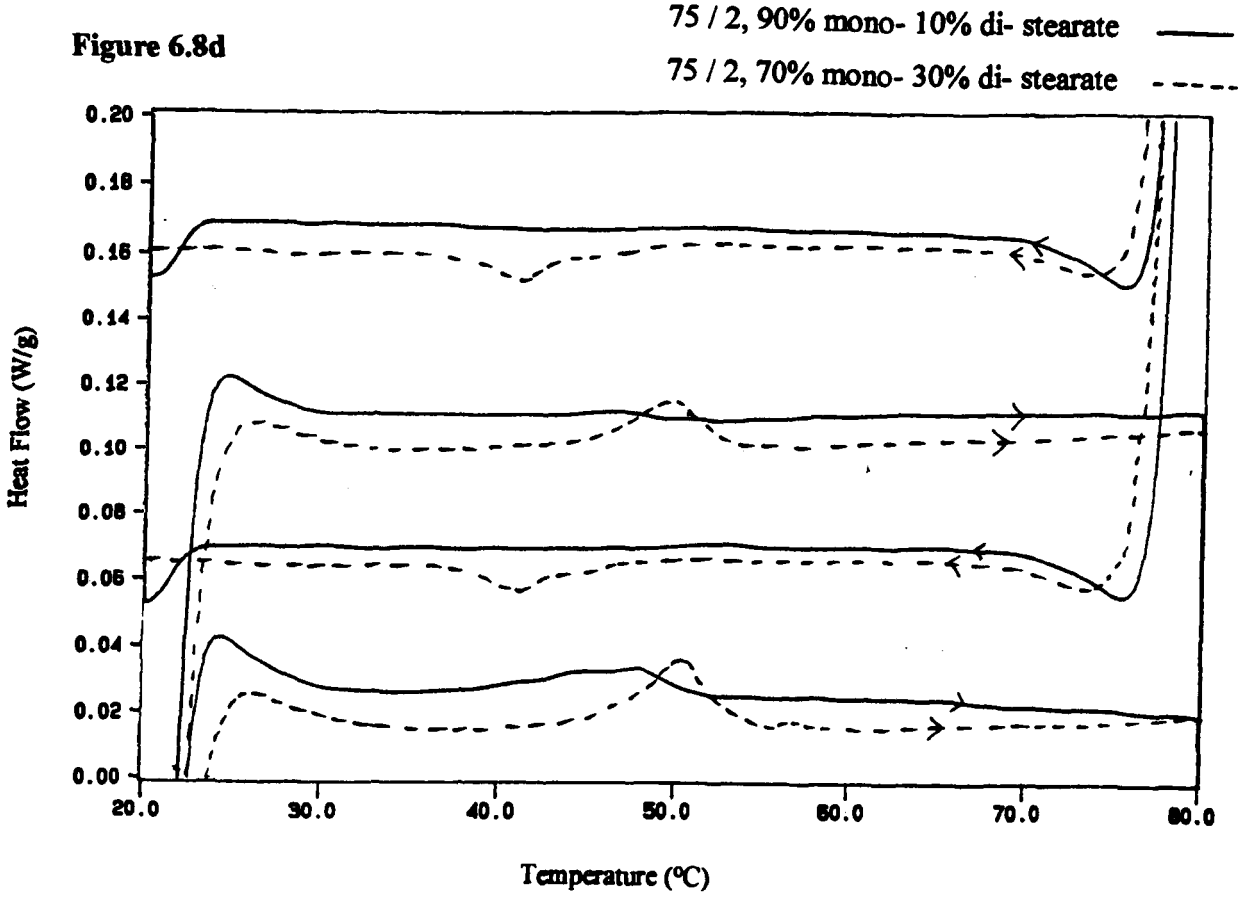

The DSC transitions observed in samples of 75%w/w Sweetose and 2%w/w sucrose ester were all observed to have a slightly lower enthalpy than 20%w/w sucrose ester in water sample. For the purpose of this discussion, 75% Sweetose 2% sucrose ester mixtures will be abbreviated to 75/2.

The phase transitions observed in 75/2 S270 occurred at similar temperatures to 20% w/w solutions of S270 with two distinct endothermic peaks at 45 and 62°C and two exothermic peaks at 38 and 54°C whereas 75/2 S770 resembled more closely that of crystalline than 20%w/w S770, with endothermic peaks at 45 and 56°C and exothermic peaks at 40 and 49°C.

75/2 S1170 had one endothermic peak and two exothermic peaks, at 47, 38 and 41°C respectively, unlike crystalline and 20% w/w S1170 which were single component in both transitions.

75/2 S1570 had a single melting and freezing transition, occurring at 49 and 40°C respectively. S1570 crystals were also one component, however the endothermic peak had a shoulder towards the lower temperature end of the scale, which in 20% w/w S1570 was developed into a separate peak at 46°C, alongside that at 48°C.

75/2 S1670 was single component in both melting and freezing, at 48 and 39°C, similar behaviour to 20% w/w S1670 and unlike crystalline S1670 which displayed two peaks which were attributed to melting, at 50 and 46°C.

75/2 with 100% sucrose mono-stearate did not undergo any detectable phase transition between 20 and 80°C, as found with 20% w/w mono-stearate, which was liquid in this temperature range. This behaviour is very different to crystalline samples of sucrose mono-stearate which melted at 40°C and froze at 30°C due to the solubility of sucrose mono-stearate in aqueous solution.

Sucrose di-stearate is insoluble in aqueous solution and hence it was not possible to compare the trace from a 20% w/w or 75/2 di-stearate sample. Mixtures of 75% Sweetose and 2% sucrose ester were prepared using ratios of mono- to di- stearate of 90/10 and 70/30. Whilst 100% mono-stearate displayed no phase transitions, 90/10 had a small endothermic peak and 70/30 had both an endothermic and exothermic peak.

The results indicate that 75% Sweetose 2% sucrose ester mixtures undergo a phase transition between 20 and 80°C if they contain at least a small quantity of di-stearate. The endothermic phase transition observed occurred at approximately 48°C for all the sucrose stearate samples containing at least 50% mono-ester. This relationship was also apparent in the study of crystalline sucrose stearates of Section 6.3, see Figure 6.3g. Since sucrose di-stearate melted at 62°C the endothermic phase transition observed in 75/2 mixtures at 48°C was not the melting of the pure di-ester component. Sucrose mono-stearate was observed to be soluble in 75/2 mixtures, and as such can have no melting point in this range. Therefore the endothermic transition observed at 48°C must be the melting of the mixture of mono- and di- stearate, described in Section 6.4.

Figure 6.8e illustrates the transition enthalpy and temperature for the first endothermic peak in the commercial sucrose stearates. The mono- and di- ester composition was given in section 6.3. The enthalpy values were normalised to the value per gram of sucrose ester in the sample, a factor of 50.

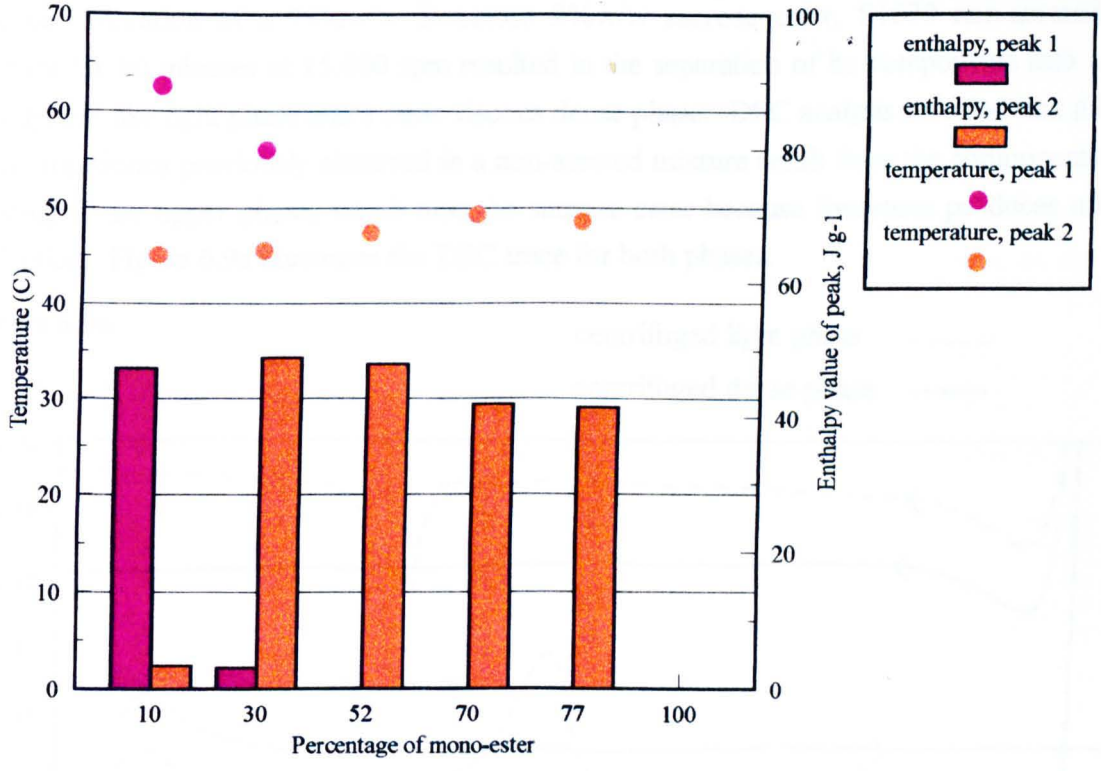

Figure 6.8e

The enthalpy and temperature of the first endothermic transition for 2% w/w sucrose esters containing mono- and di- stearate in 75% w/w Sweetose.

6.9 Centrifugation of a non-aerated 75%w/w Sweetose 2%w/w sucrose ester mixture

The centrifugation of a 75%w/w Sweetose 2%w/w sucrose ester, S1670 non-aerated mixture for 90 minutes at 15,000 rpm resulted in the separation of its components into a cloudy, gel-like light phase and a clear viscous dense phase. DSC analysis revealed that all phase transitions previously observed in a non-aerated mixture result from the components residing in the upper phase, which must be sucrose ester because Sweetose produces nil deflection. Figure 6.9a illustrates the DSC trace for both phases.

Figure 6.9a

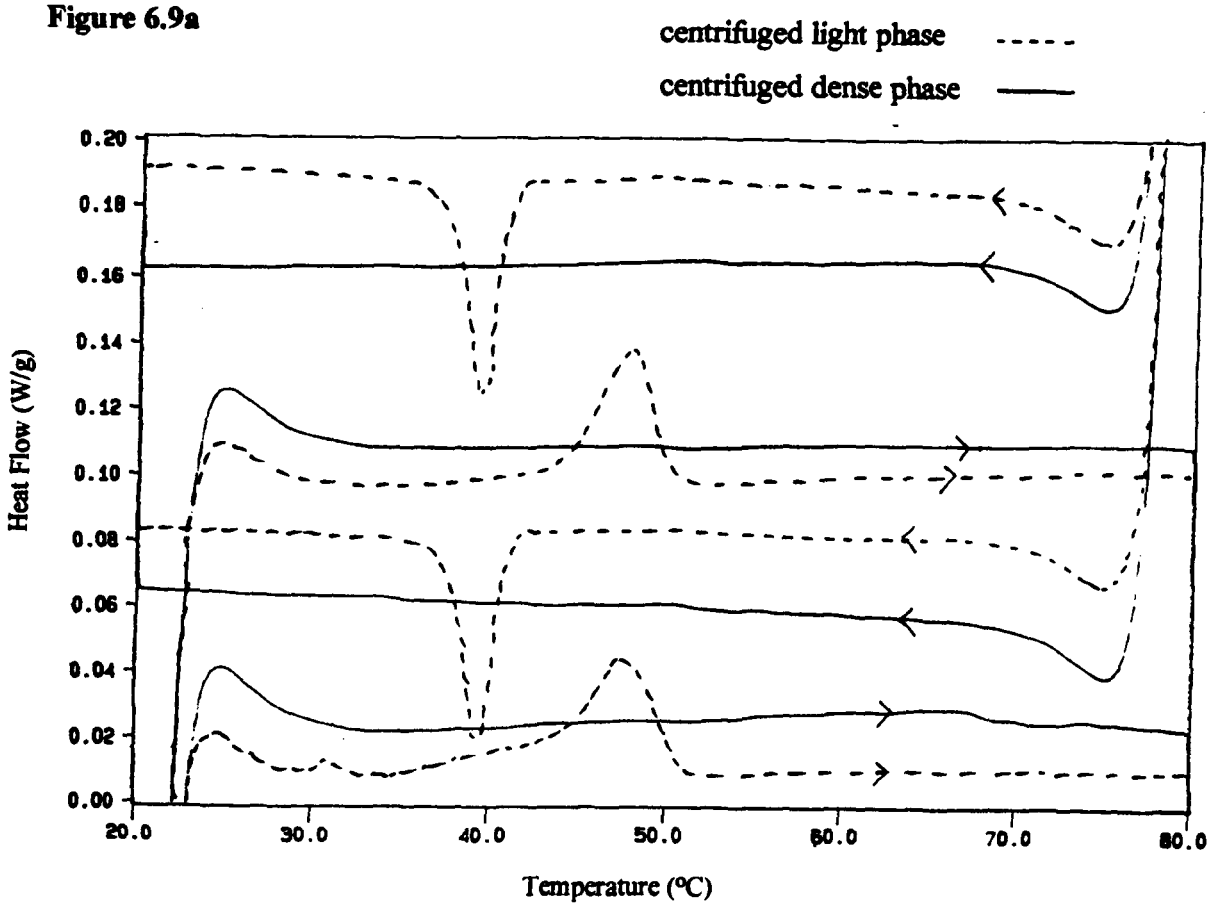

The ester content of the two separate phases was analysed using gel permeation chromatography by D. Mayes at Unilever Research, Colworth Laboratory. Details of the method can be found in the internal Unilever report[3]. The light phase contained all the sucrose ester in the non-aerated mixture, of the total sucrose ester detected in the light phase, 69.5% was mono-, 25.7% was di- and 4.8% was tri- ester, a similar ratio to the 77:20:3 ratio found in S1670. The dense phase did not contain sufficient sucrose ester for analysis and must therefore be an aqueous solution of Sweetose. Sucrose mono-stearate was soluble in water and might have been detected in the aqueous Sweetose layer, since this was not the case it was concluded that all of the sucrose mono-stearate was incorporated in a mixed liquid crystalline phase with the insoluble di- and higher stearates.

6.10 The effect of alkyl chain length on 2%w/w sucrose esters in 75%w/w Sweetose

Figure 6.10a illustrates the phase transitions observed in 75/2 sucrose behenate, B1570 and 75/2 sucrose palmitate P1570, both containing similar ratios of mono-, di- and higher esters.

The phase transitions in 75/2 B1570 occurred between 60 and 70°C, however the exothermic peak was split into two components, whereas in the crystalline and 20% w/w samples it was single. 75/2 P1570 displayed single endo- and exo-thermic peaks, as did both 20% w/w and crystalline P1570.

Figure 6.10a

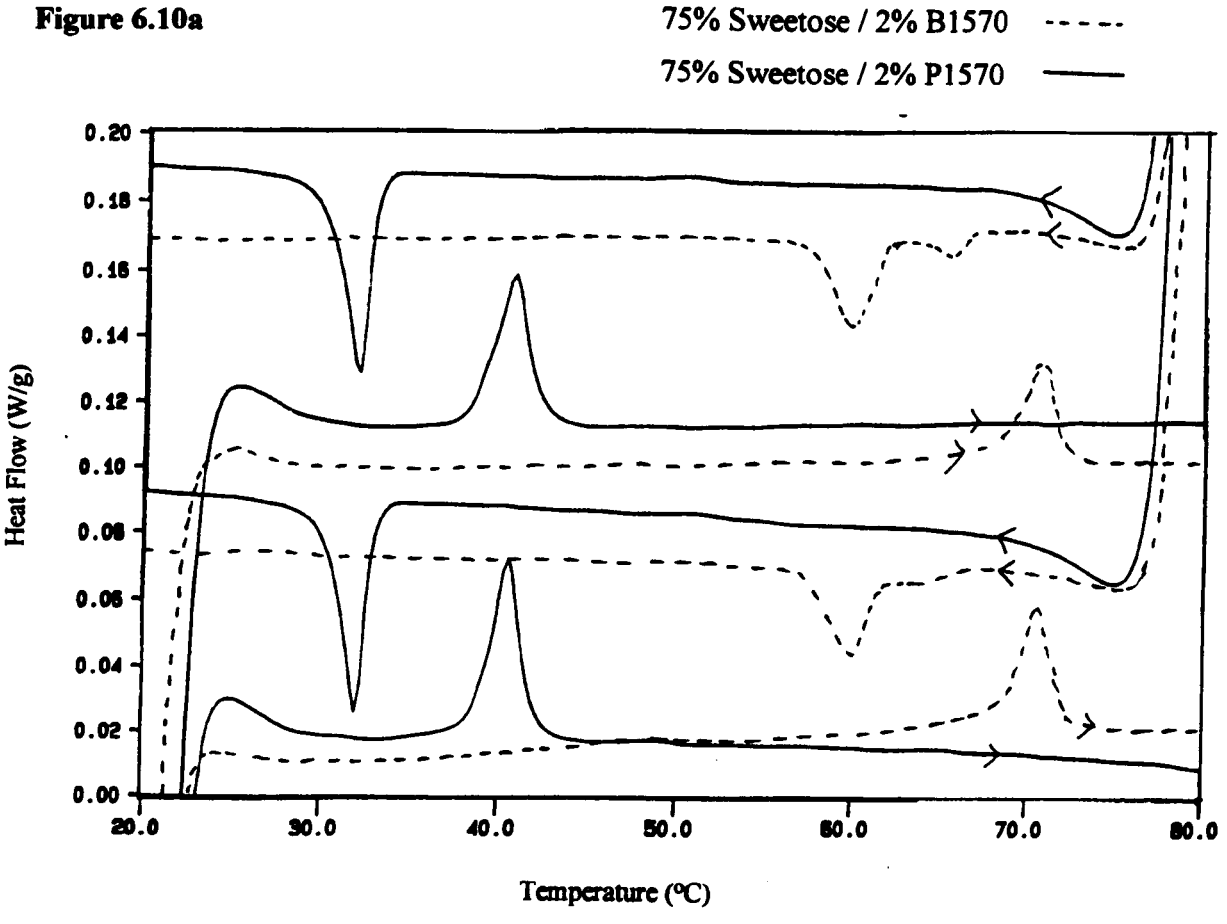

Figure 6.10b illustrates a comparison of the enthalpy and temperature for the first endothermic transition for P1570, S1570 and B1570, a commercial blend of sucrose palmitate, stearate and behenate respectively. All three are blends of mono-, di- and higher esters with similar component ratios; P1570 contains 66:28:6, S1570 contains 70:25:5 and B1570 contains 66:28:7 percent mono- to di- to tri-. The results indicated that both the temperature and the enthalpy of transition increased with alkyl chain length.

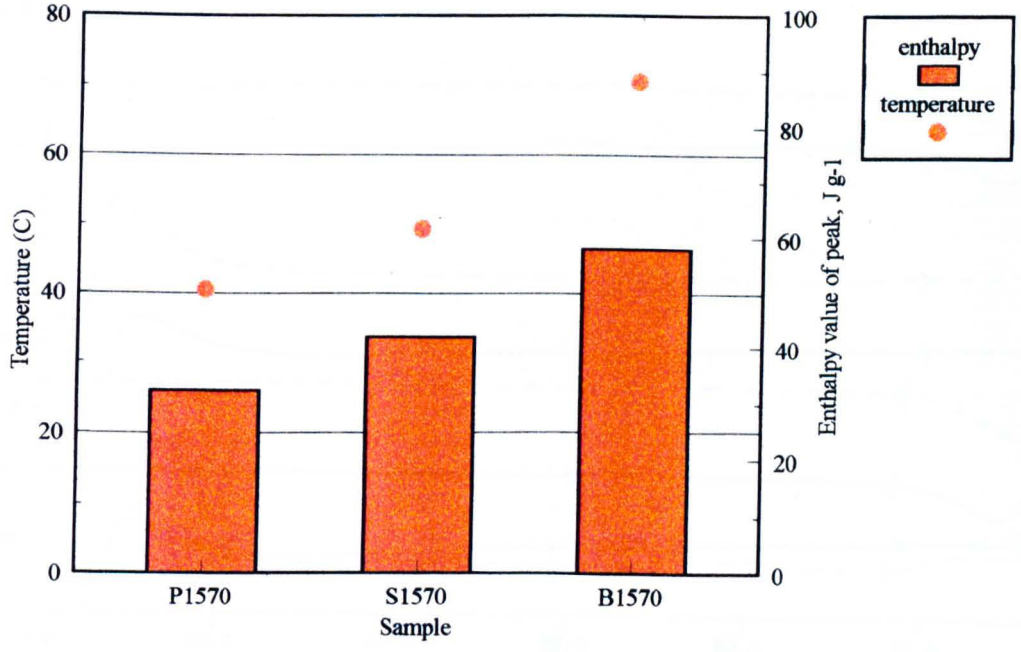

Figure 6.10b

The enthalpy and temperature of the first endothermic transition of 75% Sweetose 2% sucrose ester non-aerated mixtures, comparing the effect of chain length in three samples P1570, S1570 and B1570.

Non-aerated mixtures of 75% Sweetose and 2% sucrose ester were also produced using the sucrose esters, mono-caprylate C_8, mono-caprate C_{10}, mono-laurate C_{12} and mono-palmitate C_{16}, Figures 6.10c&d. All of the samples displayed no phase transition between 20 and 80°C, as was also observed with sucrose mono-stearate. The commercial sucrose palmitate and sucrose stearate, P1570 and S1670, containing mixed mono- and higher esters both displayed phase transitions at temperatures lower than would be expected for di-esters alone, indicating that a portion of di-ester is necessary for the formation of a mixed crystal and thus the observance of a phase transition. Samples containing mixed mono- and higher esters, of sucrose caprylate, caprate and laurate were not available for study and for this reason no conclusion could be drawn about the effect of the alkyl chain length on the phase transition if indeed one would be observed. The trend of decreasing enthalpy and temperature, in the first endothermic transition, with decreased chain length, in B1570, S1570 and P1570, compared in Figure 6.10b, suggests that at shorter chain lengths the phase transition temperature will be below 20°C and therefore no phase transition would be observed.

Figure 6.10c

75 / 2, 100% mono-caprylate (C_8) ——

75 / 2, 100% mono-caprate (C_{10}) - - - -

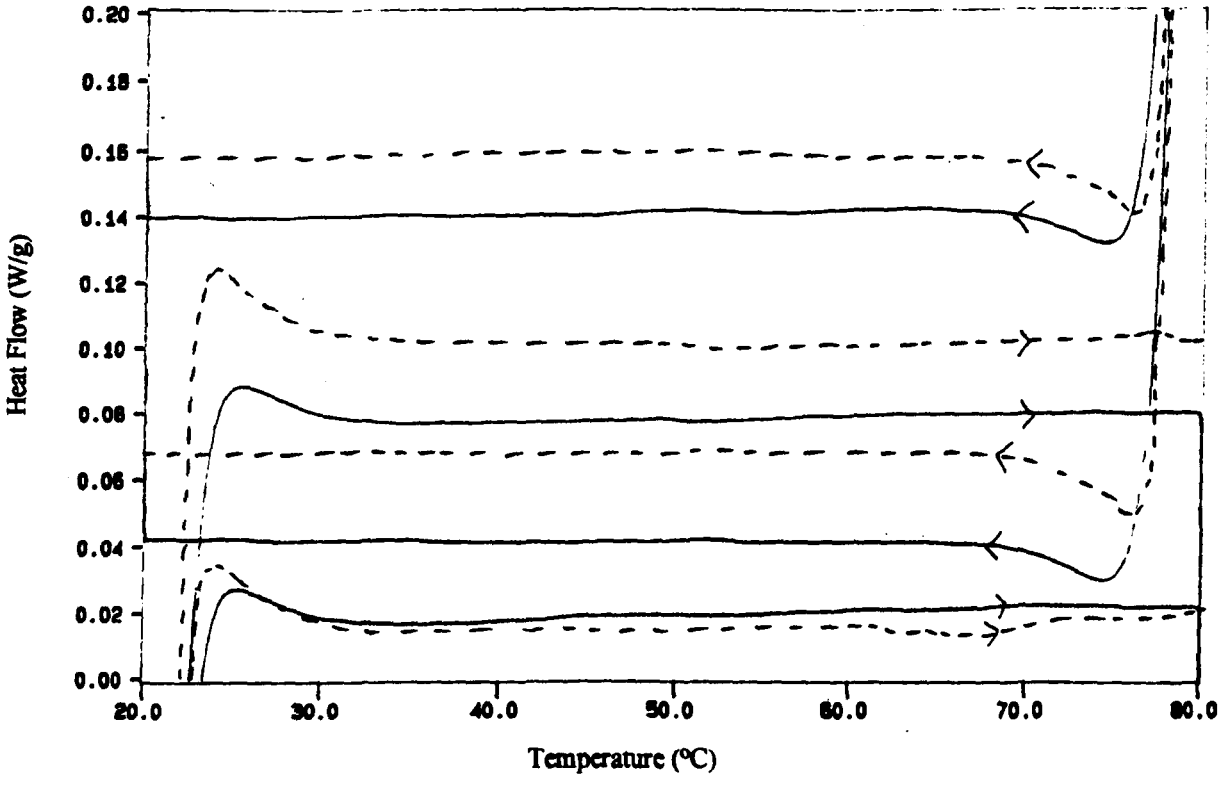

Figure 6.10d

75 / 2, 100% mono-laurate (C_{12}) - - - -

75 / 2, 100% mono-palmitate (C_{16}) ——

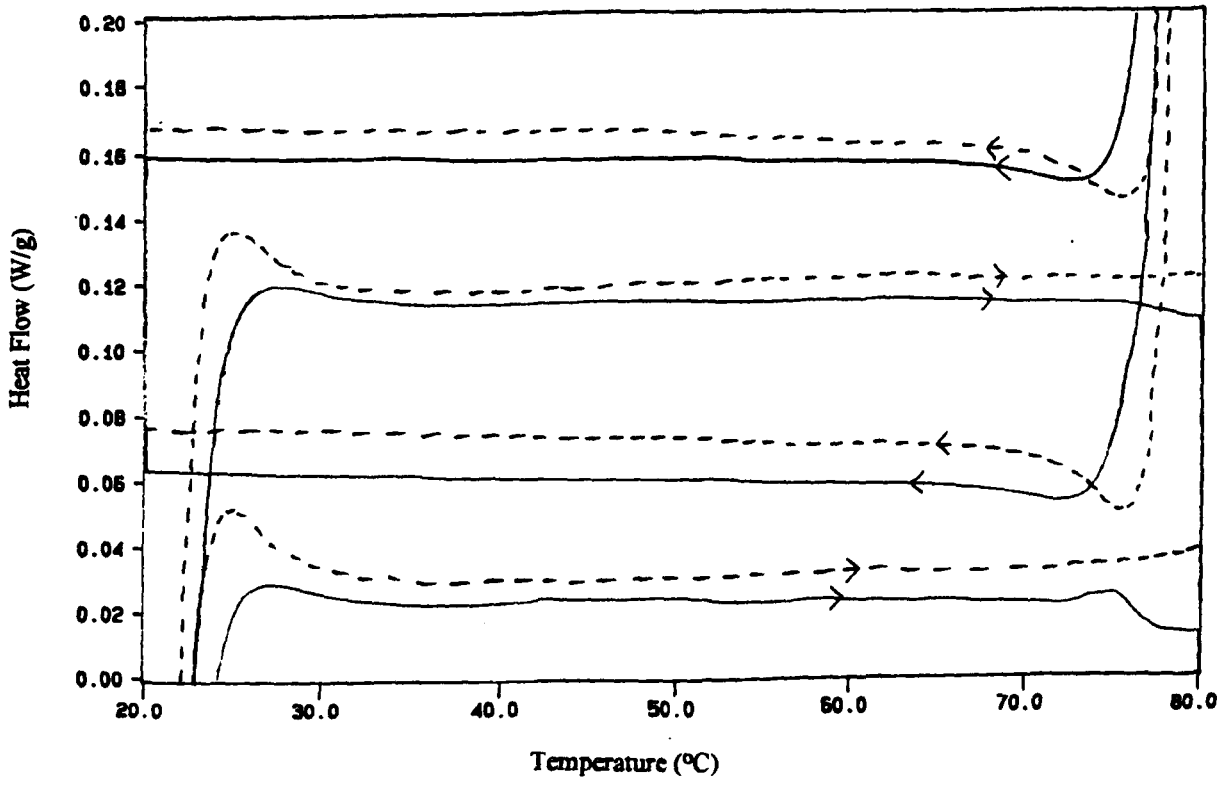

The table below presents the data for all of the 75%w/w Sweetose 2%w/w sucrose ester non-aerated mixtures described above, in the form of number of peaks observed, temperature (°C) and ΔH value (J g^{-1} of sucrose ester within the sample).

Table 6.10a

75 % w/w Sweetose / 2 % w/w sucrose ester

75 / 2	No. of Peaks		1st heat run		rpt heat run		1st cool run		rpt cool run	
sample	*heat*	*cool*	*temp*	*ΔH*	*temp*	*ΔH*	*temp*	*ΔH*	*temp*	*ΔH*
S270	2	2	45.04	3.35	45.09	3.20	38.78	-5.30	38.82	-4.10
			62.62	47.50	63.49	41.00	54.07	-45.50	54.04	-43.00
S770	2	2	45.48	49.00	45.47	total	40.98	total	40.95	total
			56.0	3.10	56.0	39.5	49.2	-47.00	49.2	-50.00
S1170	1	2	47.38	48.00	47.64	44.00	37.9	total	37.9	total
			-	-	-	-	41.26	-47.50	41.35	-47.00
S1570	1	1	49.31	42.00	49.18	28.50	40.33	-31.00	40.34	-31.00
S1670	1	1	48.60	41.50	48.68	31.50	39.22	-28.5	39.30	-27.50
P1570	1	1	40.50	32.5	40.69	31.50	31.89	-35.5	31.88	-35.50
B1570	1	2	70.64	58.00	70.76	62.00	59.86	total	59.82	total
			-	-	-	-	63.9	-68.5	65.8	-66.50
mono-C18	0	0	-	-	-	-	-	-	-	-
90/10 m/di	1	0	47.77	15.50	-	-	-	-	-	-
70/30 m/di	1	1	50.60	25.5	49.67	16.5	41.32	-43.50	41.23	-11.5
mono-C16	0	0	-	-	-	-	-	-	-	-
mono-C8	0	0	-	-	-	-	-	-	-	-
mono-C10	0	0	-	-	-	-	-	-	-	-
mono-C12	0	0	-	-	-	-	-	-	-	-
*cent light	1	1	47.52	0.800	47.93	0.840	39.43	-0.870	39.43	-0.850
cent dense	0	0	-	-	-	-	-	-	-	-

* Enthalpy value per gram of sample.

Work presented in earlier chapters, using TEM and diffraction techniques has shown that, in a 75%w/w Sweetose 2%w/w sucrose ester, non-aerated mixture, the sucrose ester is in a bilayer liquid crystalline arrangement. The melting transition observed in all mixtures containing mono- and higher ester, was therefore attributed to the melting of the alkyl chains within the bilayer into a more disordered arrangement. A more detailed discussion of the nature of this liquid crystalline phase transition appears in Chapter 15.

The previous sections have all been concerned with non-aerated samples of various constitution, the following sections refer only to samples which have been aerated to form gas microcells.

6.11 Aerated samples containing gas microcells

Foams were prepared, as described in Chapter 2, using a mixture of 75% Sweetose and 2% sucrose ester. After two hours aeration the foams contained gas microcells, the exact nature of the surface of these microcells was examined by TEM and the results are described in Chapter 5.

Many foams were prepared, using different sucrose esters:-

- all the commercial sucrose stearates
- sucrose palmitate, P1570 and sucrose behenate B1570
- sucrose mono-stearate, sucrose mono-palmitate
- a 70:30 mix of mono- to di- stearate
- light and dense phases of a naturally drained foam containing sucrose stearate
- sucrose stearate, S1670, at different aeration speeds.
- sucrose stearate with added cholesterol

The phase transitions observed were found to be largely the same as those in the equivalent non-aerated mixtures, an indication that the liquid crystal material in the non-aerated samples remains, but TEM results showed it was not in the same arrangement after aeration. As a result of the similarity, only some of the above samples will be discussed in detail; the aerated 75% Sweetose 2% S1670, the phases of a naturally drained foam, the effects of aeration speed and the addition of cholesterol.

The DSC traces of the remaining samples with a short description are presented towards the end of the section, the data are listed together in Table 6.14a, in the form of temperature, (^{o}C) and enthalpy, (J g^{-1} of sucrose ester in the sample).

Figure 6.11a illustrates the DSC measurements of an aerated and a non-aerated 75%w/w Sweetose 2%w/w S1670 mixture, the data are in Table 6.11a. Both had a melting peak at 48^{o}C and a freezing peak at 39^{o}C, however the enthalpy of the first melting peak in the aerated sample was lower than that of the non-aerated sample, the repeat freezing peaks were identical.

Table 6.11a

75 / 2	No. of Peaks		1st heat run		rpt. heat run		1st cool run		rpt. cool run	
S1670 sample	*heat*	*cool*	*temp*	*ΔH*	*temp*	*ΔH*	*temp*	*ΔH*	*temp*	*ΔH*
aer	1	1	46.83	8.05	47.67	30.55	39.35	-24.95	39.79	-34.4
non-aer	1	1	48.60	41.5	48.68	31.5	39.22	-28.5	39.30	-27.5

Figure 6.11a

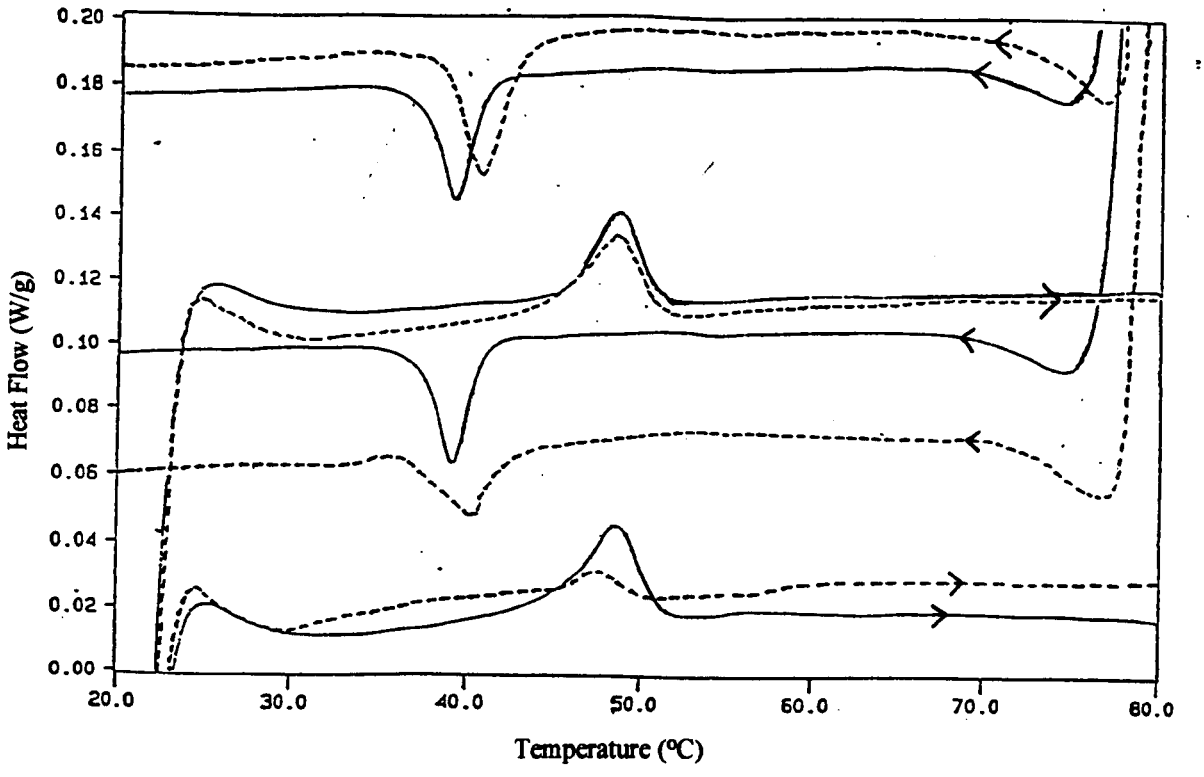

The identical phase transition temperature and similar enthalpy of transition in both cases suggested that the same transition was occurring before and after aeration. The first endothermic transition in the aerated sample was smaller than that of the non-aerated sample but after heating to 80°C and cooling to 20°C and re-heating the transition was identical. Heating an aerated sample to 80°C is sufficient to melt the chains in the sucrose ester and give them the mobility required to leave the microcell surface and enter the bulk where they can reform bilayers on cooling. Re-heating would thus be no different from heating a sample that had not been previously aerated. If the phase transition was due to liquid crystalline sucrose ester, as suggested, then this liquid crystal material must also be present in the aerated sample. The lower enthalpy of the first melting peak was attributed to the material being present as a monolayer at the gas cell surface with the alkyl chains having contact only with their neighbour and not with the other half of a bilayer. The enthalpy required to cause chain melting within a monolayer is intuitively less than that required for the same process within the interior of a bilayer hence the low enthalpy observed on the first heating of the microcells. If this liquid crystalline material melted on heating and returned to the bulk where it formed bilayers on cooling, then the enthalpy observed on re-heating would be no different to that observed on heating a previously non-aerated sample, thus explaining the difference between the traces for non-aerated and aerated 75% Sweetose 2% sucrose ester, S1670.

Foams containing gas microcells remained stable for up to 1 year when stored at 4°C, if however they were stored at room temperature, 20°C, they drained very slowly until, after 6 months there was an obvious clear liquid beneath the white foam layer. Samples of the clear liquid and the surviving foam layer were removed and any phase transitions between 20 and 80°C were measured by DSC, as before, Figure 6.11b. The data are given in Table 6.11b. In addition to the DSC analysis, gel permeation chromatography was used to determine the sucrose ester content of both light and dense phases.

Figure 6.11b

75 / 2 naturally drained foam light phase ——

75 / 2 naturally drained foam dense phase - - - -

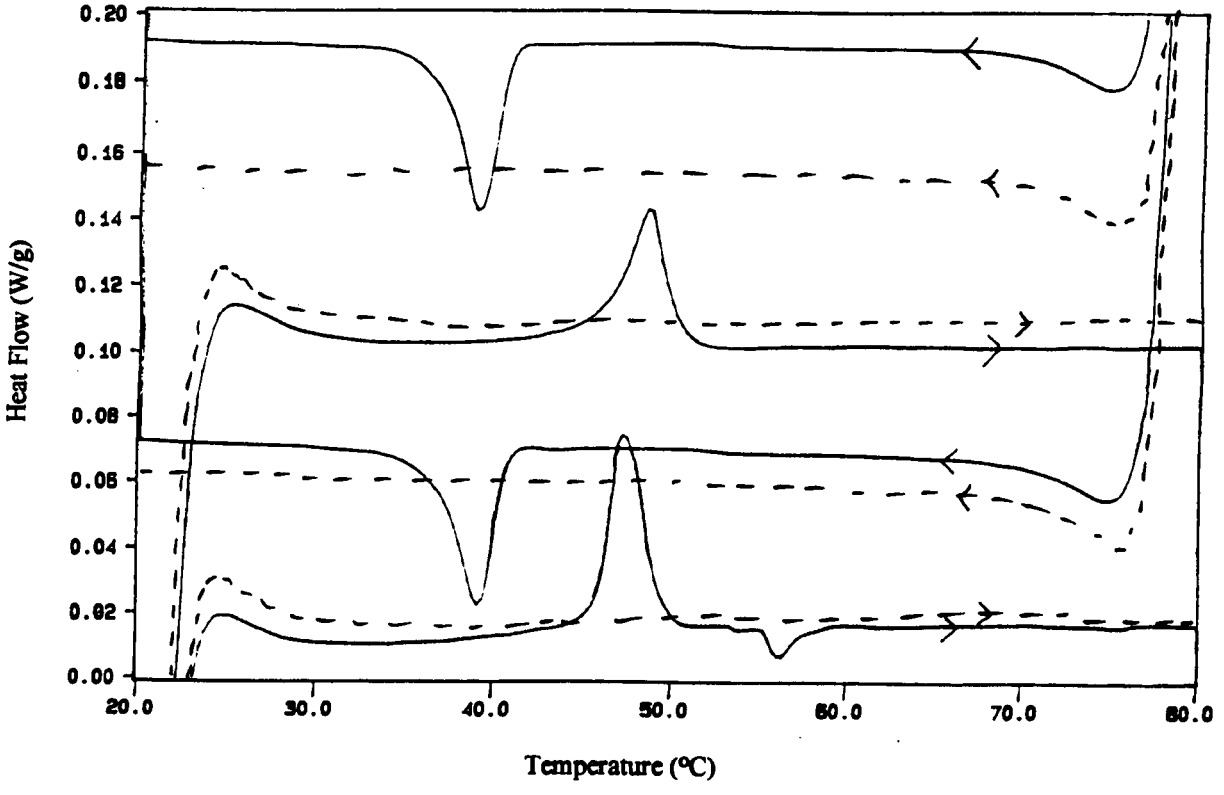

Table 6.11b

75 / 2	No. of Peaks		1st heat run		rpt. heat run		1st cool run		rpt. cool run	
sample	*heat*	*cool*	*temp*	*ΔH*	*temp*	*ΔH*	*temp*	*ΔH*	*temp*	*ΔH*
drain light	1	1	47.29	41.15	48.56	37.15	39.12	-38.65	38.97	-40.50
drain dense	0	0	-	-	-	-	-	-	-	-

The foam fraction melted at 48°C and froze at 39°C. These temperatures were the same as those of a standard preparation of aerated 75% Sweetose 2% S1670. The lower fraction showed no measurable phase transitions. Gel permeation chromatography, courtesy of D. Mayes[3] at Unilever Research, Colworth Laboratory, revealed that the light

phase contained all of the sucrose ester within the sample. Of the total amount of sucrose ester detected, 71.7% was mono-, 23% was di- and 5.3% was tri- ester, this ratio is similar to that of the S1670 used in the preparation, i.e. 77% mono-, 20% di- and 3% tri- ester. No sucrose ester was detected in the dense liquid, most likely to be Sweetose solution. The results of the separation of the upper and lower fractions of a drained foam were similar to those of the upper and lower fractions of a non-aerated mixture, after centrifuging to achieve separation, as seen previously, in Figure 6.9a.

6.12 The effect of aeration speed on mixtures of 75 % w/w Sweetose and 2 % w/w S1670

The effect of aeration speed on the volume fraction of gas incorporated during aeration is described in Chapter 10; slow aeration speeds were observed to have a negligible effect on the gas microcells and the resulting phase volume but fast speeds result in rapid aeration followed by an increase in observed viscosity and a very rapid decrease in phase volume. This increased viscosity was attributed to the loss of water vapour through evaporation by the increased agitation of the mixture. 75%w/w Sweetose 2%w/w sucrose ester S1670 gas microcells were prepared by the method described in Chapter 2 with the exception that the aeration speed and time was varied as follows:-

- 2 hours at speed 1, 120 rpm.
- 6 minutes at speed 3, 750 rpm
- 90 minutes at speed 3, 750 rpm.

These were compared with a standard preparation of gas microcells which lasts for 2 hours at speed 2, 324 rpm.

DSC traces are displayed in Figures 6.12a&b. The table below describes the data in the form of number of peaks observed, temperature (°C) and enthalpy value (J $g^{-1}$of sucrose ester in the sample).

Table 6.12a

75 % w/w Sweetose / 2 % w/w S1670 / aeration speed

Speed &	No. of Peaks		1st heat run		rpt heat run		1st cool run		rpt cool run	
Time	*heat*	*cool*	*temp*	*ΔH*	*temp*	*ΔH*	*temp*	*ΔH*	*temp*	*ΔH*
6 min sp. 3	1	1	46.83	29.55	47.44	27.6	39.06	-25.65	38.68	-28.40
1.5 hr's sp. 3	1	1	47.23	18.35	48.12	43.85	36.91	-46.40	37.49	-48.55
* 2 hr's sp. 2	1	1	46.83	8.05	47.67	30.55	39.35	-24.95	39.79	-34.40
2 hr's sp. 1	1	1	45.85	19.05	46.95	26.80	39.39	-27.30	39.01	-33.15

* A standard prep, illustrated in Figure 6.11a

All samples contained 75% w/w Sweetose and 2% w/w S1670, hence any differences should only be due to the aeration process. All phase transitions occurred at temperatures

characteristic of S1670 and in all cases the enthalpy of the first endothermic peak was larger than that of the second and the two exothermic peaks were of equal size.

6 minutes at speed 3, and 2 hours at speeds 2 and 1 produced gas microcells with similar phase transition profiles, that is with a single endo- and exo- thermic peak, at 48 and 39°C respectively. 90 minutes at Speed 3 however produced transitions with a greater enthalpy. The initially low water concentration meant a large percentage of the whole can be lost through evaporation and hence the weight fraction of sucrose ester increases dramatically, with a consequent increase in the enthalpy required for melting.

Figure 6.12a

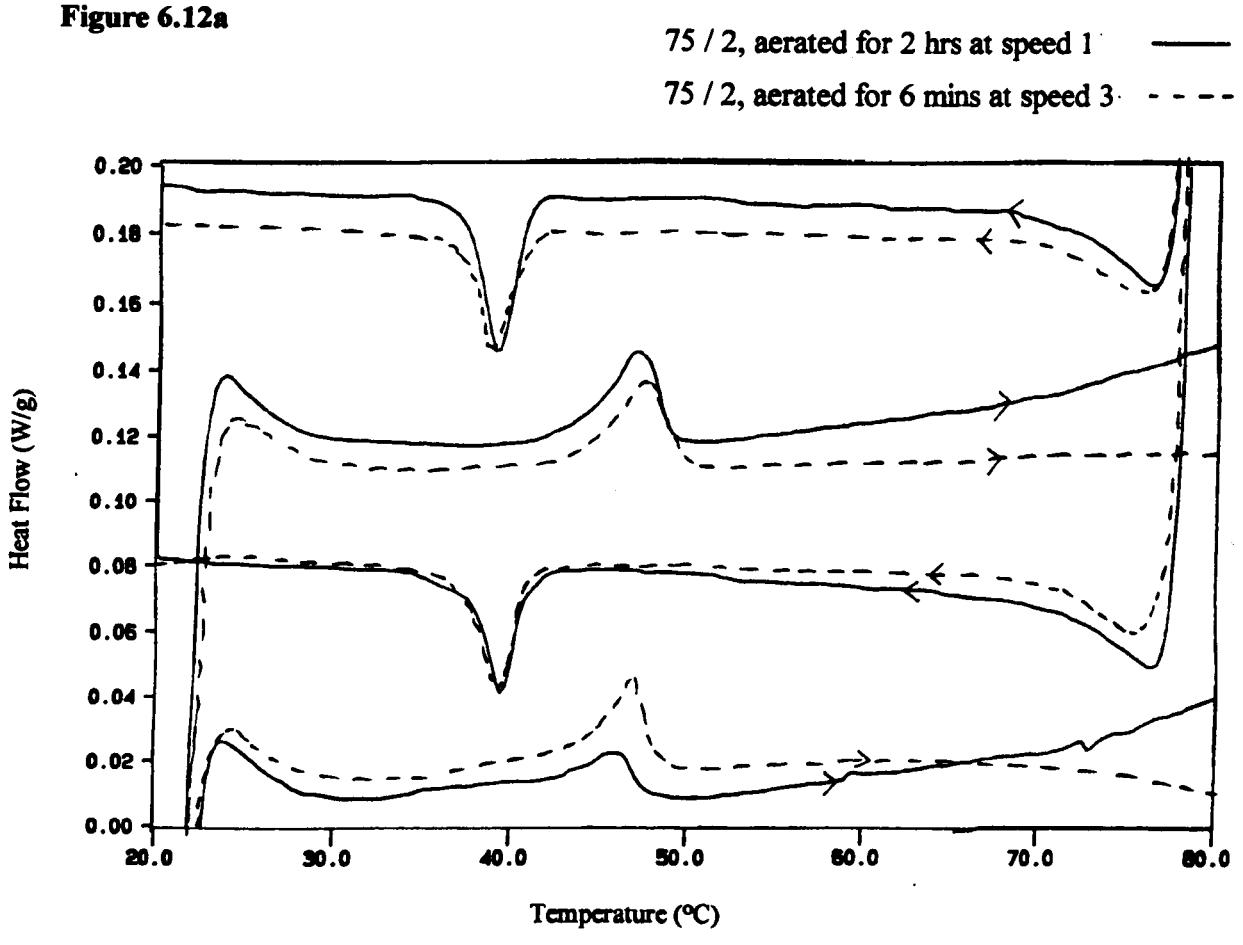

Figure 6.12b

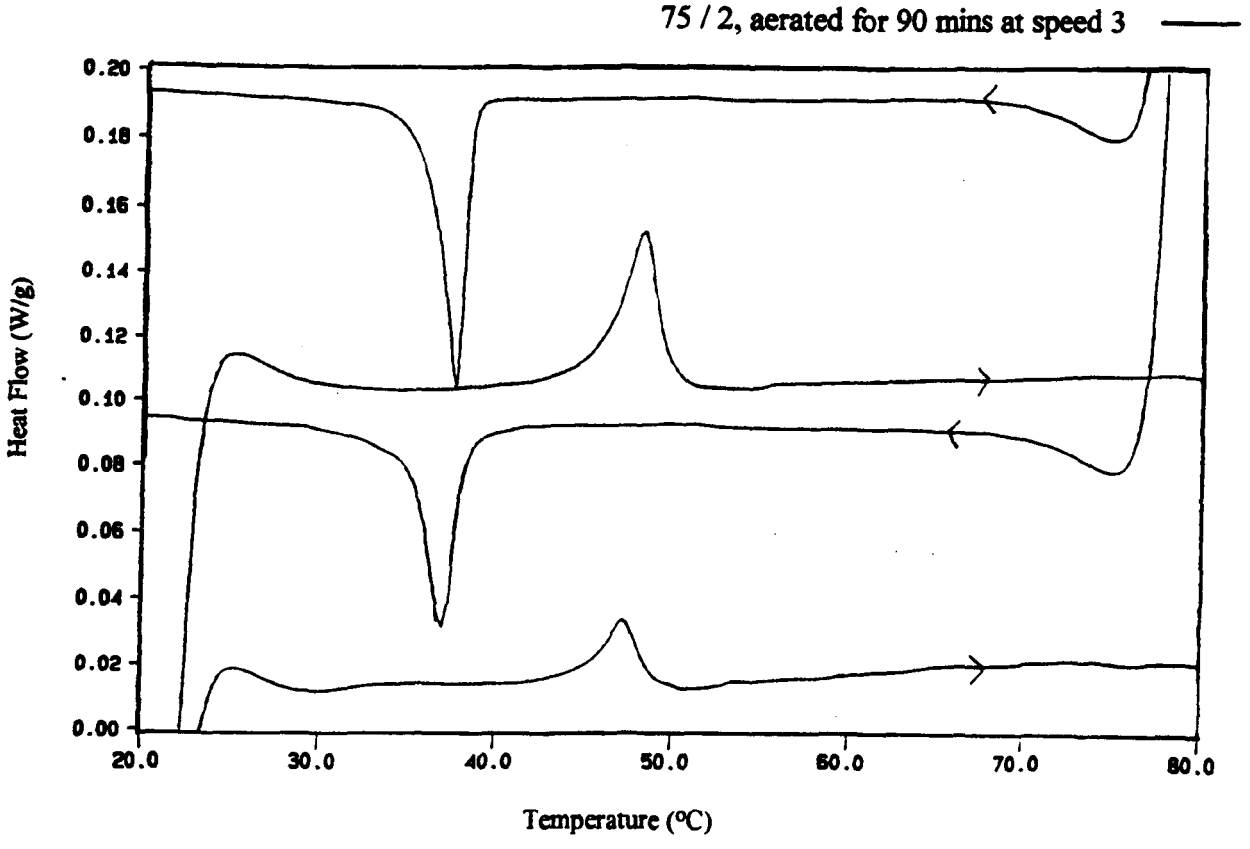

6.13 The addition of cholesterol to 75% Sweetose 2% sucrose ester before aeration

Cholesterol is known[2,4,5,6] to affect the interplanar spacing between alkyl chains in a bilayer. According to Rothman and Engelman[7] the first six or seven carbon atoms from the head group of the amphiphile which are in contact with the bulky cholesterol molecule become more ordered whilst those carbon atoms further down the chain become more fluid, but the overall effect is to increase the spacing between the chains and the layer becomes more fluid. In Chapter 5 (TEM), cholesterol was observed to cause the disruption of the regular geodesic domains on the surface of the gas microcells. If the surface of a microcell contains an ordered monolayer of sucrose ester and the addition of cholesterol disrupts the close packing then the monolayer can be expected to become less ordered and the temperature and enthalpy of the order-disorder, or chain melting, transition observed by DSC will be reduced. The effect of cholesterol addition on the phase transition temperature was observed for 75% Sweetose 2% sucrose ester samples, in which the 2% w/w sucrose ester component was made up of sucrose ester and cholesterol in the ratios, 95/5, 85/15 and 70/30.

The DSC traces are given in Figures 6.13a-c. The phase transition temperature for the endothermic peak in a mixture containing no cholesterol was 46°C. The figures show that the temperature and enthalpy of this transition decreased with cholesterol concentration. In the 70/30 sample no phase transition was observed, indicating that the alkyl chains had become more fluid and were above their chain melting temperature.

Figure 6.13a 2% w/w sucrose ester made up of 95:5, S1670:cholesterol

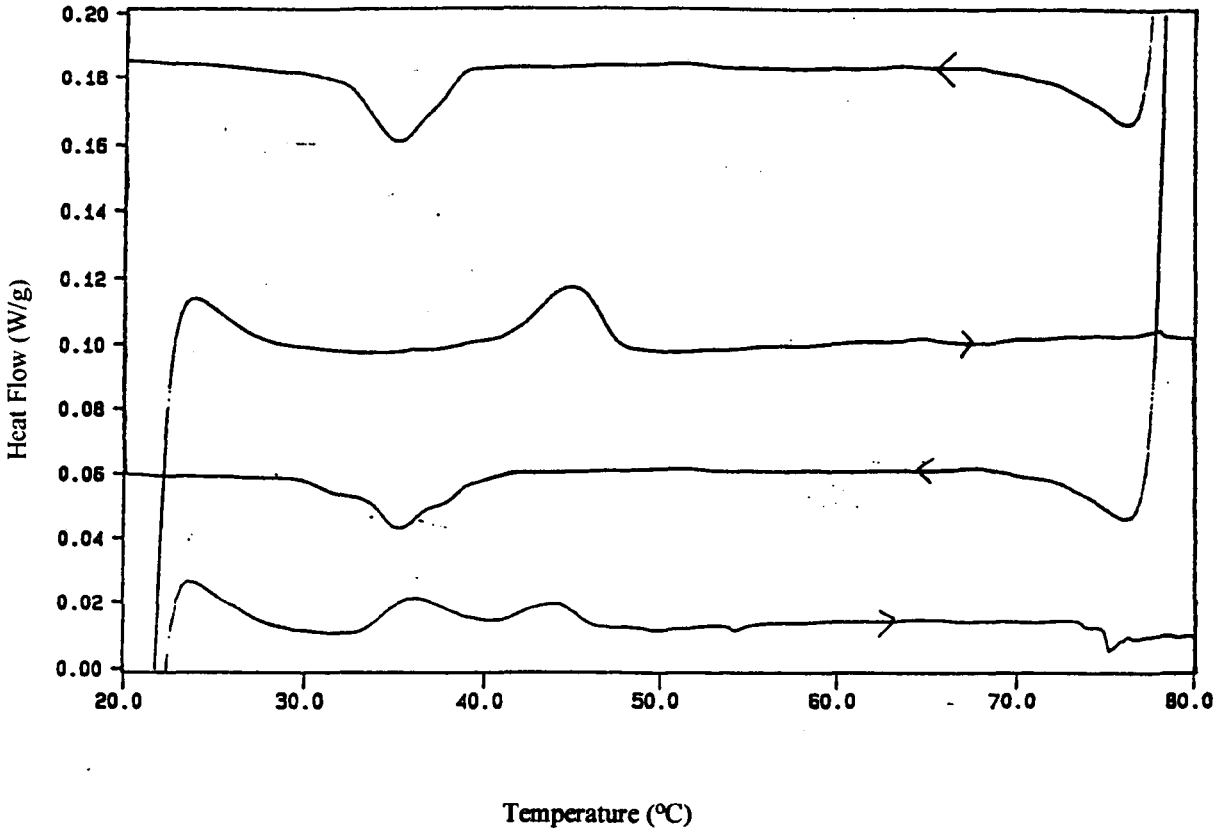

Figure 6.13b 2% w/w sucrose ester made up of 85:15, S1670:cholesterol

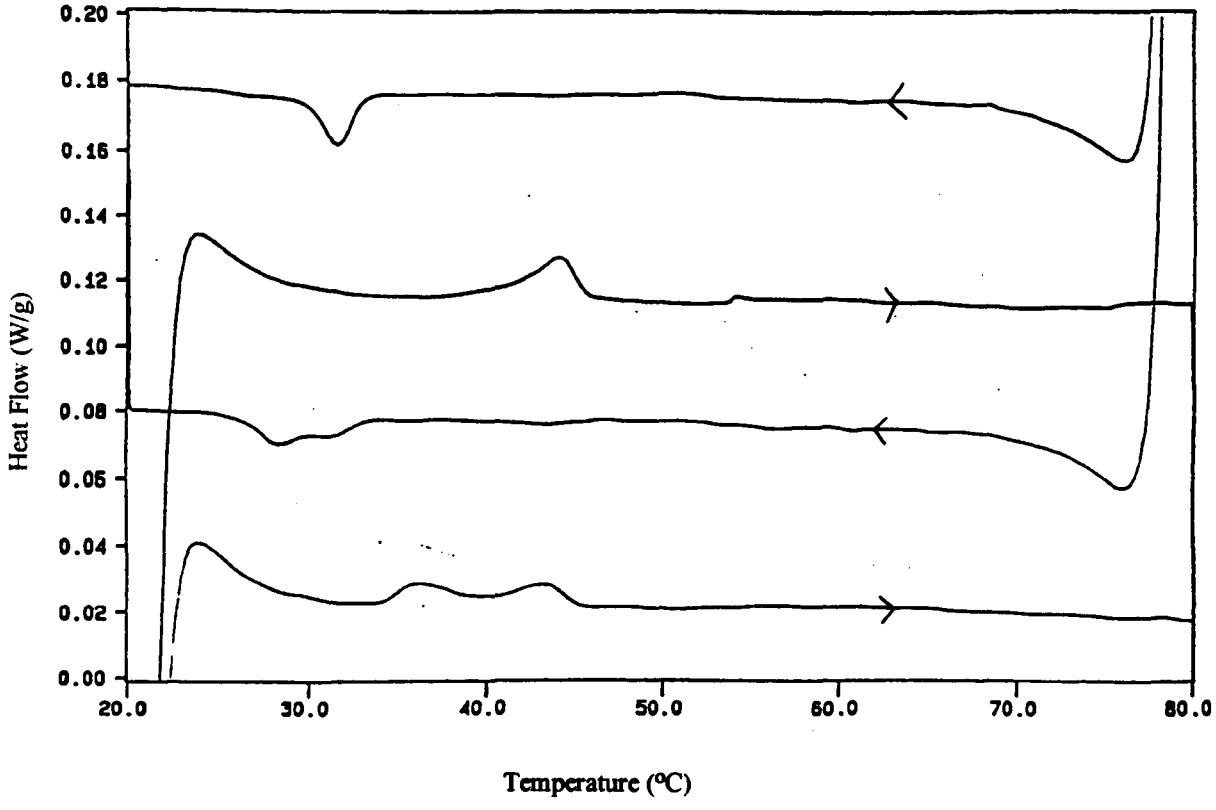

Figure 6.13c 2% w/w sucrose ester made up of 70:30, S1670:cholesterol

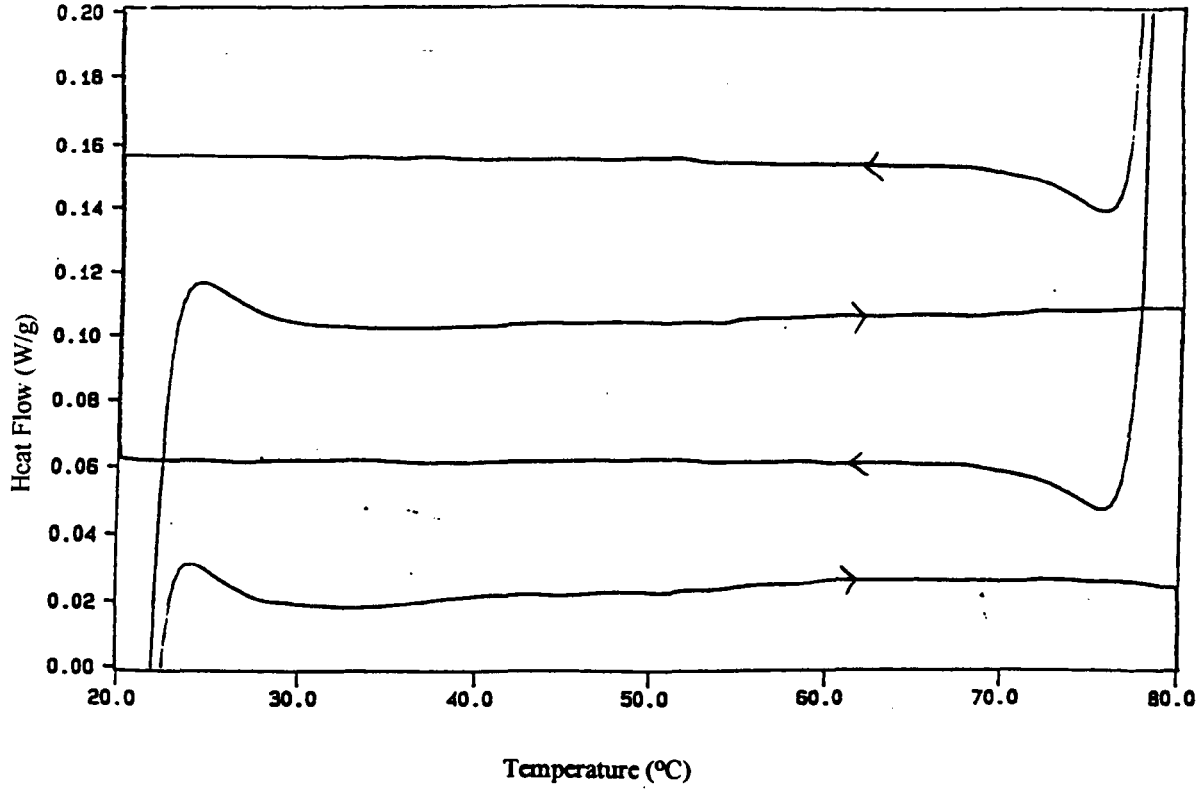

In the 95/5 sample the melting transition had two components, at 36 and 43°C, on second heating there was only one component, at 44°C. The freezing transition occurred at 35°C. In the 85/15 sample the melting phase transitions occurred at the same temperature but their enthalpy was reduced. The freezing transition occurred at a lower temperature, 28°C, and also had a lower enthalpy. The 70/30 sample displayed no phase transitions between 20 and 80°C. The reduced enthalpy and reduced temperature of transition with increased cholesterol concentration is an indication of the increased fluidity of the alkyl chains, requiring less energy to achieve complete melting. The sample containing a 70/30 ratio displayed no phase transition because it was totally fluid above 20°C.

The effect of cholesterol in disrupting the packing between alkyl chains in liquid crystal phases is well understood. The observation that cholesterol disrupts the surface domain structure and the chain melting transition was taken as evidence for the presence of liquid crystalline sucrose ester below its chain melting temperature at the surface of the gas microcells. A lamellar phase sucrose ester below its chain melting temperature is referred to as a gel phase, as previously described in Chapter 1.

6.14 The remaining aerated 75% Sweetose 2% sucrose ester samples

Samples of the commercial blended sucrose stearates, sucrose mono-stearate and sucrose mono-palmitate together with the commercial sucrose palmitate, P1570 and sucrose behenate, B1570 were analysed, Figures 6.14a-f.

Aerated 75/2S270, displayed similar phase transitions as non-aerated 75/2 S270, with melting peaks at 38 and 45°C, and freezing peaks at 55 and 62°C, there was no difference between the first and repeat cycle. Aerated 75/2S770 was found to have only one distinguishable melting transition which occurred at 45°C unlike non-aerated 75/2 S770 which had two, at 45 and 56°C, both however had two freezing peaks, at 41 and 50°C, Figure 6.14a.

Aerated 75/2 S1170 alkyl chains melted at 46°C and froze at 38 and 41°C. The enthalpy of the first melting transition was considerably lower than that of the repeat in the case of the aerated S1170 sample only. Aerated 75/2 S1570 also displayed a single melting and freezing transition, with peaks at 46 and 38°C respectively. As seen with S1170, the enthalpy of the first melting transition is much lower than that of the second, again only in the aerated sample, Figure 6.14b.

Figure 6.14a

75 % Sweetose / 2 % S270 aerated - - - - -

75 % Sweetose / 2 % S770 aerated ——

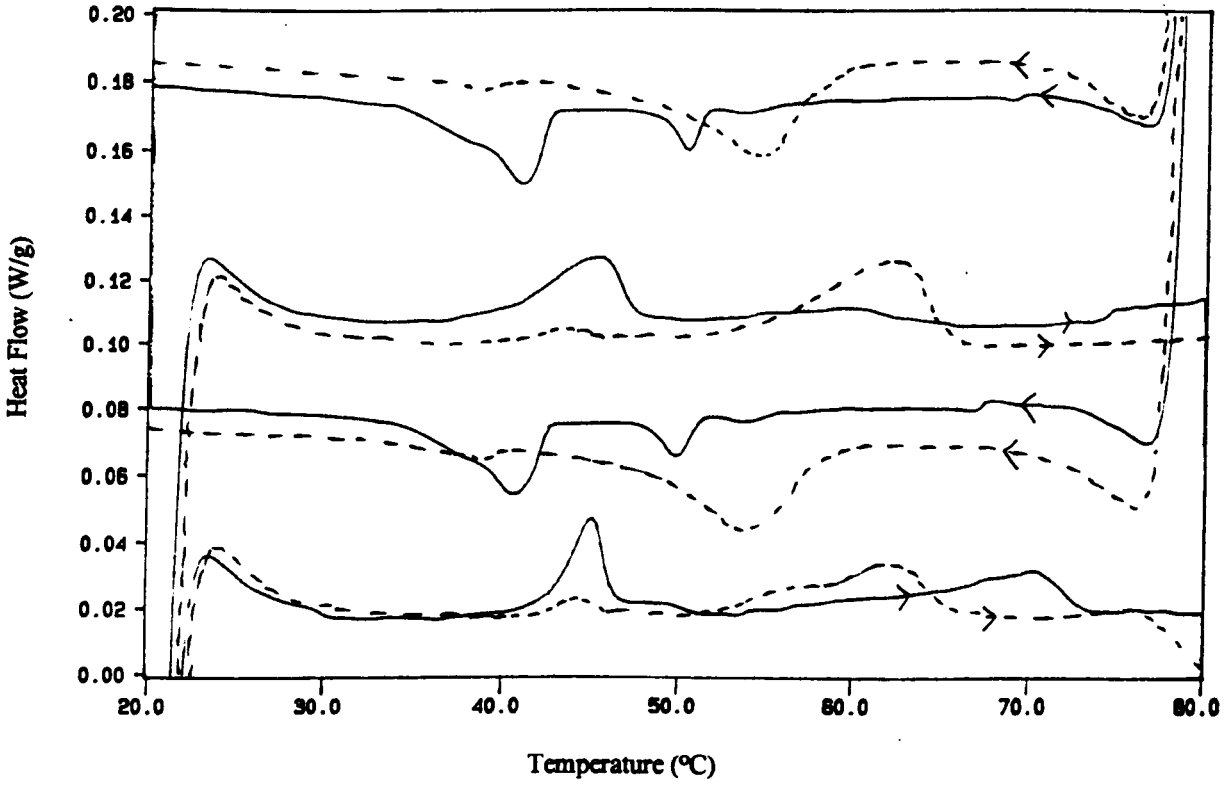

Figure 6.14b

75 % Sweetose / 2 % S1170 aerated - - - - -

75 % Sweetose / 2 % S1570 aerated ——

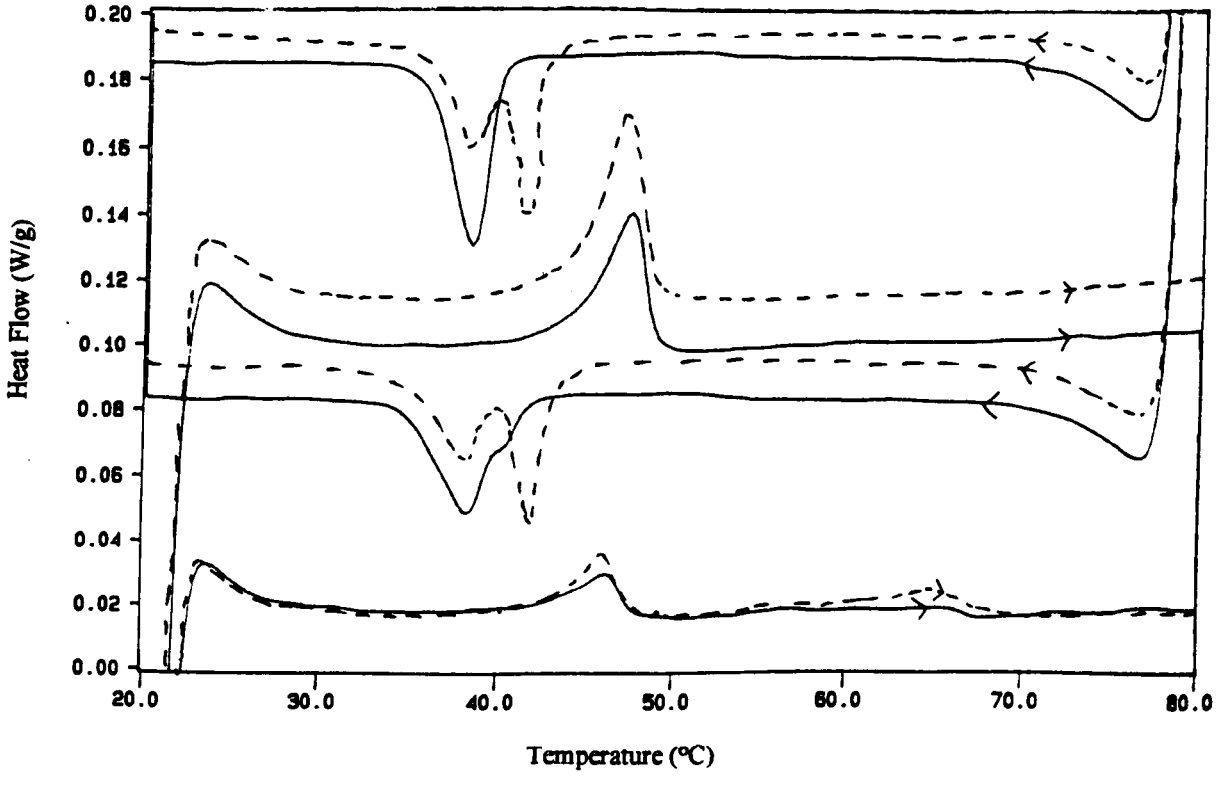

Aerated 100% mono-palmitate and 100% mono-stearate samples both displayed no measurable phase transition between 20 and 80°C which indicated that in both samples the alkyl chains were fluid above 20°C. The sample containing 70% mono- and 30% di-stearate melted at 48°C and froze at 42°C, Figures 6.14c&d. Some portion of di-stearate was found to be necessary for the observance of a phase transition in the non-aerated samples also.

Aerated 75/2 B1570 displayed the same melting and freezing transitions as non-aerated 75/2 B1570, melting at 70°C and freezing at 59 and 65°C. In common with non-aerated B1570, the enthalpy of the 65°C transition increased on the repeat cycle, Figure 6.14e.

Aerated 75/2 P1570 alkyl chains melted at 40°C and froze at 30 and 33°C, the enthalpy of the melting transition increased on the second cycle. The transition temperatures were similar to those of non-aerated 75/2 P1570, however the non-aerated sample had one freezing peak, at 32°C, whereas the aerated sample had 2 peaks, at 30 and 33°C, Figure 6.14f.

Figure 6.14c

75 % Sweetose / 2 % S1670 aerated ——

75 / 2, 100 % mono-palmitate aerated - - - -

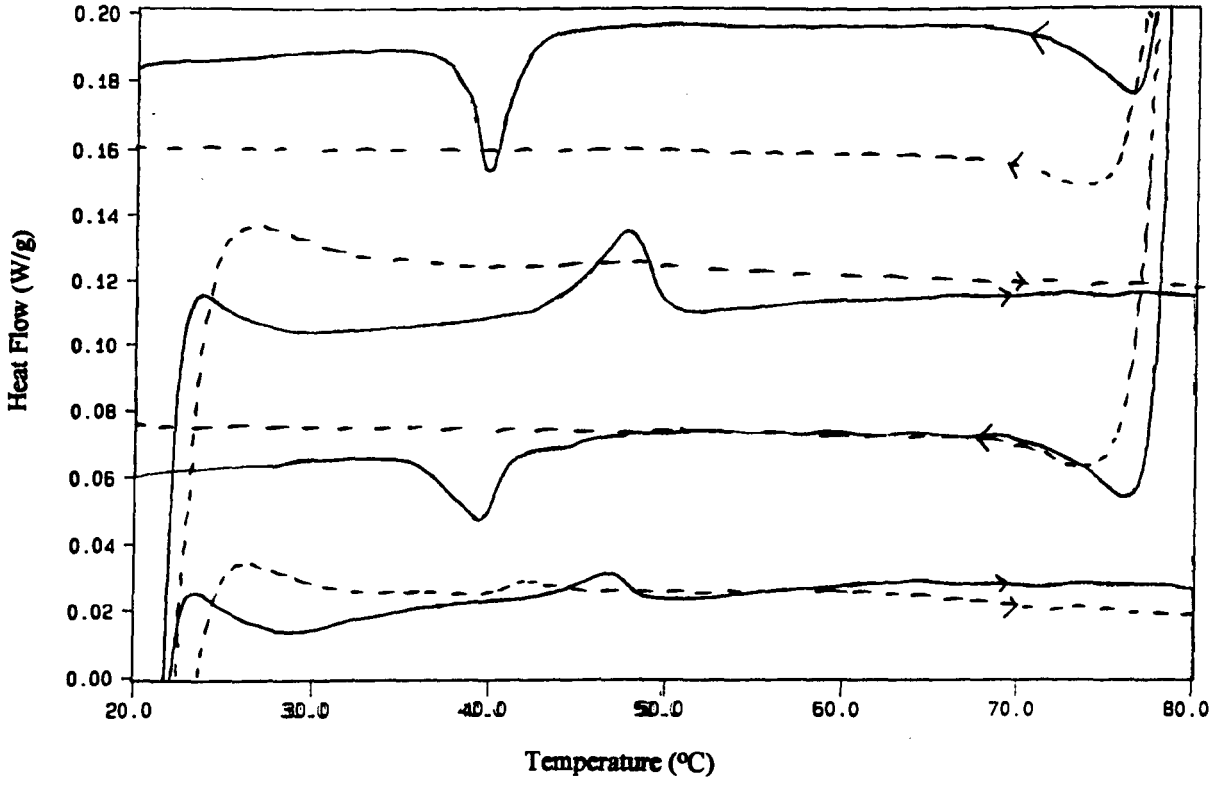

Figure 6.14d

75 / 2, 100 % mono-stearate aerated - - - -

75 / 2, 70 % mono- 30 % di- C_{18} aerated ——

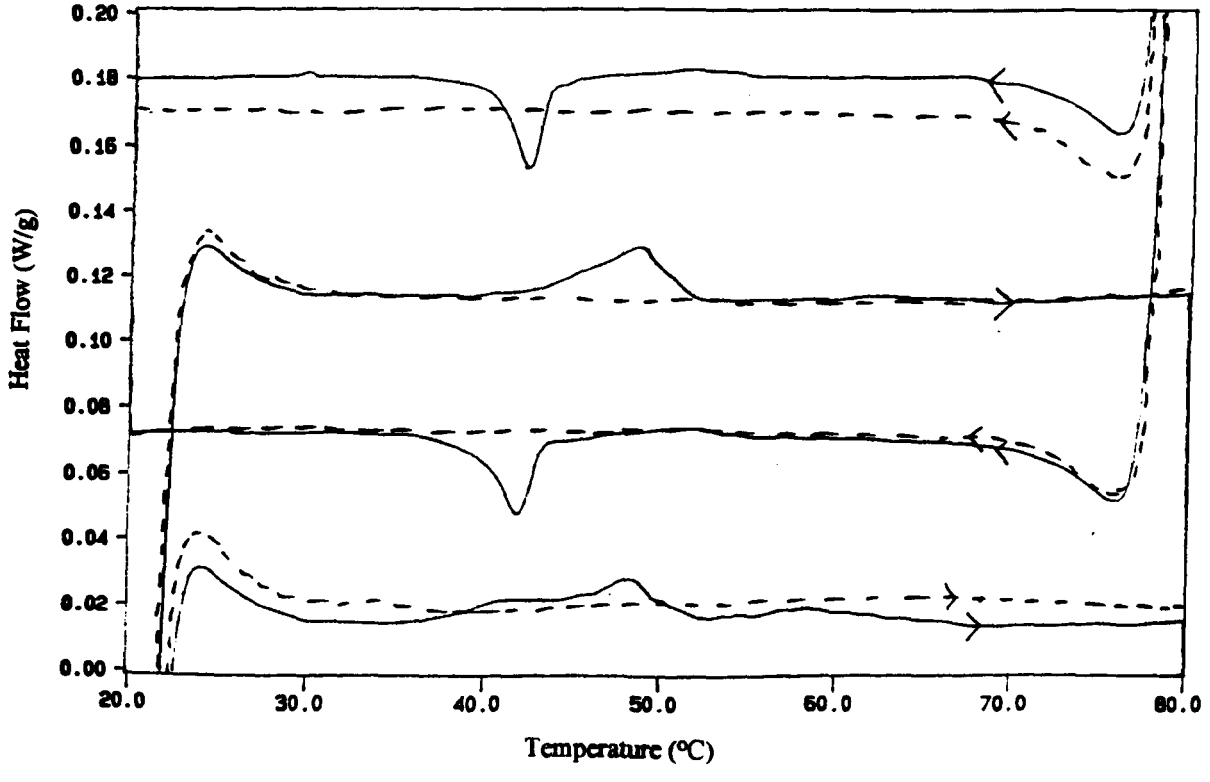

Figure 6.14e

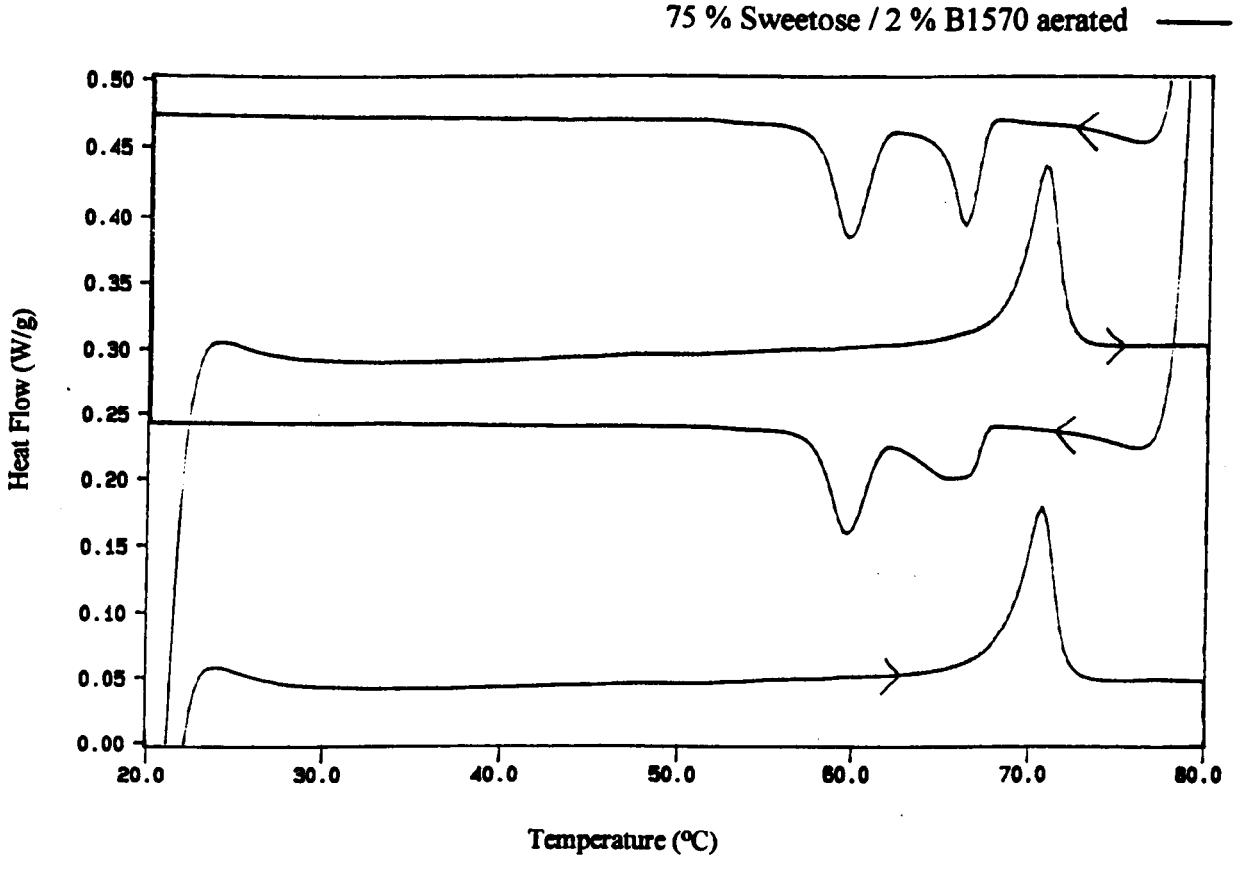

Figure 6.14f

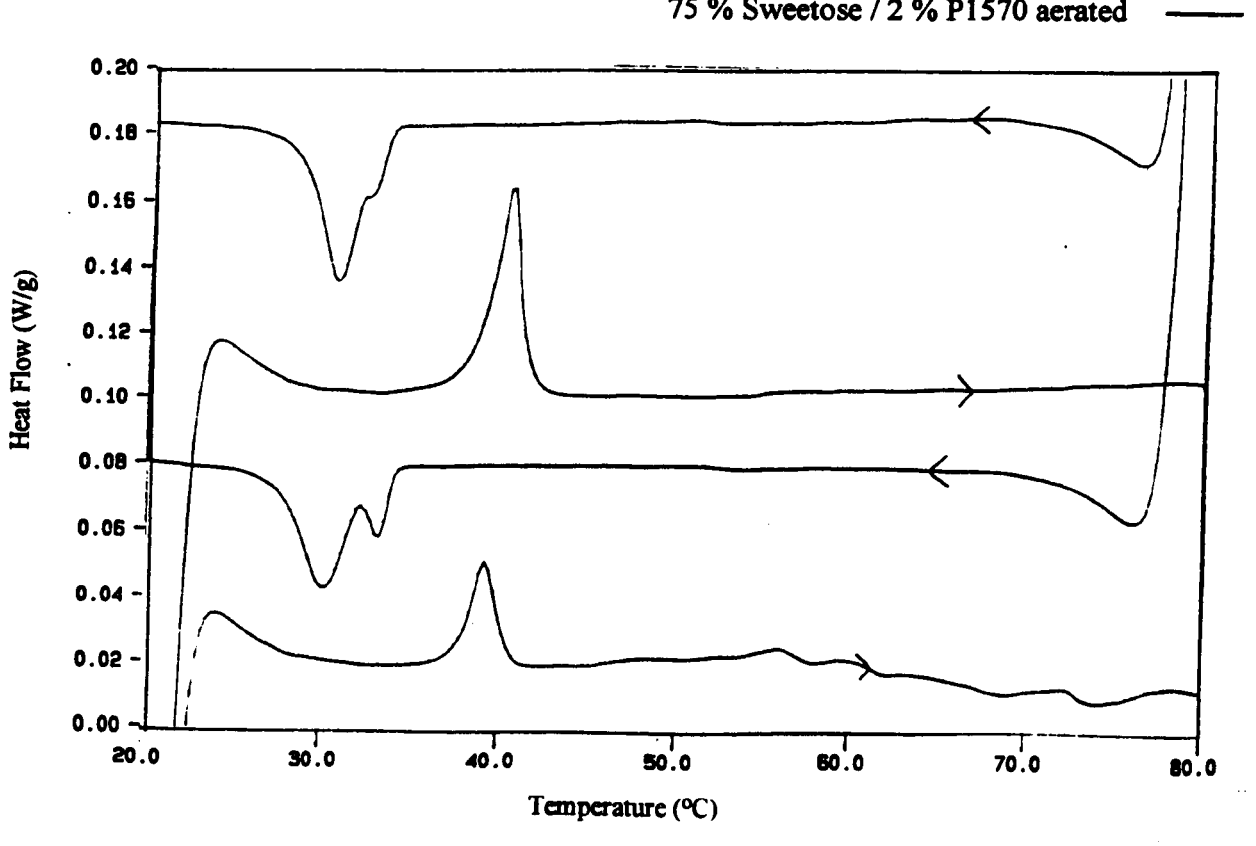

The enthalpy and temperature of the first endothermic transition for an aerated mixture of 75%w/w Sweetose 2%w/w sucrose ester containing the commercial sucrose stearates with a blend of mono- and higher esters was plotted as a function of mono-stearate concentration, assuming that the sample contained only mono- and di- stearate. Figure 6.14g illustrates the comparison.

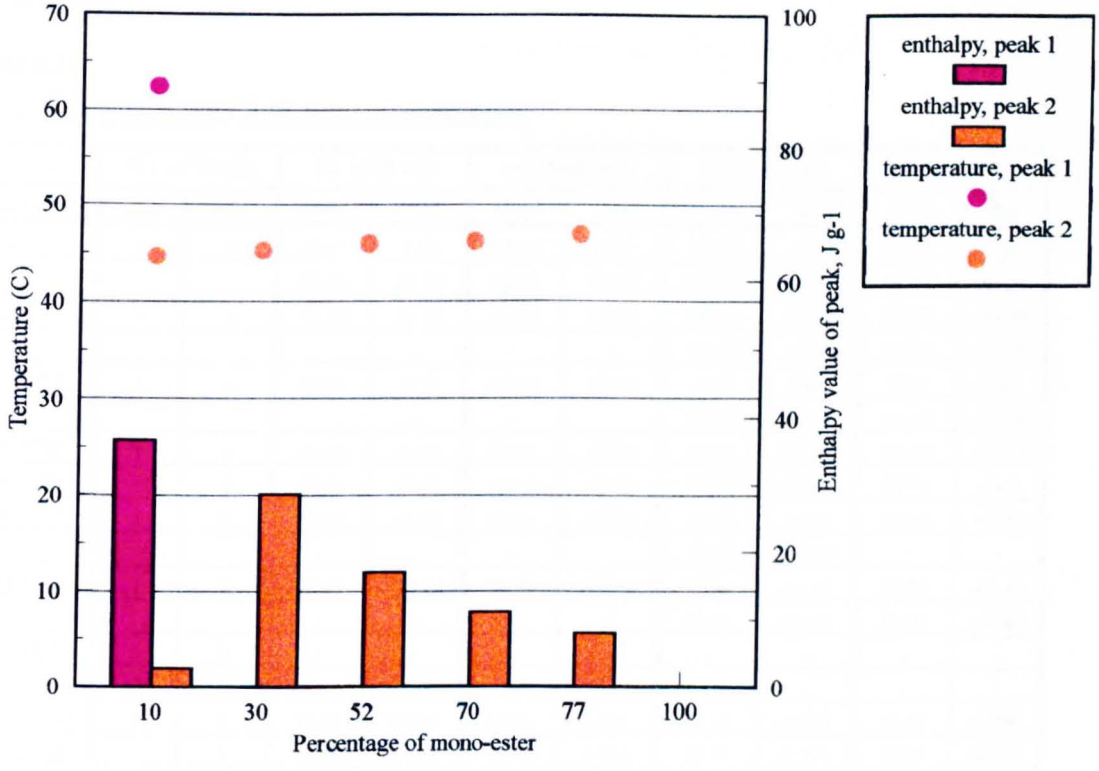

Figure 6.14g

At 10% mono-stearate concentration there were two components in the melting transition, a peak at 46°C and one above 60°C, the peak above 60°C was attribute to the pure di-stearate component. This behaviour was observed in the non-aerated mixtures also. In the other samples containing both mono- and di-stearate there was a single melting transition at 46°C. In Section 6.5 the component melting at 46°C in mixtures of mono- and di-stearate was shown to be a solid solution of mono- in di- stearate. The enthalpy of this transition at 46°C was greatest in the sample with 30% mono-stearate and it decreased with increasing mono-stearate concentration, because of the decreasing amount of di- in which to solubilise the mono-stearate. 100% mono-stearate did not show any phase behaviour within this temperature range, thought to be because the alkyl chains in the sample were fluid. In all samples the enthalpy of the first melting transition was less than the enthalpy required to melt the equivalent non-aerated sample. This was attributed to the relative ease of melting the monolayer arrangement of the sucrose ester on the gas

microcell surface. The enthalpy of the repeat melting transition for the aerated samples was identical to that in the non-aerated equivalent.

The table below describes the data for all the aerated sample discussed, in the form of number of peaks observed, temperature (°C) and enthalpy value (J g^{-1} of sucrose ester in the sample).

Table 6.14a

75 % w/w Sweetose / 2 % w/w sucrose ester

75 / 2	No. of Peaks		1st heat run		rpt. heat run		1st cool run		rpt. cool run	
sample	*heat*	*cool*	*temp*	*ΔH*	*temp*	*ΔH*	*temp*	*ΔH*	*temp*	*ΔH*
S270	2	2	44.61	2.60	43.87	2.20	38.65	-3.60	38.78	-1.45
			62.48	36.80	62.58	53.65	53.87	-53.9	54.34	-61.25
S770	1	2	45.22	28.70	45.02	24.15	40.61	-27.45	40.88	-26.50
			-	-	-	-	49.83	-5.95	50.30	-5.60
S1170	1	2	45.91	17.2	47.10	53.00	37.7	total	38.2	total
			-	-	-	-	41.68	-55.25	41.41	-53.30
S1570	1	1	46.19	11.25	47.39	40.25	38.27	-37.45	38.37	-44.05
S1670	1	1	46.83	8.05	47.67	30.55	39.35	-24.95	39.79	-34.4
P1570	1	2	39.23	17.55	40.34	40.55	30.15	total	30.63	-43.15
			-	-	-	-	33.0	-41.80	-	-
B1570	1	2	70.65	112.35	70.70	106.15	59.56	-65.25	59.50	-63.85
			-	-	-	-	65.48	-48.75	66.07	-46.40
mono-C16	0	0	-	-	-	-	-	-	-	-
mono-C18	0	0	-	-	-	-	-	-	-	-
70/30 m/di	1	1	48.26	0.495	48.51	0.423	41.88	-0.322	42.18	-0.290
* drain light	1	1	47.29	0.823	48.56	0.743	39.12	-0.773	38.97	-0.810
drain dense	0	0	-	-	-	-	-	-	-	-

* enthalpy data per gram of sample.

6.15 References

1 Glasstone, S. (1946); 'Textbook of Physical Chemistry', 2nd Ed., Van Nostrand, New York.

2 Fitzgerald, M.; PhD Thesis, University of Reading, 1996.

3 Mayes, D.; "Gel permeation chromatography of sucrose esters", Unilever Internal Report, 1996.

4 Levine, Y.K. and Williams, M.H.F.; Nature New Biol.,**230**, 69, (1971).

5 Rand, R.P. and Luzzati, V.; Biophys. J., **8**, 125, (1968).

6 Lecuyer, H. and Dervichan, D.G.; J. Mol. Biol., **45**, 39, (1969).

7 Rothman, J.E. and Engelman, D.M.; Nature New Biol., **237**, 42, (1972).

CHAPTER 7

Confocal scanning laser microscopy

7.0 CONFOCAL SCANNING LASER MICROSCOPY

Imaging was done by D. Ferdinando at Unilever Research, Colworth laboratory, using a Biorad MRC-600 Confocal Scanning Laser Microscope. Confocal imaging enables non destructive optical sectioning, by limiting the detection to the focal plane, all out of focus regions of the sample appear black. The specimen is scanned by an Argon ion laser and the in-focus fluorescence emission is focused onto a photodetector thus building a two-dimensional image. A small aperture is positioned in front of the detector to prevent out of focus light from reaching the detector, Figure 7.0a.

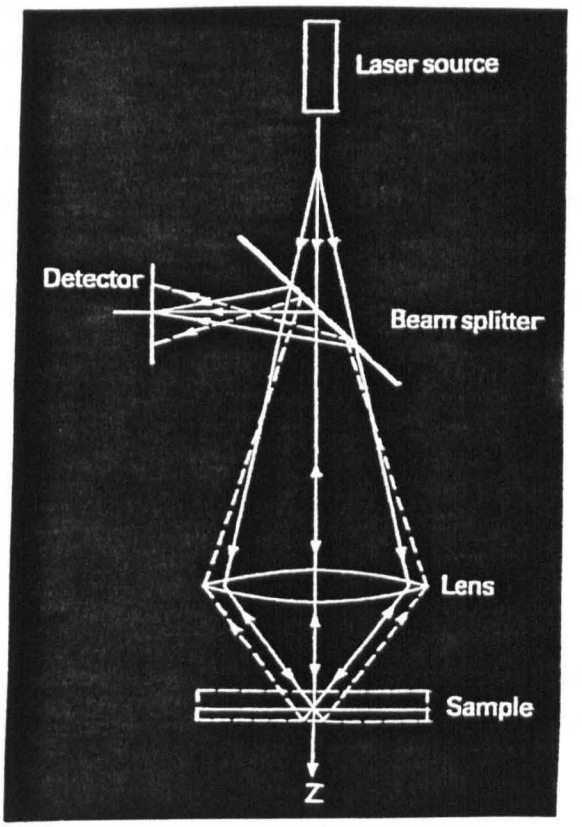

Figure 7.0a

Non-aerated samples containing 75% Sweetose and 2% sucrose ester were prepared, as described in Chapter 2, to examine the effects of different ratios of Sweetose to sucrose ester and the ratio of mono- to di- and higher esters in the sucrose ester. To some samples a fluorescence probe was added to obtain more detailed information. The dye used was Nile Blue A Oxazone, $C_{20}H_{18}N_2O_2$, supplied by Sigma Chemicals, a hydrophobic dye, crystals of which were added to the sample 24 hours before viewing, to allow diffusion to occur. This dye is commonly known as Nile Red.

On some occasions during preparation, small air bubbles became trapped in the matrix and further small bubbles were trapped during the addition of Nile Red crystals. These bubbles are not gas microcells and account for the presence of air bubbles in a non-aerated mixture. These air bubbles were observed to display unusual surface characteristics, thought to be because they also have sucrose ester at their surfaces, and have also been investigated. 75% Sweetose was clear and non-fluorescing when viewed by confocal microscopy, not illustrated.

7.1 Effect of Sweetose concentration

Non-aerated samples were prepared with 10% increments in Sweetose concentration. The samples are illustrated in Figures 7.1a-f, with respectively increasing Sweetose. In all cases the mixture was heterogeneous, the insoluble material observed was attributed to liquid crystalline sucrose ester as described in previous chapters. With increasing Sweetose concentration the sucrose ester material appeared to become more concentrated, possibly due to the decreasing water content causing phase separation of the sucrose ester. The degree of heterogeneity was more clearly visible when viewed directly down the microscope.

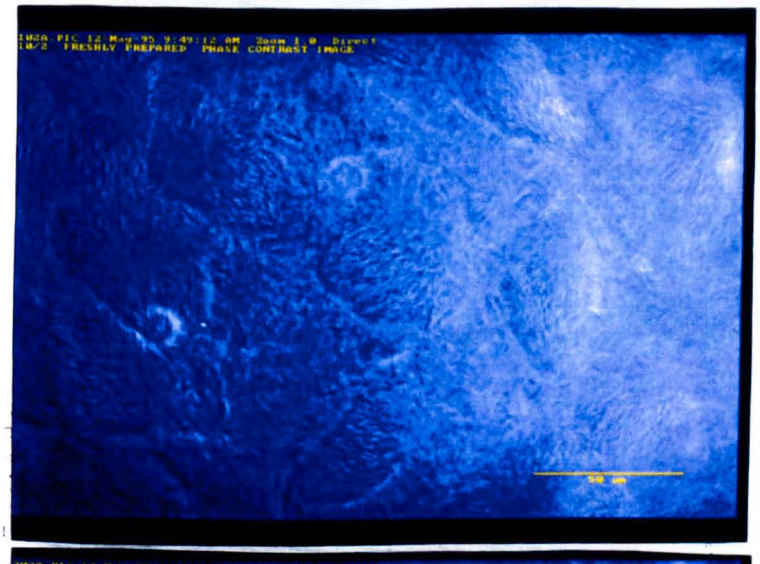

Figure 7.1a

10% Sweetose 2% sucrose ester

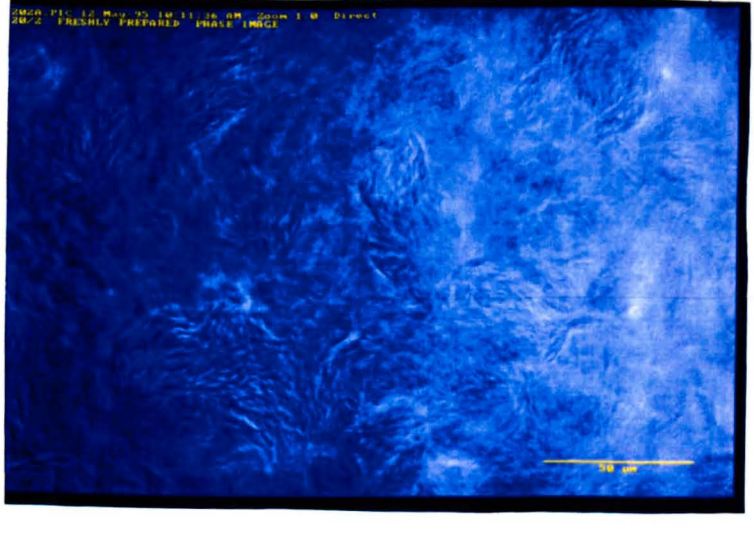

Figure 7.1b

20% Sweetose 2% sucrose ester

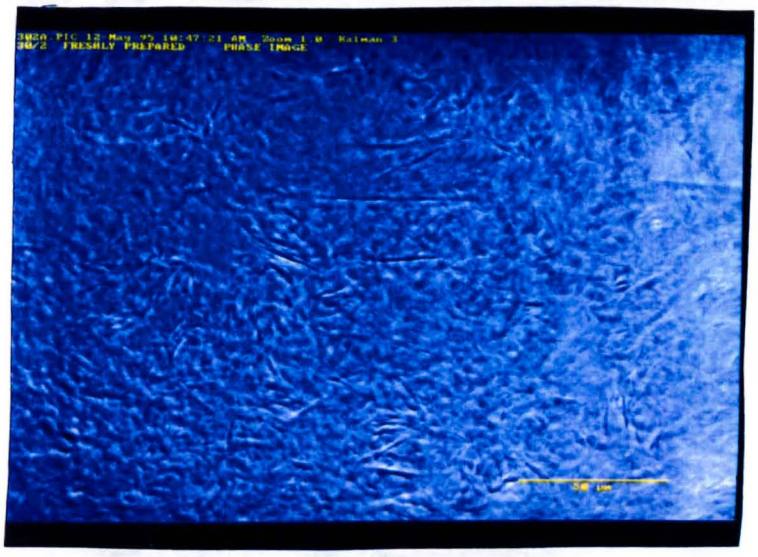

Figure 7.1c

30% Sweetose 2% sucrose ester

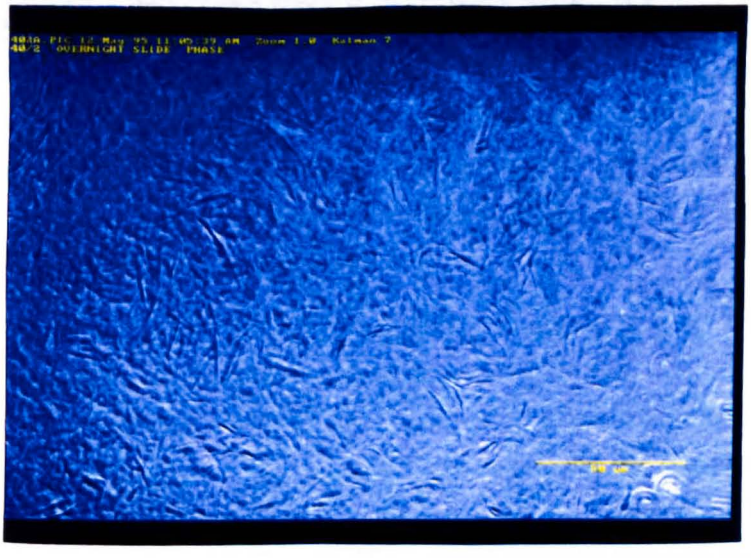

Figure 7.1d

40% Sweetose 2% sucrose ester

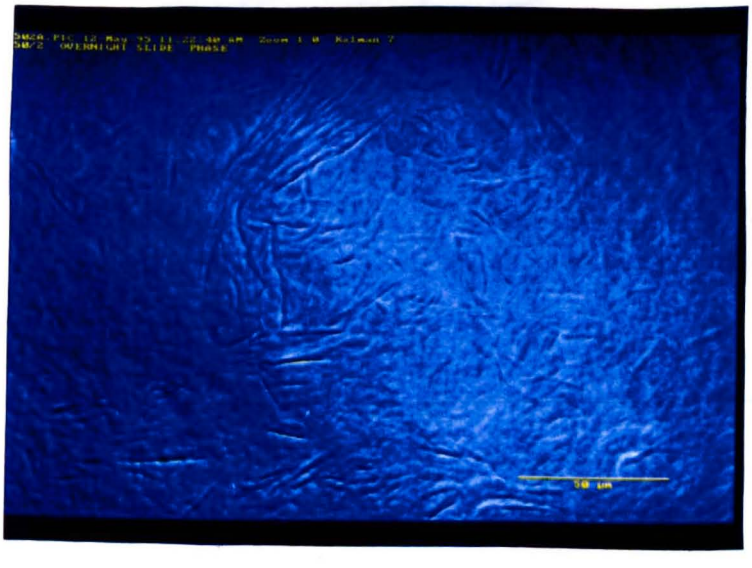

Figure 7.1e

50% Sweetose 2% sucrose ester

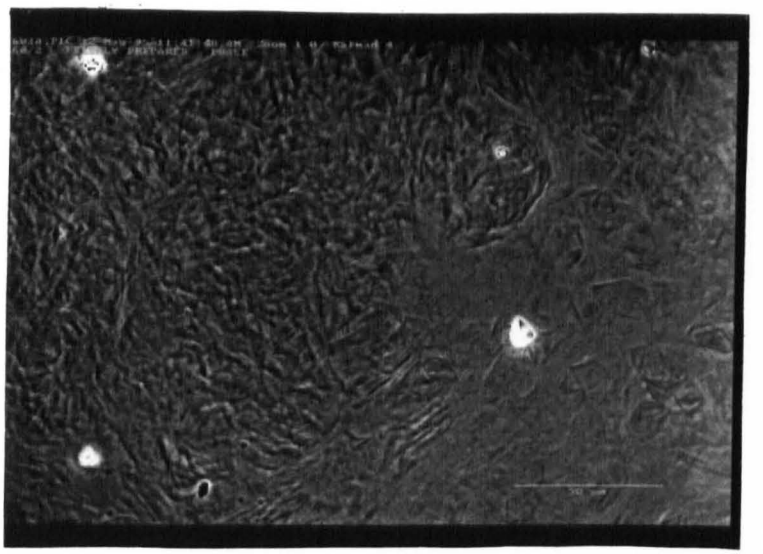

Figure 7.1f
60% Sweetose 2% sucrose ester

7.2 Incidental air bubbles in the presence of a fluorescent probe

In the introduction to this chapter it was mentioned that large gas bubbles become trapped during the preparation of non-aerated mixtures. To these non-aerated samples was added a few crystals of hydrophobic fluorescent dye. The sample was allowed to stand overnight to allow for the process of diffusion. Figures 7.2a-f illustrate the surfaces of trapped bubbles under laser illumination.

The surfaces of these trapped bubbles fluoresce brightly when viewed with laser light. A series of dark structures were observed on both small and large gas cells with apparently random surface density, the concentration of Sweetose and sucrose ester, within the limits 20-75% Sweetose and 1-8% sucrose ester, did not affect their arrangement. Figure 7.2a shows a gas cell viewed at a focal plane near its equator. Figure 7.2b shows a composite image, produced by overlaying vertical sections through the gas cell surface, revealing the outer surface of the upper hemisphere. It was not possible to subtract the fluorescing regions seen in the background on Figure 7.2a, thus after the overlay of many optical sections their concentration appears to have increased dramatically in Figure 7.2b, in reality, this was not the case.

The arrangement of these dark structures at the surface of the air bubble varies according to surface coverage, see Figures 7.2 b-d. These structures are peculiar to the surface of the gas cell surface and are seen to flow when viewed directly, however they were not seen to migrate into the matrix. No characteristic behaviour was found; within any sample the bubbles displayed almost random patterns of surface coverage. Figure 7.2e illustrates adjacent bubbles within a sample of 20% Sweetose 2% sucrose ester; one bubble has partial coverage while the other has nearly total coverage.

Figure 7.2f illustrates a portion of a bubble surface at high magnification.

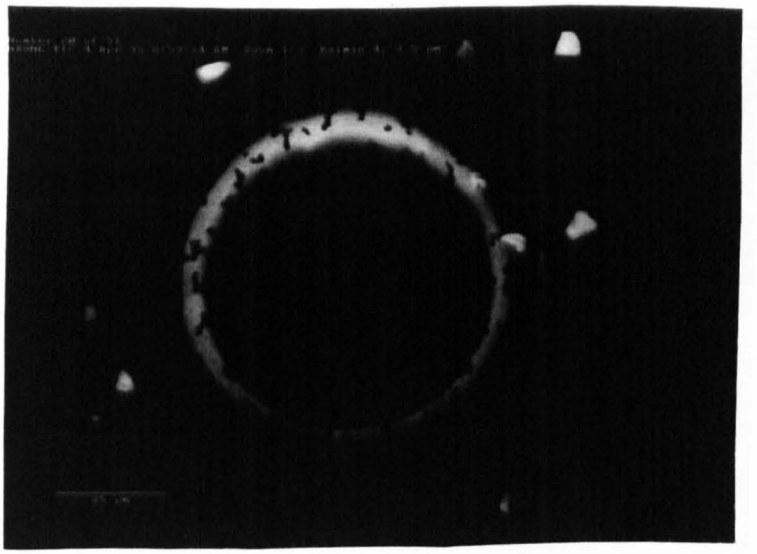

Figure 7.2a
Incidental air bubble within a non-aerated matrix, bubble surface fluoresces under laser light.

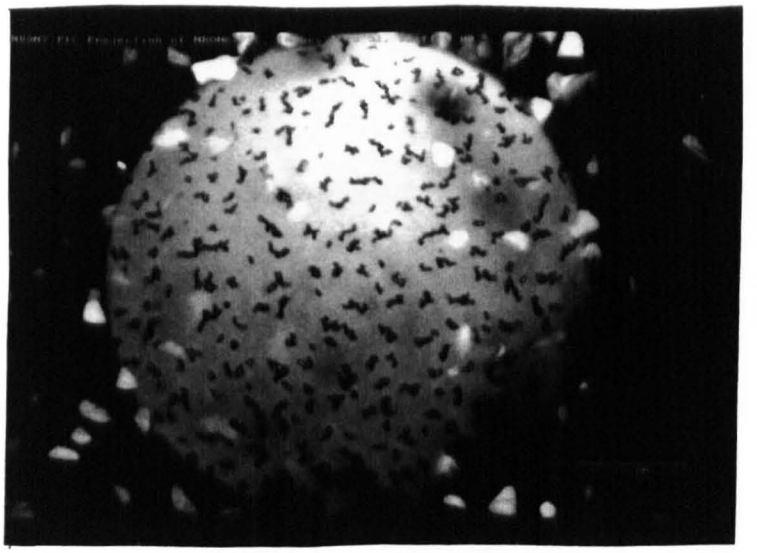

Figure 7.2b
Composite image of many optical sections similar to Fig. 7.2a. Upper hemisphere of bubble fluoresces revealing dark structures.

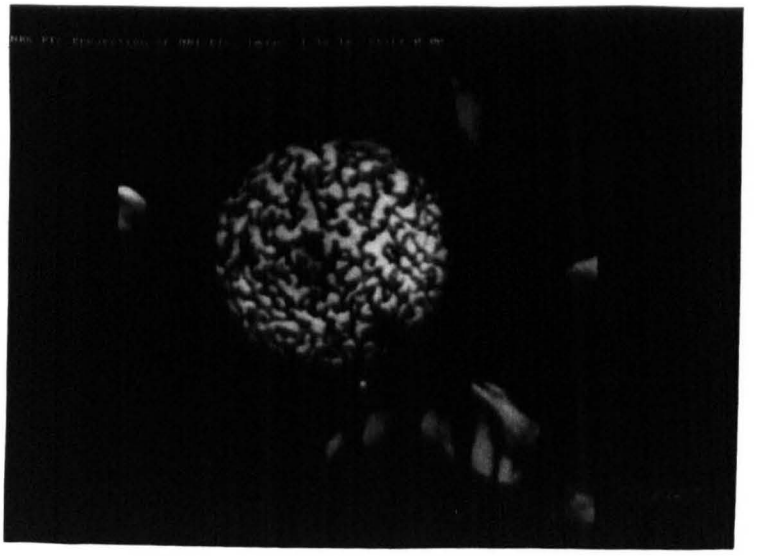

Figure 7.2c
Composite image of a different gas bubble under laser light.

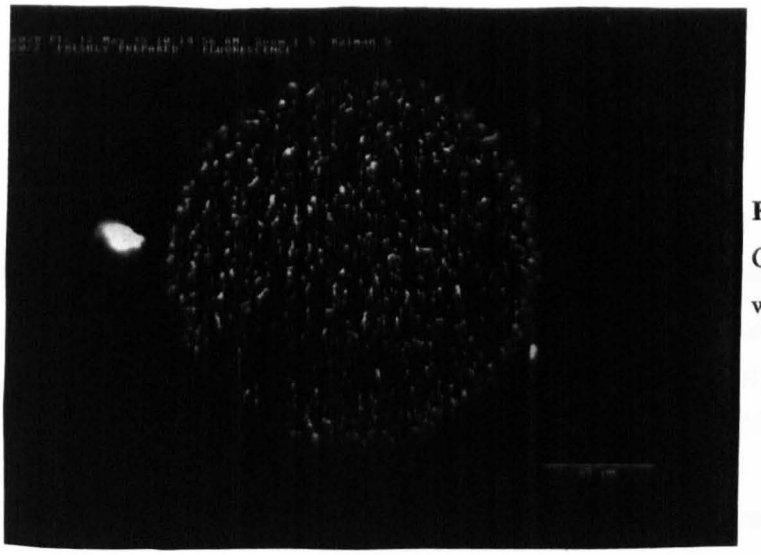

Figure 7.2d
Gas bubble in a non-aerated mixture with a high coverage of dark structures.

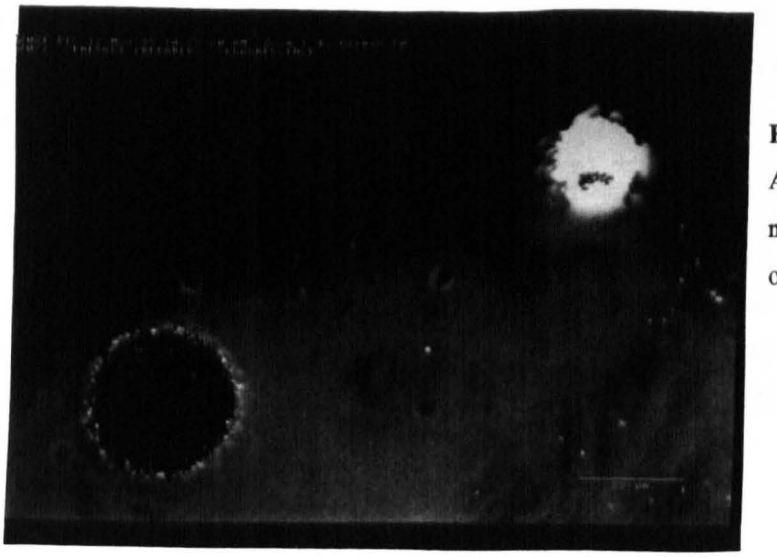

Figure 7.2e
Adjacent bubbles in a non-aerated mixture with different concentrations of dark structures at their surface.

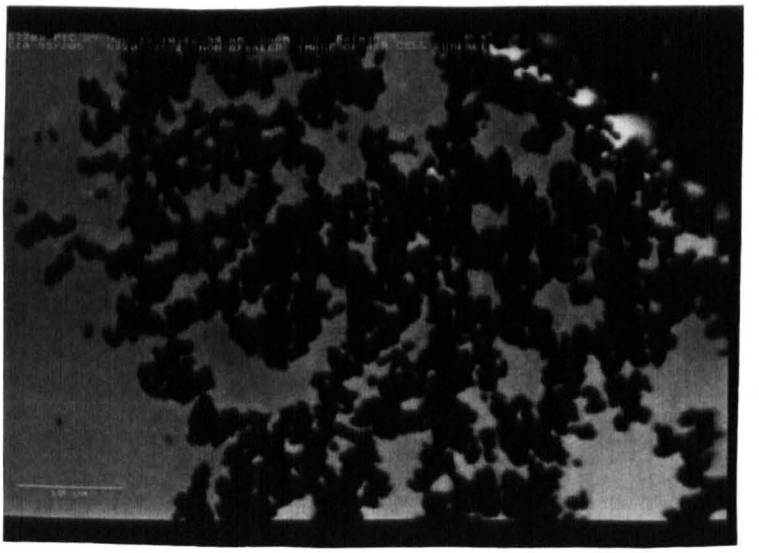

Figure 7.2f
Dark structures at the surface of an air bubble at high magnification.

The fluorescent regions of the background were viewed using bright field illumination, and attributed to small regions of the liquid crystalline sucrose ester seen in Figures 7.1a-f which had absorbed some of the dye. Crystals of Nile Red were easily distinguished, as large highly fluorescent needles, these are not illustrated.

7.3 Observation of the surface of a large bubble while heating to 60°C

Figure 7.3a shows a gas bubble with dark surface structures. Some liquid crystalline sucrose ester can be seen in the matrix although this is slightly beneath the plane of focus. The sample, on the microscope slide, was heated slowly to 60°C. At approximately 45°C the structures began to melt and disappear. At 50°C they were no longer visible. No further change occurred on heating. Figure 7.3b shows the same gas cell at 60°C. Notice also that the heterogeneity in the matrix is no longer visible. Figure 7.3c shows the cell at 55°C. As the sample was cooled dark regions began to appear on the cell surface. Notice the re-appearance of needle-like structures within the matrix. Figure 7.3d shows the cell after 20 minutes at 22°C. With prolonged cooling these dark regions increase in size and develop an angular appearance.

Figures 7.3 a-d are shown over page.

Fluorescent probes have been used by other workers to investigate insoluble monolayers of long chains fatty acids, spread at the air/water interface. They observed dark domains on a bright background very similar to those seen on the air bubble in Figure 7.3. This will be discussed at the end of the chapter.

Figures 7.3 a-d

Changes in the surface of a single large bubble with temperature.

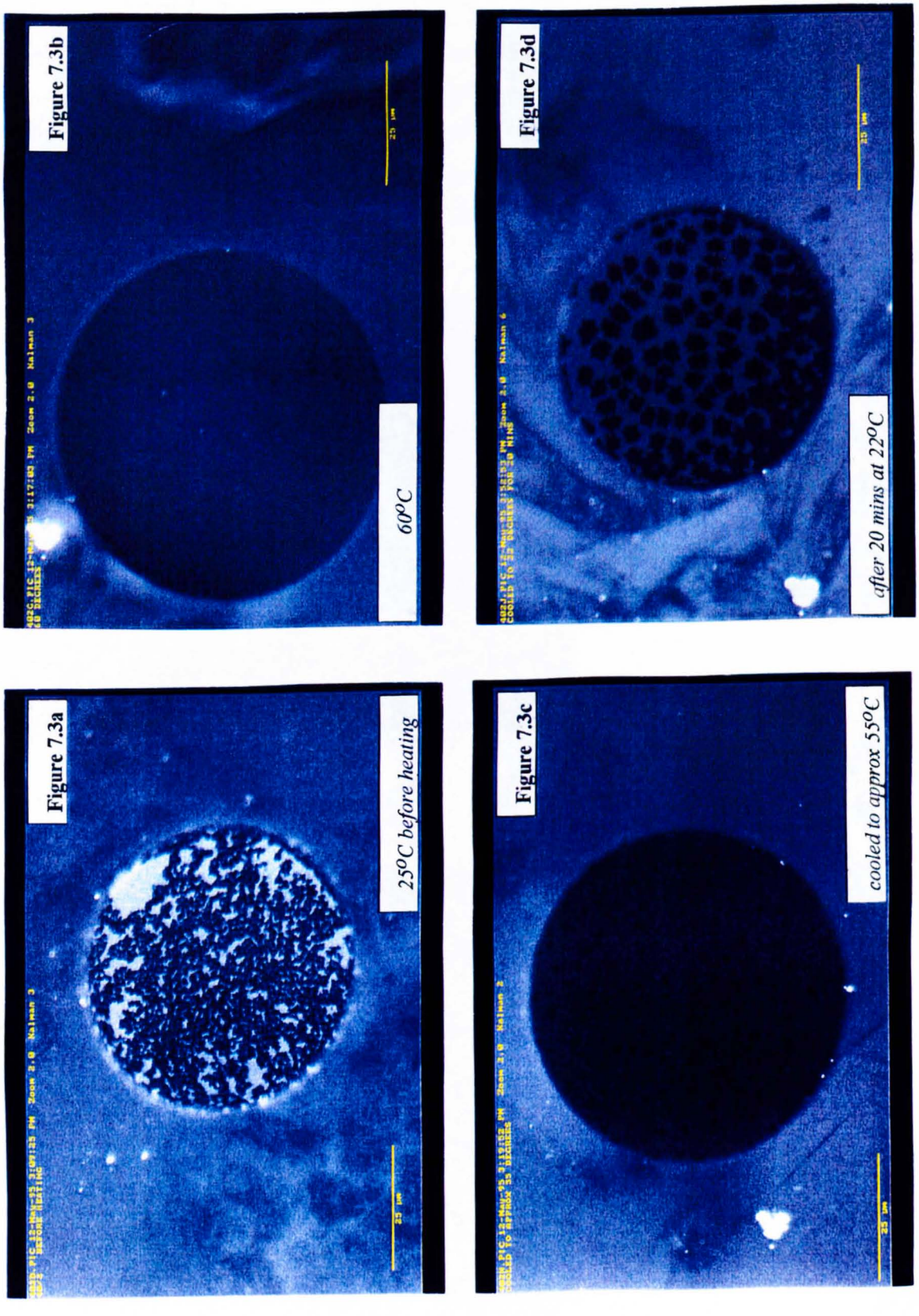

7.4 The effect of sucrose ester concentration at 20%w/w Sweetose in the sample.

Non-aerated mixtures of 20%w/w Sweetose concentration and sucrose ester (S1670) concentrations of 2%, 5% and 8%w/w are compared. The 2%w/w sucrose ester sample is illustrated in Figure 7.1b.

Figure 7.4a illustrates the 5% sucrose ester sample in polarised light. The regions of anisotropy are liquid crystalline sucrose ester as discussed previously. Figure 7.4b illustrates 5% sucrose ester using both phase contrast (LHS) and fluorescence imaging.

In Figures 7.4b&c it can be seen that at this low Sweetose concentration (20%w/w) the liquid crystal phase fluoresces less brightly than its surrounding liquid.

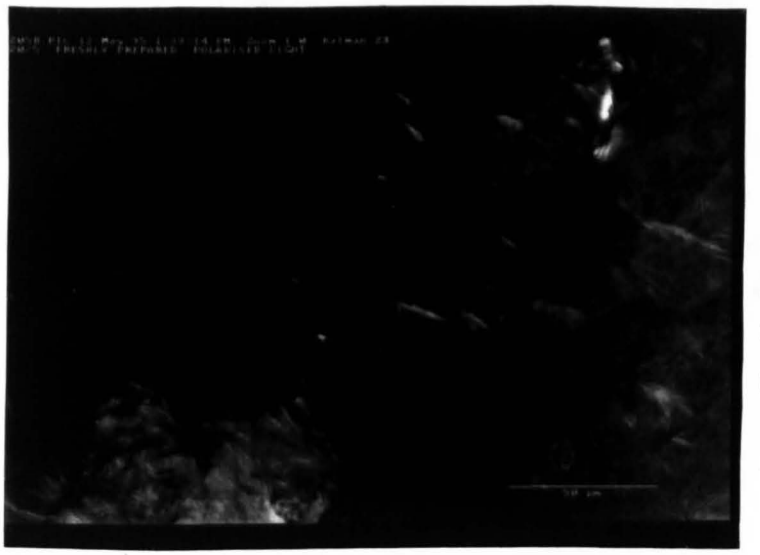

Figure 7.4a
20% Sweetose 5% sucrose ester
polarised light microscopy

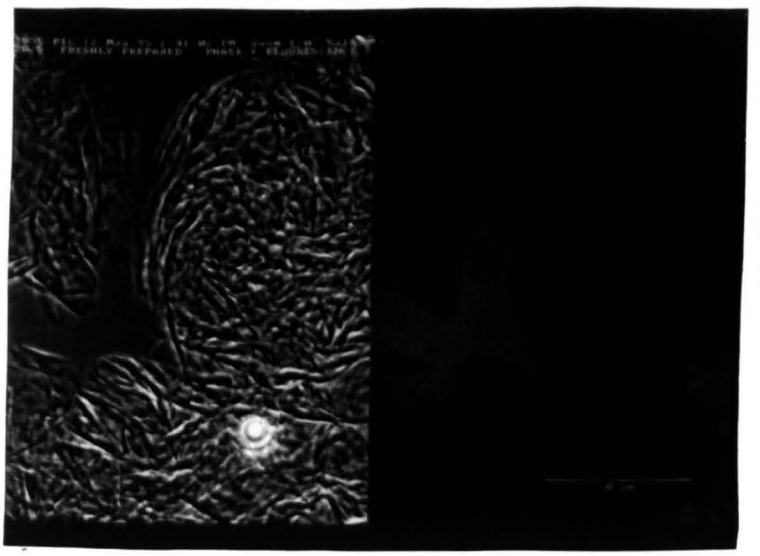

Figure 7.4b
20% Sweetose 5% sucrose ester
LHS:fluorescence RHS:bright field

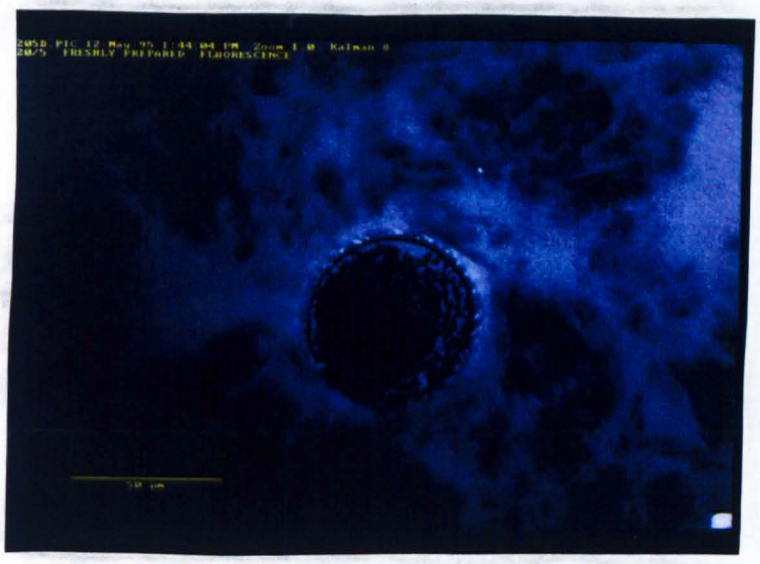

Figure 7.4c
20% Sweetose 5% sucrose ester fluorescence microscopy

Figures 7.4d-f illustrate the 20%w/w Sweetose 8%w/w sucrose ester sample, as expected, from the results of optical microscopy, the liquid crystalline material observed appeared to be more dense than that in both the 5% and 2%w/w sucrose ester samples. Figure 7.4d is a bright field image whereas Figures 7.4e&f are fluorescence images, the liquid crystals fluoresce less brightly than their surroundings.

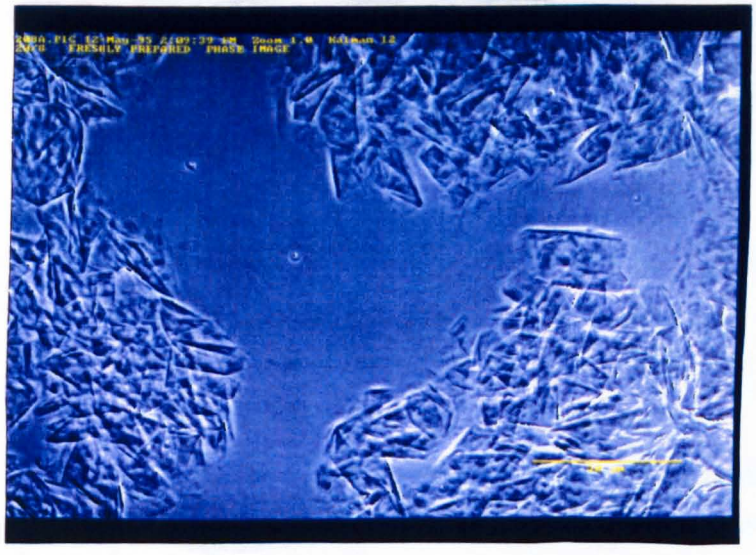

Figure 7.4d
20% Sweetose 8% sucrose ester bright field microscopy

Figure 7.4e
20% Sweetose 8% sucrose ester
Fluorescence microscopy

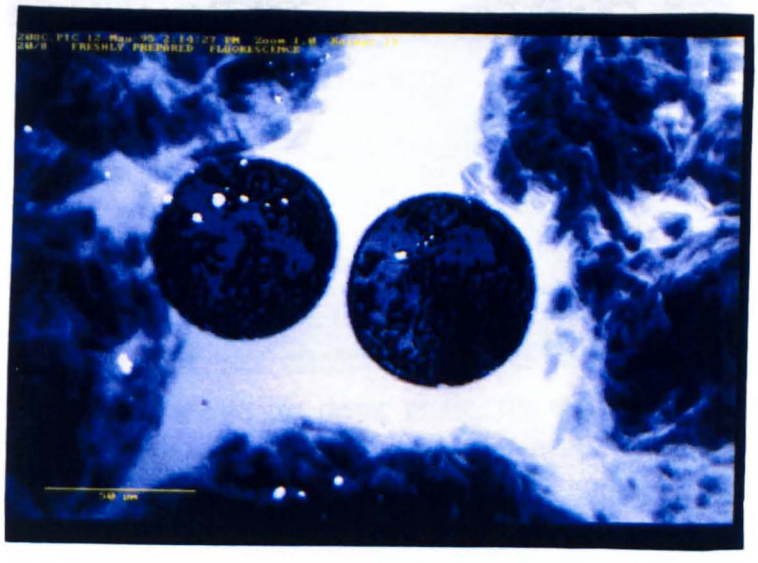

Figure 7.4f
20% Sweetose 8% sucrose ester
fluorescence microscopy

7.5 Non-aerated 75% Sweetose 2% sucrose ester after centrifuging.

A sample of non-aerated 75% Sweetose 2% sucrose ester S1670 was centrifuged in order to separate the phases for examination. The sample split into a dense liquid, resembling Sweetose, above which was an opaque, viscous gel.

Figures 7.5a&b show the light phase of the non-aerated mixture after centrifuging, Figure 7.5a is imaged using bright field and Figure 7.5b with laser light, Figure 7.5c shows the dense phase. The light phase was found to contain material similar to that observed in other non-aerated mixtures before centrifuging; the material had a spherical arrangement but within that constraint its optical appearance was very similar. Comparison of the two Figures revealed the material to be anisotropic as would be expected if it were liquid crystal.

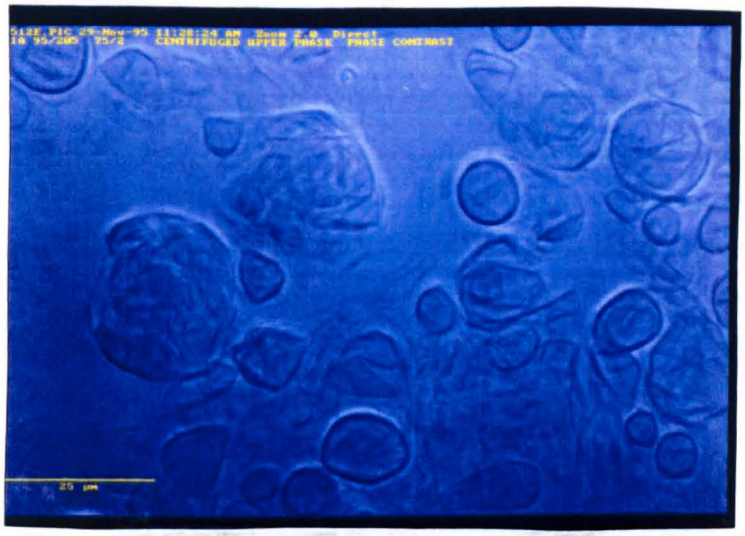

Figure 7.5a
light phase after centrifuging
bright field microscopy

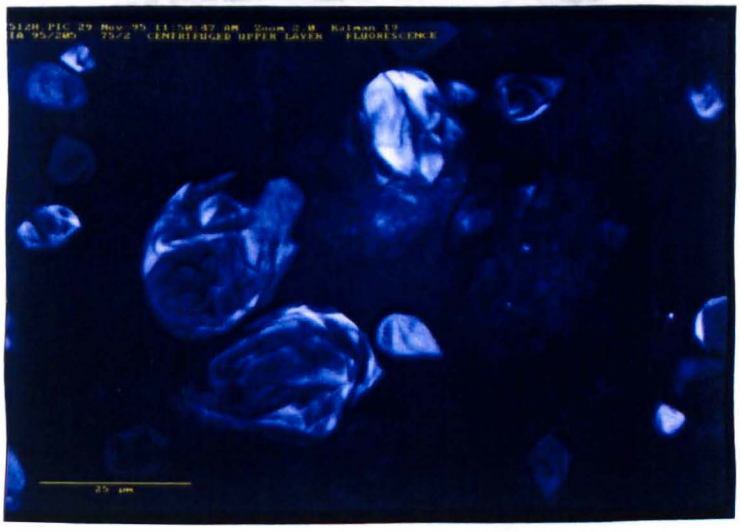

Figure 7.5b
light phase after centrifuging
polarised light microscopy

Figure 7.5c shows the dense phase, the sample was clear and isotropic with disparate fragments of sucrose ester remaining, due to incomplete centrifugation or contamination of the layers during separation.

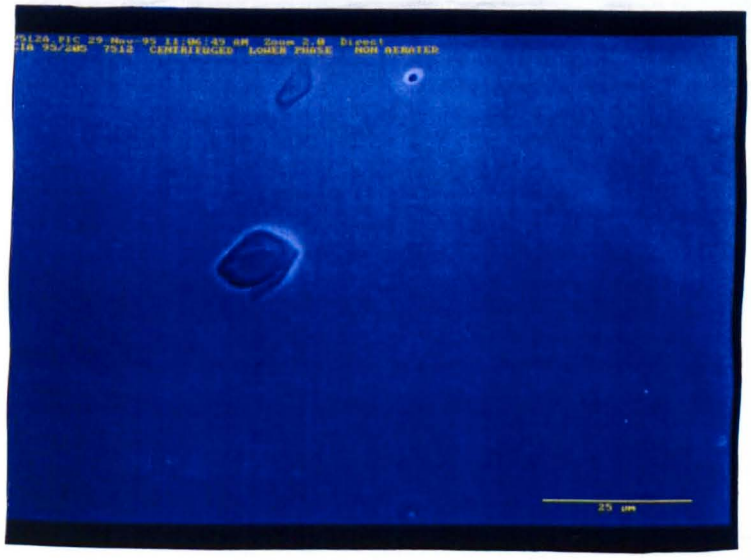

Figure 7.5c
Dense phase after centrifuging non-aerated 75% Sweetose 2% sucrose ester S1670

In Chapter 6, results of DSC measurements in conjunction with gel permeation chromatography measurements on a centrifuged non-aerated mixture and a standard non-aerated mixture are presented. Gel permeation chromatography revealed the light material to contain all the sucrose ester within the sample, none was found in the dense phase. DSC studies showed that a phase transition occurred at 48°C in the light fraction of the centrifuged non-aerated mixture which was not observed in the dense fraction, and in addition, this phase transition had a similar enthalpy and temperature as that of the standard non-aerated mixture. The likely conclusion is that the dense phase is Sweetose alone and that all of the sucrose ester is in the form of liquid crystals in the light phase, it is these liquid crystals which are visible in Figures 7.5 a&b.

7.6 The ratio of mono- to di- and higher esters within the sucrose ester.

Non-aerated mixtures containing 75% Sweetose and 2% sucrose ester were prepared using the commercial sucrose esters. The composition of commercial sucrose esters is discussed in Chapter 2.

Sucrose esters S1670, S1570, S1170 and S770 with respectively increasing di- and higher ester content were viewed under normal bright-field illumination, Figures 7.6a-d. It was observed that, with increased hydrophobic character the mixture became more granular in appearance. This was explained by the decreasing solubility of the sucrose ester in Sweetose.

Figure 7.6a

75% Sweetose 2% sucrose ester S1670, 77% mono-, 20% di- and 3% tri- ester

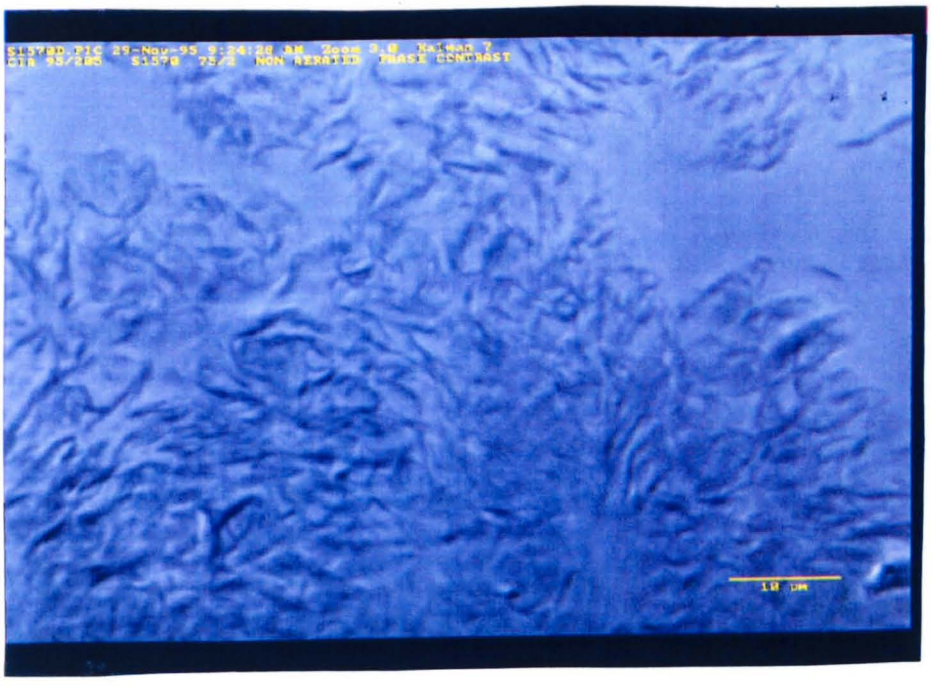

Figure 7.6b

75% Sweetose 2% sucrose ester S1570, 70% mono-, 25% di- and 12% tri- ester

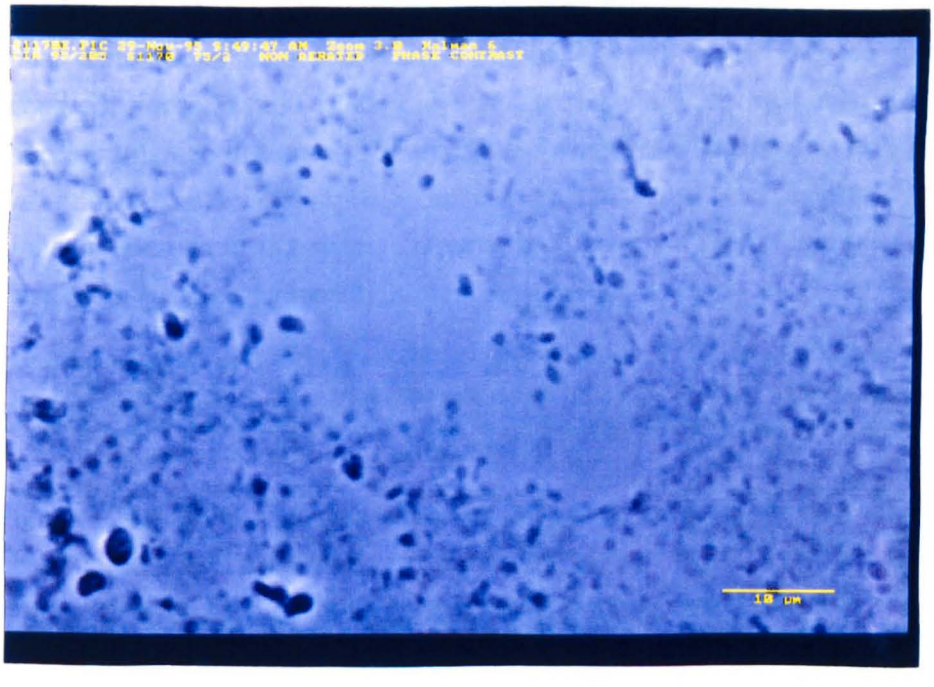

Figure 7.6c

75% Sweetose 2% sucrose ester S1170, 52% mono-, 36% di- and 12% tri- ester

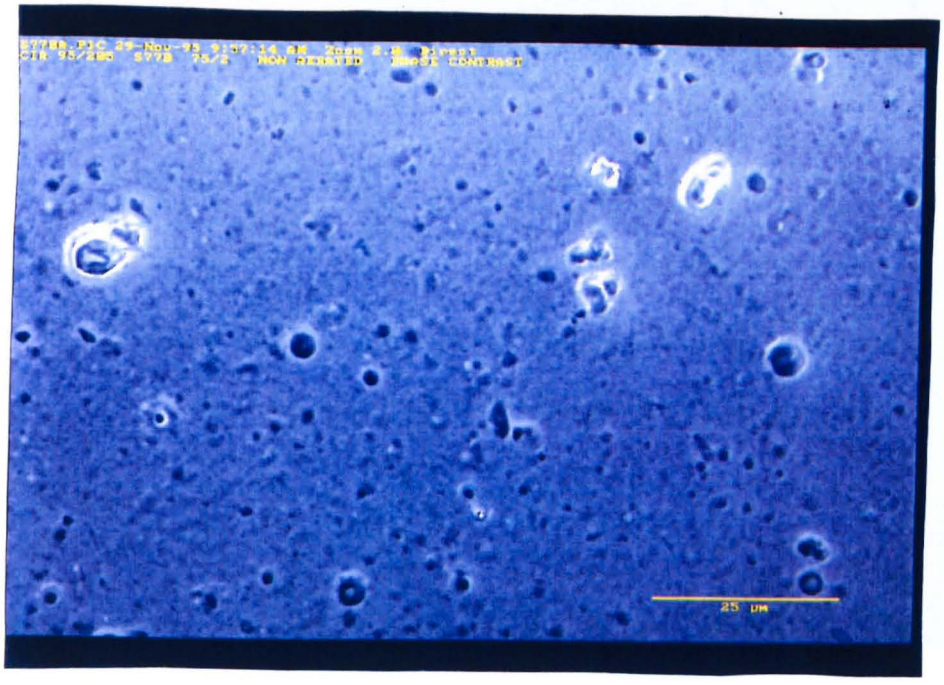

Figure 7.6d

75% Sweetose 2% sucrose ester S770, 29% mono-, 40% di-, 31% tri-/higher ester

7.7 The ratio of mono- to di-stearate in non-aerated mixtures

Small volumes of non-aerated mixtures of 75% Sweetose and 2% sucrose ester were prepared, the total mass of sucrose ester required was divided according to the required ratio of mono- to di- ester. The mono- and di-stearate fractions used in this determination were not commercial samples. Sucrose mono-stearate was from a sample provided by Unilever Research Vlaadigan Laboratory. Sucrose di-stearate was provided by M. Fitzgerald, Reading University.

Figures 7.7a&b illustrate sucrose ester containing 100% mono-stearate under phase contrast and fluorescence illumination respectively. In both cases a negligible amount of heterogeneous sucrose ester, was observed.

Figures 7.7c&d illustrate sucrose ester containing 90% mono- and 10% di-stearate under phase contrast and fluorescence illumination respectively. The visible sucrose ester phase is more widespread than in the case of 100% mono-stearate.

Figures 7.7e&f illustrate sucrose ester containing 70% mono- and 30% di- stearate. The visible sucrose ester appears to be more concentrated and granular than before.

Figure 7.7a

Non-aerated 75% Sweetose 2% sucrose ester, comprising 100% mono-stearate, bright-field.

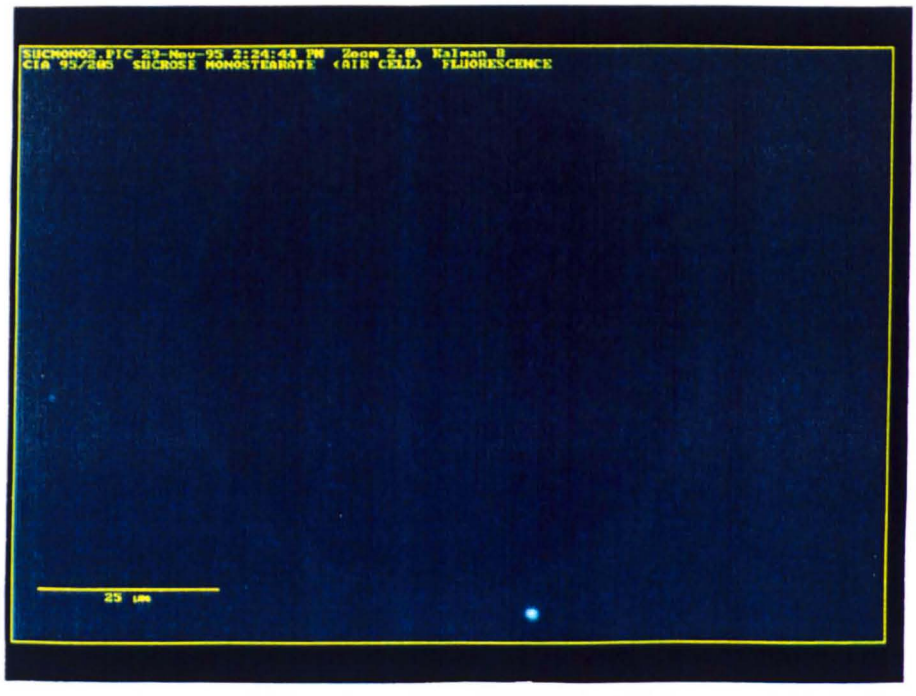

Figure 7.7b

Non-aerated 75% Sweetose 2% sucrose ester, comprising 100% mono-stearate, fluorescence

Figure 7.7c

Non-aerated 75% Sweetose 2% sucrose ester, comprising 90% mono-, 10% di-stearate, bright-field.

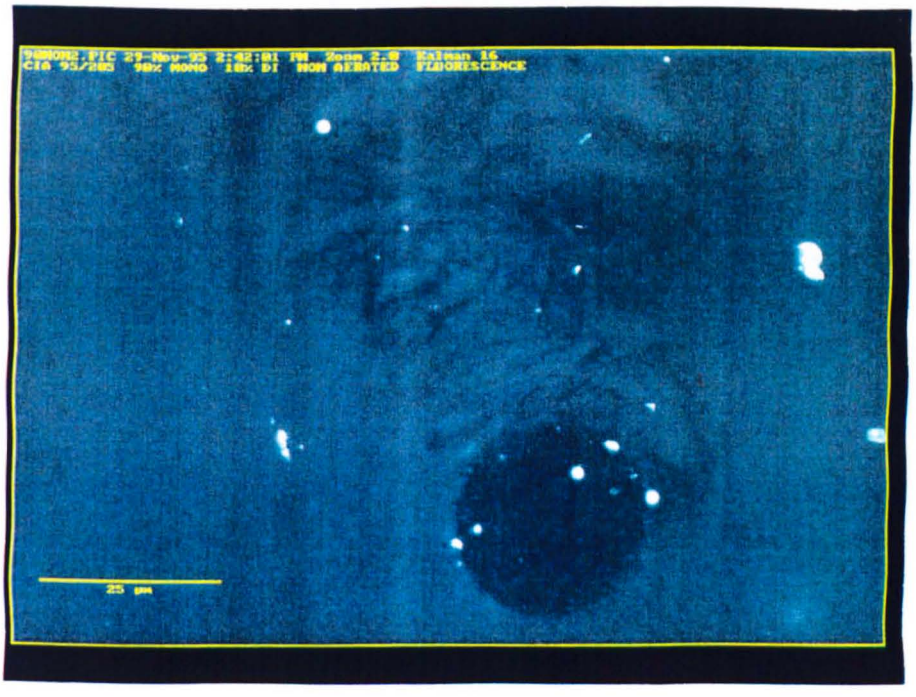

Figure 7.7d

Non-aerated 75% Sweetose 2% sucrose ester, comprising 90% mono-, 10% di-stearate, fluorescence

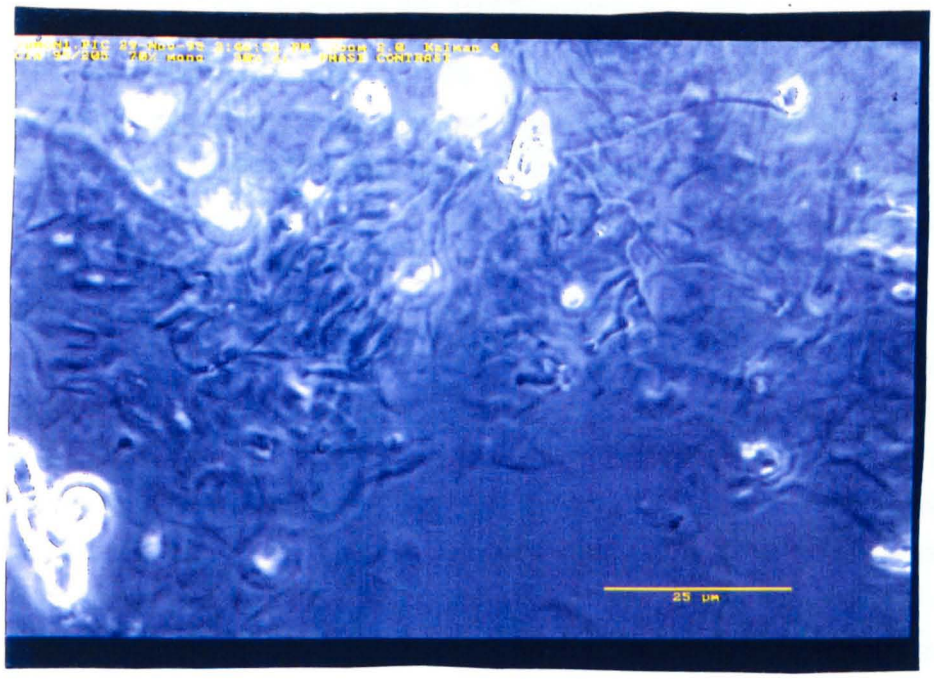

Figure 7.7e

Non-aerated 75% Sweetose 2% sucrose ester, comprising 70% mono-, 30% di-stearate, bright-field.

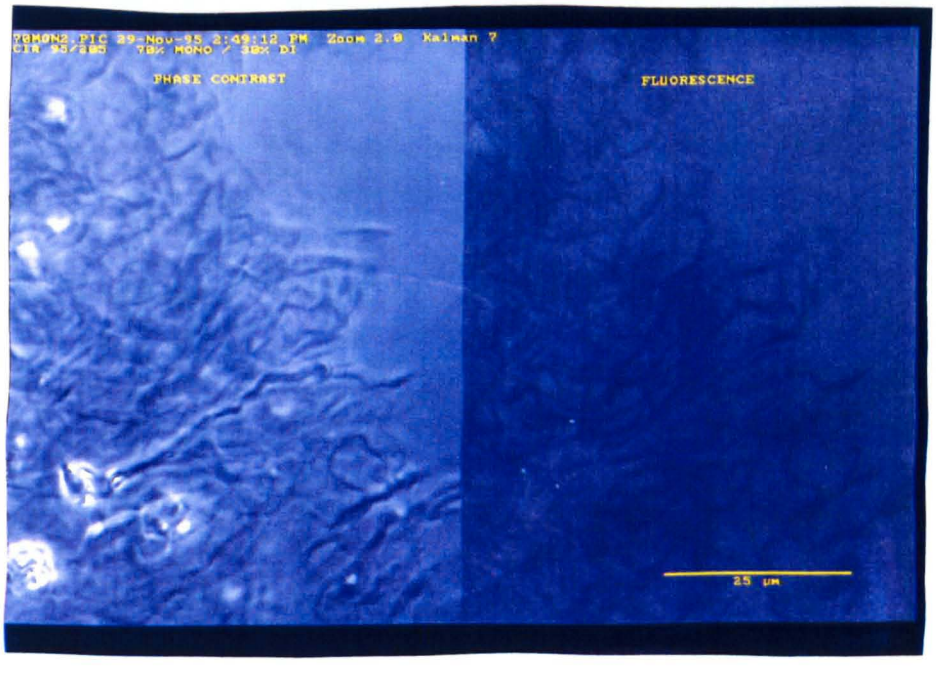

Figure 7.7f

Non-aerated 75% Sweetose 2% sucrose ester,

comprising 70% mono-, 30% di-stearate, bright-field / fluorescence

7.8 Non-aerated 75% Sweetose 2% B1570 mixture

The non-aerated mixture of 75% Sweetose and 2% sucrose ester B1570, sucrose behenate, appeared to be different from previously observed samples of non-aerated sucrose stearate, S1670. Both sucrose esters contain similar ratios of mono- to di- and tri-esters, approximately 70:25:5%. The behenate mixture was heterogeneous, with visible regions of liquid crystalline sucrose ester as expected, but rather than having the appearance of flat overlapping plates, like the stearate sample, they resembled closely packed small spheres. Figure 7.8a illustrates the sample under bright-field (LHS) and laser illumination (RHS). Air bubbles trapped within the mixture were observed to be surrounded by dark aggregates as already described in section 7.3. As discussed previously, these dark figures resemble aggregates floating in the surface. In the absence of further evidence the dark regions were tentatively attributed to regions of the sucrose ester monolayer in a liquid-condensed form co-existing with sucrose ester in a liquid-expanded form. Only the liquid expanded region of the monolayer fluoresces and hence the dark regions appear to float in a liquid monolayer.

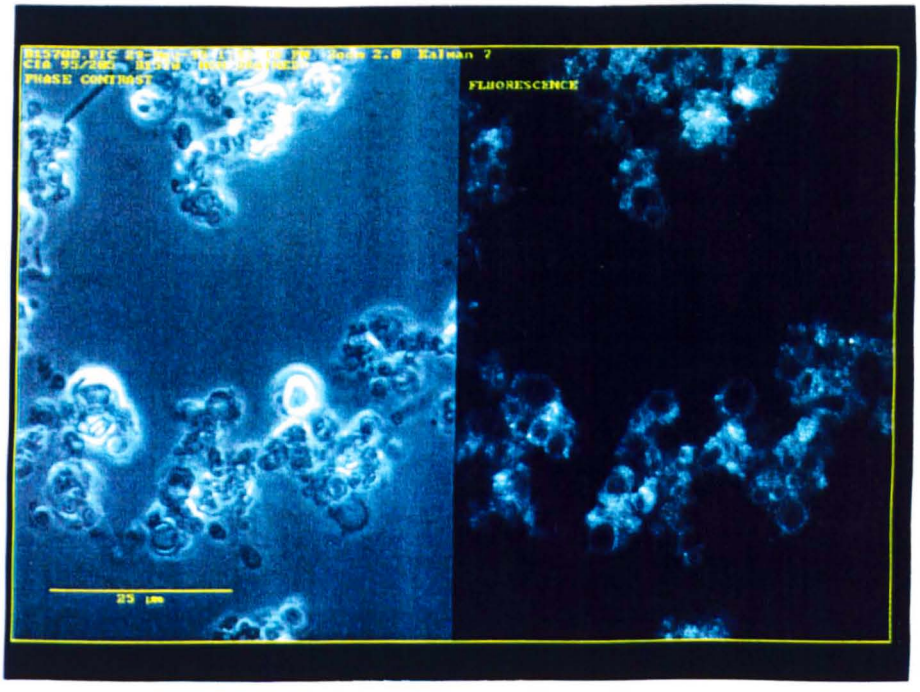

Figure 7.8a

Non-aerated 75% Sweetose 2% sucrose ester, B1570.

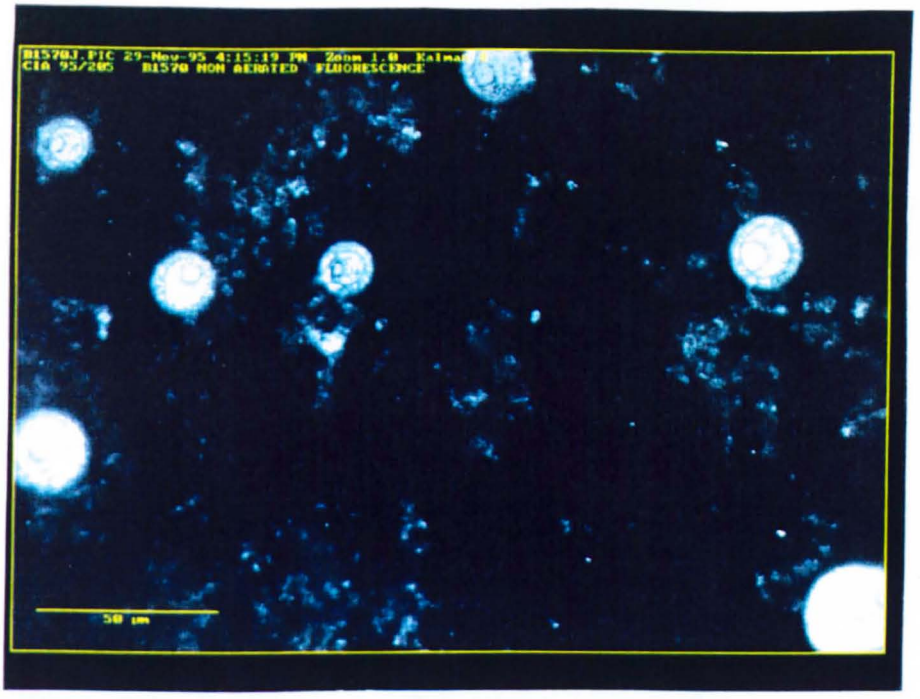

Figure 7.8b

Non-aerated 75% Sweetose 2% sucrose ester, B1570.

7.9 Aerated 75% Sweetose 2% sucrose ester gas microcells after centrifuging

A sample of a 75% Sweetose 2% sucrose ester S1670 foam was centrifuged at 18,000 rpm for 1 hour to concentrate the gas microcells in the upper fraction of the sample, both the resulting upper and lower fractions were examined. TEM observations, presented in Chapter 5, showed that the gas microcells pack closer together and become less spherical after centrifuging but their surface structure remains intact. Figure 7.9a illustrates the upper fraction containing the gas microcells, seen as a dispersion of bright spheres with diameters measuring approximately 1 micron. Figure 7.9b illustrates these at maximum magnification. Figure 7.9c illustrates the dense fraction after centrifuging; the clear viscous liquid was homogeneous and isotropic.

DSC measurements, in conjunction with gel permeation chromatography, discussed in Chapter 6, revealed that the upper fraction contained sucrose ester whereas the lower fraction did not. This was also the case after centrifuging a non-aerated mixture, thus it is likely that the material surrounding the gas cells is the same material observed in non-aerated mixtures, i.e. liquid crystalline sucrose ester. Thermal measurements on the upper fraction revealed a phase transition at 48^{o}C, a similar transition was observed in both aerated and non-aerated mixtures with the same composition.

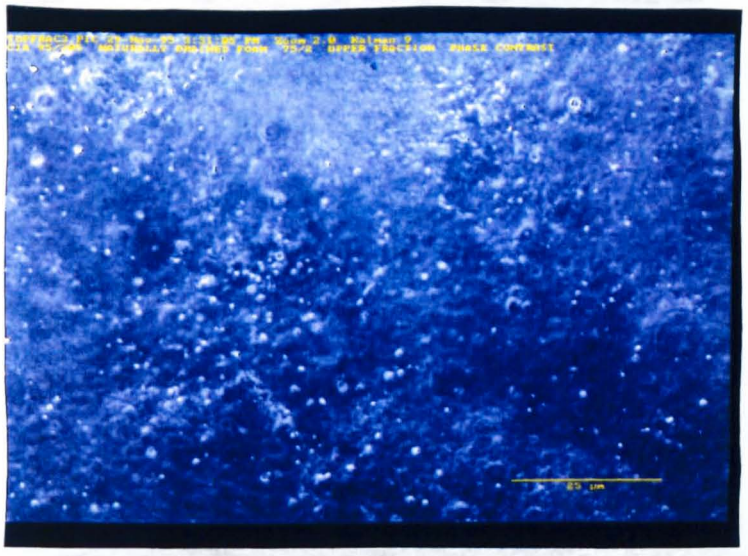

Figure 7.9a
Gas microcells in the upper fraction of a foam after centrifuging

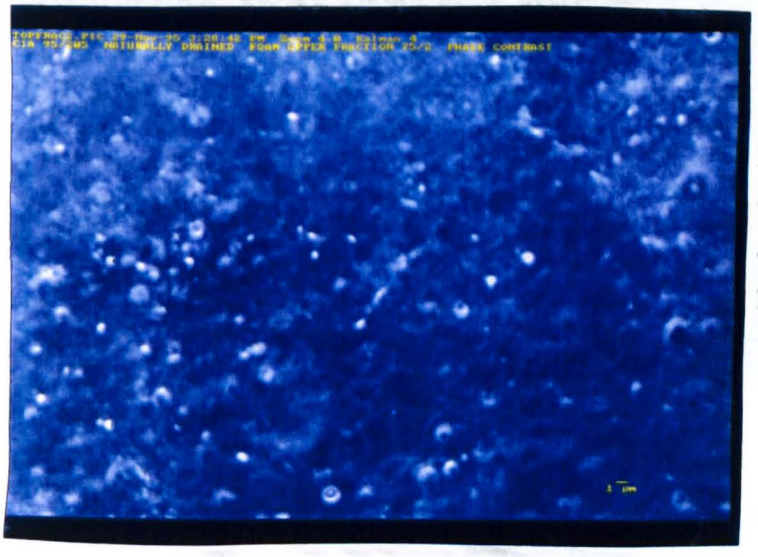

Figure 7.9b
Gas microcells in the upper fraction of a foam after centrifuging, high magnification.

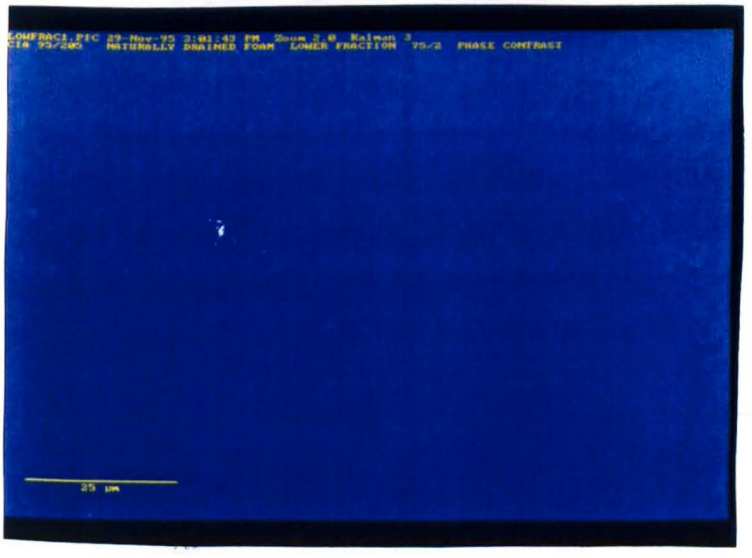

Figure 7.9c
Dense fraction after centrifuging a gas microcell foam.

With further centrifugation, the gas microcells beneath the surface pack more closely together and those at the top become completely drained, the illustration in Figure 7.9d shows a portion of this top layer, the sample was dry and white and resembled a fine spiders web.

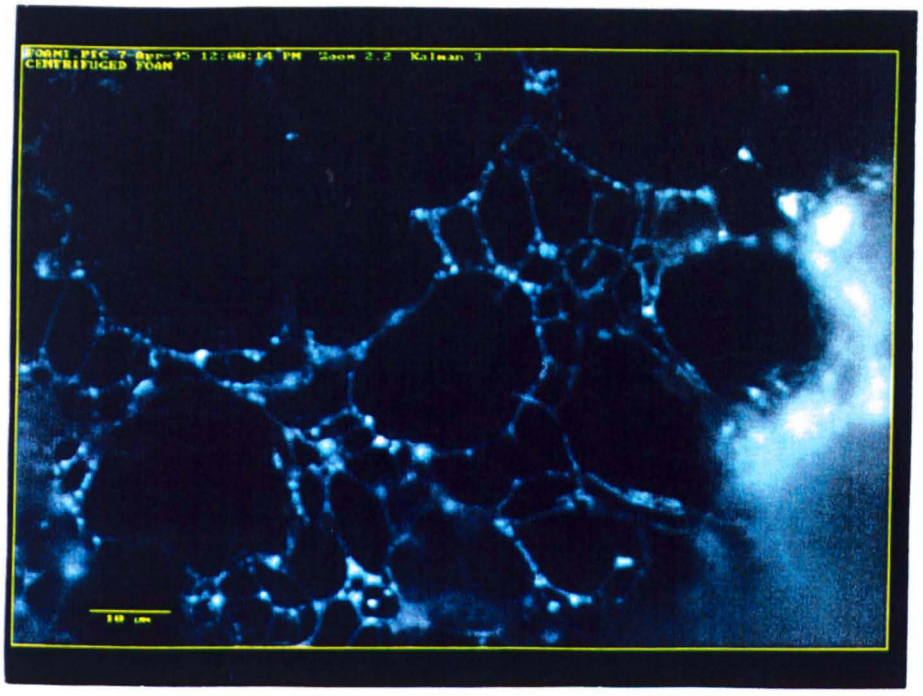

Figure 7.9d

Surface of a gas microcell foam after centrifuging. The foam drains, leaving dry, white, solid threads, which resemble a dry polyhedral foam.

7.10 Insoluble monolayers

Condensed monolayers of long chain fatty acids at the air/water interface have been shown to exist in three distinct phases, according to the surface pressure in the film[1,2,3]. These phases are generally referred to as gaseous, expanded and condensed films. The properties of these films differ according to the area of the surface which is available to each molecule. At very low surface pressure each molecule occupies a large area and is thus highly mobile, these are referred to as gaseous films. At intermediate pressures the molecules occupy less area. They do not have sufficient room to lie flat but remain randomly tilted between the horizontal and vertical. The molecules have less mobility than in the gaseous phase and the film is referred to as liquid-expanded. At higher surface

pressures the area per molecule is smaller than before, the alkyl chains become packed side-by-side as they would be in a liquid hydrocarbon, this is referred to as a liquid-condensed film. Further compression results in a solid film with very low compressibility in which the alkyl chains are packed tightly as they would be in a solid hydrocarbon. This is illustrated schematically in Figure 7.10a.

Generalised Pressure-Area isotherm for insoluble monolayers at the air-water interface[4]

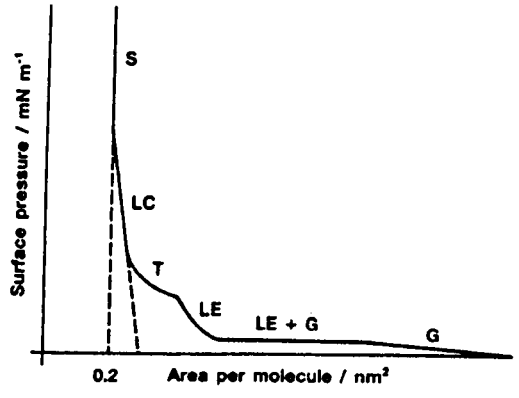

Film States
G - gaseous
LE - liquid-expanded
T - transition
LC - liquid-condensed
S - solid

Figure 7.10a

The transition between the different film states above can also be dependent upon temperature. In liquid-condensed films, at acid pH, the alkyl chains are packed side-by-side with a very low mobility, heating the film causes the alkyl chains to become fluid and the film reverts to the liquid-expanded phase. This chain melting transition is the two-dimensional equivalent of the L_β to L_α phase transition described in Chapter 1. The chain melting temperature varies according to the length of the alkyl chain. Short chain length amphiphiles generally have a low chain melting transition temperature and are thus liquid at room temperature and behave according to the surface pressure-area isotherm above. Stearic acid chains melt at 28°C and exist in the condensed state at room temperature. At low compression the stearic acid molecules do not separate completely from one another because the cohesion between the hydrocarbon chains is strong enough to maintain the film molecules in small islands of condensed film. This means that the film maintains a low surface pressure during compression until the islands join at which point the surface pressure rises rapidly and a tightly packed condensed monolayer results[5]. The limiting surface area at high pressures for all amphiphiles with single saturated alkyl chains and sufficiently small head groups is always found to be about 21 Å^2 per molecule, that is the same as the minimum area per hydrocarbon chain calculated for a bilayer when the hydrocarbon chains are perpendicular to the hydrocarbon surface. In monolayers consisting of amphiphiles with two alkyl chains per head group, the head groups cannot approach as close to each other as amphiphiles with a single chain. Thus the minimum

area per head group at high pressure tends to be about 40Å^2 instead of 20Å^2. The chain melting temperature of amphiphiles is not only dependent on the length of the chain but also on the size of the head group and the magnitude of the electrostatic interactions between adjacent head groups. The chain melting temperature for sucrose stearate in the bulk phase, measured by DSC in Chapter 6, was 48°C.

A technique for illustrating the state of aggregation of surfactant molecules in an insoluble monolayer was recently developed by Mohwald[6]. He added a surface active fluorescent dye molecule to the insoluble monolayer, at very low concentration. The dye was only soluble in the regions where the monolayer was in a liquid-expanded state. Thus gaseous and liquid-condensed films were non-fluorescing. The character of the film was evident from the intensity of the fluorescence. He observed the behaviour of monolayers of L-α-dipalmitoyl phosphatidic acid in a Langmuir trough with increasing surface pressure.

At low surface pressure the film he observed contained both gaseous and liquid expanded regions. The regions observed were circular which he explained was due to the effect of line tension minimising the area of contact between the two phases. The area occupied by each phase depended upon the surface pressure. Figure 7.10b illustrates a schematic diagram of his observations.

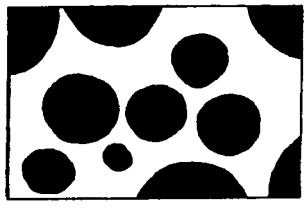

Low surface pressure

Large dark gaseous regions in a bright liquid-expanded film.

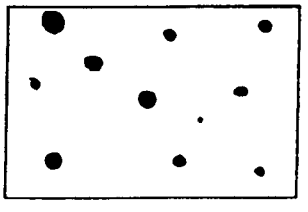

Intermediate surface pressure

Small dark gaseous regions in a bright liquid-expanded film.

Figure 7.10b

As the monolayer was further compressed, beyond a homogeneous liquid-expanded state, a transition region between liquid-expanded and liquid-condensed was reached. The liquid-condensed phase appeared darker than the liquid-expanded phase because the high compression means they can solubilise fewer dye molecules. The monolayer appeared to contain dark, circular islands randomly spaced within a bright fluorescent sea. With further compression the dark regions became more numerous and more regular, all were approximately the 17 microns in diameter. At high surface pressure the islands of liquid-condensed material became packed into a hexagonal array, surrounded by a bright liquid-expanded background. Mohwald explained the formation of this hexagonal lattice by the

presence of electrostatic forces. At very high pressures the film became fully liquid-condensed. These observations are illustrated schematically in Figure 7.10c.

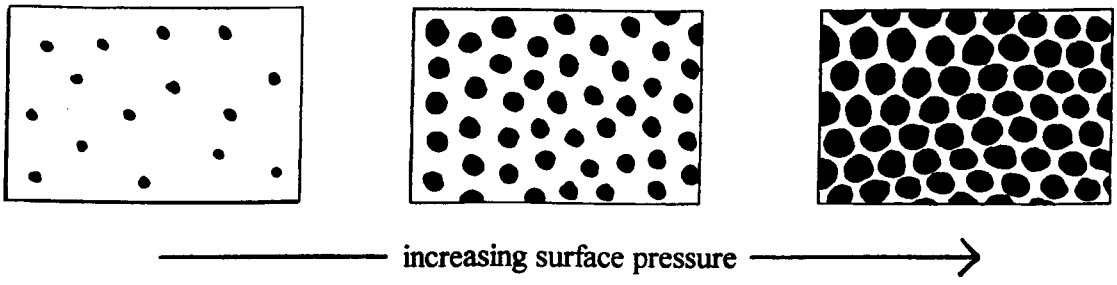

increasing surface pressure →

Small dark liquid-condensed regions nucleate in a bright liquid-expanded film.

Dark liquid-condensed regions expand to become equidistant and of equal size in a bright liquid-expanded film.

Dark liquid-condensed regions form a hexagonal lattice within the remains of a bright liquid-expanded film.

Figure 7.10c

Other workers have investigated the behaviour of stearic acid monolayers[7,8,9,10], Rondelez[11] used fluorescence microscopy to investigate phase transitions in stearic acid monolayers. He investigated the transition between the liquid-expanded and liquid-condensed phases, observing that this transition was a strong function of temperature, with the region in which the two phases co-exist narrowing as the temperature increased towards the chain melting temperature. Above the chain melting temperature the liquid-expanded phase became indistinguishable from the liquid-condensed phase. In the region near to the chain melting temperature the properties of the system were observed to become very peculiar, Widom[12] observed that the line tension between the two phases approached zero and for this reason the liquid-condensed domains were no longer circular. Losche and Mohwald[13] investigated L-α-dimyristoyl phosphatidic acid monolayers and found that the shape of the domains was influenced by the electrostatic charge between the head groups. Lee and McConnell[14] investigated the changes in domain shapes which could be brought about by changes in the surface pressure of the monolayer. In summary the domain shapes and sizes are determined by a competition between line tension at the domain boundary and dipole-dipole electrostatic repulsion between the molecules in the domains. Line tension acts to reduce the length of the interface between the liquid-expanded and liquid-condensed phases and thus favours circular domains whilst electrostatic repulsion forces tend to maximise the distance between molecules and thus favour non-circular shapes[15,16,17,18]. Characteristic domain shapes, reproduced from the paper by Losche and Mohwald[13] are given below, Figure 7.10d.

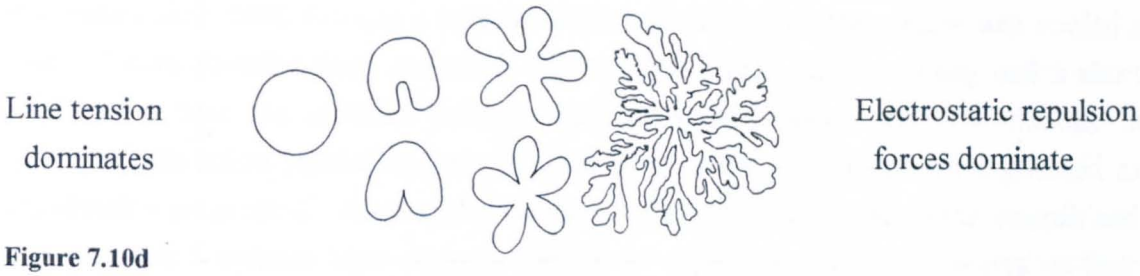

Figure 7.10d

Diagram reproduced from the paper of Losche and Mohwald[13].

This fluorescence microscopy technique was used to investigate the surface of air bubbles, trapped within a 75% Sweetose 2% sucrose ester non-aerated matrix. This matrix was known to be heterogeneous, containing a sucrose stearate gel phase within a 75% Sweetose aqueous phase. The results of this investigation were given previously, in Section 7.2. For information, Figure 7.10e illustrates the surface of one of these trapped air bubbles. These trapped air bubbles are not gas microcells and they are not thought to have a regular domain structure at their surface because they have not undergone the shearing process during aeration. TEM investigations also indicated that expanding surfaces do not contain structured domains. These trapped air bubbles were relatively large and were assumed to be expanding due to disproportionation rather than shrinking.

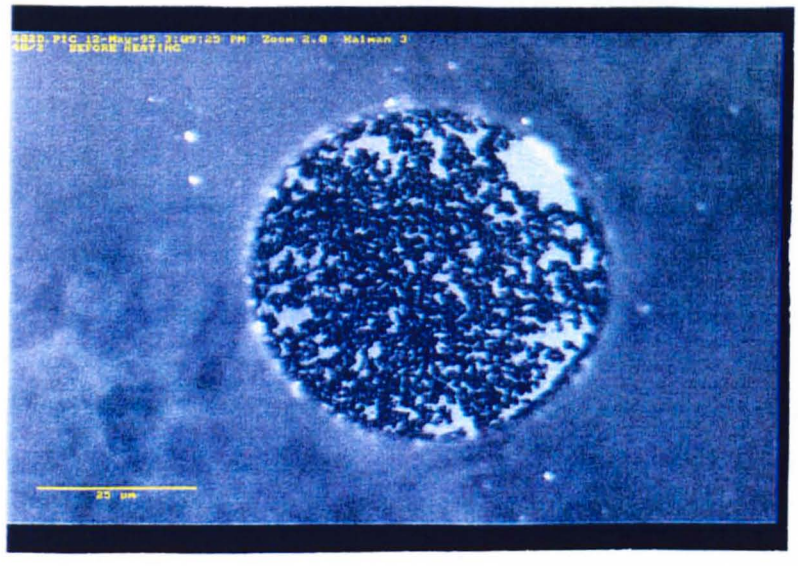

Figure 7.10e

The surface of the bubble was observed to be fluid when viewed directly. The dark domains traversed the surface but did not move into the surrounding matrix.

It was stated above that the equilibrium shape of domains observed was the result of competition between line tension at the interface and electrostatic forces of repulsion. When these domains were heated, as was previously illustrated in Figure 7.3, they melted

at approximately 50°C forming a homogeneous surface. When the surface was cooled a series of dark domains were nucleated, Figure 7.3c. After further cooling and a short equilibration time the domains became regularly spaced plates, about 3 microns in diameter, with spikes protruding into the surrounding surface, these spikes lengthened as equilibration progressed. After initial nucleation the expanding plates were smooth and circular, after 5 minutes their diameter ceased to expand and spikes appeared at their surface. These spikes grew slowly during the observation time, with a decreasing rate until, after 20 minutes, observation was ceased in the knowledge that equilibrium was not reached but that any further changes might only be observed after many hours.

The observation that the sucrose ester phase melted at 50°C was taken as an indication that the sucrose ester at the surface must be below its chain melting point when at room temperature. Thus the dark domains observed on the surface of the bubble are unlikely to be due to the compressive effect of surface pressure on a liquid-expanded phase but possibly to the tendency of the stearate chains to form islands of condensed phase at this temperature, due to the mixture of mono- and di- and tri- stearates contained in the blended sucrose ester used in this experiment. These conclusions are based on observation of the surface of an air bubble by fluorescent light during heating and cooling, and the DSC evidence that sucrose ester S1670, undergoes a phase change at this temperature which was attributed to a chain melting transition in the alkyl chains. It is not possible to observed the surface of a gas microcell during heating and cooling because of its small diameter. It is also experimentally problematic to examine the surface of a Sweetose/sucrose ester mixture using a Langmuir trough because of the high viscosity of the mixture and the tendency of the sucrose ester to separate from the Sweetose mixture on heating.

The incidental gas bubble containing the surface domains had not previously been heated and thus its surface was the result of the transference of sucrose stearate from the bulk liquid crystal, gel phase. Heating the bubble changed the appearance of these domains, this was attributed to the condensation of a mixture of mono- and higher stearates at the surface after heating. The constitution of the monolayer after heating was different to that before, thus explaining the changed appearance of the surface under fluorescent light.

7.11 Summary

The separation of both a non-aerated mixture and a foam into their two components, respectively a liquid crystalline phase and the gas microcells, each surrounded by viscous matrix revealed that in both cases all of the sucrose ester in the sample was contained in the liquid crystal and the gas microcells. The effect of increased Sweetose concentration

on a non-aerated mixture of Sweetose and 2%w/w sucrose ester was to increase the amount of liquid crystalline material observed, because the 80%w/w hydrophilic solids content of Sweetose dramatically decreased the concentration of water. Changing the ratio of mono- to di- and higher esters affected the appearance of the liquid crystal phase. The mono-stearate sample formed a liquid crystalline phase only when it was mixed with di-stearate, when mono-stearate was the major component the liquid crystal resembled overlapping planes but with the further addition of di- and higher stearate the phase became more granular in appearance. This is consistent with the observation of a phase change by DSC and of domain formation by TEM in mixtures of mono- and di- stearate but not in pure mono-stearate. Substituting B1570 for S1670 did not affect the formation of the heterogeneous phase, however its appearance was granular, resembling the more hydrophobic sucrose esters, possibly due to the lower solubility and increased rigidity of the longer chain length behenate esters.

The surface of an incidental gas bubble was seen to contain small, black particles with a random arrangement, on a brightly fluorescing gas bubble surface. This was attributed to the presence of liquid-condensed and liquid-expanded regions within a sucrose ester monolayer surrounding the gas bubble, the dark regions corresponding to the liquid-condensed phase. Heating melted the monolayer at the phase transition temperature observed by DSC, 48°C, on cooling the regions re-condense in an arrangement which balances the forces of line tension at the interface and electrostatic repulsion between the head groups.

Gas microcells were observed by confocal microscopy, however with diameters in the range of 1-2 micron their surfaces were too small to resolve.

7.12 References

[1] Langmuir, I.; J. Am. Chem. Soc., **39**, 1848, (1917)

[2] Adam, N.K.; Physics and Chemistry of Surfaces pp. 39-55

[3] Harkins, W.D.; Physical Chemistry of Surface Films, pp. 106-117, 1952, Rheinhold, London.

[4] Clint, J.H.; "Surfactant Aggregates", publ. Blackie, 1992.

[5] Davies, J.T. and Rideal, E.K.; "Interfacial Phenomena", Academic Press, New York, (1961)

[6] Mohwald, H.; Thin Solid Films, **159**,1, (1988).

[7] Smith, R.D. and Berg, J.C.; J. Coll. Int. Sci., **74**, 1, 1980.

[8] Gaines, G.L.,Jr.; in "Insoluble monolayers at liquid-gas interfaces", Wiley (interscience), New York, 1966.

[9] Ries, H.E., Jr, and Walker, D.C.; J. Colloid Sci. **16**, 361, (1961)

[10] Ries, H.E., Jr.; J. Colloid Sci. **9**, 535, (1954)

[11] Rondelez, F.; in 'The physics of amphiphilic layers' Ed. J. Meunier, D. Langevin and N. Boccara, publ. Springer Verlag, 1987.

[12] Widom, B.; in 'Phase transitions and critical phenomena, vol. 2, C. Domb and M.S. Green eds., (Academic Press, London 1976)

[13] Losche, M. and Mohwald, H.; J. Coll. Int. Sci. **131**, 1, (1989)

[14] Lee, Ka Yee C. and McConnell, M.; J. Phys. Chem. 1993, **97**, 9532

[15] Andelman, D., Brochard, F. and Joanny, J.; J. Phys. Chem. 1987, **91**, 6417

[16] McConnell, H.M. and Moy, V.T.; J. Phys. Chem. 1988, **92**, 4520

[17] Vanderlick, T.K. and Mohwald, H.; J. Phys Chem. 1990, **94**, 886

[18] McConnell, H.M.; J. Phys. Chem. 1992, **96**, 3167

CHAPTER 8

Rheology

8.0 RHEOLOGY

8.1 Introduction

Non-aerated mixtures of Sweetose and sucrose ester at room temperature have been shown in previous chapters to contain liquid crystalline bilayers of sucrose ester, separated by a solution of Sweetose. These bilayers were observed using TEM and detected by DSC. Their concentration was dependent on the ratio of Sweetose to sucrose ester in the mixture. The handling characteristics of the mixture were affected by the amount of liquid crystalline sucrose ester present. In an attempt to quantify this affect, rheological measurements on Sweetose and mixtures of Sweetose and sucrose ester have been made. The mixtures of Sweetose and sucrose ester were prepared as described in Chapter 2, i.e. with the remaining sample weight made up with water.

8.2 Theory

When a material is deformed under a shear stress the adjacent elements within that material undergo relative motion. By studying the rheology of the material it is possible to gain information about any interactions between the particles and between the particles and the medium. When the deforming stress is removed materials tend to respond in one of 3 ways; they return to their original shape, in which case their behaviour is described as elastic, they remain in their new position and are described as viscous, or they recover partially in which case they are described as viscoelastic. In general, solids usually have elastic behaviour and simple liquids have viscous behaviour.

The deformation of a material under shear[1]

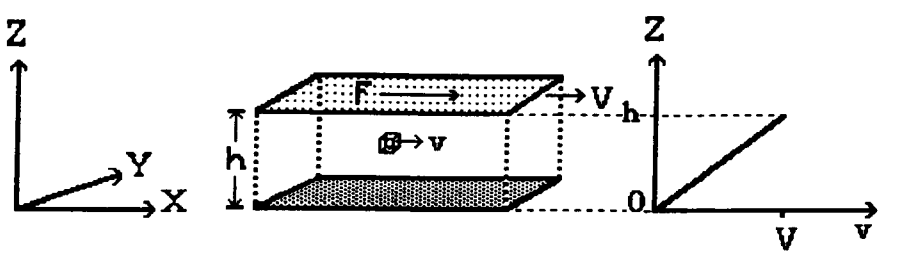

Figure 8.2a

Figure 8.2a represents a fluid between two parallel plates a distance h apart. A shearing force F is applied to the upper plate causing it to move with a relative velocity V in the x-direction. The lower plate remains stationary. Assuming that there is no slip at the surface of either of the plates then the velocity of movement, v, of an element of the fluid increases linearly from Z=0, to V at Z=h.

PAGE
MISSING
IN
ORIGINAL

The force per unit area applied to the material is called the shearing stress, σ, and it causes a deformation or strain, γ. In ideal liquid-like behaviour the applied shearing stress is directly proportional to the time rate of strain, or rate of shear, $\frac{d\gamma}{dt}$, which is the ratio of V/h.

$$\text{Shear stress, } \sigma = \eta \cdot \frac{d\gamma}{dt} \text{ where } \eta \text{ is the viscosity and } \gamma \text{ is the strain.}$$

Fluids whose viscosity is independent of the rate of shear are called Newtonian liquids. In Newtonian liquids the flow pattern tends to be laminar, in which case the viscosity can be well defined for a given temperature and pressure and will be independent of σ and γ. For concentrated solutions or those containing aggregates or particles, deviations from Newtonian flow are observed due to the formation of velocity gradients within the liquid and the flow is described as non-Newtonian. The viscosity is the ratio of shear stress to shear strain. In Newtonian materials these are directly proportional to one another. Where the behaviour is non-Newtonian it is more usual to describe the slope of the shear stress vs. shear rate curve and the viscosity is referred to as the apparent or differential viscosity.

If the apparent viscosity increases with shear strain γ then the fluid is described as shear thickening. If the reverse occurs then it exhibits shear thinning. If there is no initial response to the imposition of stress, but flow begins after a certain stress level is reached then this is described as pseudoplastic behaviour. These are illustrated in Figure 8.2b.

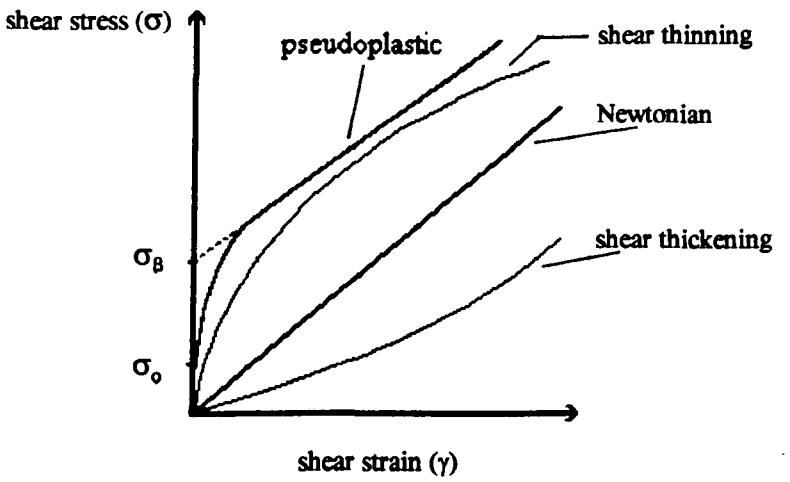

Figure 8.2b

Where the material exhibits pseudoplastic behaviour, as illustrated above, the minimum stress required to cause the material to flow, is called the yield stress and is specific to the particular material. If after flow has begun the relationship between shear stress and shear strain becomes linear then the behaviour is described as Bingham flow. The gradient at

high shear is called the differential viscosity and is related to the shear stress by the equation,

$$\sigma - \sigma_B = \eta_\Delta.\gamma \quad \text{where } \sigma_B \text{ is the Bingham yield stress.}$$

This behaviour can be caused by a continuous structural network which imparts rigidity to the sample and must be broken down before flow can occur. In many cases the yield stress exhibited by a material is time dependent. i.e. if the strain is applied quickly the yield stress may be high whereas the material will flow if the strain is applied more slowly.

In colloidal systems containing aggregated particles a high shear rate will tend to break down the aggregates releasing any solvent which was immobilised and hence the viscosity of the mixture reduces and the behaviour is described as shear-thinning. Materials containing asymmetric particles tend to be shear thinning because the high shear aligns the previously random orientation of the particles and thus they disturb the flow lines to a lesser extent. In these systems the apparent viscosity is a factor of the balance between the randomness and alignment and between aggregation and dispersion of the particles within the medium. In some media the apparent viscosity increases with an increased rate of shear. This behaviour is described as shear-thickening and often occurs in materials which contain densely packed particles in a limited supply of solvent. When the material is sheared the interparticle distance increases to allow the particles to flow past one another. This has a dilatant effect, which with a limited supply of solvent causes an increase in the apparent viscosity.

It sometimes happens that the apparent viscosity of a suspension depends both on the shear rate and the time for which the system has been sheared. This is an indication that the structure in the system, which determines the apparent viscosity, is being altered at a rate which can be observed during the time period of the measurement. The most common phenomenon of the type is called positive thixotropy. This is where the apparent viscosity at a particular shear rate decreases with time, usually because the shearing process is causing a gradual breakdown in the structure of the material. If the process is continued for long enough then a steady state equilibrium value of the shear stress can be achieved, however this is not always possible or practical. If a steady state is not achieved then measurements of shear stress across a range of shear strains from low to high and back will result in a hysteresis loop, Figure 8.2c. The closer the system is to its steady state the smaller will be the area of the loop.

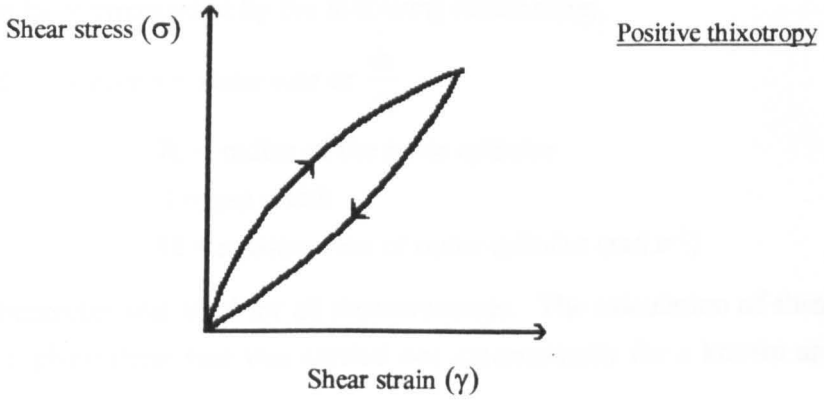

Figure 8.2c

A more detailed discussion of rheological behaviour is given by Hunter[2].

8.3 Measurement of viscosity

To measure viscosity it is necessary to establish a state of steady flow across the sample. In this study a concentric cylinder viscometer was used, consisting of two co-axial cylinders with the sample contained in the gap.

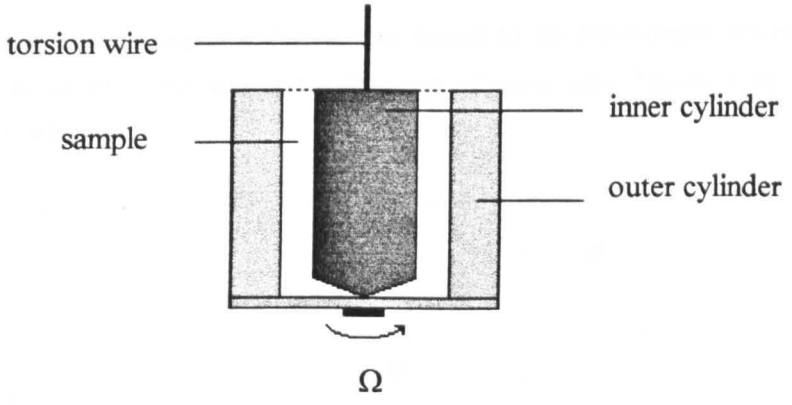

Figure 8.3a

The outer cylinder is rotated at a constant rate, Ω rad s^{-1}, and the inner cylinder is fixed in place by a torsion wire. The viscous drag of the liquid against the surface of the inner cylinder causes it to twist. The restoring torque which must be applied to the wire to prevent rotation of the inner cylinder is measured.

The gap width must be small to maintain a constant shear rate across the sample. The shear rate can then be approximated by the following relationship,

$$\dot{\gamma} = \Omega R_i/d \qquad \text{where } \dot{\gamma} = \text{shear rate or } \frac{d\gamma}{dt}$$

R_i = radius of the inner cylinder

d = gap width

Ω = rotation rate of outer cylinder (rad s^{-1})

A Bohlin VOR Rheometer was used for all measurements. The calculation of shear stress and viscosity, for a given shear rate was carried out automatically for a known apparatus geometry.

8.4 Experimental

Measurements of viscosity as a function of shear rate were carried out on the following samples;

- 75% w/w Sweetose in water at 25°C.
- A mixture of 75%w/w Sweetose with 1% w/w sucrose ester, S1670 at 20°C.
- Mixtures of 60%w/w Sweetose with 1, 2, 3 & 4% w/w sucrose ester, S1670 at 20°C.
- Mixtures of 2%w/w sucrose ester S1670 with 20, 40, 60 and 75% Sweetose at 20°C.

The 75%w/w Sweetose in water solution was found to be Newtonian across a range of shear rates, i.e. its shear stress was not a function of shear rate, Figure 8.4a. Its average viscosity was 73 mPa s.

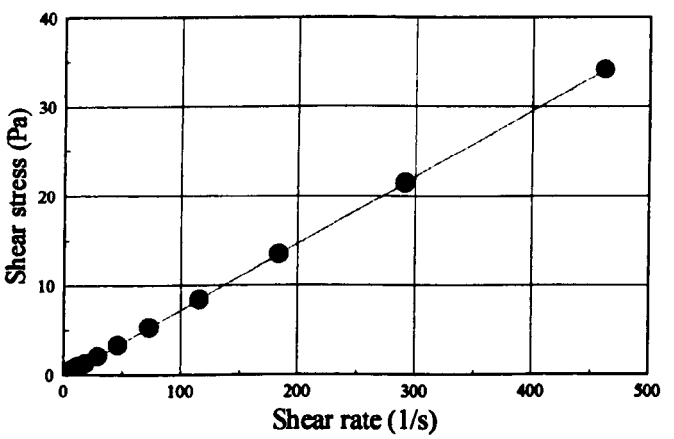

Figure 8.4a

Shear stress vs. shear rate for a 75%w/w solution of Sweetose in water.

When 1%w/w sucrose ester S1670 was added to 75%w/w Sweetose to form a non-aerated mixture, as described in Chapter 2, the rheological behaviour of the resultant mixture was shear-thinning, with an initial yield stress. The value of the yield stress depended on the rate of shear and the interval of sampling, although only one example is

illustrated. Figure 8.4b illustrates the viscosity and shear stress for a non-aerated mixture of 75%w/w Sweetose 2%w/w sucrose ester S1670 as a function of time.

The run conditions were as follows;

Shear rate - 1.459 x 10^{-1} (s^{-1})	Range 0.5 - 79 %
Number of measurements - 900	Measuring system - C25
Measurement interval - 0.1secs	Torque element - 4.13 g cm

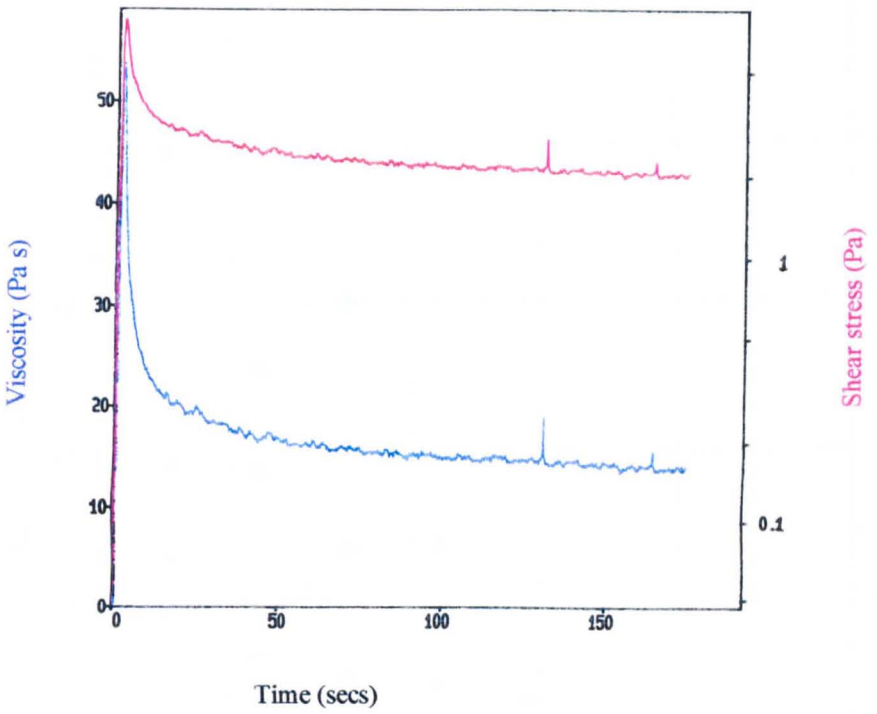

Figure 8.4b

Viscosity and shear stress as a function of time for a non-aerated mixture of 75%w/w Sweetose and 1%w/w sucrose ester S1670

Neat Sweetose is a highly viscous liquid and thus it was expected that the viscosity of any non-aerated mixtures with Sweetose would be affected by its concentration. Confocal microscopy evidence indicated that the amount of sucrose ester present as liquid crystalline bilayers was affected by both the concentration of Sweetose and of sucrose ester. It was anticipated that the amount of bilayer structuring within the sample would affect its viscosity. Figures 8.4c&d illustrate the viscosity of a number of samples containing both Sweetose and sucrose ester as a function of shear rate. Figure 8.4c illustrates the effect of changing the concentration of sucrose ester in a non-aerated mixture with 60% Sweetose. The shear rate was varied from low to high shear and back in all the samples. The sucrose ester concentration was varied between 1 and 4%w/w. The sample containing 1%w/w sucrose ester was the least viscous, across the range of shear rates measured. In all the

Viscosity of mixtures of 60%w/w Sweetose with sucrose ester, S1670 at different w/w concentrations vs. shear rate.

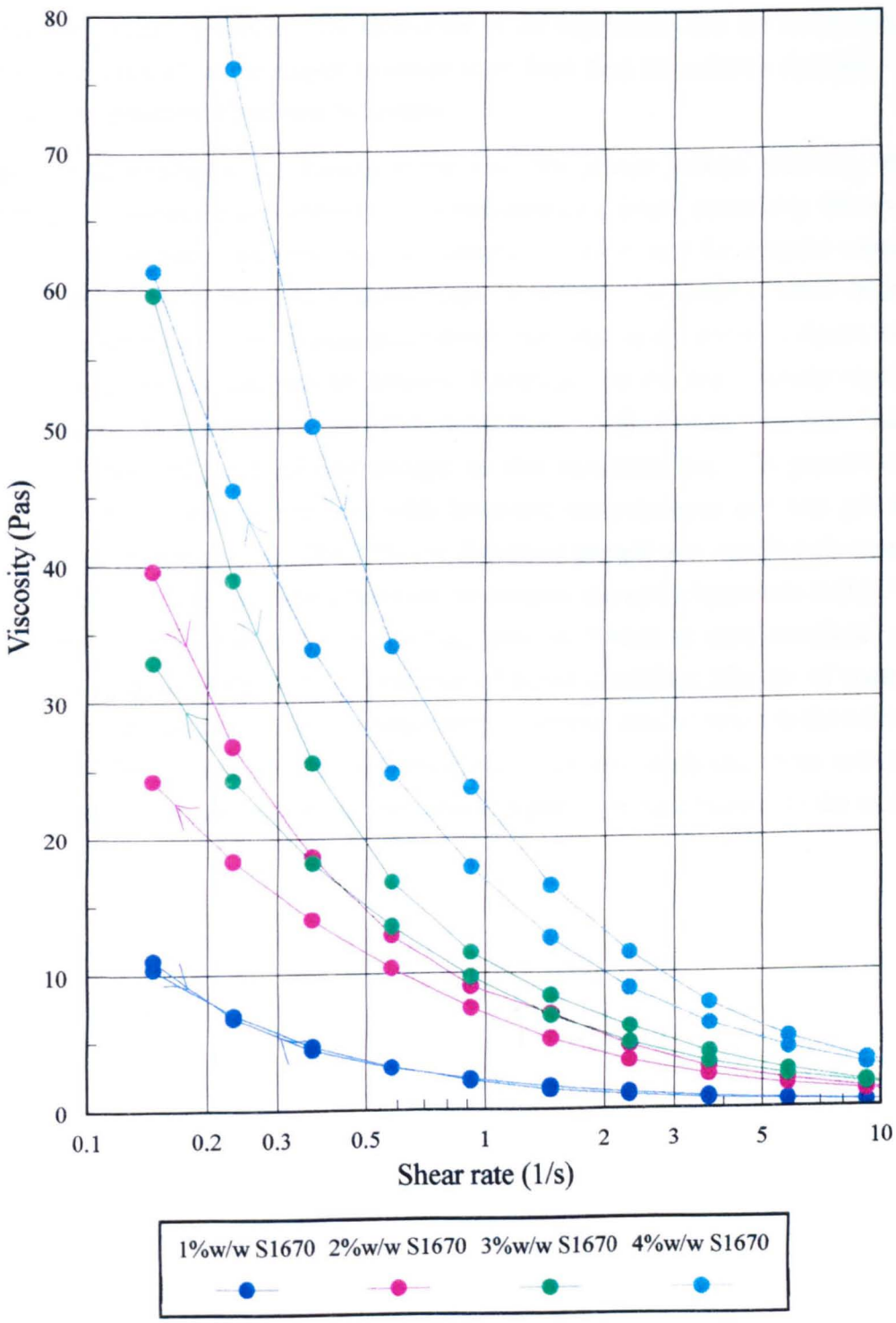

Figure 8.4c

samples the viscosity was greatest at low shear rates. The sample containing 4%w/w sucrose ester was the most viscous due to its containing the largest amount of liquid crystalline sucrose ester bilayers, as previously observed by optical microscopy in Chapter 3. In the samples containing 2, 3 and 4%w/w sucrose ester, a hysteresis in the measured viscosity was observed which was attributed to a breakdown in the sucrose ester bilayer structure within the sample. The time-scale of the experiment and the continuous shearing process did not allow the bilayer structure to re-form thus the reduced viscosity. This is an example of positive thixotropic behaviour.

Figure 8.4d illustrates the changes in the viscosity of non-aerated mixtures, effected by altering the Sweetose concentration in a non-aerated mixture containing 2%w/w sucrose ester. The viscosity was measured as a function of shear rate for samples containing 20, 40, 60 and 75%w/w Sweetose concentration, as before. The range of shear rates sampled was extended by an order of magnitude down from that in the previous figure, to account for the relatively low viscosity of 20%w/w Sweetose. At this low viscosity rapid shearing was expected to result in the immediate breakdown of the few sucrose ester bilayers that were observed by confocal microscopy at this concentration. In general terms the viscosity of the mixture increased with Sweetose concentration and was greatest in all samples at low shear rates. The 75%w/w Sweetose sample was significantly more viscous than the rest. At very low shear rates all the samples showed a hysteresis in their viscosity. The observance of thixotropic behaviour, even in Sweetose concentrations as low as 20%w/w, is an indication of the presence of liquid crystalline bilayers of sucrose ester. The area of the hysteresis loop increased with Sweetose concentration in the mixture, for a constant 2%w/w sucrose ester concentration. This was attributed to an increase in the amount of sucrose ester present in the form of liquid crystalline bilayers in the mixture.

Viscosity of mixtures of 2%w/w sucrose ester S1670
with Sweetose at different w/w concentrations vs. shear rate.

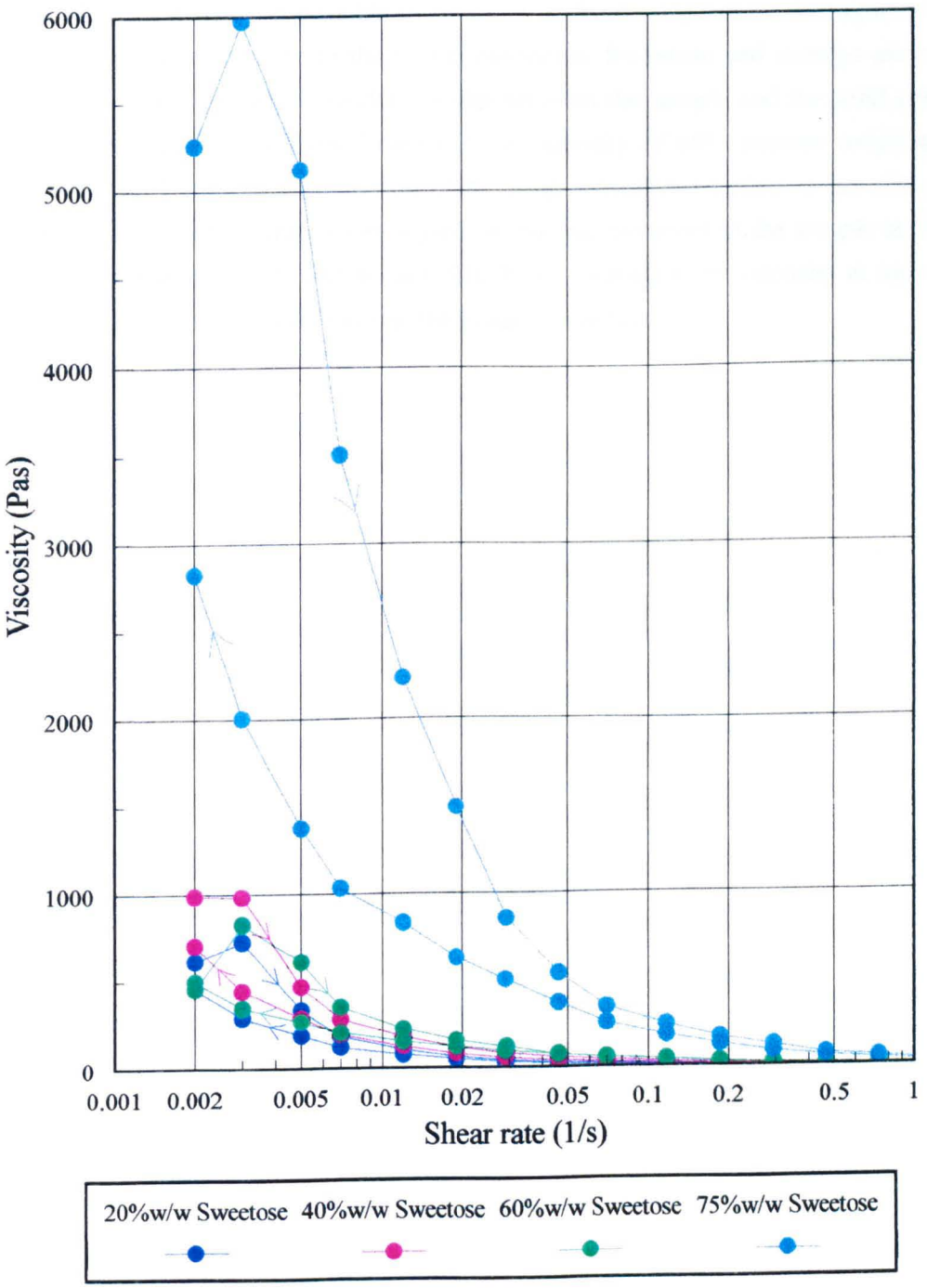

Figure 8.4d

PAGE
MISSING
IN
ORIGINAL

The shear rate, shear stress and viscosity data, together with details of run conditions, temperature etc. for Figures 8.4c&d are given in Appendix A1.

DSC investigations, described in Chapter 6, showed that a phase transition occurred at 48°C which was attributed to the melting of the alkyl chains in the sucrose ester bilayer. The above measurements were made at 25°C. Measurement of the viscosity at 60°C was attempted but it was not possible to obtain a uniform temperature throughout the sample and prevent the separation of the two components, Sweetose and sucrose ester. With the sample at 60°C there was considerable slip between the sample and the solid surface of the cylinders. Fitzgerald[3] obtained data for the viscosity of 60% sucrose solution with 2, 5 and 10%w/w S1670 at both 25 and 60°C using a roughened plate to prevent the sample slipping. He observed that where a yield stress was observed in the sample at 25°C it was no longer present at 60°C and at each S1670 concentration the viscosity at low shear rates was an order of magnitude lower at the lower temperature.

8.5 References

[1] Hunter, R.J.; "Introduction to modern colloid science", Oxford University Press.

[2] Hunter, R.J.; "Foundations of colloid science Vol. 2", Oxford University Press, 1992.

[3] Fitzgerald, M.; PhD Thesis, University of Reading, 1996.

CHAPTER 9

Density of non-aerated mixtures

9.0 DENSITY OF NON-AERATED SWEETOSE SUCROSE ESTER MIXTURES

Samples of non-aerated mixtures were prepared as previously described. Density measurements were not made until the non-aerated sample was at least 24 hrs old; this was to allow the sample to approach equilibrium after cooling. Density measurements were taken by means of a graduated syringe. A $2cm^3$ syringe was filled with non-aerated sample and weighed. Known aliquots were dispensed and the syringe was re-weighed until no further sample remained. This process was repeated for several samples of each non-aerated mixture and an average density calculated. For the more dilute samples a pipette was used to dispense a known volume of sample for weighing. The data are presented in appendix A2, the results are displayed in Table 9.0a, below. Figure 9.0a illustrates the linear relationship between density and Sweetose concentration which exists at 2% sucrose ester S1670 concentration. Within the observed range of sucrose ester concentrations the density of the mixture appears to depend only on the Sweetose concentration.

Table 9.0a
Density of non-aerated Sweetose sucrose ester mixtures at 20°C

% Sweetose	% S1670	Density (g/cm^3) (2dp)
0	2	0.93 ± 0.004
10	2	1.02 ± 0.004
20	2	1.06 ± 0.02
30	2	1.11 ± 0.02
40	2	1.15 ± 0.02
50	2	1.19 ± 0.02
60	2	1.24 ± 0.02
70	2	1.27 ± 0.02
75	2	1.30 ± 0.02
20	5	1.06 ± 0.02
50	5	1.19 ± 0.02

% Sweetose	% S1670	Density (g/cm^3) (2dp)
20	8	1.05 ± 0.02
50	8	1.16 ± 0.02
75	1.5	1.28 ± 0.02
75	1	1.28 ± 0.02
75	0.5	1.28 ± 0.02
75	0.1	1.29 ± 0.02
75	0.01	1.28 ± 0.005
75	0.001	1.28 ± 0.005
75	0.0002	1.29 ± 0.005
75	0.0001	1.29 ± 0.005

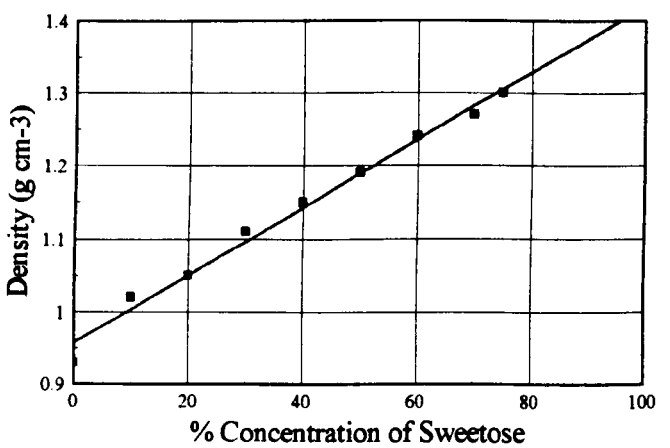

Figure 9.0a

Density of 2%w/w sucrose ester, S1670, solution with a range of Sweetose concentrations

The density of 2%w/w sucrose ester in water, in the absence of Sweetose was measured to be 0.934 g cm^{-3}, extrapolation of the best-fit line through the data for the density of 2% sucrose ester in the presence of Sweetose produced a value of 0.96 g cm^{-3} for the density of 2%w/w sucrose ester in water. Whatever the true value both are below the density of pure water at this temperature, 1.00 g cm^{-3} (2dp). The observation that a 2% sucrose ester solution was slightly less dense than pure water was attributed to a change in the partial molar volume of the water molecules in the presence of sucrose ester molecules.

CHAPTER 10

Surface tension

10.0 SURFACE TENSION MEASUREMENTS

Surface tension measurements were made on both aqueous solutions of sucrose ester and non-aerated mixtures containing Sweetose. A Kruss K12 Processor Tensiometer, using the Du Noüy ring technique, was used for the measurements on aqueous solutions. The surface tension of the, more viscous, non-aerated mixtures was measured using the spinning-drop technique. The spinning drop apparatus used was engineered to a University of Bristol design by V. Bailey Prototype Engineering (Windsor) Ltd. The instrument has been fully described by Newton[1].

10.1 Measurement of surface tension by the Du Noüy Ring technique

In this method the force required to detach a ring from the surface is measured using a torsion-wire arrangement. The ring is dipped into the surface and removed slowly whilst measuring the force exerted. The force exerted on the balance at the point of detachment is proportional to the surface tension of the liquid.

Theory

Surface tension is defined as the force acting perpendicular to a line of unit length drawn in the liquid surface. With a ring in contact with the surface then the total contact length is $4\pi R$, since the ring has an inner and outer edge, where R is the mean radius.

Thus surface tension, $\gamma = \dfrac{m \cdot g \cdot F}{4 \cdot \pi \cdot R}$

where, m = mass of liquid raised above the surface by the ring
g = a gravitational constant
F = a correction factor

The value of the correction factor F allows for the shape of the liquid surface and the consequent pressure difference. F depends upon R^3/V, where V is the volume of liquid raised above the surface, and R/r, where 2r is the distance between the inner and outer radii of the ring. These correction factors are tabulated[2] for different values of R^3/V and R/r.

The cell used to contain the liquid was thermostatted by means of a double wall through which water was circulated at the required temperature. The apparatus was contained within a perspex case to maintain constant temperature in a saturated atmosphere and to minimise dust and vibration.

10.2 Measurement of interfacial tension by the spinning-drop technique

Introduction

When a tube containing a liquid and a drop of a less dense fluid phase, is rotated about the horizontal axis, the drop will tend to find an equilibrium position along the axis. As the angular velocity is increased the drop will become more elongated, eventually forming a long cylinder with hemispherical ends. For any such system, there will be a characteristic drop shape dependant upon the speed of rotation and surface tension. A state of equilibrium exists wherein the forces of rotation are balanced by surface tension forces. The spinning fluids are housed in a parallel bore cylindrical glass tube which has first been calibrated. Calibration involves the measurement of the combined magnification factor of the dense liquid, the glass wall and the optical system. Rotation of the glass tube elongates the drop and measurements of drop length, diameter and angular velocity are recorded. This is illustrated schematically in Figure 10.2a.

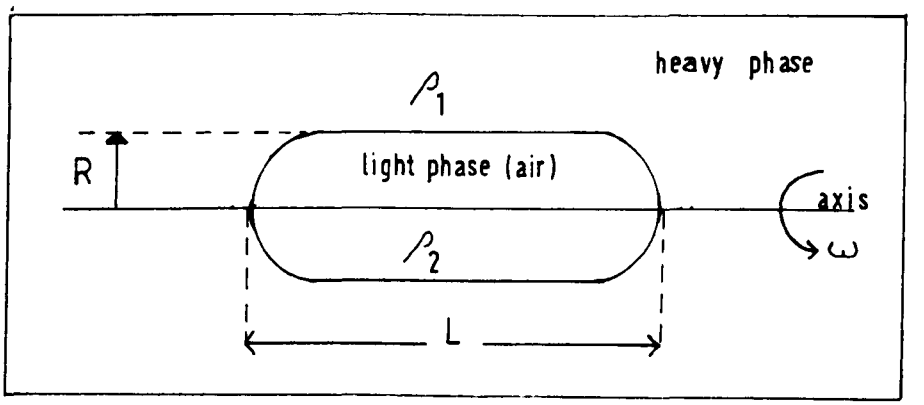

Figure 10.2a

Cross-section through a drop

Calibration

The refractive index of the medium and the curvature of the glass cell wall cause the drop diameter to be magnified, the drop length is unaffected by these. The measuring system was calibrated using a syringe needle of diameter 1.3mm. The tube was filled with the medium under test and the syringe needle was fixed along the axis of the tube using two pieces of cork at both ends. Measurements of the diameter of the syringe were taken using the eyepiece at different positions along the length. The tube, containing the syringe and test medium, was rotated through 90^o, 180^o and 270^o and the measurements repeated. A micrometer screw gauge was used to measure the real diameter of the syringe needle at positions along its length. The calculation of magnification factors is given in Appendix A3.

Theory

Measure drop length, L (mm) and diameter $D_{meas.}$

Calculate the actual diameter of the drop (mm). $D_{real} = D_{meas.}$ x Mag. Factor

Calculate $\frac{L}{D_{real}}$. Let $\frac{L}{D_{real}} = \frac{X}{Y}$

Using the tables of drop shape parameters, calculated by Newton[1], obtain ϕ and Y/r by interpolation.

Interfacial Tension γ (mN m^{-1}), $$\gamma = \frac{F \cdot \Delta\rho \cdot D_{real}^3}{\phi \cdot T^2 \cdot \left[Y_r\right]^3}$$

where $\Delta\rho$ = heavy phase density - light phase density

T = time period (msec rev-1) = 60000/speed(rpm)

F = a numerical factor = 1233.7

The numerical factor F results from the conversion of angular velocity to a time period and the measurement of the drop diameter rather than the radius.

In the calculation of surface tension by the spinning-drop technique the following mean values of density and magnification factor have been applied throughout, Table 10.2a. Density measurements were detailed in Chapter 9 and the calibration procedure was explained above. It has been assumed that these values do not change significantly with temperature or concentration of sucrose ester, beneath the chain melting temperature of 48°C.

Table 10.2a

Sample	Density (g cm^{-3})	Magnification Factor
20% Sweetose 2% S1670	1.06	1.35
40% Sweetose 2% S1670	1.15	1.40
75% Sweetose 2% S1670	1.30	1.43

10.3 Calculation of the area per molecule at the surface from surface tension data

The area of the surface occupied by a surfactant head group is dependent on the electrostatic interactions between adjacent head groups and both the hydrophilic and hydrophobic phases and the volume occupied by the alkyl chains. The balance of forces can be offset by the addition of certain solutes, e.g. the addition of salt to the aqueous phase will reduce the extent of the electrical double layer surrounding each head group causing them to pack more closely and thus their area at the surface will decrease. Measurements of the area occupied per head group can give a good indication of the environment in which the surfactant exists.

Calculation

Using the Gibbs adsorption equation, calculate the surface excess concentration, Γ (mol m^{-2})

The Gibbs equation $\Gamma = \frac{-1}{R \cdot T} \cdot \frac{d\gamma}{d \log c}$ where,

$\frac{d\gamma}{d \log c}$ is the gradient of the surface tension vs. log concentration graph.

Then calculate the area per molecule, A (m^2), using the equation , below

$$A = \frac{1}{\Gamma \cdot N_A}$$

This is also referred to as the area per head group at the surface.

Symbols, Γ = surface excess concentration (mol m^{-2})

c = concentration of surface active agent in aqueous solution (mol m^{-3})

T = temperature (K)

R = molar gas constant (8.3143 J K^{-1} mol^{-1})

γ = surface tension (N m^{-1})

N_A= Avogadro's Constant (6.0225×10^{23})

A = cross sectional area per molecule at the interface (m^2)

10.4 Surface tension of sucrose ester in dilute Sweetose and dilute KCl solutions

The surface tension of sucrose ester, S1670 in dilute Sweetose and in dilute KCl at 25°C measured using the Du Nouy ring technique is displayed in Figures 10.4a&b. Surface tension values are presented in Tables 10.4a-d. Other parameters are given in Appendix A3.

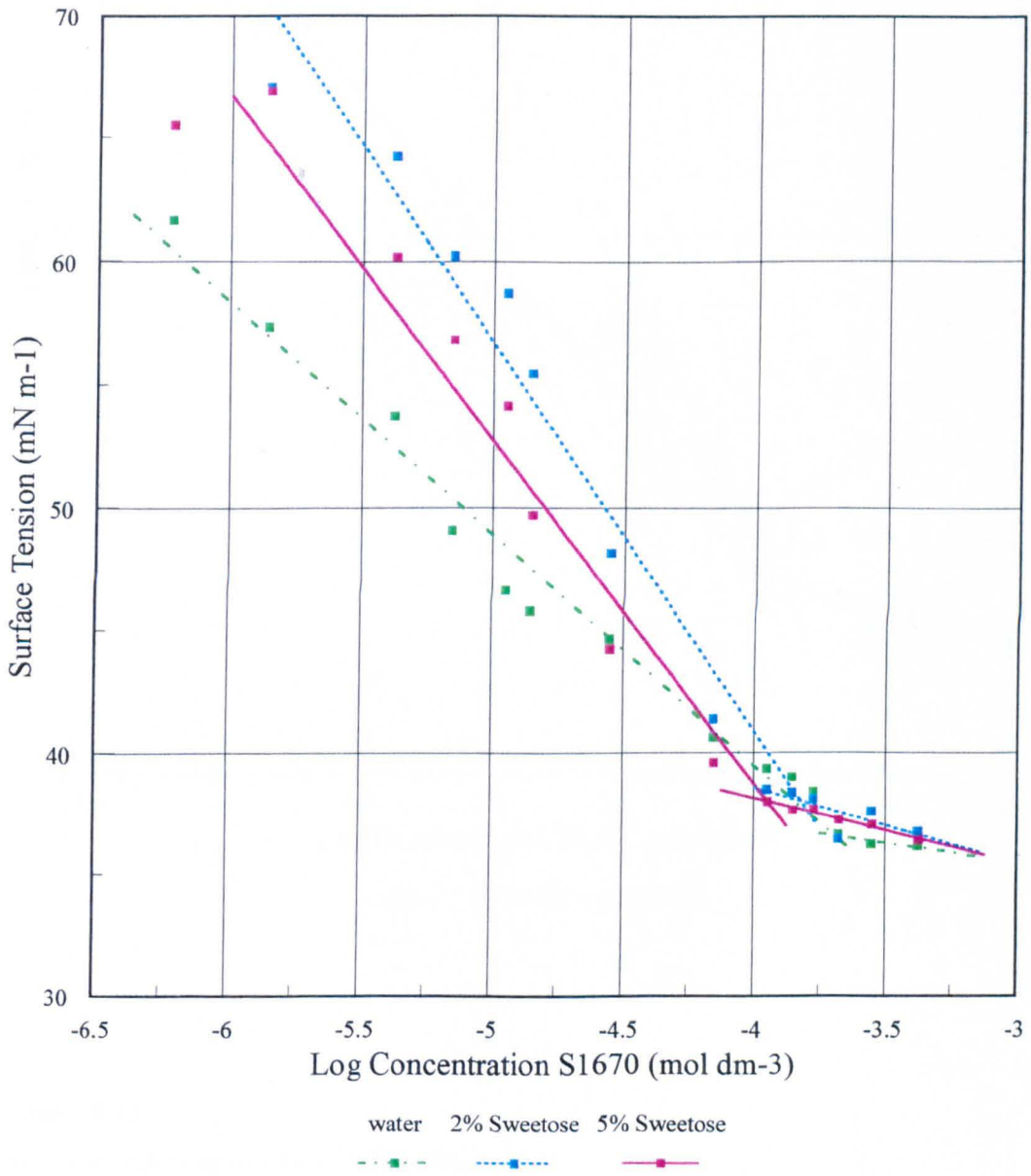

Figure 10.4a

Surface tension of sucrose ester in dilute Sweetose solution

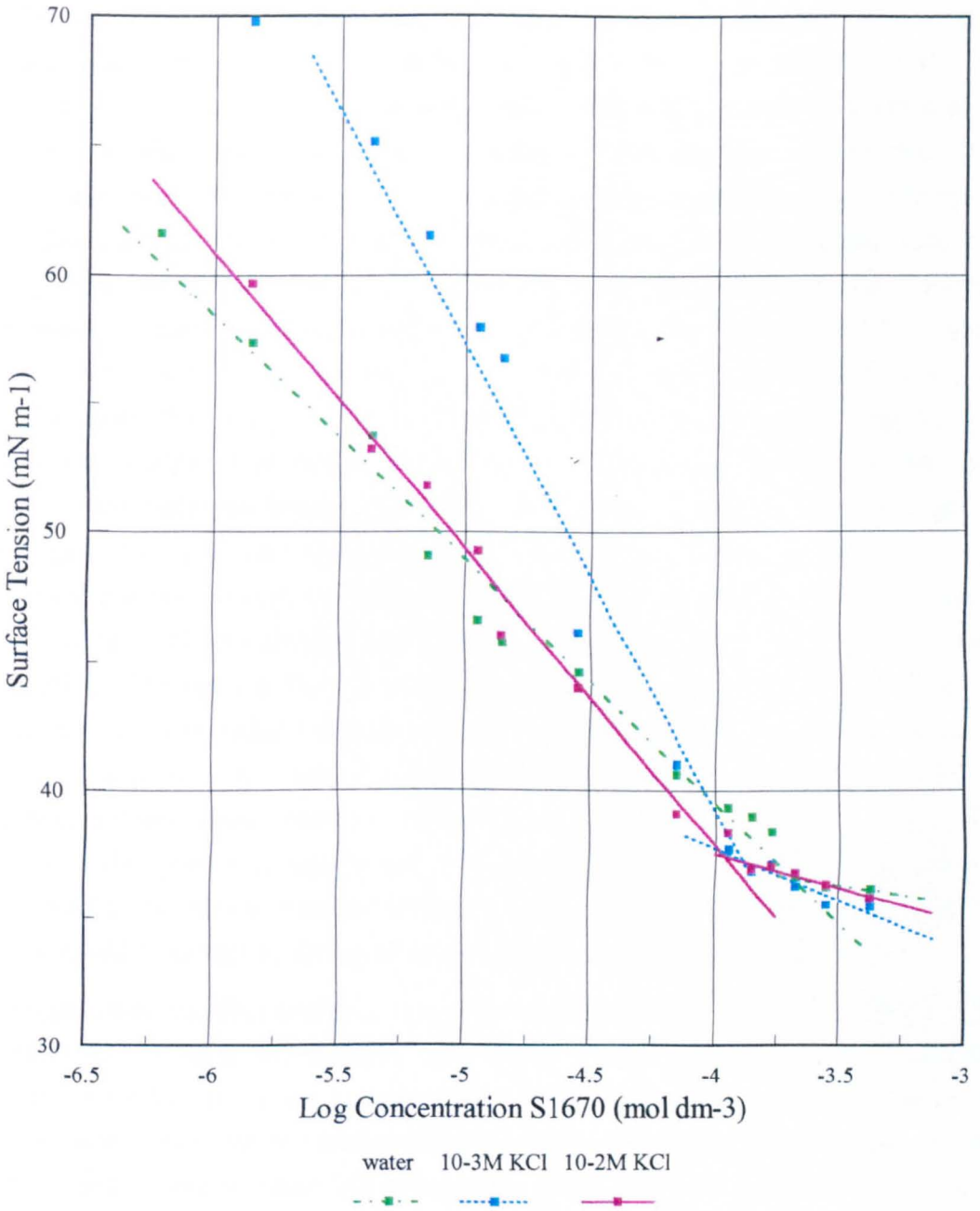

Figure 10.4b

Surface tension of sucrose ester in dilute KCl solution

In Figure 10.4a dilute Sweetose was observed to increase the surface tension for a given concentration of sucrose ester below the cmc. At 1.4 x 10^{-5}mol dm^{-3}, S1670 concentration in water, the surface tension was 45.78 mN m^{-1}, which increased to 55.49 mN m^{-1} in the presence of 2%w/w Sweetose. This increase was attributed to the competing effect of Sweetose at the surface and its ability to hydrogen bond with the water and thus partially rebuild the hydrogen bonding network, which drives the sucrose ester away from the surface and into the bulk solution. This effect was observed in the decreased critical micelle concentration, 2 x 10^{-4} mol dm^{-3} in water but 1 x 10^{-4} mol dm^{-3} in 2%w/w Sweetose. In the presence of 5%w/w Sweetose the surface tension of the S1670, above the cmc., was again higher than that in water, but less than in 2%w/w Sweetose. The increased surface tension was an indication that the Sweetose had restored much of the hydrogen bonding network. At very low Sweetose concentrations, the 6 hydrogen bonding sites on each glucose molecule in the Sweetose can partially restore the hydrogen bonding network but when the concentration is increased the effect became less pronounced. This was thought to be because the glucose molecules themselves became disruptive. The cmc. in 5%w/w Sweetose was further reduced to 7.5 x 10^{-5} mol dm^{-3} because of the competition with the glucose molecules in the Sweetose for the available water. The characteristic raising of the surface tension of aqueous solutions is typical of lyophilic solutes whose negative adsorption at the surface causes the restoration of otherwise disrupted hydrogen bonds. An example of a lyophilic solute is an ionic salt, these tend to be repelled from the surface in order to maintain a complete hydration shell, which would otherwise be disrupted by the gaseous region above the surface.

In Figure 10.4b an effect similar to that of Sweetose addition was observed on the addition of dilute KCl to the S1670 solution. In a similar fashion the more dilute KCl sample had the greatest effect on surface tension, which was partially negated by the further addition of salt. Above the cmc. the surface tension in pure water was almost constant at 36 mN m^{-1}, in the presence of dilute KCl however the solutions were slow to reach their limiting tension at this value.

In water, the surface tension of S1670 above the cmc. was nearly constant at 36mN m^{-1}, indicating that a limit had been reached. In Sweetose the surface tension continued to fall above the cmc, approaching the value for the surface tension of S1670 in water above the cmc, as the S1670 concentration increased. This behaviour indicated that another component was slightly surface active. The sucrose ester itself is a blend of mono- di- and tri- esters which might cause this effect but since it was accentuated by the presence of Sweetose it seems more likely that the Sweetose itself is slightly surface active.

The following table lists the measured values of surface tension with sucrose ester S1670 concentration.

Surface tension measurement data

Table 10.4a

S1670 Concentration			Average Surface Tension mN m^{-1}		
% w/w	mol dm^{-3}	Log Conc	Water	2% Sweetose	5% Sweetose
3×10^{-2}	4.255×10^{-4}	-3.374	36.14	36.75	36.40
2×10^{-2}	2.817×10^{-4}	-3.550	36.22	37.59	37.02
1.5×10^{-2}	2.113×10^{-4}	-3.675	36.62	36.44	37.23
1.2×10^{-2}	1.690×10^{-4}	-3.772	38.39	38.11	37.67
1×10^{-2}	1.409×10^{-4}	-3.851	39.01	38.37	37.64
8×10^{-3}	1.127×10^{-4}	-3.948	39.35	38.49	37.99
5×10^{-3}	7.042×10^{-5}	-4.152	40.64	41.39	39.60
2×10^{-3}	2.817×10^{-5}	-4.550	44.63	48.17	44.22
1×10^{-3}	1.409×10^{-5}	-4.851	45.78	55.49	49.71
8×10^{-4}	1.127×10^{-5}	-4.948	46.64	58.73	54.16
5×10^{-4}	7.042×10^{-6}	-5.152	49.09	60.23	56.86
3×10^{-4}	4.225×10^{-6}	-5.374	53.74	64.23	60.19
1×10^{-4}	1.409×10^{-6}	-5.851	57.37	67.07	66.93
4.3×10^{-5}	6.056×10^{-7}	-6.218	61.64		65.52

Table 10.4b

S1670 Concentration			Average Surface Tension mN m^{-1}		
% w/w	mol dm^{-3}	Log Conc	Water	10^{-3}M KCl	10^{-2}M KCl
3×10^{-2}	4.255×10^{-4}	-3.374	36.14	35.45	35.77
2×10^{-2}	2.817×10^{-4}	-3.550	36.22	35.50	36.30
1.5×10^{-2}	2.113×10^{-4}	-3.675	36.62	36.25	36.77
1.2×10^{-2}	1.690×10^{-4}	-3.772	38.39	37.12	37.06
1×10^{-2}	1.409×10^{-4}	-3.851	39.01	36.85	36.92
8×10^{-3}	1.127×10^{-4}	-3.948	39.35	37.71	38.36
5×10^{-3}	7.042×10^{-5}	-4.152	40.64	41.04	39.11
2×10^{-3}	2.817×10^{-5}	-4.550	44.63	46.17	44.01
1×10^{-3}	1.409×10^{-5}	-4.851	45.78	56.76	46.05
8×10^{-4}	1.127×10^{-5}	-4.948	46.64	57.96	49.29
5×10^{-4}	7.042×10^{-6}	-5.152	49.09	61.54	51.79
3×10^{-4}	4.225×10^{-6}	-5.374	53.74	65.16	53.21
1×10^{-4}	1.409×10^{-6}	-5.851	57.37	69.76	59.67
4.3×10^{-5}	6.056×10^{-7}	-6.218	61.64		

Analysis

The critical micelle concentration and area per head group were calculated, from the preceding figures.

Regression Analysis	Water	2%w/w Sweetose	5%w/w Sweetose
Intercept	1.726×10^{-3}	-3.837×10^{-2}	-3.093×10^{-2}
Gradient	-9.4422×10^{-3}	-1.9239×10^{-2}	-1.6863×10^{-2}
Correl. coefficient	-0.989	-0.9918	-0.9919
crit. micelle conc. (mol dm^{-3})	2.37×10^{-4}	1×10^{-4}	7.5×10^{-5}
limiting surface tension	36	40	38.5
temperature (°C)	25	25	25
Area per head group (nm^2)	0.44	0.21	0.24

Regression Analysis	10^{-3}M KCl	10^{-2}M KCl
Intercept	-4.673×10^{-2}	-8.044×10^{-3}
Gradient	-2.0981×10^{-2}	-1.1483×10^{-2}
Correl. coefficient	-0.9866	-0.9929
critical micelle concentration	1.22×10^{-4}	1.10×10^{-4}
limiting surface tension	38	37.5
temperature (°C)	25	25
Area per head group (nm^2)	0.20	0.36

The area per head group measurements assume that the only surface active molecules at the interface belong to the sucrose ester. The mean area per head group at the surface in pure water was $0.44nm^2$. Upon the addition of Sweetose or KCl the surface tension was seen to rise, with an accompanying decrease in the area per head group, to 0.21 nm^2 in 2%w/w Sweetose $0.24nm^2$ in 5%w/w Sweetose, $0.20nm^2$ in 10^{-3}mol dm^{-3} and $0.36nm^2$ in 10^{-2} mol dm^{-3} KCl solution. As expected the largest effect was observed with the low solute concentration.

10.5 Surface tension of non-aerated mixtures of Sweetose, sucrose ester and water

The surface tension of non-aerated mixtures of Sweetose, sucrose ester, S1670, and water were measured by the spinning-drop technique, using air as the less dense phase. Solutions of 2%w/w sucrose ester in 20, 40 and 75%w/w solutions of Sweetose in water were measured as a function of temperature. The samples were placed into the tube at room temperature, an air bubble was injected and the tube was slowly warmed by circulating hot water through a surrounding water jacket. This was carried out with the tube spinning at 1000rpm, until the required temperature was reached. After equilibration, at a particular temperature, and measurement of the surface tension the

sample was heated again. Measurements were recorded on both heating and cooling of the sample in the tube. The samples were observed to begin melting at approximately 50°C.

The results are displayed in Figure 10.5a and listed at the end of the section in Table 10.5a.

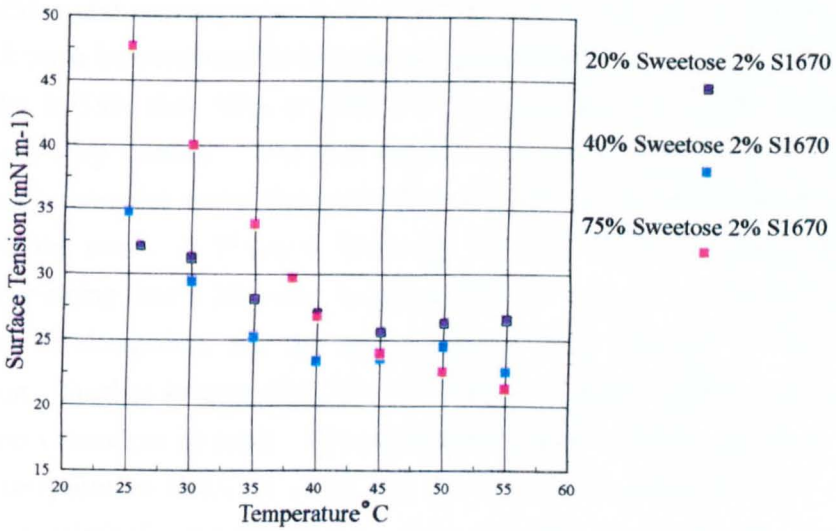

Figure 10.5a

Surface tension of mixtures of Sweetose and 2% sucrose ester S1670 as a function of temperature.

All mixtures contained 2%w/w concentration of sucrose ester and either 20, 40 or 75%w/w Sweetose concentration. The surface tension decreased with temperature in all cases, the gradient was greatest in 75% Sweetose and least in 20% Sweetose. Between 40 and 45°C the gradient decreased. Above this temperature the surface tension was not seen to change significantly.

The values of the surface tension of 2%w/w sucrose ester in 20 and 40%w/w Sweetose at 25°C were very similar but the value in 75%w/w Sweetose was much higher. Rheological measurements, seen in Figure 8.4d, on 2%w/w sucrose ester with 20, 40 and 75%w/w Sweetose also showed a disproportional increase in the viscosity of the mixture between 40%w/w Sweetose and 75%w/w Sweetose. Microscopy evidence showed that in non-aerated mixtures some of the sucrose ester is arranged in the form of liquid crystalline bilayers. The amount of sucrose ester arranged in bilayers increases with Sweetose concentration for a given amount of sucrose ester. The observation of a disproportional increase in both viscosity and surface tension between 40 and 75%w/w Sweetose was thought to be due to the increased concentration of sucrose ester bilayers in the mixture and the large proportion of the total sample volume they occupy. The larger the fraction of the total volume occupied by the sucrose ester bilayers, the smaller will be the volume

of the lubricating Sweetose matrix. The reduced lubrication will result in a higher viscosity.

The spinning drop technique measures the surface tension by measuring the angular velocity required to elongate a drop. The density of the light and dense phases is accounted for but the rheological characteristics are not. Non-aerated mixtures of Sweetose and sucrose ester were observed, in Chapter 8, to possess a large yield stress which must be overcome before the sample will flow. The value of this yield stress will be greater in 75% than 40% or 20%w/w Sweetose because of the amount of sucrose ester bilayers they contain. The rheological differences between the 75, 40 and 20%w/w Sweetose samples mean that their flow characteristics inside the spinning drop tube will not be the same. A 75%w/w Sweetose 2%w/w sucrose ester mixture will require more rapid spinning than a 20%w/w Sweetose 2%w/w sucrose ester sample to achieve the same degree of elongation, and this may not simply be a function of the difference in surface tension. Further investigation of this is required before direct comparison of the surface tension values can be made. The significant finding of the measurements of surface tension with temperature in Figure 10.5a was the observation that above 50°C the surface tension remains relatively constant and at approximately the same value for each of the three samples measured.

Chapter 6 describes DSC measurements on non-aerated mixtures of 75%w/w Sweetose 2%w/w sucrose ester and water in which an endothermic phase transition, attributed to the melting of the alkyl chains, was observed at 48°C. This phase transition temperature was within the temperature region in which the sucrose ester surface tension gradients changed in Figure 10.5a which implies that the surface tension of the mixtures remains relatively constant above 50°C because the alkyl chains are above their transition temperature.

In order to investigate the behaviour of sucrose ester in 75% Sweetose, above its chain melting temperature non-aerated samples of 75% Sweetose with different concentrations of sucrose ester were prepared in the standard way. These were allowed to stand at 4°C for 24 hours prior to measurements being made. The sample, containing a single air bubble, was added to the spinning-drop tube at room temperature, the tube was sealed within the apparatus which was then warmed to 55°C. During this warming process the tube was kept spinning at 1000rpm in order that the bubble should remain in the central region of the tube and aligned about its axis. The temperature inside the water jacket was monitored until a constant 55°C was reached. The previously opaque samples were seen to melt and become transparent. The surface tension of many non-aerated samples containing 75%w/w Sweetose and a range of sucrose ester concentrations was measured at 55°C, see Figure 10.5b. At 55°C the sample is above the chain melting transition temperature as described in Chapter 6. The data is listed in table 10.5b.

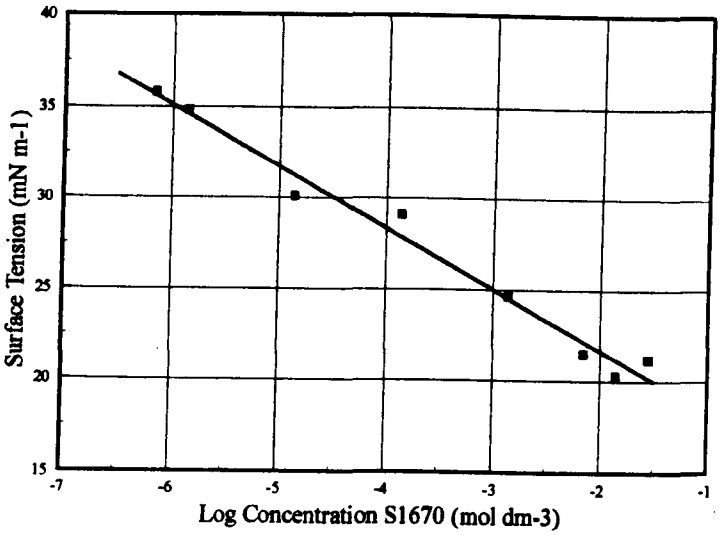

Figure 10.5b

Surface tension of sucrose ester S1670 in 75% Sweetose at 55°C

By measuring the gradient of the line and hence the surface excess concentration of sucrose ester the area per head group was found to be 1.33nm^2, which is consistent with the low values of surface tension measured, between 20 and 35mN m^{-1} over the range of concentrations studied.

The surface tension of a mixture of 75%w/w Sweetose 2%w/w sucrose ester as a function of temperature was illustrated in Figure 10.5a. The surface tension was 47mN m^{-1} at 25°C compared to 21mN m^{-1} at 55°C. At 55°C the hydrocarbon chains within the bilayer were thought to be in a fluid state and the observance of a large head group area and low surface tension is consistent with this. An attempt to measure the surface tension of sucrose ester in 75% Sweetose at 25°C was made, however the heterogeneous mixtures of Sweetose and sucrose ester separated during spinning and consistent results could not be obtained.

Surface tension results

Table 10.5a

Surface Tension of 2% sucrose ester in Sweetose as a function of temperature

	Surface Tension ($mN\ m^{-1}$) of 2% S1670		
Temperature °C	20% Sweetose	40% Sweetose	75% Sweetose
25	32.1	34.7	47.5
30	31.2	29.4	39.9
35	28.1	25.2	33.7
38			29.6
40	27.0	23.4	26.7
45	25.6	23.6	23.9
50	26.3	24.5	22.5
55	26.5	22.6	21.2

Table 10.5b

Surface Tension of 75% Sweetose as a function of sucrose ester concentration at 55°C

% conc'n S1670	conc ($mol\ dm^{-3}$)	Log conc	Surface Tension ($mN\ m^{-1}$)
2	2.817×10^{-2}	-1.550	21.2
1	1.409×10^{-3}	-1.851	20.3
0.5	7.042×10^{-3}	-2.152	21.5
0.1	1.409×10^{-3}	-2.851	24.7
0.01	1.409×10^{-4}	-3.851	29.1
1×10^{-3}	1.409×10^{-5}	-4.851	30.1
1×10^{-4}	1.409×10^{-6}	-5.851	34.8
5×10^{-5}	7.042×10^{-7}	-6.152	35.8

The magnification factor used for the surface tension measurements is given in Appendix A3. No account of the effect of heating on this figure was taken, due to the experimental difficulty of preventing the separation of the components, Sweetose and sucrose ester, before measurement was complete.

10.6 Summary

Surface tension measurements on solutions of sucrose ester in water revealed that the addition of dilute Sweetose or dilute salt to the solution increases the extent of the hydrogen bonding network in the water, which is evidenced by an increase in the surface tension of the solution for a given sucrose ester concentration.

The surface tension of non-aerated mixtures of Sweetose, sucrose ester and water at 25°C was found to be a function of temperature and of Sweetose concentration. The surface tension increased with the concentration of Sweetose at 2%w/w sucrose ester. This effect was attributed to the presence of sucrose ester arranged in liquid crystal bilayers. Previous techniques have demonstrated that the proliferation of the bilayers increases with Sweetose concentration for a fixed concentration of sucrose ester. The effect of sucrose ester concentration in 75% Sweetose at 25°C was not measured.

When non-aerated Sweetose, sucrose ester and water mixtures are heated to 50°C their surface tension decreased. The range of this decrease increased with the Sweetose concentration of the mixture. Sweetose concentrations of 75, 40 and 20%w/w mixed with 2%w/w sucrose ester and water were measured. All three samples reached a surface tension of between 25 and 35mNm^{-1} when heated to 50°C, above this temperature their surface tension changed very slightly with further increases in temperature. This behaviour was thought to coincide with the observation of a melting phase transition by DSC in non-aerated mixtures at 48°C. The phase transition was attributed to the melting of the alkyl chains of the sucrose ester within the liquid crystal bilayers.

The surface tension of 2%w/w sucrose ester in 75%w/w Sweetose in water solution at 55°C was 21mN m^{-1} compared to 47mN m^{-1} at 25°C. The area per sucrose ester head group was measured to be approximately 1.33nm^2 in solutions of 75%w/w Sweetose at 55°C, whereas the area per head group in water at 25°C was 0.44nm^2. The increase in the area of the sucrose ester head group at the interface at 55°C over that at 25°C, not accounting for the change in solvent, is consistent with the observation of a chain melting transition at 48°C. Above the transition temperature the alkyl chains have a greater flexibility and can be expected to occupy a larger volume, which is reflected in the increased area occupied by each of the head groups. It is likely that the different head group areas are affected the solvent. The surface tension of sucrose ester in 75%w/w Sweetose at 25°C was not measured because of practical difficulties so direct comparison of the effect of temperature on head group area is not possible.

The rheological behaviour of non-aerated mixtures of Sweetose and sucrose ester is not accounted for in the calculations of surface tension. It was hoped that by allowing the samples to reach equilibrium, by spinning for 30 minutes at the required speed and temperature, before any measurements were made the factor of the yield stress of the

sample would be negated. When the samples were heated to at least 55°C and the alkyl chains had melted the viscosity of the samples reduced, as did the size of their yield stress. The surface tension measured was lower at 55°C than at 25°C. An alternative explanation for this behaviour might be the decrease in the sample viscosity on heating causing it to elongate at lower speeds and thus a lower value of surface tension would be recorded.
The reduction in surface tension with temperature might be due to either or both of the above explanations. The situation could be clarified by measuring the surface tension of 75%w/w Sweetose in water, without the addition of sucrose ester, at 25 and 55°C and by making further measurements on the surface tension of sucrose ester at progressively increasing concentrations of Sweetose. The limited number of experiments carried out in this study were sufficient to discover the water-structure making effect of Sweetose in water and the change in surface tension on heating non-aerated mixtures of Sweetose and sucrose ester above 50°C. A similar change in the properties of non-aerated mixtures at 50°C was also observed by other techniques; DSC and confocal and polarising microscopy. These observations are relevant to understanding of the formation of gas microcells from mixtures of Sweetose and sucrose esters however a detailed explanation of this behaviour was not necessary.

10.7 References

1 Newton, R.; PhD Thesis, University of Bristol, 1984.

2 Harkins, W.D. and Jordan, H.F.; J. Am. Chem. Soc., **52**, 1751, (1930).

CHAPTER 11

Gas phase volume

11.0 MEASUREMENT OF GAS PHASE VOLUME DURING AERATION

In order to measure the gas phase volume incorporated during the aeration process it was assumed that the density of the mixture was entirely due to the Sweetose/sucrose ester mixture and not due to the gas phase. The density of the mixture was measured at regular intervals of time, up to 2 hours. The density of the non-aerated equivalent mixture was previously calculated, see Chapter 9. The non-aerated mixture was assumed to have zero phase volume of gas.

The gas phase volume was calculated using the following equation,

$$\phi_{air} = 1 - \frac{\rho_{mixture}}{\rho_{nonaerated}}$$

where, ρ = density (g cm^{-3})
ϕ = volume fraction

Density of non-aerated mixtures,
75% Sweetose 2% sucrose ester, 1.30 g cm^{-3}
50% Sweetose 2% sucrose ester, 1.19 g cm^{-3}
40% Sweetose 2% sucrose ester, 1.15 g cm^{-3}
30% Sweetose 2% sucrose ester, 1.10 g cm^{-3}

Contrary to the effect of Sweetose concentration, the concentration of the sucrose ester employed has a negligible effect on the density of the non-aerated mixture at a given Sweetose concentration, see Chapter 9.

The total weight of foam prepared was 500g in all cases. The foam was prepared by the standard method as described in Chapter 2. 2.5cm^3 aliquots were removed at regular intervals of time using a graduated plastic syringe. The density of the mixture was measured by weighing the syringe and contents, dispelling 0.5cm^3 and re-weighing, repeating until no mixture remained in the syringe. The average weight of 0.5cm^3 was calculated and hence the density of the mixture. The data are given in appendix A4.

Four variables have been investigated:-

1. The effect of Sweetose concentration at 2%w/w sucrose ester, S1670.
2. The effect of sucrose ester, S1670, concentration at 75%w/w Sweetose.
3. The effect of the nature of sucrose ester employed, at 75%w/w Sweetose.
4. The effect of aeration speed, using 75% Sweetose 2% sucrose ester, S1670.

11.1 The effect of Sweetose concentration

30,40,50 and 75%w/w Sweetose mixtures with 2% S1670 were each aerated for two hours. Aeration occurred more rapidly with higher Sweetose concentrations. 80% gas phase volume was achieved in 30 minutes with 75% Sweetose, compared to 90 minutes in 30% Sweetose.

75% Sweetose reached a maximum of 80% phase volume at 30 minutes, further whipping resulted in loss of the gas phase, after 2 hours only 60% phase volume remained. The lower concentrations of Sweetose all reached maxima of 90% gas phase volume, higher than the 75% Sweetose sample, and retained their gas volume during the remaining aeration time. These are illustrated in Figure 11.1a.

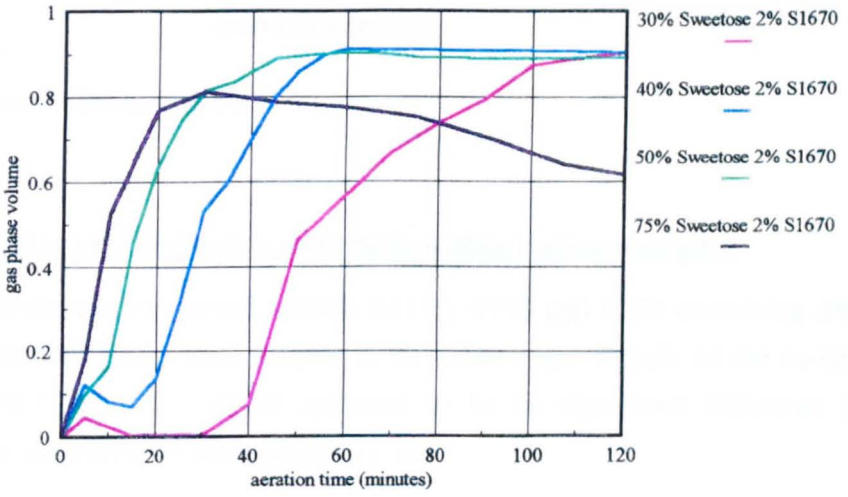

Figure 11.1a

Effect of Sweetose concentration

11.2 The effect of sucrose ester concentration

75%w/w Sweetose alone did not produce a foam on aeration for two hours. Adding sucrose ester up to 0.1%w/w caused limited aeration, 10% gas phase volume after 2 hours. A further increase to 0.2% sucrose ester produced a dramatic increase in the gas phase volume. A maximum phase volume of 50% was produced after 40 minutes, this was retained throughout the remaining aeration time. Further increases, up to 1%w/w, caused more rapid aeration and increased the maximum phase volume to 80%. Above 1% however there was negligible difference between the aeration profiles, after 30 minutes all reach a maximum of 80% phase volume, reducing to 60% on further aeration. These are illustrated in Figure 11.2a.

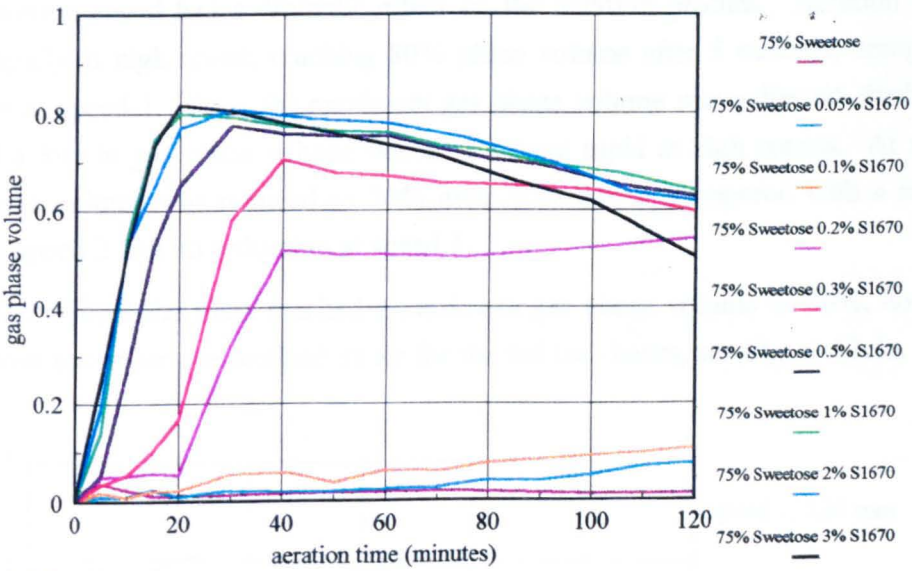

Figure 11.2a

Effect of sucrose ester concentration

11.3 The effect of mono-/di-/higher ester ratio within the sucrose ester

The commercial sucrose esters, S1670, S1170, S770 and S270 containing different ratios of the component esters were aerated in the usual way. Details of the component ratios are given in Chapter 2. There appeared to be no significant difference between the aeration characteristics of each, Figure 11.3a.

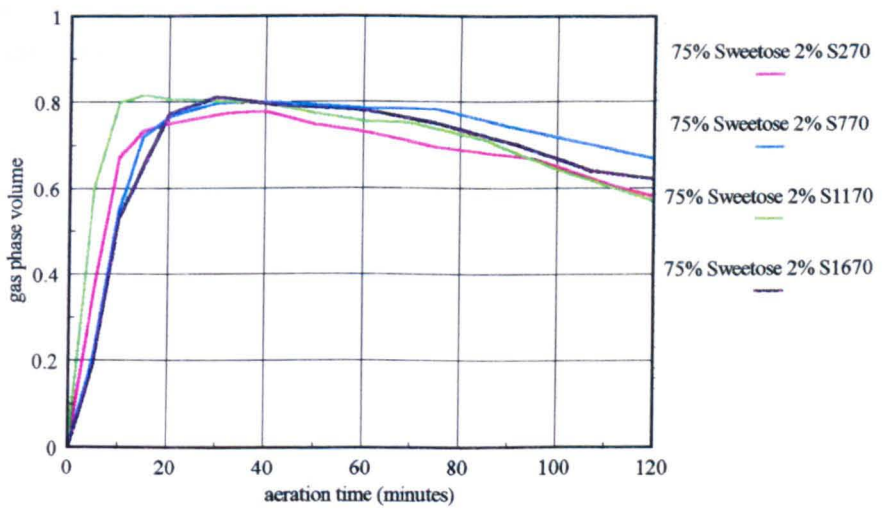

Figure 11.3a

Effect of mono-/di-/higher ester ratio within the sucrose ester

11.4 The effect of aeration speed

The aeration speed had a dramatic effect on the aeration profiles. Aeration takes place very rapidly at high speed, reaching 80% phase volume after 5 minutes, compared to 70 minutes at speed 1. Once the maximum gas phase volume was achieved, further aeration caused a loss in gas phase volume which was most rapid at high speeds. At speed 3 the gas phase volume was reduced to 30% after 90 minutes, compared with a reduction to 70% at speed 2 and no reduction at speed 1.

In all three cases the foam reached a maximum gas phase volume of 80%, however only the lowest speed sample retained its air for the full two hours, see Figure 11.4a.

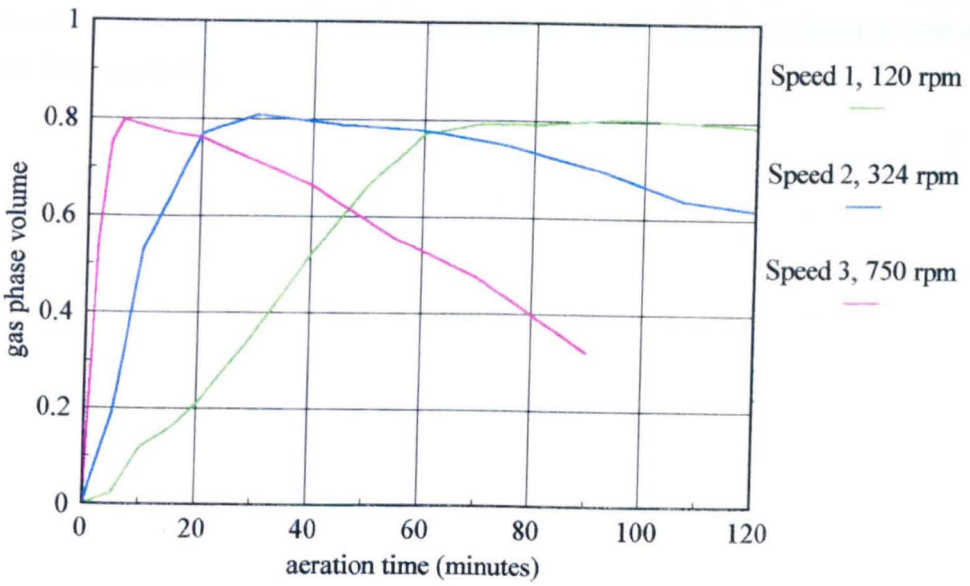

Figure 11.4a

Effect of aeration speed

11.5 Summary

It was observed that both Sweetose and sucrose ester concentration had an effect on the aeration profile. It was not possible to aerate 2%(aq) S1670 or 75%w/w Sweetose alone, however a combination of both resulted in stable gas microcells. The Sweetose concentration could be varied between 30% and 75%, with difficulties related to viscosity at both limits. Sucrose ester concentration could be varied between 0.2% and 3% although concentrations above 0.5% had a negligible effect on the incorporation of gas. Concentrations of sucrose ester greater than 3%w/w are increasingly viscous and difficult to aerate. The ratio of mono- / higher- esters within the sucrose ester did not show any effect on the incorporation of air. Aeration speed had a pronounced effect, the rate of aeration increased with speed, as expected, but at higher speeds the gas phase volume reached a maximum rapidly and then declined. In all cases the maximum gas phase volume reached was 80%.

CHAPTER 12

Scanning electron microscopy

12.0 SCANNING ELECTRON MICROSCOPY

Gas microcells were produced by the aeration of 75% Sweetose and 2% sucrose ester S1670 by the standard method. Samples of the foam were removed at intervals of time, immediately frozen, by immersion in liquid nitrogen, and stored in a deep freeze until they were fractured and replicated for examination by SEM. The samples were glassy when frozen because of their high Sweetose concentration and freezing by immersion in liquid nitrogen did not result in the formation of artefacts. The microscopy was carried out by J. Brigham at Unilever Research, Colworth Laboratory. The illustrations are qualitative because not all of the gas cells have been fractured at their diameter.

It can be seen that the gas cell number and size distribution changes with time, after 2 hours aeration there are both large and small gas bubbles in the foam. In order to investigate the effects of short-time ageing, some samples were stored at room temperature for 15 hours before freezing with liquid nitrogen. There appeared to be very little change on standing overnight, gas microcells were in existence alongside large air bubbles as before, some bubbles were surrounded by areas devoid of other cells, suggesting that their diameter had reduced during the ageing period. The cross-sections of the bubbles which had been frozen immediately after aeration were less circular, suggesting that the bubbles were less spherical, than those which had been aged for 15 hours. This is thought to be due to deformation caused by mechanical stress during the aeration process. Those bubbles which were aged for 15 hours had time to return to their equilibrium spherical shape.

During the aeration process, samples were removed at regular intervals. The following illustrations compare samples at 15, 30, 60 and 120 minutes before the ageing process. Figures 12.0 a-d are x50, Figures 12.0 e-h are x120 and Figures 12.0 i-l are x300 magnification.

Samples taken at 70, 120 and 160 minutes were examined after ageing for 15 hours. These are illustrated at x50, x120 and x300 in Figures 12.0 m-u.

SEM images of samples taken at intervals during the aeration of 75%w/w Sweetose and 2%w/w sucrose ester with water. Magnification - x50.

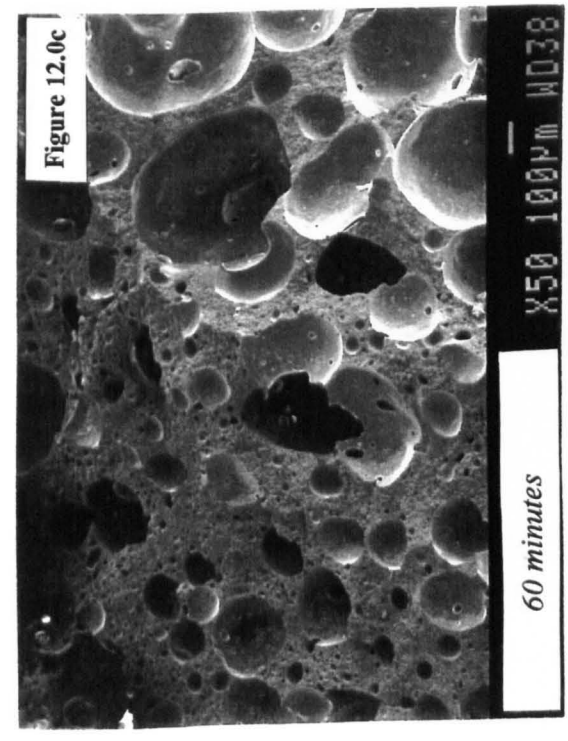

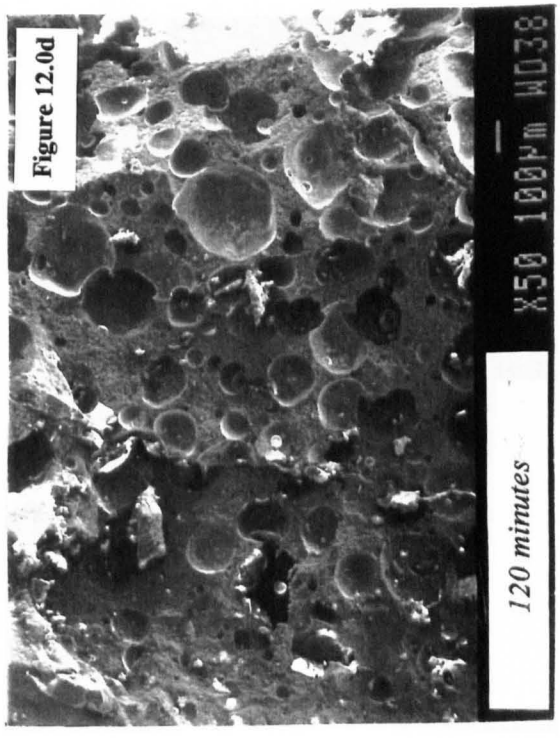

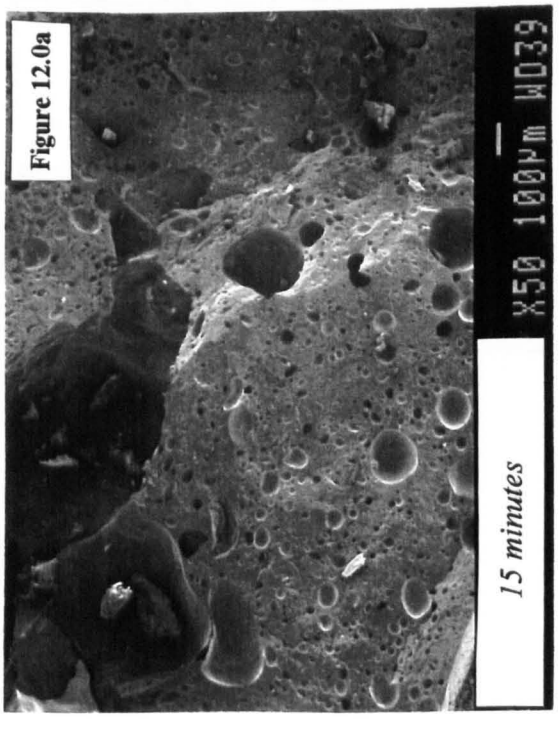

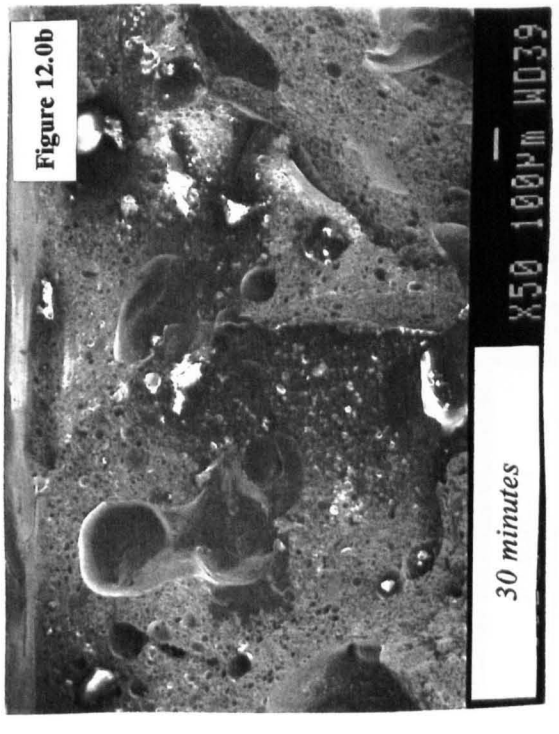

SEM images of samples taken at intervals during the aeration of 75%w/w Sweetose and 2%w/w sucrose ester with water. Magnification - x100.

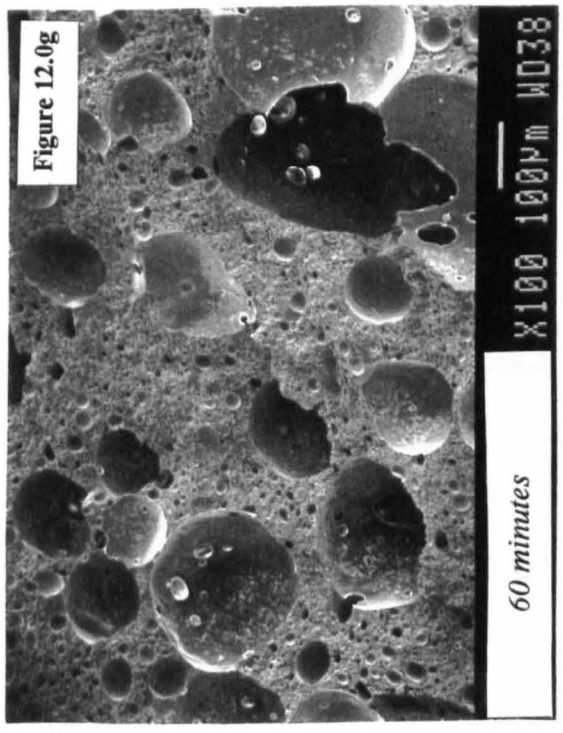

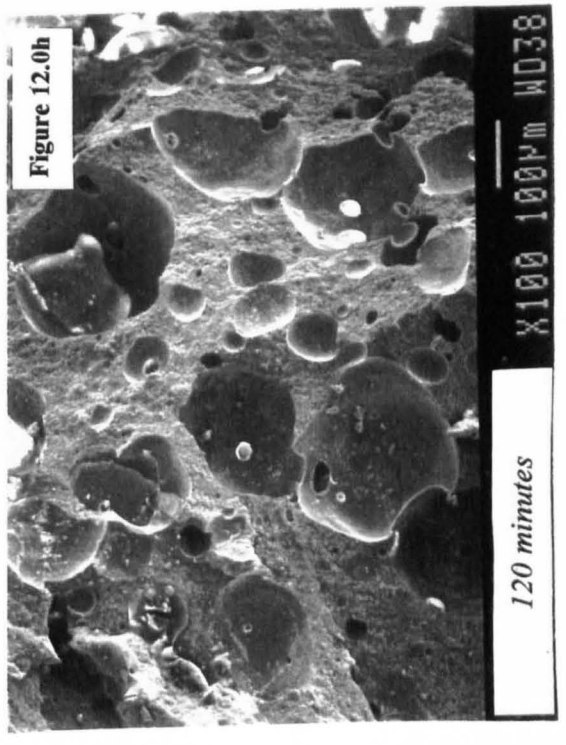

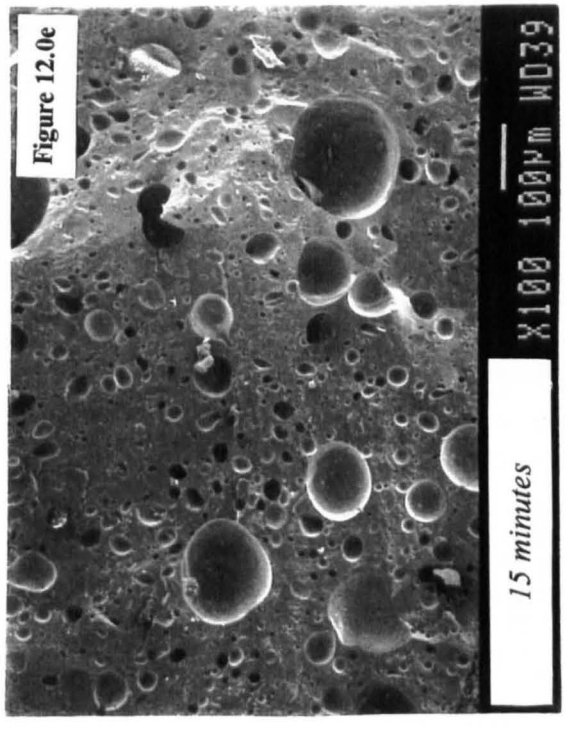

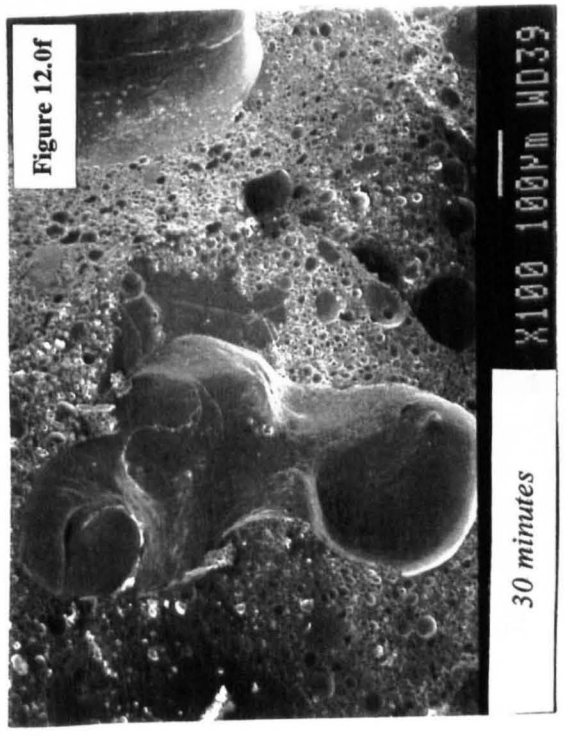

SEM images of samples taken at intervals during the aeration of 75%w/w Sweetose and 2%w/w sucrose ester with water. Magnification - x300.

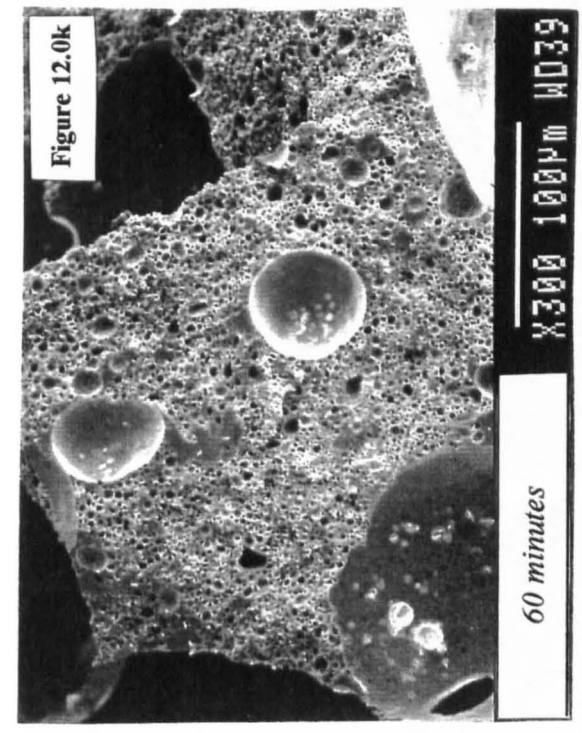

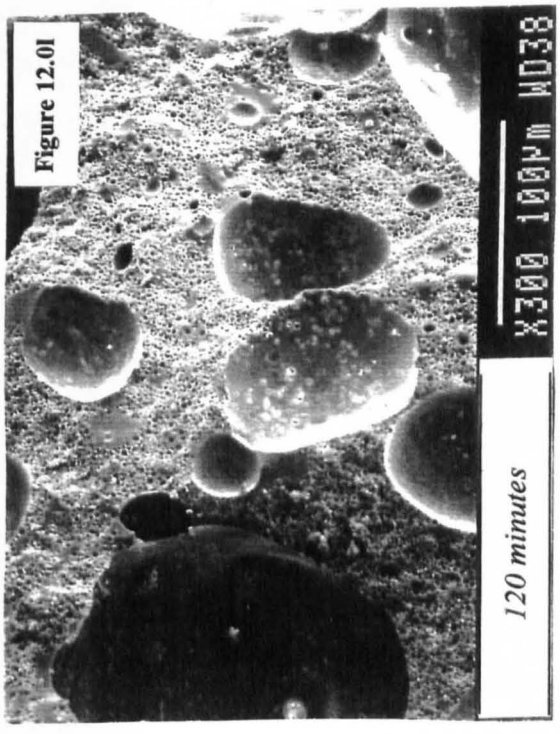

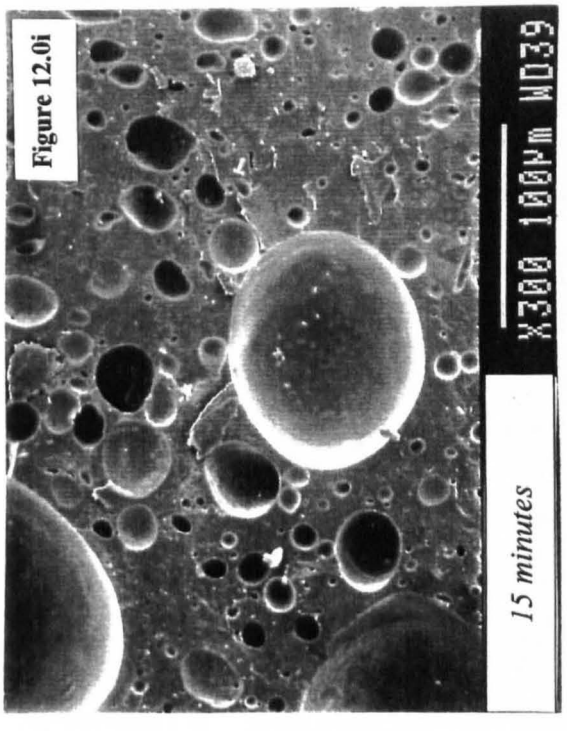

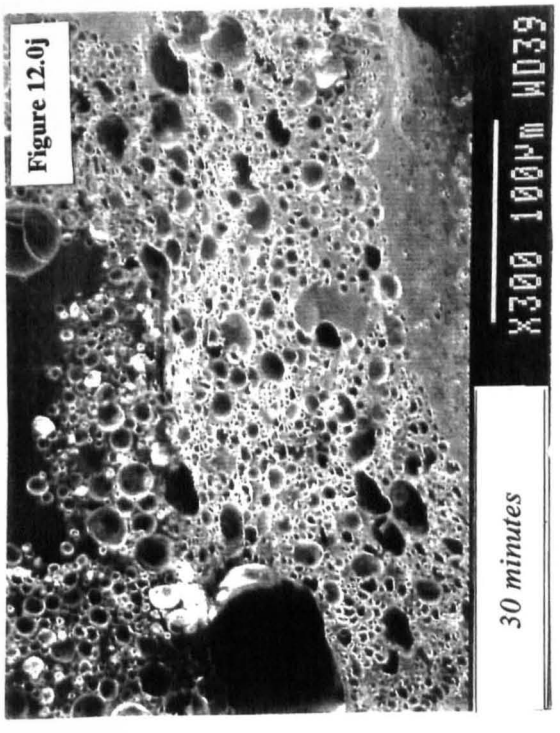

SEM images of samples taken at intervals during the aeration of 75%w/w Sweetose and 2%w/w sucrose ester with water, and allowed to stand for 15 hours at room temperature. Magnification - x 50

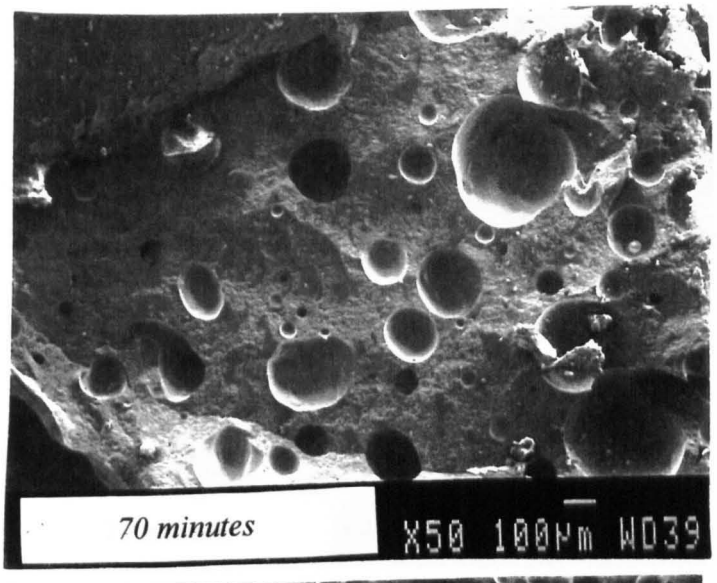

Figure 12.0m

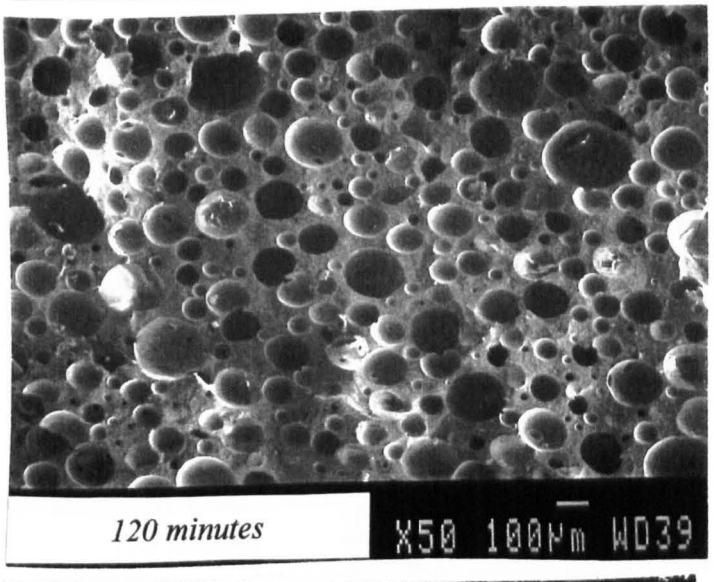

Figure 12.0n

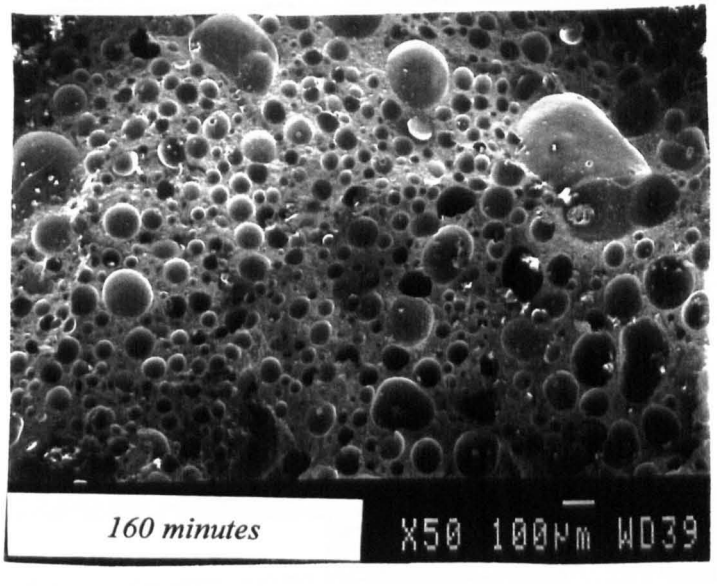

Figure 12.0o

SEM images of samples taken at intervals during the aeration of 75%w/w Sweetose and 2%w/w sucrose ester with water, and allowed to stand for 15 hours at room temperature. Magnification - x 100

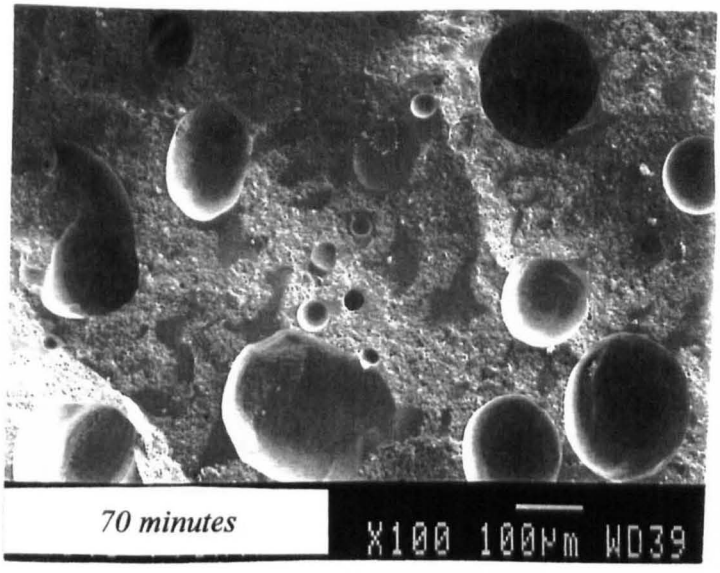

Figure 12.0p

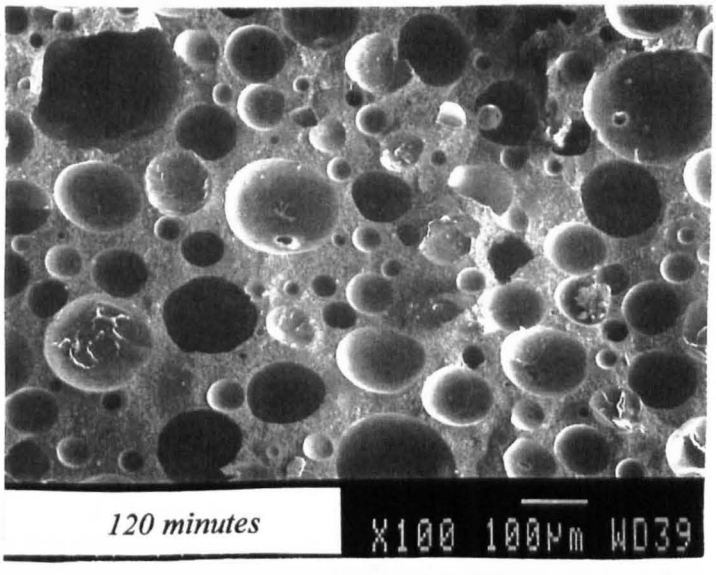

Figure 12.0q

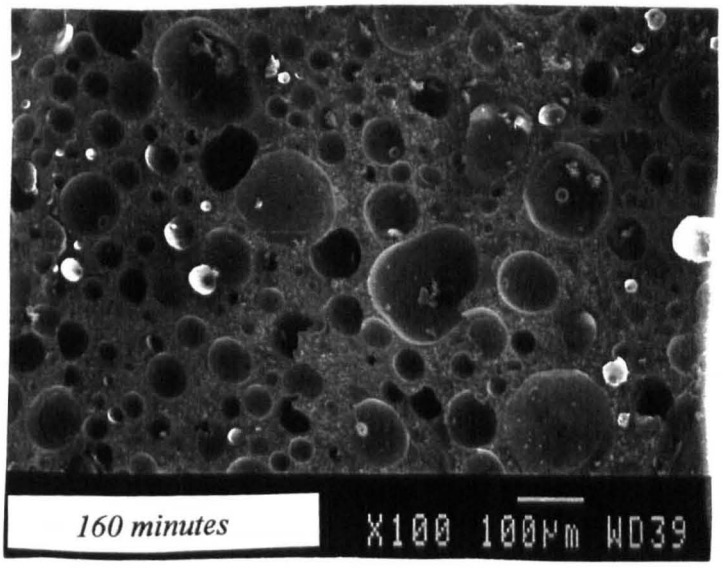

Figure 12.0r

SEM images of samples taken at intervals during the aeration of 75%w/w Sweetose and 2%w/w sucrose ester with water, and allowed to stand for 15 hours at room temperature. Magnification - x 300

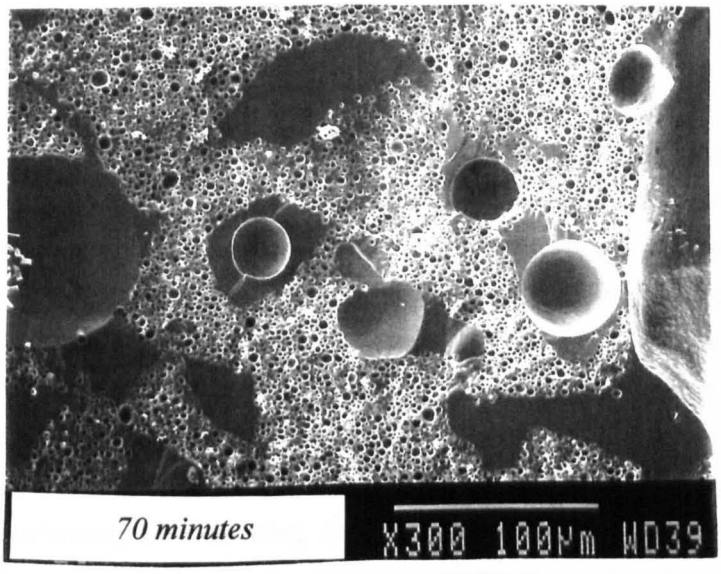

Figure 12.0s

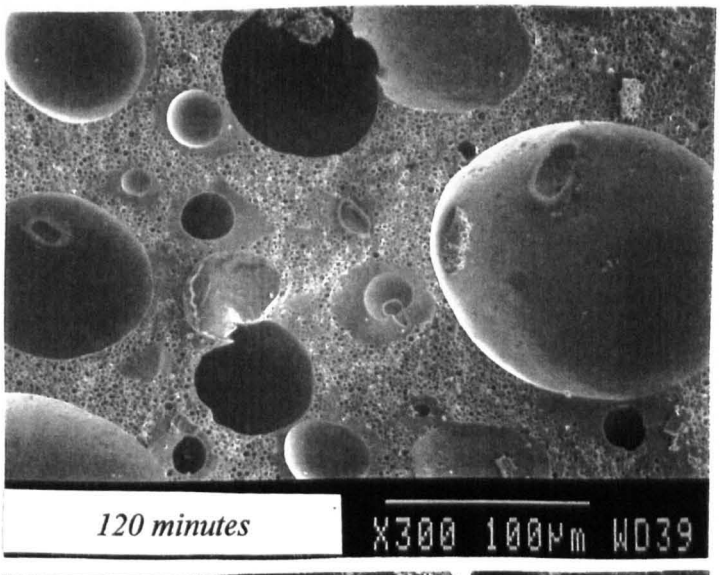

Figure 12.0t

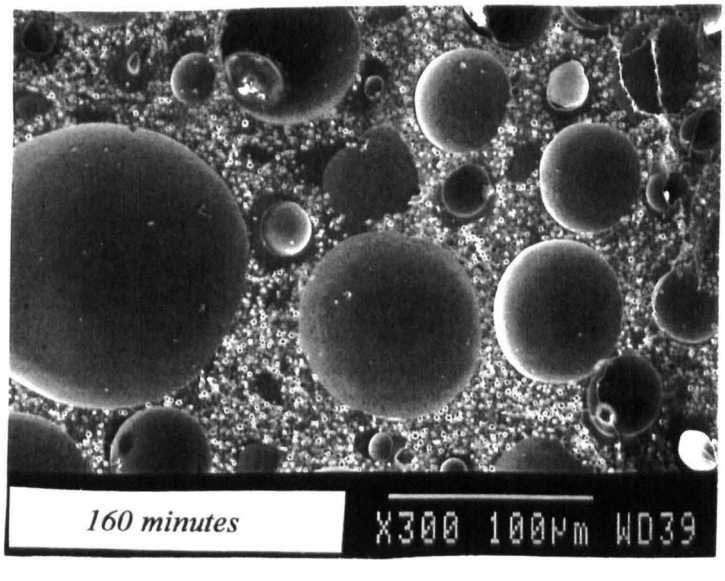

Figure 12.0u

12.1 Summary

In summary, the number of gas cells increased during aeration whilst the mean diameter decreased, after 2 hours some large gas bubbles remained. The results compare well with measurements of gas phase volume during aeration, described in Chapter 11. TEM revealed that large cells do not possess surface domain structure unlike the small gas microcells. After 15 hours ageing some cells appear to have decreased in size, these appear to be neither the very large bubbles or the gas microcells. On average, the smaller bubbles appear to have decreased and the large ones increased, this is concurrent with the process of disproportionation. If the gas cells are surrounded by a lamellar phase sucrose ester layer, then only those cells whose diameter is reduced will compress this surface and form structured domains as seen by TEM. Examination of gas microcells by TEM revealed the majority to be in the size range 0.5-5 microns, all with structured surfaces, some, with a cross-section of approximately 30 microns also possessed surface domains however gas cells larger than this were not observed to have surface domains. Within the limitations of measuring diameter after freeze fracture, those bubbles which appeared to have shrunk during the ageing period were approximately 30 microns across and were within the range of TEM. It is possible that by virtue of their shrinking these medium-sized bubbles account for the appearance of 30 micron gas microcells. The large gas bubbles do not appear to have shrunk during ageing and would thus not be expected to have a structured surface.

CHAPTER 13

Gas microcell concentration after dispersion

13.0 GAS MICROCELL CONCENTRATION AFTER DISPERSION

Dispersions of a 75% Sweetose 2% S1670 foam were made to different approximate concentrations. The dispersions were sampled at intervals and examined by optical microscopy. A haemocytometer cell, of 0.1mm depth, was used to display the sample. The gas microcells creamed to the underside of the coverslip and photographs of random areas of the surface were taken. Gas microcells in such a low viscosity medium undergo Brownian motion, the effects of this were eliminated by the use of a very fast film, Fuji Neopan 1600, black and white.

A Zeiss Particle Size Analyser was used to examine the photographs. The instrument is capable of both counting and sizing particles, however in this case it was used only to count the number of gas microcells per photograph. The reason for this was the difficulty in determining the position of the equator of the cell due to the optical effects of reflection and refraction within the bubble cell walls.

The haemocytometer slide used was calibrated across its face and had a depth of 0.1mm, thus the volume per photograph could be calculated, assuming that all gas microcells in the known sample volume were located within the cream layer. All objects which could be identified as gas microcells were counted, regardless of their position relative to the plane of focus.

Three dilution's were made, $1.6x10^{-2}$ g cm^{-3}, $1.1x10^{-2}$ g cm^{-3} and $0.5x10^{-2}$ g cm^{-3}, each was sampled at regular intervals. Figure 13.0a shows photographs of the $1.6x10^{-2}$ g cm^{-3} dispersion taken at regular intervals of time. Before sampling each dispersion was gently tipped to ensure an even distribution of the remaining gas microcells. The number of gas microcells in each picture decreases, observation by eye indicates that there is no significant change in microcell size with time. Figure 13.0b illustrates the variation of number concentration with dispersion age for each of the three dispersions. A summary of the data is given in Table 13.0a, more detailed results are given in Appendix 5.

Table 13.0a

1.6×10^{-2} g cm^{-3}		1.1×10^{-2} g cm^{-3}		0.5×10^{-2} g cm^{-3}	
time (mins)	cells per cm^3	time (mins)	cells per cm^3	time (mins)	cells per cm^3
3.75	1.91×10^9	2.83	1.47×10^9	3	0.762×10^9
10	1.84×10^9	15	1.36×10^9	15	0.491×10^9
19	2.00×10^9	27.5	0.943×10^9	39	0.377×10^9
41	1.44×10^9	43	0.925×10^9	71	0.348×10^9
80	1.00×10^9	89	0.471×10^9		
141	0.610×10^9	177	0.305×10^9		
230	0.374×10^9	240	0.156×10^9		
300	0.293×10^9				

Figure 13.0a

Photographs of a dispersion of gas microcells in water at different intervals after dilution

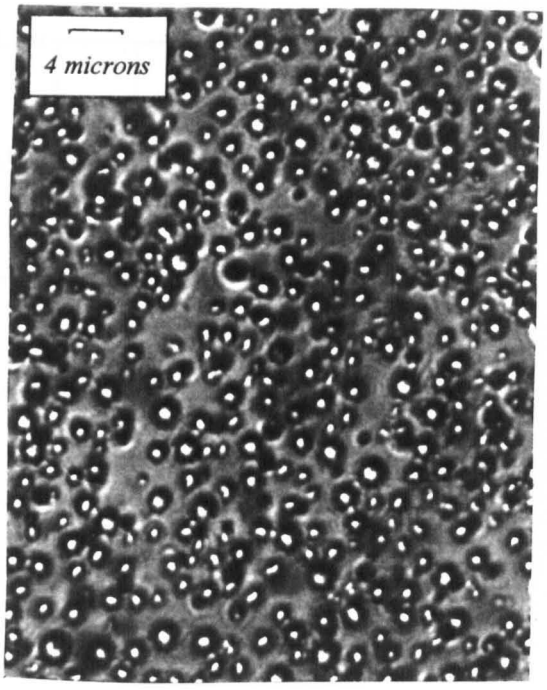

19 minutes

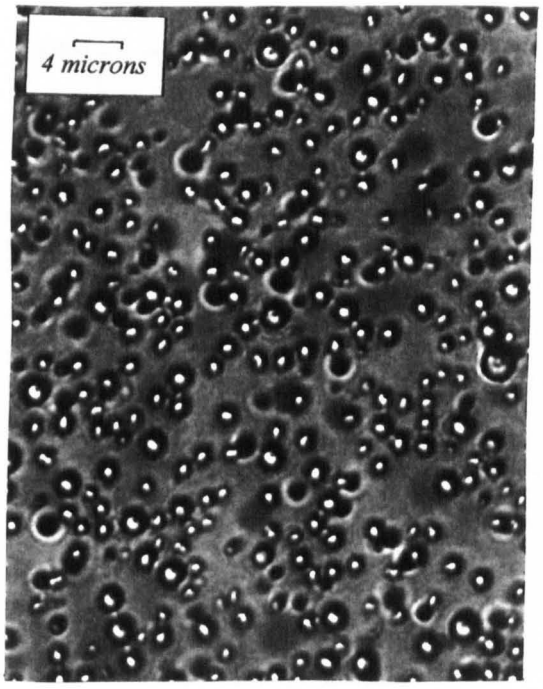

41 minutes

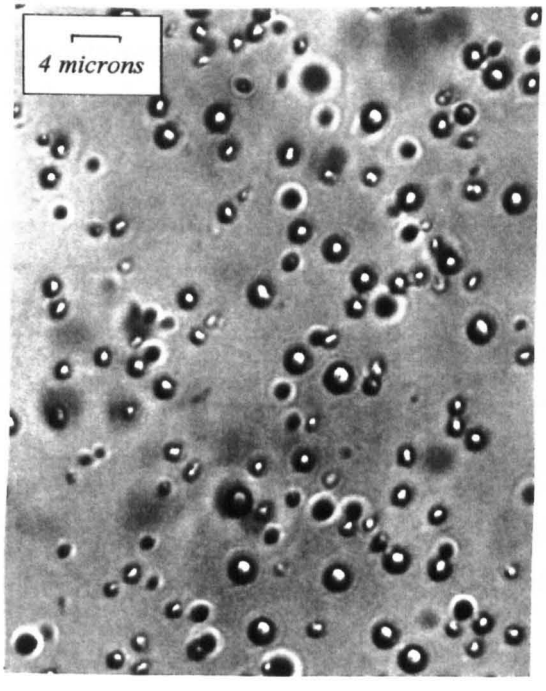

141 minutes

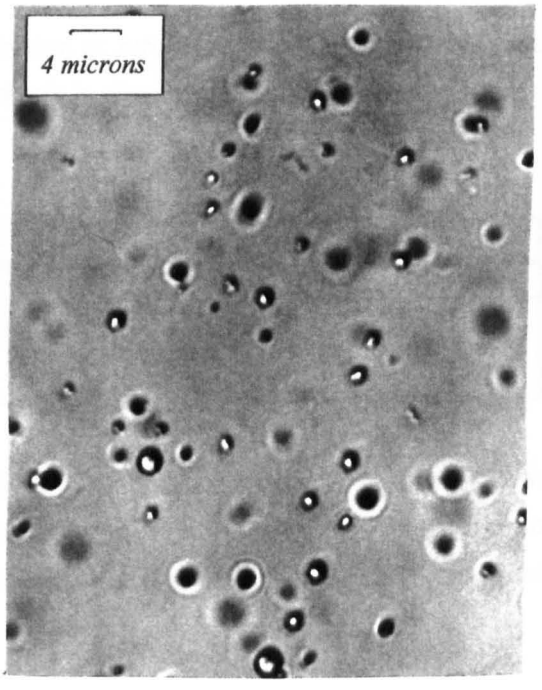

230 minutes

Figure 13.0b

An illustration of the decrease in concentration of gas microcells with dispersion age.

i) Linear plot

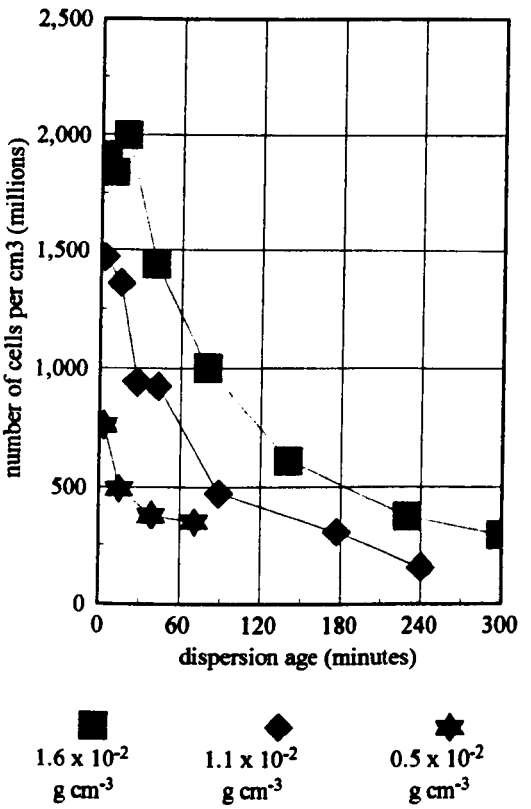

ii) Natural log plot

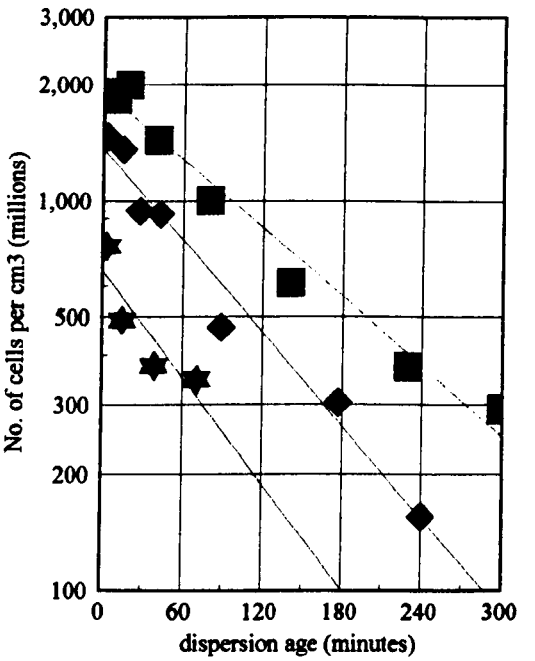

The data was extrapolated back to cell concentration at zero time, using a logarithmic plot, as shown in Figure 13.0 bii. The regression analysis is given in Table 13.0b, below.

Table 13.0b

1.6×10^{-2} g cm^{-3}		1.1×10^{-2} g cm^{-3}		0.5×10^{-2} g cm^{-3}	
gradient	-0.00680	gradient	-0.00908	gradient	-0.01038
t_0 conc (g cm^{-3})	1.92×10^{9}	t_0 conc (g cm^{-3})	1.36×10^{9}	t_0 conc (g cm^{-3})	6.56×10^{8}
correlation coefficient	-0.987	correlation coefficient	-0.986	correlation coefficient	-0.881

The poor correlation coefficient in the 0.5×10^{-2} g cm^{-3} dispersion is a result of a low number of data points, each itself based on a small sample size, this was due to experimental difficulty. The data from this dispersion is thus less reliable than that from the other two.

The normalised results are illustrated in Figure 13.0c, the results indicate that the rate of decrease in concentration is independant of the strength of the initial dispersion. Normalised data is given in Table 13.0c.

Figure 13.0c

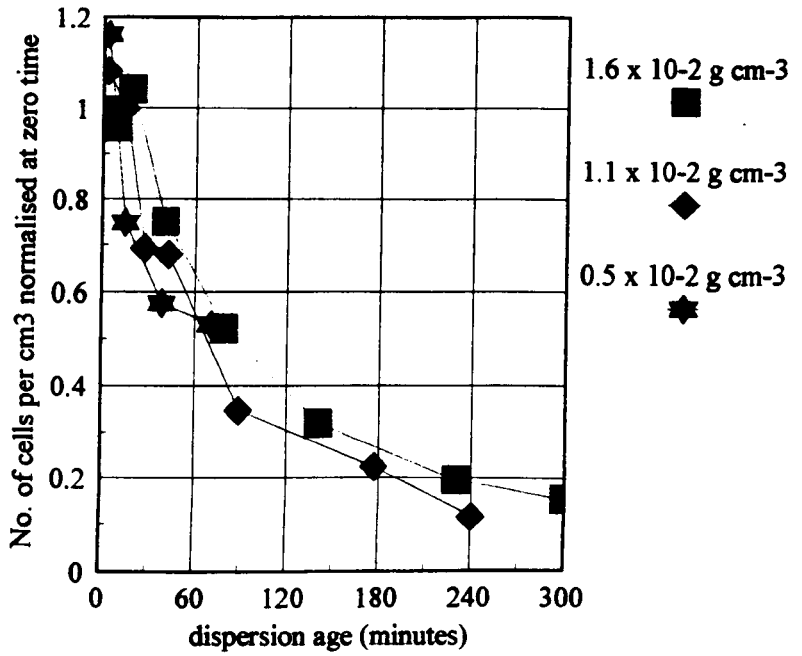

Table 13.0c

1.6×10^{-2} g cm^{-3}		1.1×10^{-2} g cm^{-3}		0.5×10^{-2} g cm^{-3}	
time	cells / cm^3 ± SD	time	cells / cm^3 ± SD	time	cells / cm^3 ± SD
3.75	0.995 ± 0.10	2.83	1.081 ± 0.09	3	1.161 ± 0.11
10	0.958 ± 0.10	15	1.000 ± 0.14	15	0.748 ± 0.03
19	1.042 ± 0.09	27.5	0.693 ± 0.09	39	0.575 ± 0.23
41	0.750 ± 0.07	43	0.680 ± 0.05	71	0.530 ± 0.11
80	0.521 ± 0.02	89	0.346 ± 0.04		
141	0.318 ± 0.05	177	0.224 ± 0.03		
230	0.195 ± 0.04	240	0.115 ± 0.01		
300	0.153 ± 0.03				

Within the limits of the standard deviation the results show that the concentration of gas microcells decreases at a rate which is independant of initial concentration. The results do not fit exactly to an exponential decay, however they are close enough for a good approximation to be made. With this assumption, the rate of decay and the number of gas microcells in the foam before dilution were estimated.

The correlation between the number of gas cells at zero time and the concentration of each dispersion.

Table 13.0d

disp. conc'n g/cm^3	cells per cm^3 at zero time	calculated cells per gram
1.6×10^{-2}	1.92×10^{9}	1.2×10^{11}
1.1×10^{-2}	1.36×10^{9}	1.2×10^{11}
0.5×10^{-2}	6.56×10^{8}	1.3×10^{11}

The results correlate very well, with the two most concentrated dispersions giving 1.2×10^{11} gas microcells per gram of foam dispersed. The results of the most dilute dispersion were different, as expected, due to the lack of raw data with which to describe the sample. The calculated concentration was 1.3×10^{11} cells per gram, a result good enough to lend credence to the rest.

The rate of concentration decay with time

The measured concentration of gas microcells is assumed to decay according to the following relationship,

$$[\text{conc}]_t = [\text{conc}]_{t=0} \cdot \exp^{-k \cdot t}$$

Figure 13.0d illustrates the data, such that the gradient of the line is equal to the rate constant k.

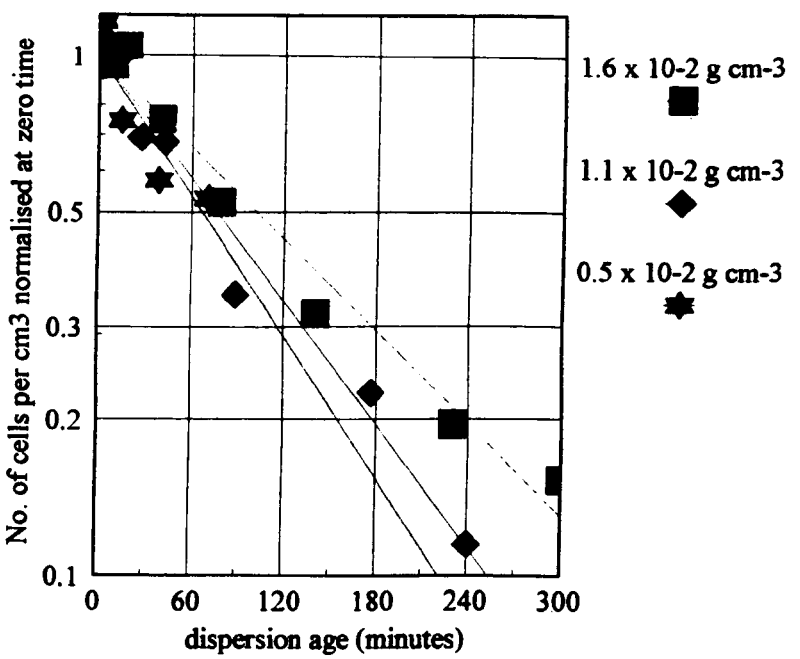

Figure 13.0d

Table 13.0e describes the results of the linear regression analysis.

Table 13.0e

1.6×10^{-2} g cm^{-3}		1.1×10^{-2} g cm^{-3}		0.5×10^{-2} g cm^{-3}	
gradient	-0.00679	gradient	-0.00907	gradient	-0.01038
t_0 conc (g cm^{-3})	1.000	t_0 conc (g cm^{-3})	1.000	t_0 conc (g cm^{-3})	1.000
correlation coefficient	-0.987	correlation coefficient	-0.986	correlation coefficient	-0.882

The mean gradient, and hence mean rate constant, of the two most concentrated dispersions is 7.9×10^{-3} min^{-1}. The result of dispersion three is deemed unreliable, due to insufficient data, and hence has not been included in the rate constant, it is not however far removed from the results of the remainder and gives confidence in their validity.

The relationship, $[\text{conc}]_t = [\text{conc}]_{t=0} \cdot \exp^{-(7.9 \times 10^{-3}) \cdot t}$ can be used to estimate the number of cells per cm^3 remaining after time, t mins. In all three dispersions, this was close to their measured standard deviations.

13.1 Summary

The results show that when 75% Sweetose 2% S1670 gas microcells are dispersed in water, the gas microcells do not remain stable. The concentration of microcells was found to decay with an approximate rate constant of 7.9×10^{-3} min^{-1}, which is not dependent on the initial concentration of the dilute dispersion. In this experiment three dispersions were made from the same foam sample and the average number of gas microcells before dispersion was estimated at 1.2×10^{11} cells per gram. This figure is an estimate, not accounting for the initial rapid loss of the large microcells, which the results of SEM and TEM have shown to be present. The large bubbles which are also present are not thought to be gas microcells, by their lack of surface structure, and hence their initial loss is not relevant to the number of gas microcells present in the foam before dilution.

Classically, when gas bubbles are dispersed in water they have been observed to possess very short lifetimes, due to the combined effects of creaming, disproportionation and flocculation[1]. Conversely, a dispersion of gas microcells shows a measurable decay in concentration with time, with cells remaining stable for up to 6 hours. The results of optical density, Chapter 14 suggest this may be as long as 24 hours. Several processes may be taking place in a dispersion of gas microcells, each of which are expected to reduce the cell stability. These are disproportionation, flocculation, creaming and dissolution of

the cell surface material. It is proposed that in the dispersion of gas microcells no one factor is responsible for their increased stability but that it is the combination of a reduction in all of the factors which delays their disappearance.

Disproportion, or Ostwald ripening, has been shown in Chapter 3 to occur on initial contact with water, a new equilibrium is reached and the rate of further disproportionation is deemed to be reduced by the presence of a liquid crystalline surface structure around the cells. The flocculation of microcells in aqueous solution was studied in Chapter 3. Limited flocculation was observed following a period of 15 hours, however this is longer than the time scale of this experiment. Flocculation is known to be a second-order process and the results appear to suggest that the process occurring is first-order, hence flocculation is not the cause of the observed behaviour. Creaming is thought to account for the initial rapid loss of the large gas cells, rising to the surface where they lose their air to the atmosphere and form a white layer which disappears after a few minutes. The smaller gas microcells however are seen to undergo Brownian motion, which hinders their progress towards the surface because of their buoyancy, hence a low rate of creaming. The surface of the gas microcells in their natural environment have been shown, by TEM to possess structured domains, which, by a combination of techniques already described are thought to be lamellar phase sucrose ester, in Sweetose, arranged at the gas microcell surface. When the gas microcells are dispersed in water some of the Sweetose and sucrose ester will dissolve. Sucrose ester is only partially soluble in water, the mono-ester fraction is sparingly soluble, whilst the di- and higher ester fractions are insoluble, hence not all of the sucrose ester will leave the cell surface. The presence of this solid structure is thought to account for the existence of each tiny gas cell, and hence its susceptibility to Brownian motion, its reduced disproportionation and the low rate of flocculation. It is proposed that, in aqueous solution, the stability of each gas microcell depends upon the lifetime of the sucrose ester 'capsule' surrounding it.

13.2 Reference

[1] Bikermann, J.J., Foams, Springer-Verlag (1973).

CHAPTER 14

Optical density

14.0 OPTICAL DENSITY

14.1 Introduction

When a sample of an aerated 75%w/w Sweetose 2%w/w sucrose ester mixture containing gas microcells is added to water the gas microcells become dispersed. Dispersions of this type were examined by microscopy in Chapter 3 and the gas microcells were observed to exist as discrete units for up to 24 hours. In Chapter 13 the number concentration of gas microcells in the dispersion was found to decrease exponentially with time. The rate of decrease was attributed to creaming and the gradual dissolution of the sucrose ester at the surface of the gas microcell into the solvent. In Chapter 3 it was observed that the rate of decrease in the number concentration was affected by the properties of the solvent used, such as salt or Sweetose concentration. In the following experiments the decrease in the number concentration of gas microcells in a dispersion was followed by measuring the decrease in optical density with time. The appearance of the dispersion changed from a milky white suspension to an almost colourless solution. The percentage transmission at 540 nm was measured using a Pye Unicam 8800 spectrophotometer. The solvent used to disperse the gas microcells was varied to observe the effect of pH, salt, S1670 and Sweetose concentration on the rate of the decrease of the number concentration of the gas microcells.

Normal practice in the standardisation of a dispersion is to mix a known mass of solute into a known volume of solvent. The instability of gas microcells when diluted renders this method impractical. Instead the following method was devised. A sample of an aerated foam, contained at the tip of a spatula, was gently swirled within a glass jar containing 500 cm^3 of solvent for 45 seconds, the spatula was removed and this time was recorded as the zero age of the dispersion. For a given volume of solvent, the percentage transmission is inversely proportional to the concentration of gas microcells. At regular intervals of time the jar was gently swirled and fresh samples were removed from the bulk dispersion and the turbidity at 540nm was measured. Measurements were continued until no further change in optical density was observed. The data were normalised to the turbidity at zero time and displayed as a function of time.

The turbidity of a dispersion is related to the percentage transmission by the following equation[1],

$$\frac{\%T}{100} = \exp^{(-\tau l)} \qquad \textit{where,} \quad \%T = \textit{percentage transmission}, \; \tau = \textit{turbidity}, \; l = \textit{path length of cell, 1cm.}$$

14.2 Using polystyrene latex as a standard to measure the effect of concentration and diameter on the percentage transmission

In Chapter 13 it was stated that in the foam before dispersion there are an average of 1.2 x 10^{11} cells per gram. The number of cells which become dispersed depends upon the mix time and the properties of the solvent, meaning that at any given time the concentration of gas microcells in the dispersion was not known. Dispersions of polystyrene latex particles with a range of diameters were dispersed to give solutions with a range of percentage transmission values. The lower the transmission the more concentrated the dispersion. The percentage transmission of these dispersions was measured across the wavelength spectrum between 400 and 700nm to determine whether the wavelength of light used was a factor in the normalised turbidity. A 2850nm latex was dispersed to an arbitrary concentration, such that its percentage transmission was between 2 and 99%. The turbidity was calculated from the percentage at each wavelength and the data was normalised to the turbidity at 540nm for each dispersion. Figure 14.2a shows the normalised turbidity across a range of wavelengths for dispersions of a 2850nm latex with a range of concentrations defined by the percentage transmission at 540nm. The data are listed in Appendix A6.

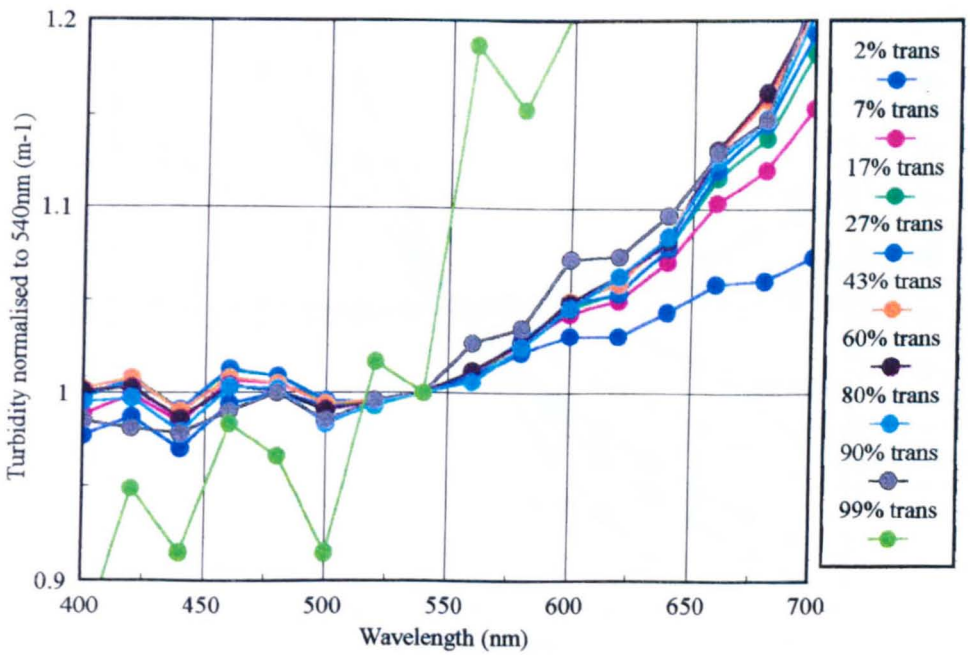

Figure 14.2a

Normalised turbidity across a range of wavelengths for different concentrations of 2850nm polystyrene latex dispersion.

The graph shows that for 2850nm spheres of polystyrene latex the normalised turbidity varied slightly with wavelength for all concentrations but where the concentration range was such that the percentage transmission was between 10 and 90% the effect was only one of wavelength and not concentration.

In order to investigate the effect of latex diameter monodisperse latices with different diameters were dispersed to an arbitrary concentration. The percentage transmission and hence turbidity of these latex dispersions was measured as a function of wavelength and the data were normalised to the turbidity at 540nm as before. The results are illustrated in Figure 14.2b. The turbidity of the 263, 490 and 850nm diameter dispersions was measured at two dilution's within 10 and 90% transmission although only one appears in the figure below. The difference between the measurements was small confirming that concentration is not a major factor in determining the turbidity after normalisation. Dispersions of gas microcells made from 75% Sweetose and 2% sucrose ester were shown in Chapter 13 to behave as a dispersion of spheres whose concentration decreases with time. A dispersion of microcells in water was made, as described in the introduction, and sampled after 15 minutes and 14 hours. The turbidity across the range of wavelengths was calculated from measurements of the percentage transmission and normalised to the turbidity at 540nm which is illustrated for comparison in Figure 14.2b. All the data relating to Figure 14.2b are listed in Appendix A6.

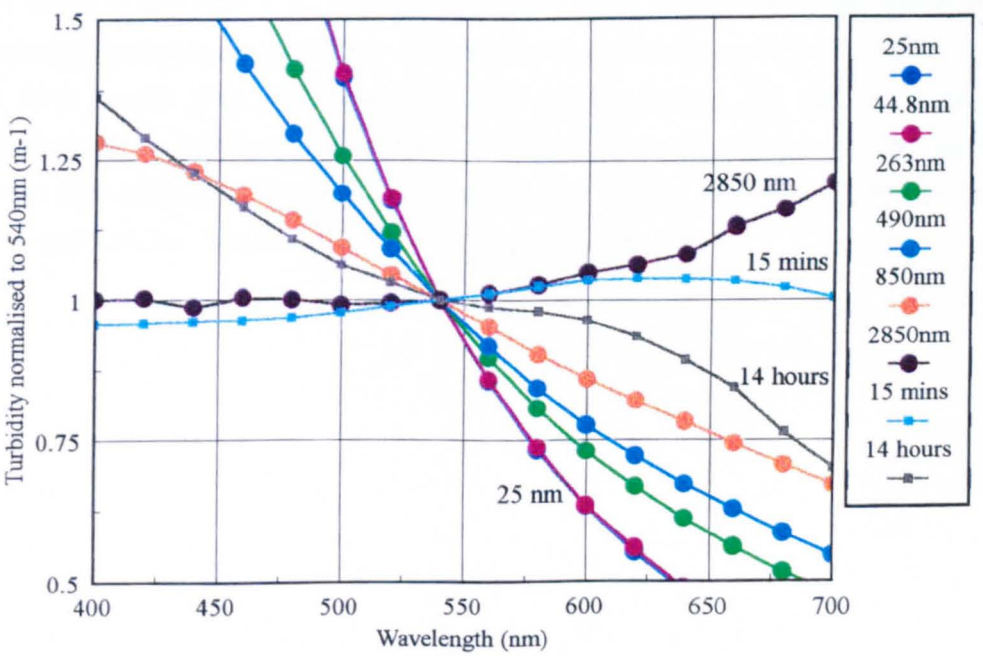

Figure 14.2b

The effect of particle diameter on the normalised turbidity across a range of wavelengths. Included on the graph is the data for samples of a dispersion of gas microcells in water after 15 minutes and 14 hours.

The figure illustrates that the turbidity values of the latices normalised to 540nm show an effect which was attributed to the latex diameter, since concentration effects were shown to be negligible; at long wavelengths the normalised turbidity increased with the diameter of the latex. The data for the dispersion of gas microcells at different times of sampling were different, the sample after 15 minutes had a higher normalised turbidity at longer wavelength than the one after 14 hours and both curves lay between those of the 2850 and 850nm polystyrene latex dispersions. The gas microcell samples were taken from the same dispersion, and concentration effects have been shown to be negligible, hence the change in normalised turbidity must be due to a change in the diameter of the gas microcells. The trend in the normalised turbidity of the polystyrene latices with different diameter indicated that the diameter of the gas microcells had decreased. This conclusion was reached with caution because the refractive index difference between dispersions of polystyrene latex and dispersions of gas microcells limits the extent to which it is justifiable to quantify the change in diameter.

14.3 Examining the relative stability of dispersions of gas microcells in various solvents

With the assumption that the normalised turbidity at any wavelength is not dependant on the initial dispersion concentration, a series of gas microcell dispersions were prepared. The solvent used was varied as follows; water, 0.001, 0.2 and 0.5%w/w sucrose ester, S1670 in water, 5 and 10% w/w Sweetose in water, pH 2.5 (with HCl) and 10^{-2}M NaCl. The percentage transmission at 540nm was measured as a function of time over 24 hours, taking a fresh sample from the dispersion, after gently swirling, for each measurement. The percentage transmission at zero time was calculated by extrapolation. The turbidity values were then calculated and normalised to the turbidity at zero time. The results are shown in Figure 14.3a. The data are listed in Appendix A6.

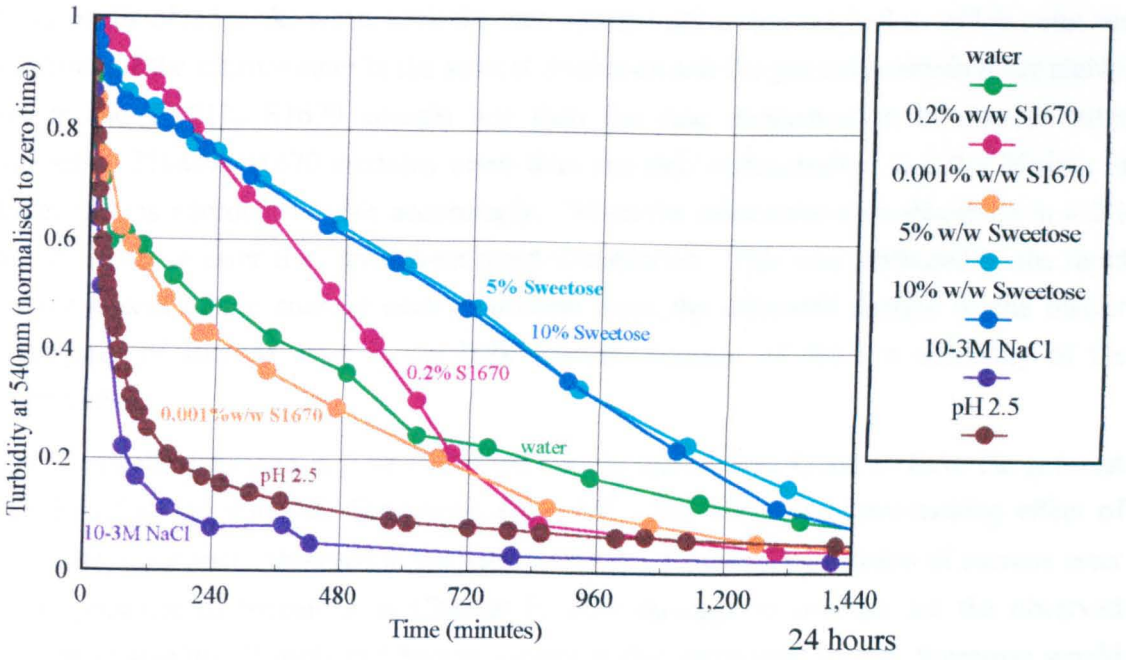

Figure 14.3a

The decay in turbidity at 540nm with time, normalised to the value at zero time, for dispersions of gas microcells in various solvents.

In all samples the normalised turbidity fell during the 24 hour period. The rate at which it fell varied according to the solvent in which the microcells were dispersed. The rate decreased most dramatically in 10^{-2}mol dm^{-3} NaCl and at pH 2.5, the natural pH for gas microcells is 5.5. This behaviour was attributed to the screening effect of the electrolyte on the electrical double layer surrounding each microcell leading to its flocculation. In Chapter 3 gas microcells were previously observed to flocculate in 10^{-2} mol dm^{-3} KCl. Clusters of flocculated microcells are more buoyant than single microcells and their increased size makes them less susceptible to Brownian motion, hence they cream faster to the surface, which reduces the turbidity of the dispersion more rapidly. If the rate of turbidity decay is an indication of the stability of the dispersion then the microcells in Sweetose and 0.2% S1670 remained more stable than those in water. The microcells dispersed in 0.001%w/w S1670 were marginally less stable than those dispersed in water, the difference was not thought to be significant. Those dispersed in 0.5%w/w S1670 flocculated so rapidly that dispersion was not possible, in Chapter 3 gas microcells dispersed in 2%w/w S1670 were also observed to flocculate rapidly. This behaviour was explained in terms of the limited solubility of S1670 in water above its cmc of 2×10^{-4} mol dm^{-3} at this temperature. 0.001%w/w S1670, a concentration of 1.4×10^{-5} mol dm^{-3}, is below the cmc whereas 0.2%w/w, a concentration of 2.8×10^{-3} mol dm^{-3}, is above the

cmc. When gas microcells were dispersed in these solvents, the sucrose ester at their surfaces dissolved in the water until the cmc concentration was reached at which point the solubility of the sucrose ester in the solvent decreases and the gas cells remain more stable. Water and 0.001% S1670 contain less than the cmc concentration of sucrose ester whereas 0.2%w/w S1670 contains more than the cmc concentration and the lifetime of dispersed gas microcells varies accordingly. When the microcells were dispersed in 0.5% and 2% sucrose ester they underwent rapid flocculation. This was attributed to the rapid rearrangement of the sucrose ester molecules from the microcell surface to the bilayer aggregates of sucrose ester in the bulk solution because of the low solubility of the amphiphiles.

Gas microcells dispersed in 5 or 10% Sweetose in water were found to have the greatest stability of all the aqueous dispersions examined. The water structure-making effect of Sweetose, previously observed in the measurements of the surface tension of sucrose ester in the presence of Sweetose in Chapter 9, were thought to account for the observed increase in stability. Results in Chapter 3 suggest that dispersion in neat Sweetose would yield the maximum stability. The optical density technique was not used to examine dispersions in neat Sweetose or any other highly viscous liquid because of the introduction of extra air bubbles during the dispersion of the microcells which distort the measurements of percentage transmission.

Other researchers[2,3] have used the technique of measuring optical density as a function of wavelength to calculate the radius of gyration and the diffusion coefficient of aqueous dispersions of particles. A similar analysis was not carried out in this discussion due to the limited knowledge of concentration that results from the arbitrary dispersion of constantly changing gas-filled microcells.

14.4 References

[1] Kerker, M.; "The scattering of light and other electromagnetic radiation", Academic Press Inc., London, 1969.

[2] Lothian, G.F. and Chappel, F.P.; J. Appl. Chem., p.475, Nov., 1951.

[3] Heller, W., Bhatnagar, H.L. and Nakagaki, M.; J. Chem. Phys., **36**, 1163, 1962.

CHAPTER 15

Discussion

15.0 DISCUSSION

15.1 Introduction

Gas microcells are the name given to the small spherical air bubbles produced during the aeration of a mixture of Sweetose, water and sucrose ester surfactant. The diameter of these bubbles varies within the range of 0.1 to 20 μm. TEM revealed them to have a structured surface, comprising regular domains, approximately 50-100nm in diameter, protruding from the surface of each cell into the surrounding matrix. These bubbles have an unusually high stability to drainage and disproportionation, common causes of instability in foams, and were known to resist drainage for over 12 months when stored at 4°C. For this reason and because of their unusual surface structure they are referred to as gas microcells to differentiate them from other air bubbles, such as those found in detergent foams, which in general do not possess these characteristics.

The aim of this work was to study the gas microcells in order to gain an understanding of why they have a distinctive surface structure and what it consists of. These objectives were achieved by the use of many and varied techniques, some of which were found to be of negligible benefit. Despite the description given in the introduction of the gas microcells being discrete stable spherical gas cells dispersed in a viscous matrix they did not submit to all of the classical methods of analysis of emulsions. Foams containing gas microcells are very viscous which makes them difficult to analyse. When the microcells are dispersed in water they have a dynamic instability which makes them unsuitable for techniques such as light scattering because their number concentration is constantly decreasing. Their instability to even low salt concentrations caused them to flocculate in the Coulter Counter. The techniques described in this thesis are those which yielded the best information.

The gas microcells were composed of small cells of air in a continuous mixture of Sweetose and sucrose ester. The mixture before aeration was found to contain liquid crystal bilayers of sucrose ester within a matrix of Sweetose. Figure 15.1a illustrates the sucrose ester bilayers in a non-aerated mixture, by TEM. After aeration, the gas microcells themselves were found to possess a rigid surface which had a varied structure according to the blend of sucrose esters used. Figure 15.1b illustrates a number of gas microcells produced by the aeration of the non-aerated mixture seen in Figure 15.1a, also by TEM. Dispersions of gas microcells in water remained stable for up to 24 hours in water or indefinitely if dispersed in neat Sweetose, the presence of salt caused flocculation. This chapter aims to discuss in more detail the results of each of the previous chapters in terms of their relation to non-aerated mixtures, individual gas microcells and dispersions of microcells.

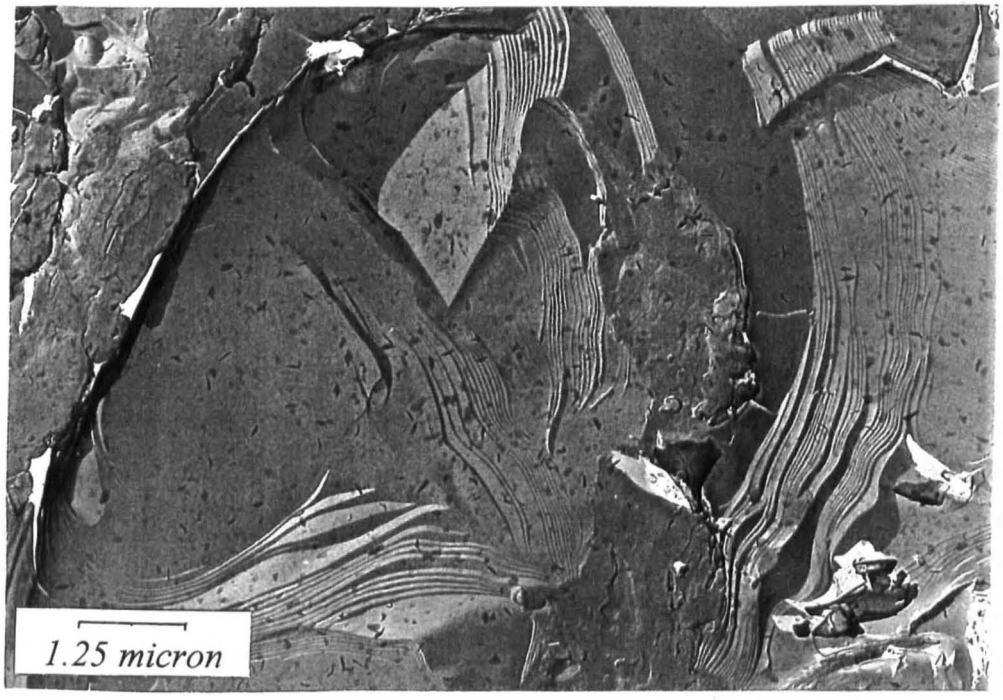

Figure 15.1a

A non-aerated mixture of 75% Sweetose, 2%w/w sucrose ester, S1670, and water, showing sucrose ester bilayers in a matrix of aqueous Sweetose, by TEM.

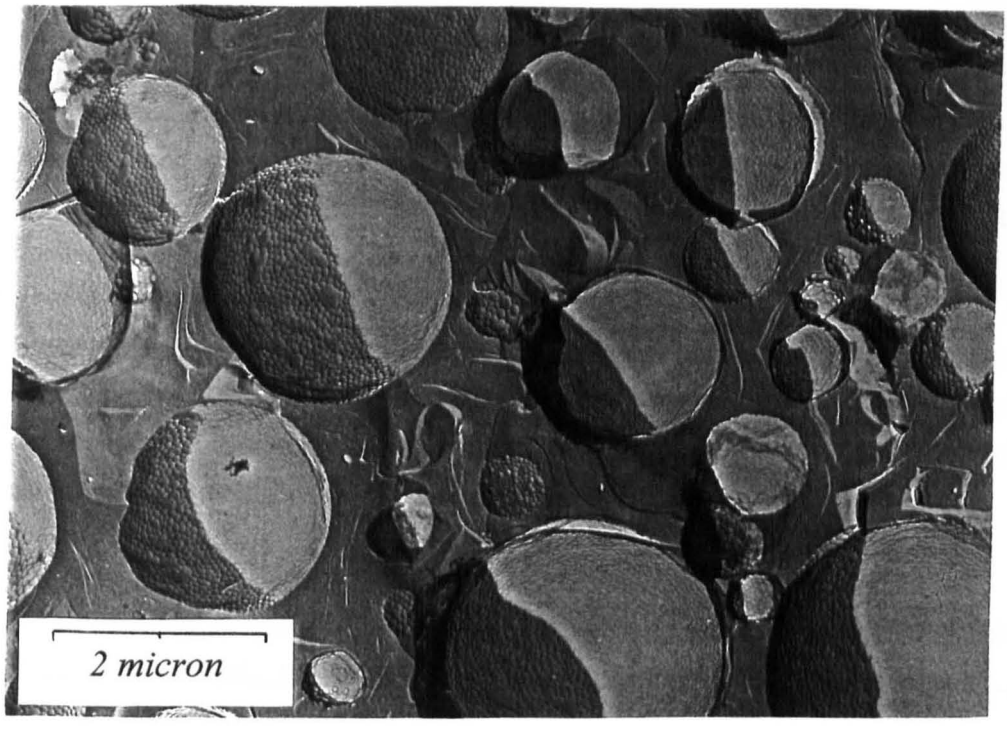

Figure 15.1b

Gas microcells produced by the aeration of a mixture of 75%w/w Sweetose, 2%w/w sucrose ester, S1670, and water. TEM image.

15.2 The mixture before aeration.

The preparation of a non-aerated mixture was largely the same as that of the gas microcells, without the aeration. For this reason the character of this material was assumed to be very relevant to the structure of gas microcells. The sucrose esters, being insoluble in water at room temperature, were mixed with water and heated to 70°C to form a solution, Sweetose at the same temperature was added to the solution and stirred to disperse the sucrose ester, which had a tendency to separate from the Sweetose. The mixture so obtained was viscous and opaque after cooling. Solutions of sucrose ester in water alone formed a gel on cooling. The non-aerated mixture of Sweetose, water and sucrose ester was examined by various microscopy techniques and found to contain regions of optical anisotropy. Comparison with solutions containing sucrose ester in water alone revealed these to be discrete regions of sucrose ester in an optically isotropic matrix. X-ray and neutron diffraction experiments on the non-aerated sample revealed that it was sucrose ester arranged as liquid crystalline bilayers, this was confirmed by the use of TEM. Gel permeation chromatography proved that all of the sucrose ester in the sample was in the liquid crystal phase and the matrix was a solution of Sweetose and water.

Optical microscopy examination of sucrose esters in water revealed that no mesophases were formed at weight concentrations of only 2% w/w which is equivalent to 2.8×10^{-2} mol dm^{-3} and yet the addition of 75%w/w Sweetose was sufficient to cause the sucrose ester to phase separate. The extent to which the phase separation occurred increased with the Sweetose concentration of the mixture, according to the observations of confocal microscopy. In hydrogen bonded solutions the minimisation of the extent to which the water network is disrupted, tends to be the driving force for micellisation. The observation that adding high concentrations of Sweetose to water causes the sucrose ester to form lamellar phase indicates an increase in the water structure in the presence of Sweetose, rather than the reverse. The solids concentration in Sweetose is 80%w/w so in a 75%w/w sample Sweetose solution with 2%w/w sucrose ester the total water concentration is 38% of the sample weight as opposed to 98% in the sample containing 2%w/w of sucrose ester in water alone. Sweetose itself is an oligosaccharide containing low molecular weight solutes with a distribution of glucose units between 1 and 9.

15.3 Calculating the number of hydrogen bonding units in Sweetose compared to the number of water molecules, at 75%w/w Sweetose and 30%w/w Sweetose concentration.

Consider 100g of a non-aerated mixture of 75%w/w Sweetose and 2%w/w sucrose ester, composed of 70% mono-stearate and 30% di-stearate.

Sweetose is an oligosaccharide composed of glucose units, illustrated in Figure 15.3a.

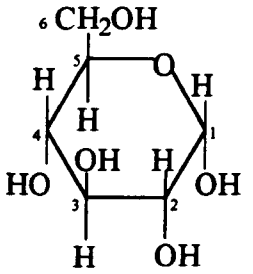

Molecular weight
of each glucose unit = 166

Figure 15.3a
A molecule of α-d-Glucopyranose,
described here as 1 glucose unit.

Thus the mass of 1 molecule of glucose = 166 / 6.022 x 10^{23} = 2.758 x 10^{-22}g

Sweetose is 80% solids therefore in 100g of a sample, which is 75%w/w Sweetose in water, there are 60g of Sweetose solids.
In 60g of Sweetose solids there are 60 / 2.758 x 10^{-22} = 2.175 x 10^{23} glucose units.

The water content of the above mixture is 23g + 15g (from the Sweetose) = 38g and the molecular weight of water = 18g
By the above calculation, there are 1.27 x 10^{24} water molecules in 38g of water. So, there are 2.18 x 10^{23} glucose molecules and 1.27 x 10^{24} water molecules in the non-aerated mixture described.

Each glucose molecule has 12 potential hydrogen bonding sites, thus there are approximately 2.6 x 10^{24} hydrogen bonding sites and 1.3 x 10^{24} water molecules. That is there are twice as many hydrogen bonding sites as water molecules. This would indicate that the amount of water in the system is low, which combined with the surface tension evidence that Sweetose increases the water structure was thought to explain the high degree of phase separation observed at a relatively low sucrose ester concentration.

When the concentration of Sweetose used in the non-aerated mixtures was reduced to 30%w/w Sweetose in water, the amount of liquid crystalline sucrose ester observed by light microscopy was reduced. The above calculation was repeated to find whether the effect could be explained in terms of the water content of the mixture.

In a 100g sample of 30%w/w Sweetose there are 24g of glucose solids. This is equivalent to 8.70 x 10^{22} glucose molecules, or 1.04 x 10^{24} hydrogen bonding sites. The water content of such a mixture is 6g from the Sweetose and 68g added to the mix, = 74g, which is equivalent to 2.47 x 10^{24} water molecules. Thus in 30%w/w Sweetose there are 1.0 x 10^{24} hydrogen bonding sites and 2.5 x 10^{24} water molecules.

In a 30%w/w Sweetose in water mixture there are twice as many water molecules as hydrogen bonding sites on the glucose molecules, the reverse of the situation which exists at 75%w/w Sweetose in concentration. If as proposed, the Sweetose increases the extent of the hydrogen bonding network then a decrease in its concentration in favour of increased water would cause the structuring of the network to decrease and by the hydrophobic effect the driving force for aggregation of the sucrose ester would be reduced explaining the observation of less liquid crystalline sucrose ester.

In 2%w/w sucrose ester, containing a blend of 70% mono-stearate and 30% di-stearate, the approximate number of hydrogen bonding sites on the head groups was also calculated to see whether it would have any substantial effect on the ratio of hydrogen bonding sites to water molecules.

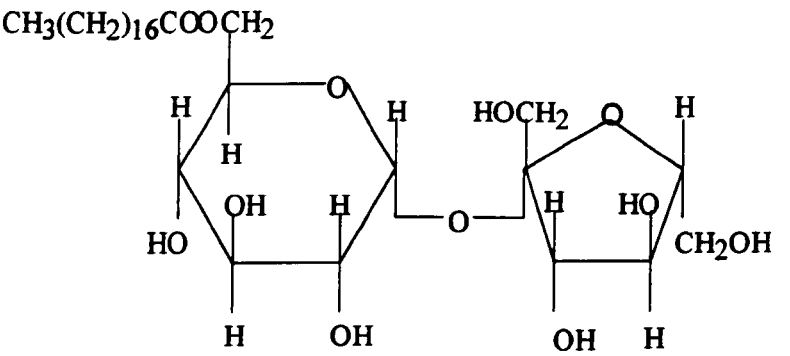

Figure 15.3b

A molecule of sucrose mono-stearate

In 2g of sucrose ester there is 1.4g of mono-stearate and 0.6g of di-stearate.
The molecular weight of mono-stearate is 636g and that of di-stearate is 917g.

There are 1.33×10^{21} molecules of mono-stearate and 3.94×10^{20} molecules of di-stearate in 2g of sucrose ester containing 70% mono-stearate and 30% di-stearate..

Each sucrose ester molecule has a sucrose head group, thus the total number of head groups is 1.72×10^{21}. On each head group there are 21 possible hydrogen bonding sites, thus the total number of hydrogen bonding sites in the sucrose ester is 3.62×10^{22}. This is two orders of magnitude smaller than the number of hydrogen bonding sites in Sweetose and thus would not effect the dynamics of the above calculations.

The above calculation revealed that at low Sweetose concentrations there are more water molecules than hydrogen bonding sites in Sweetose whereas at high Sweetose concentrations the reverse is true. Surface tension measurements on sucrose ester in the presence of dilute Sweetose revealed that for a given concentration of sucrose ester the surface tension increased upon the addition of Sweetose. This was attributed to the increased hydrogen bonding at the water surface. It was assumed that this would also be accompanied by an increase in the extent of hydrogen bonding within the bulk solution. The formation of lamellar phase sucrose ester in high concentrations of Sweetose was thus attributed to the strongly hydrophilic character of the Sweetose molecules causing an increase in the hydrophobic effect. The spaces between the sucrose ester bilayers were thought to be occupied by the Sweetose solution. Gel permeation chromatography proved that no sucrose ester was dissolved in the Sweetose solution. All of the sucrose ester was present as liquid crystalline bilayers. For this reason, it was assumed that the Sweetose did not interact with the sucrose ester in any other way. Its use as a viscosity modifier is discussed later.

15.4 Rheological measurements on non-aerated mixtures of Sweetose and sucrose ester

Rheological measurements on 75%w/w Sweetose in water and non-aerated mixtures of Sweetose, sucrose ester and water revealed that although solutions of Sweetose in water are Newtonian, in the presence of sucrose ester they become shear thinning, with a large hysteresis loop and a quantifiable yield stress. This behaviour was attributed to the presence of liquid crystalline bilayers of sucrose ester and their breakdown during shear. The viscosity of the non-aerated mixture and the area of the hysteresis loop was found to be strongly dependant on the concentration of liquid crystalline sucrose ester present, which was proven by microscopy and DSC evidence to be dependant upon the concentration of both Sweetose and sucrose ester. Rheological measurements on non-aerated mixtures of sucrose, sucrose ester and water at 20°C and 60°C by Fitzgerald[1] showed that the viscosity and the extent of shear thinning in these mixtures were reduced on heating. The observation, by Fitzgerald, that the viscosity and the degree of shear thinning, in mixtures of Sweetose, water and sucrose ester, reduces on heating to 60°C concurs with the behaviour of similar mixtures when investigated by other techniques. Evidence of an endothermic phase transition at 48°C by DSC was attributed to the melting of the alkyl chains in the sucrose ester bilayers. The observation that optically anisotropic mixtures of Sweetose, sucrose ester and water became more isotropic on heating above 50°C was also attributed to the melting of the alkyl chains in the sucrose ester bilayers.

15.5 DSC measurements on non-aerated mixtures of Sweetose and sucrose ester

DSC measurements were carried out on the different sucrose esters in a variety of states, from pure crystals to aqueous solutions and mixtures with Sweetose. With sucrose esters containing a mixture of mono- and di- ester, independently of their environment, an endothermic phase change was observed at 48°C which was attributed to the hydrocarbon chain melting transition in a solid solution of both mono- and di- ester. This explains the reduced viscosity at high temperatures. Where the sucrose ester used contained only mono-ester no phase change was observed which agreed with the observation, by confocal microscopy, that no liquid crystalline material was formed in a mixture of 75%w/w Sweetose and 2%w/w sucrose ester when the sucrose ester contained only mono-ester.

DSC measurements on crystalline sucrose esters containing different blends of sucrose mono- and di- stearate revealed the formation of mixed crystal of mono- in di-stearate and di- in mono- stearate. The phase changes observed in crystalline samples of sucrose ester were also observed in mixtures of sucrose ester in 75%w/w Sweetose in water solutions. The only exception to this was that sucrose mono-stearate was soluble in 75%w/w Sweetose hence no phase transition was observed. The alkyl chain melting transition observed at 48°C in a mixture of 75%w/w Sweetose in water with 2%w/w sucrose stearate was attributed to the melting of the chains in a mixed liquid crystal of mono- in di-stearate. The alkyl chain melting transition temperature, observed in mixtures of Sweetose, water and sucrose ester, was affected by the chain length of the sucrose ester. Sucrose palmitate melted at 40°C whereas sucrose behenate melted at 70°C, when both contained the same blend of mono- and higher esters.

When a non-aerated mixture of 75%w/w Sweetose in water and 2%w/w sucrose ester was centrifuged, it separated into two layers, a dense clear liquid and a light opaque phase. DSC analysis on the two phases revealed that only the light phase showed any phase transitions. Gel permeation chromatography showed that this was because only the light phase contained sucrose ester, the dense clear liquid was a solution of Sweetose and water.

In conclusion non-aerated mixtures of 75%w/w Sweetose, water and 2%w/w sucrose ester exist as a heterogeneous mixture of liquid crystalline sucrose ester in an aqueous Sweetose matrix, provided that the sucrose ester used is composed of mono- and di- ester. The liquid crystal is a mixture of mono- in di-ester arranged in a bilayer formation. This conclusion is based on the behaviour of sucrose stearate; sucrose palmitate and sucrose behenate are believed to have similar characteristics by virtue of their thermal characteristics observed by DSC. Sucrose esters whose chain lengths were shorter than that of sucrose palmitate were soluble in 75%w/w Sweetose and did not form liquid crystals. Sucrose esters whose chain lengths were between that of sucrose palmitate and

sucrose behenate were not investigated but it is expected that they would form liquid crystals whose phase transition temperature varies according to the alkyl chain length.

15.6 Gas microcells produced by the aeration of Sweetose, sucrose ester and water

A comparison of the thermal analysis of the mixtures before aeration and the results of TEM on gas microcells produced after aeration, containing blends of sucrose mono-, di- and tri- esters revealed some interesting relationships. Where the sucrose ester contained only mono-ester no surface structure and no DSC phase change was observed. When up to 30%w/w of di-ester was added to the mono-ester a DSC phase change was observed and the microcells possessed a regular hexagonal and pentagonal domained surface structure. When the di-ester component was further increased however the phase changes observed began to alter progressively and the surface structure on the microcells became less regular. Thus for the observation of a phase change by DSC it was necessary to use a mixture of mono- and di- esters, but for regular structure on the microcells the di-ester component had to be less than 30%w/w.

An aerated sample of 75%w/w Sweetose in water and 2%w/w sucrose ester was left to stand for 6 months at room temperature. The foam drained partially, leaving a white particulate foam layer above a clear viscous liquid. Gel permeation chromatography was used to analyse both fractions. The foam layer contained all of the sucrose ester in the sample, none was found in the lower liquid, which was therefore a solution of Sweetose and water. The foam layer contained solid white particles which, by TEM, resembled the honeycomb arrangement of hexagonal and pentagonal domains seen on the surface of the gas microcells, despite the fact that no gas microcells remained after drainage. It was concluded that all of the sucrose ester in the sample was at the surface of the gas microcells which were suspended in a viscous matrix of Sweetose in water.

The DSC evidence showed that the phase transition occurring in the aerated mixture had a close resemblance to that occurring in the non- aerated mixture. There was an endo- and exo- thermic phase transition in samples before and after aeration. These transitions were attributed to the melting and freezing of the alkyl chains. The enthalpy of the endothermic transition in the aerated sample was slightly lower than that of the non-aerated sample, for the same Sweetose and sucrose ester concentration. When the melting and freezing process was repeated using the same samples the enthalpy of the endothermic transition was identical. This was attributed to a re-arrangement of the sucrose ester molecules in the aerated sample caused by the melting of the alkyl chains, with the resulting arrangement having the same enthalpy of transition as that in a non-aerated sample.

In the aerated sample the sucrose ester is at the surface of the gas microcell whereas in the non-aerated sample it is present in liquid crystalline bilayers in the bulk. Heating the sucrose ester above 48°C melts the alkyl chains and increases their solubility in aqueous Sweetose. Heating the aerated sample above 48°C was thought to allow the sucrose ester to migrate from the surface of the gas microcell and into the Sweetose matrix. The endothermic phase change observed on melting the aerated sample for the second time was the same as that observed in melting a non-aerated mixture. This suggests that the sucrose ester in the aerated sample migrates from the surface of the microcell into the Sweetose matrix when the sample is heated where it forms bilayers which crystallise on cooling. When the aerated sample is heated for a second time the melting process is that of melting the alkyl chains in a bilayer, which is the same process as that occurring in the non-aerated sample. The lower enthalpy of transition in the melting of the aerated sample is an indication that less energy is required to melt the alkyl chains of the sucrose esters on the surface of the microcells than in a liquid crystalline bilayer.

15.7 The process of aeration

In order to observe the aeration process more closely photographs of a non-aerated mixture after stirring for a few minutes by hand were taken. These showed that as the number of air bubbles increased the liquid crystalline sucrose ester began to disperse and became less visible due to the shearing process.

Measurements on the phase volume of gas incorporated during aeration showed that a minimum of 0.2%w/w sucrose ester was required to aerate a solution of 75%w/w Sweetose. A minimum of 30%w/w Sweetose was also required for aeration of 2%w/w sucrose ester. This was attributed to the need for a minimum viscosity to reduce the drainage and creaming rate of the matrix, in addition, at Sweetose concentrations lower than 30%w/w both confocal microscopy and DSC evidence showed that the quantity of sucrose ester in the liquid crystalline arrangement was reduced. TEM investigations revealed that when a low sucrose ester concentration, such as 0.2%w/w, was used the microcells were very few and had a large diameter, but all possessed a regular surface structure.

These observations, by TEM and by measuring gas phase volume on foams, with a minimum concentration of sucrose ester were attributed to the limiting of the total surface area of the microcells produced, by the concentration of sucrose ester in a lamellar phase before aeration.

15.8 Sucrose ester at the surface of a gas microcell

The sucrose ester is arranged at the surface of the gas microcell and the microcells observed by TEM have a regularly structured surfaces consisting of hexagonal and pentagonal domains that protrude into the matrix.

The alternative arrangements for the packing of the sucrose ester around the gas microcell surface might be any of the following.

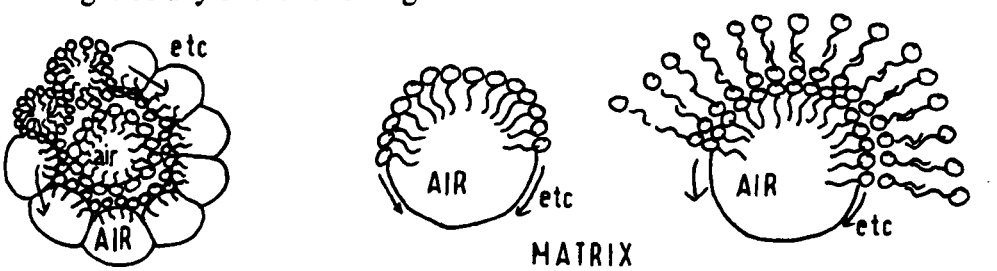

Model 1 *Model 2* *Model 3*

Figure 15.8a

Model one consists of an arrangement of close packed spherical vesicles around the surface of the air bubble. When viewed from the outside by TEM this would resemble a gas microcell. A fracture across its diameter would reveal a double layered shell, being the inside and outside edges of the vesicle.

In models two and three the surface of the gas bubble is surrounded by either a monolayer or odd numbers of multilayers of sucrose ester. Fracture around the diameter in the multilayer model would be expected to resemble a ring surrounded by bilayers which would look like steps, as observed in the TEM of a non-aerated mixture containing bilayers. In the monolayer model, fracture around the diameter would reveal a ring with a sharp edge.

Figure 15.8b illustrates a gas microcell after freeze fracture and shadow coating for examination by TEM.

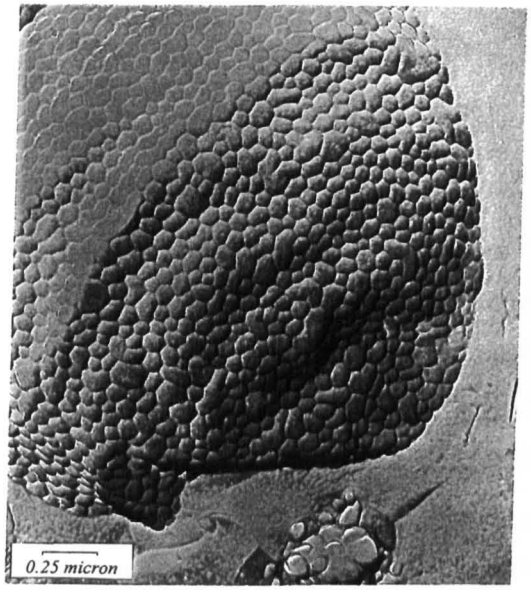

Figure 15.8b

A gas microcell made from the aeration of 75%w/w Sweetose and 2%w/w sucrose ester. Fracture across its centre reveals the inside surface of a hemisphere. The surface contains hexagonal and pentagonal domains which protrude into the matrix. This can be clearly seen at the perimeter of the microcell.

The gas microcell in Figure 15.8b is typical of the appearance of the majority of gas microcells after freeze fracture. The perimeter of the microcell was sharp with no indication of the presence of vesicles or a multilayer but the surface was not circular, as it would be if the microcell was a perfect sphere. If the surface of such a sphere was rippled then it might resemble the cross section observed in reality. TEM revealed the presence of bilayers in a non-aerated mixture so it was expected that if the microcell was surrounded by multilayers or vesicles of sucrose ester then they would have been visible in the illustration above. Therefore the surface was likely to consist of a monolayer of sucrose ester. The quantity of sucrose ester required to form a monolayer on each of the gas microcells in a foam was calculated, for comparison with the amount of sucrose ester available.

15.9 The mass of sucrose ester required to form a monolayer on each gas microcell

This was calculated for a foam at 25°C, assuming a monodisperse distribution of 2 micron diameter gas microcells and an average head group area of $0.44nm^2$.

The area occupied by 1 molecule on the surface of the microcell = $0.44nm^2$
The area of the surface of a 2 micron diameter gas microcell = $4\pi r^2 = 1.2566 \times 10^{-11}m^2$.

$$\frac{1.2566x10^{-11}}{0.44x10^{-18}} = 2.86x10^{7} \text{ molecules on the surface of 1 bubble,}$$

$\div N_A = 4.743 \times 10^{-17}$ moles of sucrose ester on the surface.

Average molecular weight of S1670,accounting for the ratio of mono-/ di-/ tri- esters = 720
$\therefore$ the mass of S1670 in a monolayer, on a 2 micron diameter bubble = 3.415×10^{-14}g.

$$\text{Volume of spheres} = \frac{4}{3} \cdot \pi \cdot r^3,$$

thus for a 2 micron diameter gas cell the volume is 4.189×10^{-18} m^3.

The density of the mixture after 2 hours aeration = 0.52g cm^{-3} = 5.2×10^5 g m^3.
The volume of 100g of this foam = 1.923×10^{-4} m^3.
Assuming a 70% packing fraction, the available volume = 1.346×10^{-4} m^3.

If all are 2 micron diameter spheres then there would be 3.213×10^{13} spheres.

Therefore the total mass of sucrose ester required for a monolayer on each microcell is,
$3.213 \times 10^{13} \times 3.415 \times 10^{-14} = 1.0974$g in 100g of sample.

In the preparation of gas microcells 2g in 100g is used.

Assuming a monodisperse distribution of 2 micron diameter gas cells, with a 70% packing fraction and an area per head group for each sucrose ester molecule of 0.44nm^2 then 1.0974g of sucrose ester would be required to form a monolayer on each of the microcells in a sample weighing 100g.

In reality many of the microcells are smaller than 2 microns in diameter and thus the total surface area is likely to be higher than calculated, in which case the amount of sucrose ester available would be further restricted.
In the measurement of the number concentration of gas microcells after dispersion it was estimated that the number of gas microcells in a foam before dispersion was 1.2×10^{11} cells per gram. If this figure is used in the calculation above, then the average diameter of the gas microcells with all of the above assumptions would be 0.5 microns. A foam containing gas microcells with a monodisperse distribution of gas microcells of 0.5 micron diameter would have a larger total surface area than one containing microcells with an average diameter of 2 microns, for the same phase volume of gas.

This calculation demonstrates therefore that the quantity of sucrose ester added to the mixture with Sweetose is only sufficient to form a monolayer coverage on all of the microcells.

15.10 Structuring of the surface of the gas microcell

From a comparison of the results of DSC and TEM on gas microcells containing mixtures of mono- and di- esters we know that the shape of the domains on the surface are dependant on the blend of esters used. This discussion of the mono or multilayer arrangement has not accounted for this as yet. In the monolayer model, the fracture

criteria for a mixture with 70% mono- and 30%- di ester, i.e. the formation of regular domains protruding from the gas cell surface into the matrix, would be satisfied if the surface layer was forced to bend to accommodate the different geometry's of the component sucrose esters. The DSC measurements showed that the alkyl chains within the sucrose esters were beneath their chain melting temperatures at room temperature and that the sucrose ester was a mixed solid of mono in di ester. Thus the sucrose ester layer at the surface of the microcell would be expected to have a degree of rigidity. When a drained foam was examined by TEM the remains of a solid particulate material was observed whose structure might have originated from the regular domains on the outside of the microcells. The survival of this structure after the drainage of the foam was taken as further evidence of a rigid surface.

It was observed that microcells prepared from non-aerated mixture that was freshly prepared and still warm at the start of the aeration process were spherical, the average surface was smooth although it contained small protruding domains. Microcells prepared from non-aerated mixture of the same proportion that had been stored for 24 hours at 4°C were not perfectly smooth and spherical. They had regular domains on their surface but there was a secondary ripple in the surface. This was attributed to the increased rigidity in the bilayers of the non-aerated mixture after having been cooled for 24 hours prior to aeration.

The mechanism for the deliverance of a sucrose ester monolayer onto the surface of a microcell was probably the shearing of the bilayers of sucrose ester by the mixer blade followed by the well of air. As further bubbles are introduced the bubble surface shears the bilayers, across the hydrocarbon chains because these are the weakest plane, depositing the exposed alkyl chains of the sucrose ester at the gas cell surface. The rigidity of the chains helps to prevent the layer from breaking up. Initially more than a monolayer will reside on each gas cell but as the shearing continues the process of comminution will increase the number of cells until each one has a monolayer of sucrose ester and the total surface area can increase no further.

This process explains the requirement for at least 30%w/w Sweetose concentration. If the viscosity of the matrix was low then the mixture would not elongate on shearing and the comminution process would be disrupted moreover, the low matrix viscosity would accelerate the processes of drainage and creaming and de-stabilise the foam.

SEM showed that after two hours aeration some very large gas bubbles remained, meaning that in relative terms all of the gas microcells were small bubbles. The surface of the large cells should also contain a monolayer of sucrose ester, yet TEM observations suggest that only the small cells have a regular domain structure at their surface.

In the process of reaching equilibrium, all foams undergo the process of disproportionation, or Ostwald ripening, wherein all the bubbles try to equalise the internal pressure of the gas they contain. The value of their internal pressure is governed by the surface tension and the radius of curvature, thus for an equal surface tension the small cells have a larger internal pressure which will tend to force some of the air to diffuse out so that the cell shrinks further. The larger cells on the other hand have a lower internal pressure and will tend allow the air to diffuse in. This results in an overall expansion of the larger cells at the expense of the smaller cells. The process would continue until all of the small cells have disappeared if it is not checked. The presence of a rigid sucrose ester monolayer at the surface of each microcell might be such an inhibitor. We know that the sucrose ester is insoluble in 75% Sweetose at room temperature thus the monolayer will not dissolve off the surface of the cell. Once aeration has ceased there is no mechanical force to remove the monolayer thus it is very likely that it will remain at the surface. As the small gas cells shrink the area available to the monolayer shrinks and the monolayer is forced to bend. The exact structure of the monolayer at the microcell surface was observed to be dependant on the constitution of the sucrose ester blend. However in all blends which form a rigid monolayer, that is all blends that display a phase transition, a structured surface is observed. The observance of a lack of structuring on the surface of the large gas cells was due to the fact that the sucrose ester monolayer was contained on an expanding surface and it was not forced to buckle.

In the knowledge that the exact shape of the surface domains was a result of the composition of the monolayer, the following calculations aim to interpret the weight fractions used in terms of the ratio of the number of molecules of mono- ester to di-ester.

The sucrose esters used were blends of mono-stearate, di-stearate and tri-stearate. The molecular weight of these was 636, 917 and 1197g respectively.

In 1g of crystalline sucrose ester, containing a 70:30 ratio of mono- to di- stearate there is 0.7g of mono-stearate and 0.3g of di-stearate. This corresponds to 1.1006×10^{-3} moles of mono-stearate and 3.2715×10^{-4} moles of di-stearate, or 6.63×10^{20} molecules of mono-stearate and 1.97×10^{20} molecules of di-stearate. This is a ratio of the number of molecules of mono-/di- of 3:1. Each di-stearate molecule has two alkyl chains, so the ratio of the number of alkyl chains in the monolayer originating from the mono- and di- stearate is 3:2.

By the same method, the ratio of the number of alkyl chains in the monolayer which originate from the mono-, di- and tri- stearate molecules is given below.

In 90/10 ratio of mono:di the ratio of molecules is 13:2.
In 70/30 ratio of mono:di the ratio is 3:2.
In 70/25/5 ratio of mono:di:tri, or S1670, the ratio is 26:12:3.
In 52/36/12 ratio of mono:di:tri, or S1170, the ratio is 8:8:3.
In 30/40/30 ratio of mono:di:tri, or S770, the ratio is 2:3.4:3.

The ratios above are the ratios of the number of hydrocarbon chains in a monolayer consisting of the blends of sucrose esters used in the investigation by DSC analysis and TEM. The microcells were observed to possess regular hexagonal and pentagonal domains at their surface in those samples in which the percentage of the di- and higher ester component was less than 30% of the total weight. In this case the calculations above show that the alkyl chains from the mono-stearate are in the majority. In the S1170 sample the percentage of the mono-stearate component was 52%, but the ratio of the alkyl chains was 8:11, i.e. the majority of the alkyl chains originated from the di- and higher esters. The sample did not exhibit regular surface structuring. With a further increase in the percentage if di- and higher esters in the sample the proportion of the alkyl chains in the monolayer which derive from mono-stearate decreases rapidly, as does the regularity of the surface structuring on the microcells.

In the DSC analysis of the crystalline sucrose esters, mixed crystals, of mono- in di- ester were formed across the range of possible compositions, except where the concentration of di- ester was very low and crystals of di- in mono- were formed. At intermediate concentrations in which the weight percentage mono-stearate concentration was greater than 50% both types of mixed crystal were formed. This phase behaviour also related to liquid crystalline sucrose ester in 75%w/w Sweetose in water. At 50% mono-stearate the phase behaviour of the mixed esters was found to be slightly different. At this composition only one type of mixed crystal was formed, a crystal of mono- in di-stearate. At this composition the ratio of alkyl chains deriving from mono- and di- stearate was 8:8:3, that is the number of chains from the mono- and di- stearate is equal, and there is a small component from the tri-stearate. At this ratio neither the mono- or di- component dominates hence the formation of only one type of mixed crystal.

The calculations above treat the alkyl chains deriving from the different esters as being one and the same. In reality the chains are attached to a single head group and thus the bending of the monolayer under compression will be dictated by the dominant component. Where the mono-stearate dominates the monolayer can have a smaller radius of curvature than in the case where the di-stearate dominates. TEM observations concur with this

statement. That is the microcells with a higher di-stearate component had more planar surfaces than those with a higher mono-stearate component.

15.11 Gas microcells dispersed in aqueous solvents

Gas microcells were also dispersed in aqueous solvents and light microscopy was used to demonstrate the existence of discrete microcells. Gas microcells are small stable air bubbles which have been proven to possess a rigid monolayer of sucrose ester surfactant at their surface. The sucrose ester has been demonstrated to be soluble in water up to its cmc concentration but above this it forms bilayer aggregates due to its low solubility at room temperature. The large concentration gradient which dispersion in water induces was expected to cause the gradual dissolution of the sucrose ester from the monolayer. Measurements of the optical density with the age of the dispersion showed that the stability of the microcells was affected by the solvent used for their dispersion.

Dispersion of gas microcells in dilute salt solutions caused rapid flocculation, whereas dilute Sweetose and sucrose ester solutions increased the stability. Dispersion in concentrations of sucrose ester below the cmc of 2×10^{-4} mol dm^{-3} were only negligibly different from dispersion in water. When the sucrose ester concentration was slightly above the cmc the microcells were more stable than when dispersed in water, but further increases in the sucrose ester concentration above the cmc caused the microcells to flocculate very rapidly, such that it was not possible to form a dispersion. The relative instability of gas microcells in Sweetose and dilute sucrose ester solutions was believed to be due to the rate at which the sucrose ester dissolves from the surface of the gas microcell and into solution. The observation that dilute salt, increased temperature and low pH cause the microcells to flocculate is behaviour typical of a charge stabilised dispersion in which the shielding of the electrical double layer surrounding the particle is affected by the addition of salt which causes flocculation. Optical microscopy observations showed that when gas microcells are flocculated by dilute salt solution they remain as discrete spherical units rather than aggregating to form a single bubble. This is further evidence of the rigid sucrose ester shell which surrounds the microcells.

15.12 Summary

When low concentrations of a blend of sucrose mono- and di- esters are dispersed in water they form an optically isotropic solution, but when the same concentration of sucrose ester is mixed with 75% Sweetose, the hydrophilicity of the Sweetose causes the sucrose ester to phase separate into liquid crystal bilayers. When the non-aerated mixture containing liquid crystal bilayers is aerated the shearing process coats the surface of each air bubble

with sucrose ester. After two hours the gas bubbles become very small and each one contains a monolayer of sucrose ester at its surface. The concentration of sucrose ester limits the total surface area of the microcells. During and following aeration the process of disproportionation occurs, resulting in the preferential shrinkage of the microcells in favour of the large bubbles. As a result the surface shrinks and the monolayer is compressed. The limited solubility of sucrose ester in a 75%w/w Sweetose in water mixture at room temperature means that the sucrose ester is unable to leave the surface of the microcell. The monolayer itself is in a fairly rigid state at room temperature because the alkyl chains are below their melting transition, which confers on the microcells their stability to centrifugation and other processes which would otherwise be expected to destroy a gas cell. They are stable in a dispersion for as long as a sucrose ester monolayer can remain at the surface of the gas cell and the gas cell can remain as a discrete entity.

15.12 **References**

1 Fitzgerald, M.; PhD Thesis, University of Reading, 1996.

Conclusion

CONCLUSION

It was known that stable foams could be made by the aeration of a mixture of Sweetose, sucrose stearate and water. The air bubbles within this foam were between 0.1 and 20 μm in diameter and each possessed a regularly structured surface comprising regularly spaced hexagonal and pentagonal domains. These bubbles were called gas microcells because of their high stability and characteristic surface structure.

This project was aimed at explaining the high stability of the foams and the reason for their surface structure. In addition the gas microcells were dispersed in various solvents to investigate their relative instabilities when removed from their natural environment.

Mixtures of 75%w/w Sweetose and 2%w/w sucrose stearate in water, before aeration, were found to contain liquid crystalline bilayers of sucrose ester, dispersed in a matrix of Sweetose in water, provided the sucrose stearate used was a blend of mono- and di-stearate. The sucrose ester bilayers are a mixed liquid crystal of mono- in di-stearate below its chain melting temperature. These become sheared during the aeration process and are deposited at the gas cell surface. The high viscosity provided by the Sweetose matrix facilitates the shearing and comminution process, as well as reducing the rate of drainage. The total surface area of the gas phase increases until all of the sucrose ester bilayers are sheared and each bubble has a monolayer at its surface.

Foams undergo the process of disproportionation because of the different Laplace pressure between the small and large bubbles. The large bubbles expand and the small ones shrink to form gas microcells . The decreasing surface area of the bubble causes compression of the monolayer. The solubility of the sucrose ester in 75% Sweetose is very low at room temperature so the sucrose ester remains on the microcell surface. The compression causes the monolayer to buckle, forming the characteristic hexagonal and pentagonal domains observed on the gas microcells. The structure of the domains depends on the ratio of mono- to di- stearate making up the sucrose ester. When the proportion of di-stearate is less than 30%, regular hexagonal and pentagonal domains are formed. As the proportion of di-stearate increases, the radius of curvature of each domain increases and their arrangement becomes less regular. The stability of the foam is not affected by the ratio of mono- to di-stearate, provided that the bubbles are surrounded by a sucrose ester monolayer, beneath its chain melting transition temperature.

The microcells remained stable when dispersed in 75%w/w Sweetose and in a non-aerated mixture of 75%w/w Sweetose and 2%w/w sucrose ester S1670 in water. When dispersed in aqueous solution they behaved like classical colloidal dispersions, i.e. they were flocculated by solutions of dilute salt and low pH. Their stability was a function of the lifetime of the sucrose ester monolayer at the surface of each gas microcell.

In summary, the foams containing gas microcells have their high stability because of a combination of factors. The high viscosity of the Sweetose reduces the rate of creaming and drainage. It also causes the sucrose stearate to phase separate, forming a gel phase of liquid crystalline bilayers which are sheared during the aeration process. The aeration process endows gas bubble with a monolayer coating of sucrose ester. This becomes compressed by disproportionation forming the domain structure observed. When it can be compressed no further it forms a rigid layer around the gas cell that retards further disproportionation. The reduction in the rate of creaming, drainage and disproportionation explains the high stability of foams containing gas microcells. When the gas microcells are removed from their natural environment they remain stable provided there is no disruption of the sucrose ester monolayer at their surface.

APPENDICES

APPENDIX A1

Rheological Measurements

Table A1 i
60%w/w Sweetose in water

Measuring system C25
Torque element 21.404 g cm
Autozero delay time 0 s
Constant delay time 15 s

Integration time 10 s
Measurement interval 20 s

Time (secs)	Temp (oC)	Shear rate (1/s)	Shear stress (Pa)	Viscosity (Pas)	Range (%)
15.3	24.9	4.614	3.539E-01	7.669E-02	0.7
40.7	24.7	7.311	5.565E-01	7.611E-02	1.1
66.1	25.1	1.159E+01	8.741E-01	7.542E-02	1.7
91.8	25	1.853E+01	1.273	6.873E-02	2.5
117.1	25	2.922E+01	2.054	7.029E-02	4
142.4	25.1	4.596E+01	3.287	7.151E-02	6.4
167.7	24.9	7.304E+01	5.266	7.209E-02	10.2
193.1	25.1	1.158E+02	8.418	7.27E-02	16.3
218.4	25	1.839E+02	1.349E+01	7.337E-02	26.1
243.9	25.1	2.911E+02	2.147E+01	7.374E-02	41.5
269.3	25	4.614E+02	3.424E+01	7.420E-02	66.2

Table A1 ii
2% w/w S1670 in 20%w/w Sweetose in water

Measuring system CP 5/30
Torque element 1.726 g cm
Autozero delay time 0 s
Constant delay time 100 s
Integration time 20 s
Measurement interval 20 s

Time (secs)	Temp (oC)	Shear rate (1/s)	Shear stress (Pa)	Viscosity (Pas)	Range (%)
100.6	25	1.865E-03	1.149	6.16E+02	4.8
221	25.1	2.941E-03	2.137	7.266E+02	8.9
341.4	25	4.627E-03	1.549	3.347E+02	6.5
461.8	25	7.353E-03	1.357	1.846E+02	5.7
582.2	25	1.166E-02	1.248	1.07E+02	5.2
702.6	25.1	1.851E-02	1.242	6.71E+01	5.2
823	24.9	2.931E-02	1.283	4.38E+01	5.4
943.4	25.1	4.645E-02	1.365	2.94E+01	5.7
1063.7	25	7.36E-02	1.524	2.071E+01	6.4
1184.1	25	1.167E-01	1.729	1.482E+01	7.2
1304.9	25.1	1.865E-01	2.025	1.086E+01	8.5
1425.4	25	2.941E-01	2.433	8.271	10.2
1545.8	25	4.627E-01	2.547	5.504	10.6
1666.2	25	7.353E-01	3.03	4.121	12.7
1786.6	25	1.166	3.583	3.074	15
1907	25.1	1.851	4.07	2.199	17
2027.4	25	2.931	4.28	1.46	17.9
2147.7	25	4.645	4.522	9.734E-01	18.9
2268.2	24.8	7.36	4.909	6.67E-01	20.5
2388.6	25	1.167E+01	5.398	4.626E-01	22.6
2509.1	25	7.36	4.395	5.971E-01	18.4
2629.5	25	4.645	3.772	8.121E-01	15.8
2749.8	25.1	2.931	3.331	1.137	13.9
2870.2	24.9	1.851	3.073	1.66	12.8
2990.6	25.1	1.166	2.838	2.434	11.9
3110.9	24.9	7.353E-01	2.582	3.512	10.8
3231.3	25.1	4.627E-01	2.256	4.876	9.4
3351.7	25	2.941E-01	1.988	6.761	8.3
3472.1	25.1	1.865E-01	1.743	9.347	7.3
3592.8	25.1	1.167E-01	1.511	1.295E+01	6.3
3713.2	25	7.36E-02	1.323	1.797E+01	5.5
3833.6	25	4.645E-02	1.172	2.523E+01	4.9
3954	25	2.931E-02	1.065	3.635E+01	4.5
4074.4	25.1	1.851E-02	9.814E-01	5.303E+01	4.1
4194.7	25.1	1.166E-02	9.248E-01	7.933E+01	3.9
4315.1	25	7.353E-03	8.881E-01	1.208E+02	3.7
4435.5	25	4.627E-03	8.727E-01	1.886E+02	3.6
4555.8	25	2.941E-03	8.565E-01	2.912E+02	3.6
4676.1	25	1.865E-03	8.594E-01	4.608E+02	3.6

Table A1 iii
2% w/w S1670 in 40%w/w Sweetose in water

Measuring system CP 5/30
Torque element 3.698 g cm
Autozero delay time 0 s
Constant delay time 100 s
Integration time 20 s
Measurement interval 20 s

Time (secs)	Temp (oC)	Shear rate (1/s)	Shear stress (Pa)	Viscosity (Pas)	Range (%)
100.6	25	1.865E-03	1.843	9.882E+02	3.6
221.1	25	2.941E-03	2.891	9.830E+02	5.6
341.5	25.1	4.627E-03	2.168	4.685E+02	4.2
461.9	25	7.353E-03	2.081	2.830E+02	4.1
582.3	25	1.166E-02	2.099	1.801E+02	4.1
702.7	25	1.851E-02	2.209	1.193E+02	4.3
823.1	25.1	2.931E-02	2.44	8.325E+01	4.8
943.5	25	4.645E-02	2.725	5.867E+01	5.3
1064	25	7.36E-02	3.02	4.104E+01	5.9
1184.3	25	1.167E-01	3.315	2.841E+01	6.5
1305	25	1.865E-01	3.599	1.930E+01	7
1425.4	25.1	2.941E-01	3.644	1.239E+01	7.1
1545.8	24.9	4.627E-01	4.059	8.773	7.9
1666.3	25.1	7.353E-01	4.615	6.276	9
1786.7	25	1.166	5.132	4.402	10
1907.1	25	1.851	5.321	2.875	10.4
2027.5	24.9	2.931	5.739	1.958	11.2
2147.9	25	4.645	6.389	1.375	12.5
2268.3	25	7.36	6.829	9.278E-01	13.3
2388.8	25	1.167E+01	7.511	6.437E-01	14.6
2509.1	25.1	7.36	6.246	8.486E-01	12.2
2629.6	25.1	4.645	5.424	1.168	10.6
2749.9	25.1	2.931	4.865	1.66	9.5
2870.3	24.9	1.851	4.437	2.397	8.7
2990.7	25.1	1.166	4.083	3.502	8
3111.1	25.1	7.353E-01	3.767	5.123	7.3
3231.5	25	4.627E-01	3.429	7.41	6.7
3352	25.2	2.941E-01	2.997	1.019E+01	5.8
3472.3	25	1.865E-01	2.64	1.415E+01	5.1
3593.1	24.9	1.167E-01	2.329	1.996E+01	4.5
3713.5	24.9	7.36E-02	2.054	2.790E+01	4
3833.8	25.2	4.645E-02	1.821	3.920E+01	3.6
3954.1	24.9	2.931E-02	1.651	5.633E+01	3.2
4074.6	25	1.851E-02	1.531	8.274E+01	3
4195	25	1.166E-02	1.435	1.231E+02	2.8
4315.3	24.9	7.353E-03	1.41	1.917E+02	2.7
4435.7	25.1	4.627E-03	1.352	2.921E+02	2.6
4556.1	25.1	2.941E-03	1.315	4.471E+02	2.6
4676.5	25	1.865E-03	1.316	7.056E+02	2.6

Table A1 iv

2% w/w S1670 in 60%w/w Sweetose in water

Measuring system CP 5/30
Torque element 3.698 g cm
Autozero delay time 0 s
Constant delay time 100 s

Integration time 20 s
Measurement interval 20 s

Time (secs)	Temp (oC)	Shear rate (1/s)	Shear stress (Pa)	Viscosity (Pas)	Range (%)
100.6	25	1.865E-03	8.616E-01	4.619E+02	1.7
221.1	25	2.941E-03	2.424	8.241E+02	4.7
341.5	25	4.627E-03	2.825	6.106E+02	5.5
461.9	25	7.353E-03	2.585	3.515E+02	5
582.3	25	1.166E-02	2.639	2.263E+02	5.1
702.7	25	1.851E-02	2.936	1.586E+02	5.7
823.1	25	2.931E-02	3.509	1.197E+02	6.8
943.5	25	4.645E-02	3.582	7.712E+01	7
1064	25	7.36E-02	4.145	5.631E+01	8.1
1184.3	25	1.167E-01	4.889	4.190E+01	9.5
1305	25	1.865E-01	5.016	2.689E+01	9.8
1425.4	24.9	2.941E-01	5.553	1.888E+01	10.8
1545.8	25	4.627E-01	5.59	1.286E+01	11.6
1666.3	25.1	7.353E-01	6.917	9.406	13.5
1786.7	25	1.166	7.887	6.766	15.4
1907.1	25	1.851	8.19	4.425	16
2027.5	25	2.931	8.561	2.921	16.7
2147.9	25.1	4.645	9.511	2.048	18.5
2268.3	25	7.36	1.071E+01	1.455	20.9
2388.8	25	1.167E+01	1.193E+01	1.023	23.3
2509.1	25.1	7.36	9.675	1.314	18.9
2629.6	24.9	4.645	8.385	1.805	16.4
2749.9	25	2.931	7.557	2.579	14.7
2870.3	25	1.851	6.928	3.743	13.5
2990.7	24.9	1.166	6.602	5.663	12.9
3111.1	25.1	7.353E-01	6.285	8.547	132.3
3231.5	25.1	4.627E-01	5.908	1.277E+01	11.5
3352	25	2.941E-01	5.6	1.904E+01	10.9
3472.3	25.1	1.865E-01	5.32	2.852E+01	10.4
3593.1	25.1	1.167E-01	4.739	4.062E+01	9.2
3713.5	25.1	7.36E-02	4.138	5.622E+01	8.1
3833.8	25.1	4.645E-02	3.462	7.453E+01	6.8
3954.1	25	2.931E-02	2.789	9.516E+01	5.4
4074.6	25.1	1.851E-02	2.26	1.221E+02	4.4
4195	25.1	1.166E-02	1.789	1.535E+02	3.5
4315.3	25.1	7.353E-03	1.505	2.047E+02	2.9
4435.7	25	4.627E-03	1.242	2.684E+02	2.4
4556.1	25	2.941E-03	1.022	3.475E+02	2
4676.5	24.9	1.865E-03	9.397E-01	5.038E+02	1.8

Table A1 v

2% w/w S1670 in 75%w/w Sweetose in water

Measuring system CP 5/30
Torque element 19.39 g cm
Autozero delay time 0 s
Constant delay time 50 s

Integration time 20 s
Measurement interval 20 s

Time (secs)	Temp (oC)	Shear rate (1/s)	Shear stress (Pa)	Viscosity (Pas)	Range (%)
50.7	25	1.865E-03	9.807	5.258E+03	3.6
121.2	25	2.941E-03	1.749E+01	5.974E+03	6.5
191.6	25	4.627E-03	2.370E+01	5.123E+03	8.8
262	25	7.353E-03	2.577E+01	3.504E+03	9.6
332.5	25	1.166E-02	2.598E+01	2.229E+03	9.7
402.9	25.2	1.851E-02	2.769E+01	1.496E+03	10.3
473.4	25	2.931E-02	2.501E+01	8.533E+02	9.3
543.7	25	4.645E-02	2.507E+01	5.397E+02	9.3
614.1	25	7.36E-02	2.535E+01	3.444E+02	9.4
684.4	25	1.167E-01	2.848E+01	2.441E+02	10.6
755.2	25	1.865E-01	3.108E+01	1.666E+02	11.6
825.6	24.9	2.941E-01	3.515E+01	1.195E+02	13.1
896	25	4.627E-01	3.236E+01	6.993E+01	12
966.4	25.1	7.353E-01	3.747E+01	5.096E+01	13.9
1036.7	25	1.166	3.573E+01	3.065E+01	13.3
1107.1	25	1.851	3.697E+01	1.997E+01	13.7
1177.4	25	2.931	3.711E+01	1.266E+01	13.8
1247.9	25.1	4.645	4.136E+01	8.904	15.4
1318.2	25	7.36	4.402E+01	5.98	16.4
1388.5	25	1.167E+01	4.889E+01	4.19	18.2
1459	25.1	7.36	4.299E+01	5.84	16
1529.5	24.9	4.645	3.984E+01	8.578	14.8
1599.9	25	2.931	3.660E+01	1.249E+01	13.6
1670.2	25	1.851	3.473E+01	1.877E+01	12.9
1740.6	24.9	1.166	3.166E+01	2.716E+01	11.8
1810.9	25.1	7.353E-01	2.940E+01	3.999E+01	10.9
1881.4	25.1	4.627E-01	2.599E+01	5.616E+01	9.7
1951.8	25	2.941E-01	2.497E+01	8.488E+01	9.3
2022.1	25.1	1.865E-01	2.339E+01	1.254E+02	8.7
2092.8	25.1	1.167E-01	2.097E+01	1.797E+02	7.8
2163.2	25	7.36E-02	1.861E+01	2.528E+02	6.9
2233.7	25.1	4.645E-02	1.724E+01	3.712E+02	6.4
2304.1	25	2.931E-02	1.485E+01	5.067E+02	5.5
2374.5	25.1	1.851E-02	1.171E+01	6.326E+02	4.4
2445	24.9	1.166E-02	9.671	8.296E+02	3.6
2515.4	25	7.353E-03	7.61	1.035E+03	2.8
2585.7	25.2	4.627E-03	6.386	1.380E+03	2.4
2656.1	25	2.941E-03	5.896	2.005E+03	2.2
2726.6	25.2	1.865E-03	5.278	2.830E+03	2

Table A1 vi
1% w/w S1670 in 60%w/w Sweetose in water

Measuring system C25
Torque element 4.13 g cm
Autozero delay time 0 s
Constant delay time 15 s
Integration time 10 s
Measurement interval 10 s

Time (secs)	Temp (oC)	Shear rate (1/s)	Shear stress (Pa)	Viscosity (Pas)	Range (%)
15.4	21.7	1.459E-01	1.606	1.101E+01	16.1
41.1	21.6	2.316E-01	1.569	6.774	15.7
66.5	21.8	3.670E-01	1.632	4.446	16.4
91.9	21.7	5.808E-01	1.783	3.071	17.9
117.3	21.8	9.193E-01	2.041	2.22	20.5
142.6	21.8	1.461	2.422	1.658	24.3
168	21.8	2.312	2.795	1.209	28
193.5	21.8	3.666	3.221	8.785E-01	32.3
218.9	21.7	5.808	3.74	6.440E-01	37.5
244.3	21.7	9.207	4.406	4.785E-01	44.2
269.7	21.6	1.459E+01	5.282	3.620E-01	53
295.2	21.7	9.207	4.046	4.395E-01	40.6
320.6	21.9	5.808	3.257	5.607E-01	32.7
346	21.8	3.666	2.717	7.410E-01	27.2
371.4	21.9	2.312	2.347	1.015	23.5
396.7	21.8	1.461	2.104	1.44	21.1
422.1	21.9	9.193E-01	1.935	2.105	19.4
447.5	21.9	5.808E-01	1.817	3.129	18.2
472.9	21.8	3.670E-01	1.72	4.687	17.2
488.3	21.8	2.316E-01	1.627	7.027	16.3
524	21.7	1.459E-01	1.519	10.41	15.2

Table A1 vii
2% w/w S1670 in 60%w/w Sweetose in water

Measuring system C25
Torque element 21.404 g cm
Autozero delay time 0 s
Constant delay time 15 s
Integration time 10 s
Measurement interval 10 s

Time (secs)	Temp (oC)	Shear rate (1/s)	Shear stress (Pa)	Viscosity (Pas)	Range (%)
15.4	21.7	1.459E-01	5.782	3.963E+01	11.2
41.1	21.6	2.316E-01	6.206	2.680E+01	12
66.5	21.8	3.670E-01	6.835	1.862E+01	13.2
91.9	21.7	5.808E-01	7.436	1.280E+01	14.4
117.3	21.8	9.193E-01	8.339	9.071	16.1
142.6	21.8	1.461	1.027E+01	7.038	19.9
168	21.8	2.312	1.080E+01	4.668	20.9
193.5	21.8	3.666	1.108E+01	3.022	21.4
218.9	21.7	5.808	1.202E+01	2.069	23.2
244.3	21.7	9.207	1.276E+01	1.386	24.7
269.7	21.6	1.459E+01	1.366E+01	9.361E-01	26.4
295.2	21.7	9.207	1.126E+01	1.223	21.8
320.6	21.9	5.808	9.926	1.709	19.2
346	21.8	3.666	9.005	2.456	17.4
371.4	21.9	2.312	8.243	3.565	15.9
396.7	21.8	1.461	7.566	5.179	14.6
422.1	21.9	9.193E-01	6.852	7.453	13.3
447.5	21.9	5.808E-01	6.04	10.4	11.7
472.9	21.8	3.670E-01	5.127	13.97	9.9
488.3	21.8	2.316E-01	4.24	18.31	8.2
524	21.7	1.459E-01	3.537	24.24	6.8

Table A1 viii
3% w/w S1670 in 60%w/w Sweetose in water

Measuring system C25
Torque element 21.404 g cm
Autozero delay time 0 s
Constant delay time 15 s
Integration time 10 s
Measurement interval 10 s

Time (secs)	Temp (oC)	Shear rate (1/s)	Shear stress (Pa)	Viscosity (Pas)	Range (%)
15.4	21.7	1.459E-01	8.691	5.956E+01	16.8
41.1	21.6	2.316E-01	9.024	3.896E+01	17.5
66.5	21.8	3.670E-01	9.385	2.557E+01	18.2
91.9	21.7	5.808E-01	9.722	1.674E+01	18.8
117.3	21.8	9.193E-01	1.060E+01	1.153E+01	20.5
142.6	21.8	1.461	1.222E+01	8.367	23.6
168	21.8	2.312	1.401E+01	6.059	27.1
193.5	21.8	3.666	1.518E+01	4.139	29.4
218.9	21.7	5.808	1.618E+01	2.786	31.3
244.3	21.7	9.207	1.721E+01	1.869	33.3
269.7	21.6	1.459E+01	1.876E+01	1.286	36.3
295.2	21.7	9.207	1.586E+01	1.722	30.7
320.6	21.9	5.808	1.397E+01	2.405	27
346	21.8	3.666	1.250E+01	3.41	24.2
371.4	21.9	2.312	1.125E+01	4.864	21.8
396.7	21.8	1.461	1.010E+01	6.911	19.5
422.1	21.9	9.193E-01	8.967	9.751	17.3
447.5	21.9	5.808E-01	7.821	1.347E+01	15.1
472.9	21.8	3.670E-01	6.663	1.816E+01	12.9
488.3	21.8	2.316E-01	5.628	2.430E+01	10.9
524	21.7	1.459E-01	4.802	3.291E+01	9.3

Table A1 ix
4% w/w S1670 in 60%w/w Sweetose in water

Measuring system C25
Torque element 21.404 g cm
Autozero delay time 0 s
Constant delay time 15 s
Integration time 10 s
Measurement interval 10 s

Time (secs)	Temp (oC)	Shear rate (1/s)	Shear stress (Pa)	Viscosity (Pas)	Range (%)
15.4	21.7	1.459E-01	1.724E+01	1.182E+02	33.4
41.1	21.6	2.316E-01	1.764E+01	7.616E+01	34.1
66.5	21.8	3.670E-01	1.833E+01	5.009E+01	35.6
91.9	21.7	5.808E-01	1.975E+01	3.400E+01	38.2
117.3	21.8	9.193E-01	2.177E+01	2.369E+01	42.1
142.6	21.8	1.461	2.397E+01	1.641E+01	46.4
168	21.8	2.312	2.645E+01	1.144E+01	51.2
193.5	21.8	3.666	2.844E+01	7.758	55
218.9	21.7	5.808	3.007E+01	5.177	56.2
244.3	21.7	9.207	3.219E+01	3.497	62.3
269.7	21.6	1.459E+01	3.484E+01	2.388	67.4
295.2	21.7	9.207	2.930E+01	3.183	56.7
320.6	21.9	5.808	2.564E+01	4.415	49.6
346	21.8	3.666	2.284E+01	6.23	44.2
371.4	21.9	2.312	2.046E+01	8.847	39.6
396.7	21.8	1.461	1.835E+01	1.256E+01	35.5
422.1	21.9	9.193E-01	1.635E+01	1.778E+01	31.6
447.5	21.9	5.808E-01	1.439E+01	2.478E+01	27.8
472.9	21.8	3.670E-01	1.242E+01	3.383E+01	24
488.3	21.8	2.316E-01	1.053E+01	4.548E+01	20.4
524	21.7	1.459E-01	8.937	6.125E+01	17.3

Density of non-aerated Sweetose / sucrose ester mixtures

% Sweetose	% S1670	Mass of vessel (g), containing volume (cm^3)(*±0.001 g*)					Mass (g) per increment				Av density, ($g\ cm^{-3}$)
	vessel										
VOLUME	*pipette*	*0*	*5*	*10*	*±0.05 cm^3*						
0	2	17.731	22.709	27.071			0.996	0.842			0.934 ± 0.004
10	2	14.507	19.588	24.697			1.016	1.022			1.019 ± 0.004
VOLUME	*syringe*	*2.5*	*2.0*	*1.5*	*1.0*	*0.5*	*±0.1 cm^3*				
20	2	6.074	5.546	5.014	4.500	3.976	0.528	0.532	0.514	0.525	1.049 ± 0.02
30	2	6.168	5.614	5.056	4.508	3.943	0.554	0.558	0.548	0.565	1.113 ± 0.02
40	2	6.084	5.504	4.943	4.391	3.817	0.581	0.560	0.553	0.574	1.134 ± 0.02
40	2	6.292	5.730	5.154	4.596	4.023	0.562	0.576	0.558	0.573	1.134 ± 0.02
50	2		5.789	5.197	4.608	4.004		0.592	0.589	0.605	1.190 ± 0.02
60	2	6.498	5.862	5.252	4.642	4.025	0.636	0.610	0.610	0.618	1.237 ± 0.02
70	2	6.584	5.920	5.295	4.654	4.041	0.664	0.625	0.641	0.614	1.272 ± 0.02
80	2	6.427	5.802	5.220	4.613		0.624	0.583	0.607		1.209 ± 0.02
20	5	6.066	5.547	5.012	4.476	3.951	0.519	0.535	0.536	0.524	1.057 ± 0.02
50	5	6.326	5.730	5.139	4.549	3.952	0.595	0.591	0.590	0.597	1.187 ± 0.02
70	5	6.639	5.982	5.349	4.724	4.066	0.657	0.634	0.624	0.658	1.286 ± 0.02
20	8	6.010	5.477	4.975	4.458	3.912	0.533	0.502	0.517	0.546	1.049 ± 0.02
50	8	6.299	5.710	5.130	4.572	3.969	0.589	0.579	0.559	0.603	1.165 ± 0.02
70	8		5.935	5.337	4.705	4.061		0.598	0.632	0.644	1.249 ± 0.02
VOLUME	*pipette*	*0*	*2*	*4*	*6*	*8*	*±0.05 cm^3*				
75	0.0002	28.065	30.6368	33.2261	35.8251	38.4045	2.5718	2.5893	2.599	2.5794	1.292 ± 0.005
75	0.001	35.8158	38.3920	40.9487	43.5137	46.0856	2.5762	2.5567	2.565	2.5719	1.284 ± 0.005
75	0.01	28.1978	30.7671	33.3298	35.8658	38.4274	2.5693	2.5627	6.340	2.5616	1.279 ± 0.005
VOLUME	*syringe*	*2.5*	*2.0*	*1.5*	*1.0*	*0.5*	*±0.1 cm^3*				
75	0.1	6.7204	6.085	5.435	4.7841	4.1291	0.635	0.650	0.651	0.655	1.296 ± 0.02
75	0.5	6.6887	6.0601	5.4066	4.7684	4.1264	0.629	0.654	0.638	0.642	1.281 ± 0.02
75	1	6.2596	5.6117	4.9731	4.3355	3.6780	0.648	0.639	0.638	0.658	1.291 ± 0.02
75	1.5	6.6921	6.0531	5.415	4.7725	4.1323	0.639	0.638	0.643	0.640	1.280 ± 0.02

APPENDIX A3

Calibration of the optical system in the Spinning-Drop Interfacial Tensiometer

The magnification factor of the optical system used in the measurements of surface tension by the spinning drop technique in Chapter 10 was calculated thus.

A syringe needle was used as the insert. It was positioned in the tube containing the sample whose surface tension was to be measured. Measurements of the diameter of the syringe needle at various positions along its length and at various angles to the cathetometer were recorded. This was done because it was not always possible to position the syringe needle precisely along the axis of the tube.

The real diameter of the syringe needle measured using a micrometer was 1.275(5) mm.

The apparent diameter of the syringe needle, when surrounded by the sample, within the tube was termed d_{meas}.

The magnification factor of the optical system = $\frac{d_{meas}}{d_{real}}$

This magnification factor includes the sample, the walls of the tube and the distance between the cathetometer and the apparatus. After calibration, the cathetometer was fixed in position relative to the apparatus.

With the syringe needle correctly positioned inside the tube, the following measurements of diameter were recorded.

In a non-aerated mixture of 75%w/w Sweetose in water and 2%w/w sucrose ester

90^{o} rotation, No.	upper surface	lower surface	Diameter (cm)	upper surface	lower surface	Diameter (cm)
0	7.895	7.710	0.185	7.887	7.701	0.186
1	7.883	7.694	0.189	7.880	7.691	0.189
2	7.998	7.718	0.180	7.903	7.720	0.183
3	7.903	7.723	0.180	7.905	7.724	0.181
		Av. diam	0.183(5)		Av. diam	0.184(7)

Average measured diameter = 0.184(13) cm

Magnification factor = 1.8413/1.2755 = 1.443(55)

The magnification factor for 75% Sweetose 2% sucrose ester was 1.443.

Then, by a similar method the magnification factor was measured for other mixtures of Sweetose and sucrose ester. The magnification factor for each Sweetose / sucrose ester concentration listed is given below.

% Sweetose	% sucrose ester S1670	magnification factor
75	2	1.443
75	1	1.409
75	0.5	1.407
75	0.1	1.424
75	0.01	1.439
75	0.001	1.430
75	0.0001	1.420

No trend in the magnification factor with sucrose ester concentration was observed. The magnification factors calculated are heavily dependant on the accurate positioning of the syringe needle in the tube. In practice this is difficult to achieve. To compensate for this the diameter was measured with the needle viewed from 4 sides. If the measured values of diameter were very different when viewed from a different angle then the measurement was repeated after re-aligning the syringe needle.

The magnification factors for the samples measured above have very similar values, which lie within the range of experimental error. The average of the above magnification factors was calculated, after discarding the lowest and highest values, so that a direct comparison between the surface tension of the samples could be made. This was taken to be the magnification factor for all the samples measured which had a Sweetose concentration of 75%. That magnification factor was 1.43.

40%w/w Sweetose and 2%w/w sucrose ester

The average diameter of the syringe, measured in a 40/2 mixture was 1.79mm.
The magnification factor was 1.404.

20%w/w Sweetose and 2%w/w sucrose ester

The average diameter of the syringe, measured in a 40/2 mixture was 1.72mm.
The magnification factor was 1.349.

For comparison, the av. diameter of the syringe needle measured in water was 1.26mm, which corresponds to a magnification factor of 1.304.

The difference between each magnification factor was attributed to the refractive index difference between the samples, however no quantitative refractive measurements were made.

Table A4i

30% w/w Sweetose 2%w/w sucrose ester, S1670 Density of the non-aerated mixture = 1.113 g cm-3

Time (mins)	volume (cm3) 2.5	2	1.5	1	0.5	Mass per 0.5g				Av mass per 0.5g	Av density g cm-3	Gas phase volume
5	6.0351	5.4949	4.9666	4.4511	3.9156	0.5402	0.5283	0.5155	0.5355	0.5299	1.060	0.048
10	6.0318	5.4958	4.9302	4.3732	3.8308	0.5360	0.5656	0.5570	0.5424	0.5503	1.101	0.011
15	6.1403	5.5911	5.0211	4.4715	3.9273	0.5492	0.5700	0.5496	0.5442	0.5533	1.107	0.006
20	6.1460	5.5887	5.0474	4.5022	3.9410	0.5573	0.5413	0.5452	0.5612	0.5513	1.103	0.009
30	6.1775	5.6225	5.0735	4.5060	3.9664	0.5550	0.5490	0.5675	0.5396	0.5528	1.106	0.007
40	4.6041	4.0900	3.9060	3.6887	3.5495	0.5141	0.1840	0.2173	0.1392	0.2637	0.527	0.526
50	4.7517	4.1845	3.8883	3.7208	3.5602	0.5672	0.2962	0.1675	0.1606	0.2979	0.596	0.465
60	4.8650	4.3690	3.9591	3.7348	3.5820	0.4960	0.4099	0.2243	0.1528	0.3207	0.641	0.424
70	4.2698	3.9575	3.8098	3.6560	3.5344	0.3123	0.1477	0.1538	0.1216	0.1838	0.368	0.670
80	4.0877	3.9184	3.7724	3.6382	3.5051	0.1693	0.1460	0.1342	0.1331	0.1457	0.291	0.738
90	3.9907	3.8694	3.7551	3.6416	3.5340	0.1213	0.1143	0.1135	0.1076	0.1142	0.228	0.795
100	3.7493	3.6685	3.5910	3.5300	3.4723	0.0808	0.0775	0.0610	0.0577	0.0692	0.138	0.876
110	3.6534	3.5887	3.5285	3.4700	3.4131	0.0647	0.0602	0.0585	0.0569	0.0601	0.120	0.892
120	3.7039	3.6470	3.5947	3.5455	3.4925	0.0569	0.0523	0.0492	0.0530	0.0529	0.106	0.905

Table A4ii

40% w/w Sweetose 2%w/w sucrose ester, S1670 Density of the non-aerated mixture = 1.153 g cm-3

Time (mins)	volume (cm3) 2.5	2	1.5	1	0.5	Mass per 0.5g				Av mass per 0.5g	Av density g cm-3	Gas phase volume
5	5.9152	5.4308	4.9222	4.4203	3.9228	0.4844	0.5086	0.5019	0.4975	0.4981	0.996	0.136
10	5.9844	5.4802	4.9542	4.411	3.8704	0.5042	0.5260	0.5432	0.5406	0.5285	1.057	0.083
15	5.8516	5.3012	4.7594	4.2233	3.7098	0.5504	0.5418	0.5361	0.5135	0.5355	1.071	0.071
20	5.8031	5.2846	4.7851	4.2734	3.8126	0.5185	0.4995	0.5117	0.4608	0.4976	0.995	0.137
25	5.36	4.9578	4.6231	4.1929	3.7846	0.4022	0.3347	0.4302	0.4083	0.3939	0.788	0.317
30	4.7724	4.4864	4.2162	3.9538	3.6969	0.2860	0.2702	0.2624	0.2569	0.2689	0.538	0.534
35	4.5939	4.3468	4.1161	3.8901	3.672	0.2471	0.2307	0.2260	0.2181	0.2305	0.461	0.600
40	4.2712	4.0912	3.9196	3.7431	3.5817	0.1800	0.1716	0.1765	0.1614	0.1724	0.345	0.701
45	3.9978	3.8784	3.7704	3.6618	3.5466	0.1194	0.1080	0.1086	0.1152	0.1128	0.226	0.804
50	3.8539	3.7686	3.6877	3.6082	3.5339	0.0853	0.0809	0.0795	0.0743	0.0800	0.160	0.861
55	3.6358	3.575	3.5192	3.4622	3.4048	0.0608	0.0558	0.0570	0.0574	0.0577	0.115	0.900
60	3.6447	3.5941	3.5435	3.49	3.4419	0.0506	0.0506	0.0535	0.0481	0.0507	0.101	0.912
65	3.6705	3.6187	3.5649	3.5131	3.4706	0.0518	0.0538	0.0518	0.0425	0.0500	0.100	0.913
85	3.6922	3.6387	3.5863	3.5347	3.4865	0.0535	0.0524	0.0516	0.0482	0.0514	0.103	0.911
100	3.6852	3.6311	3.5784	3.5293	3.4763	0.0541	0.0527	0.0491	0.0530	0.0522	0.104	0.909
120	3.6404	3.583	3.5289	3.4743	3.423	0.0574	0.0541	0.0546	0.0513	0.0544	0.109	0.906

Table A4iii

50% w/w Sweetose 2%w/w sucrose ester, S1670 Density of the non-aerated mixture = 1.190 g cm-3

Time (mins)	volume (cm3) 2.5	2	1.5	1	0.5	Mass per 0.5g				Av mass per 0.5g	Av density g cm-3	Gas phase volume
5	6.1315	5.5939	5.0622	4.5248	3.9814	0.5376	0.5317	0.5374	0.5434	0.5375	1.075	0.097
10	5.9235	5.4106	4.9344	4.4287	3.937	0.5129	0.4762	0.5057	0.4917	0.4966	0.993	0.165
15	5.0552	4.7203	4.3985	4.0734	3.7665	0.3349	0.3218	0.3251	0.3069	0.3222	0.644	0.459
20	4.573	4.347	4.1264	3.9088	3.7002	0.2260	0.2206	0.2176	0.2086	0.2182	0.436	0.633
25	4.1903	4.0307	3.8788	3.727	3.5852	0.1596	0.1519	0.1518	0.1418	0.1513	0.303	0.746
30	3.9521	3.8349	3.716	3.6095	3.5056	0.1172	0.1189	0.1065	0.1039	0.1116	0.223	0.812
36	3.9328	3.8281	3.7291	3.6307	3.537	0.1047	0.0990	0.0984	0.0937	0.0990	0.198	0.834
45	3.7453	3.6776	3.6112	3.543	3.4846	0.0677	0.0664	0.0682	0.0584	0.0652	0.130	0.890
55	3.7191	3.661	3.6025	3.5453	3.4861	0.0581	0.0585	0.0572	0.0592	0.0583	0.117	0.902
65	3.6462	3.5831	3.5278	3.4713	3.4182	0.0631	0.0553	0.0565	0.0531	0.0570	0.114	0.904
75	3.7176	3.6515	3.5874	3.5244	3.4653	0.0661	0.0641	0.0630	0.0591	0.0631	0.126	0.894
90	3.7058	3.6439	3.5799	3.5323	3.4658	0.0619	0.0640	0.0476	0.0665	0.0600	0.120	0.899
105	3.7741	3.714	3.6481	3.5814	3.5186	0.0601	0.0659	0.0667	0.0628	0.0639	0.128	0.893
120	3.7354	3.6685	3.6054	3.5532	3.486	0.0669	0.0631	0.0522	0.0672	0.0624	0.125	0.895

Table A4iv

75% w/w Sweetose 2%w/w sucrose ester, S1670 Density of the non-aerated mixture = 1.303 g cm-3

Time (mins)	volume (cm3) 2.5	2	1.5	1	0.5	Mass per 0.5g				Av mass per 0.5g	Av density g cm-3	Gas phase volume
5	6.0405	5.5313	5.0174	4.484	3.9429	0.5092	0.5139	0.5334	0.5411	0.5244	1.049	0.195
10	5.0216	4.695	4.3702	4.0968	3.7865	0.3266	0.3248	0.2734	0.3103	0.3088	0.618	0.526
20	4.2263	4.0948	3.9277	3.7899	3.6218	0.1315	0.1671	0.1378	0.1681	0.1511	0.302	0.768
30		3.9415	3.8289	3.7057	3.5757		0.1126	0.1232	0.1300	0.1219	0.244	0.813
45		4.0003	3.8594	3.733	3.5846		0.1409	0.1264	0.1484	0.1386	0.277	0.787
60		4.0145	3.8654	3.747	3.5785		0.1491	0.1184	0.1685	0.1453	0.291	0.777
75		4.08	3.9074	3.7786	3.5981		0.1726	0.1288	0.1805	0.1606	0.321	0.753
92		4.1636	3.9633	3.7911	3.5792		0.2003	0.1722	0.2119	0.1948	0.390	0.701
107				3.8955	3.6618				0.2337	0.2337	0.467	0.641
122		4.4673	4.2206	3.9829	3.7205		0.2467	0.2377	0.2624	0.2489	0.498	0.618

Table A4 v

75% w/w Sweetose 1%w/w sucrose ester, S1670 Density of the non-aerated mixture = 1.291 g cm-3

Time (mins)	volume (cm3) 2.5	2	1.5	1	0.5	Mass per 0.5g				Av mass per 0.5g	Av density g cm-3	Gas phase volume
5	6.0361	5.4766	4.9176	4.361	3.8012	0.5595	0.5590	0.5566	0.5598	0.5587	1.117	0.134
10	4.1907	3.8941	3.598	3.3325	3.042	0.2966	0.2961	0.2655	0.2905	0.2872	0.574	0.555
15	3.5786	3.4151	3.2482	3.0815	2.9175	0.1635	0.1669	0.1667	0.1640	0.1653	0.331	0.744
20	4.0517	3.9294	3.7928	3.6696	3.5321	0.1223	0.1366	0.1232	0.1375	0.1299	0.260	0.799
30	3.4175	3.2772	3.1458	3.0146	2.88	0.1403	0.1314	0.1312	0.1346	0.1344	0.269	0.792
40	4.1391	3.9948	3.85	3.7133	3.5639	0.1443	0.1448	0.1367	0.1494	0.1438	0.288	0.777
50	4.1841	4.0312	3.8794	3.779	3.6259	0.1529	0.1518	0.1004	0.1531	0.1396	0.279	0.784
60	3.5465	3.3811	3.2252	3.0735	2.9152	0.1654	0.1559	0.1517	0.1583	0.1578	0.316	0.755
70	3.6285	3.4536	3.2815	3.1412	2.9693	0.1749	0.1721	0.1403	0.1719	0.1648	0.330	0.745
80	3.648	3.462	3.282	3.11	2.936	0.1860	0.1800	0.1720	0.1740	0.1780	0.356	0.724
90	4.3897	4.1898	3.9969	3.814	3.6182	0.1999	0.1929	0.1829	0.1958	0.1929	0.386	0.701
105	4.195	3.9795	3.768	3.561	3.355	0.2155	0.2115	0.2070	0.2060	0.2100	0.420	0.675
120	4.611	4.3697	4.1375	3.9068	3.6772	0.2413	0.2322	0.2307	0.2296	0.2335	0.467	0.638

Table A4 vi

75% w/w Sweetose 0.5%w/w sucrose ester, S1670 Density of the non-aerated mixture = 1.281 g cm-3

Time (mins)	volume (cm3) 2.5	2	1.5	1	0.5	Mass per 0.5g				Av mass per 0.5g	Av density g cm-3	Gas phase volume
5	5.7982	5.1907	4.5768	3.9591	3.3332	0.6075	0.6139	0.6177	0.6259	0.6162	1.233	0.038
10	5.1244	4.6411	4.1623	3.6925	3.2305	0.4833	0.4788	0.4698	0.4620	0.4735	0.947	0.261
15	4.3164	4.0068	3.695	3.3856	3.082	0.3096	0.3118	0.3094	0.3036	0.3086	0.617	0.518
20	4.5858	4.354	4.1285	3.9013	3.6844	0.2318	0.2255	0.2272	0.2169	0.2254	0.451	0.648
30	3.8724	3.7274	3.5943	3.4511	3.2903	0.1450	0.1331	0.1432	0.1608	0.1455	0.291	0.773
40	4.2124	4.0554	3.8959	3.7462	3.5838	0.1570	0.1595	0.1497	0.1624	0.1571	0.314	0.755
50	4.2501	4.0877	3.9245	3.7654	3.5991	0.1624	0.1632	0.1591	0.1663	0.1627	0.325	0.746
60	3.6137	3.4618	3.3172	3.146	2.9728	0.1519	0.1446	0.1712	0.1732	0.1602	0.320	0.750
70	4.0169	3.8279	3.6467	3.4891	3.3095	0.1890	0.1812	0.1576	0.1796	0.1769	0.354	0.724
80	3.7003	3.4986	3.314	3.1295	2.9378	0.2017	0.1846	0.1845	0.1917	0.1906	0.381	0.702
90	3.7495	3.5496	3.3516	3.1578	2.9559	0.1999	0.1980	0.1938	0.2019	0.1984	0.397	0.690
105	3.927	3.6969	3.4722	3.2485	3.0244	0.2301	0.2247	0.2237	0.2241	0.2257	0.451	0.648
120	3.9403	3.6883	3.4412	3.21	2.9756	0.2520	0.2471	0.2312	0.2344	0.2412	0.482	0.623

Table A4 vii

75% w/w Sweetose 3%w/w sucrose ester, S1670 Density of the non-aerated mixture = 1.300 g cm-3

Time (mins)	*volume (cm3)* 2.5	2	1.5	1	0.5	Mass per 0.5g				Av mass per 0.5g	Av density g cm-3	Gas phase volume
5	5.2271	4.7411	4.2525	3.7672	3.2737	0.4860	0.4886	0.4853	0.4935	0.4884	0.977	0.249
10	4.3115	3.9899	3.6811	3.362	3.0671	0.3216	0.3088	0.3191	0.2949	0.3111	0.622	0.521
15	3.5753	3.3956	3.2284	3.0646	2.8903	0.1797	0.1672	0.1638	0.1743	0.1713	0.343	0.737
20		3.5598	3.45	3.3447	3.2027		0.1098	0.1053	0.1420	0.1190	0.238	0.817
30	3.8	3.665	3.5512	3.4251	3.2927	0.1350	0.1138	0.1261	0.1324	0.1268	0.254	0.805
40			3.8312	3.6866	3.5459			0.1446	0.1407	0.1427	0.285	0.781
		2.1	*1.7*	*1.3*	*0.9*							
55		3.5643	3.993	3.8674	3.733		0.1256	0.1344	0.1687	0.1649	0.323	0.746
70			3.3275	3.1419	2.9544			0.1856	0.1875	0.1866	0.3731	0.713
85		3.5083	3.4027	3.1803	2.9599			0.2224	0.2204	0.2214	0.4428	0.659
100			3.5072	3.2562	3.0092			0.251	0.247	0.249	0.498	0.617
120				3.76	3.4357				0.3243	0.3243	0.6486	0.501

Table A4 viii

75% w/w Sweetose 2%w/w sucrose ester, S1170 Density of the non-aerated mixture = 1.300 g cm-3

Time (mins)	volume (cm3) 2.5	2	1.5	1	0.5	Mass per 0.5g				Av mass per 0.5g	Av density g cm-3	Gas phase volume
5	4.0454	3.7899	3.5293	3.2657	3.0108	0.2555	0.2606	0.2636	0.2549	0.2587	0.517	0.602
10	3.4515	3.3174	3.1881	3.0663	2.929	0.1341	0.1293	0.1218	0.1373	0.1306	0.261	0.799
15		3.1682	3.0539	2.9615	2.8351		0.1143	0.0924	0.1264	0.1203	0.241	0.815
20	3.6447	3.5304	3.4507	3.3277	3.1983	0.1143	0.0797	0.1230	0.1294	0.1222	0.244	0.812
30	3.7695	3.6434	3.51	3.389	3.2528	0.1261	0.1334	0.1210	0.1362	0.1292	0.258	0.801
40		3.9592	3.8336	3.7104	3.561		0.1256	0.1232	0.1494	0.1327	0.265	0.796
50	4.1609	4.0266	3.8767	3.7274	3.5683	0.1343	0.1499	0.1493	0.1591	0.1482	0.296	0.772
60	3.5938	3.4371	3.2761	3.1237	2.954	0.1567	0.1610	0.1524	0.1697	0.1600	0.320	0.754
70		3.4092	3.2501	3.1043	2.921		0.1591	0.1458	0.1833	0.1627	0.325	0.750
85	3.6727	3.4825	3.2791	3.1298	2.9233	0.1902	0.2034	0.1493	0.2065	0.2000	0.400	0.692
100		3.548	3.4488	3.2182	2.9851		0.0992	0.2306	0.2331	0.2319	0.464	0.643
120		4.5155	4.2331	3.9583	3.6795		0.2824	0.2748	0.2788	0.2787	0.557	0.571

Tables A4 ix and A4 x

Table A4 ix

75% w/w Sweetose 2%w/w sucrose ester, S770

Density of the non-aerated mixture = 1.298 g cm-3

Time (mins)	volume (cm3) 2.5	2	1.5	1	0.5	Mass per 0.5g				Av mass per 0.5g	Av density g cm-3	Gas phase volume
5	5.2497	4.7084	4.1538	3.642	3.1908	0.5413	0.5546	0.5118	0.4512	0.5147	1.029	0.207
10	4.5123	4.219	3.9252	3.6308	3.3431	0.2933	0.2938	0.2944	0.2877	0.2923	0.585	0.550
15	3.7115	3.5298	3.3501	3.171	2.9819	0.1817	0.1797	0.1791	0.1891	0.1824	0.365	0.719
20	3.4791	3.3272	3.1708	3.0191	2.8644	0.1519	0.1564	0.1517	0.1547	0.1537	0.307	0.763
30	3.35	3.2175	3.1412	3.013	2.8746	0.1325	0.0763	0.1282	0.1384	0.1330	0.266	0.795
40		3.8926	3.8085	3.6803	3.5485		0.0841	0.1282	0.1318	0.1300	0.260	0.800
		1.4	1.1	0.8	0.4							
50		3.1366	3.0568	2.9738	2.8672		0.1330	0.1383	0.1333	0.1349	0.270	0.792
	2	1.5	1	0.7	0.3							
60	3.2326	3.1232	3.0105	2.9268	2.815	0.1094	0.1127	0.1395	0.1397	0.1396	0.279	0.785
	1.9	1.5	1	0.7	0.3							
75	3.2742	3.1621	3.0362	2.9466	2.8262	0.1401	0.1259	0.1493	0.1505	0.1415	0.283	0.782
	2	1.5	1.1	0.7	0.3							
90	3.3376	3.2362	3.1543	3.0223	2.8858	0.1014	0.1024	0.1650	0.1706	0.1678	0.336	0.741
	1.8	1.4	1	0.7	0.3							
105	3.3429	3.2737	3.1208	3.073	2.8527	0.0865	0.1911	0.0797	0.2754	0.1582	0.316	0.756
	2	1.6	1.2	0.8	0.4							
120	3.642	3.4985	3.3391	3.1627	2.9834	0.1794	0.1993	0.2205	0.2241	0.2146	0.429	0.669

Table A4 x

75% w/w Sweetose 2%w/w sucrose ester, S270

Density of the non-aerated mixture = 1.300 g cm-3

Time (mins)	volume (cm3) 2.5	2	1.5	1	0.5	Mass per 0.5g				Av mass per 0.5g	Av density g cm-3	Gas phase volume
5	4.8174	4.3772	3.9555	3.5346	3.1422	0.4402	0.4217	0.4209	0.3924	0.4188	0.838	0.356
10	3.7682	3.5547	3.3402	3.164	2.9496	0.2135	0.2145	0.1762	0.2144	0.2047	0.409	0.685
15	3.6129	3.438	3.2627		2.916	0.1749	0.1753		0.1733	0.1745	0.349	0.732
	2	1.6	1.2	0.8	0.4							
20	3.3585	3.2504	3.1713	3.0418	2.9101	0.1351	0.0989	0.1619	0.1646	0.1633	0.327	0.749
32	3.3118	3.1913	3.082	2.9625	2.8368	0.1506	0.1366	0.1494	0.1571	0.1484	0.297	0.772
	2	1.5	1.1	0.7	0.3							
40	3.3739	3.2463	3.1352	3.011	2.8811	0.1276	0.1389	0.1553	0.1624	0.1522	0.304	0.766
	2		1.2	0.8	0.4							
50	3.2885		3.1224	2.9913	2.8595		0.1038	0.1639	0.1648	0.1643	0.329	0.747
	2	1.6	1.2	0.8	0.4							
60	3.408	3.3022	3.1944	3.0564	2.9141	0.1322	0.1348	0.1725	0.1779	0.1752	0.350	0.730
	2.2	1.7	1.3	0.9	0.5							
75	3.4935	3.3415	3.2244	3.0662	2.9085	0.1520	0.1464	0.1978	0.1971	0.1974	0.395	0.696
	2	1.6	1.2	0.8	0.4							
95	3.6206	3.4363	3.2964	3.1148	2.9301	0.2304	0.1749	0.2270	0.2309	0.2294	0.459	0.647
111	3.8367	3.6255	3.4296	3.2297	3.0187	0.2640	0.2449	0.2499	0.2638	0.2556	0.511	0.607
120	3.824	3.6105	3.4116	3.1819	2.9525	0.2669	0.2486	0.2871	0.2867	0.2723	0.545	0.581

Tables A4 xi, A4 xii and A4 xiii

Table A4 xi

75% w/w Sweetose — Density of the non-aerated mixture = 1.300 g cm-3

Time (mins)	volume (cm3) 2.5	2	1.5	1	0.5	Mass per 0.5g				Av mass per 0.5g	Av density g cm-3	Gas phase volume
5	5.8548	5.2338	4.6075	3.96	3.3506	0.6210	0.6263	0.6475	0.6094	0.6261	1.252	0.037
15	6.0367	5.4153	4.7576	4.1032	3.462	0.6214	0.6577	0.6544	0.6412	0.6437	1.287	0.010
30	5.8829	5.2334	4.6046	3.9615	3.3154	0.6495	0.6288	0.6431	0.6461	0.6419	1.284	0.012
70	5.7716	5.1706	4.5107	3.8681	3.226	0.6010	0.6599	0.6426	0.6421	0.6364	1.273	0.021
100	5.8218	5.1377	4.5392	3.9028	3.2572	0.6841	0.5985	0.6364	0.6456	0.6412	1.282	0.014

Table A4 xii

75% w/w Sweetose 0.05%w/w sucrose ester, S1670 — Density of the non-aerated mixture = 1.300 g cm-3

Time (mins)	volume (cm3) 2.5	2	1.5	1	0.5	Mass per 0.5g				Av mass per 0.5g	Av density g cm-3	Gas phase volume
5	5.9874	5.3434	4.7056	4.0635	3.4149	0.6440	0.6378	0.6421	0.6486	0.6431	1.286	0.011
10	5.9672	5.3181	4.6714	4.04	3.3915	0.6491	0.6467	0.6314	0.6485	0.6439	1.288	0.009
15	5.9553	5.335	4.6937	4.0448	3.415	0.6203	0.6413	0.6489	0.6298	0.6351	1.270	0.023
20	5.9405	5.293	4.6528	4.004	3.3638	0.6475	0.6402	0.6488	0.6402	0.6442	1.288	0.009
30	5.898	5.266	4.6247	3.9896	3.3551	0.6320	0.6413	0.6351	0.6345	0.6357	1.271	0.022
40	5.9265	5.2963	4.642	4.0122	3.3753	0.6302	0.6543	0.6298	0.6369	0.6378	1.276	0.019
50	5.9107	5.2614	4.6402	3.9975	3.3648	0.6493	0.6212	0.6427	0.6327	0.6365	1.273	0.021
60	5.9401	5.3166	4.6738	4.0319	3.4042	0.6235	0.6428	0.6419	0.6277	0.6340	1.268	0.025
70	5.8907	5.248	4.6201	3.9868	3.3623	0.6427	0.6279	0.6333	0.6245	0.6321	1.264	0.028
80	5.849	5.2181	4.5924	3.978	3.3586	0.6309	0.6257	0.6144	0.6194	0.6226	1.245	0.042
90	5.8066	5.1744	4.5357	3.9112	3.3116	0.6322	0.6387	0.6245	0.5996	0.6238	1.248	0.040
100	5.8227	5.1974	4.5758	3.9677	3.3567	0.6253	0.6216	0.6081	0.6110	0.6165	1.233	0.052
110	5.7477	5.1366	4.5274	3.9263	3.3253	0.6111	0.6092	0.6011	0.6010	0.6056	1.211	0.068
120	5.7302	5.1137	4.5174	3.9161	3.3232	0.6165	0.5963	0.6013	0.5929	0.6018	1.204	0.074

Table A4 xiii

75% w/w Sweetose 0.1%w/w sucrose ester, S1670 — Density of the non-aerated mixture = 1.300 g cm-3

Time (mins)	volume (cm3) 2.5	2	1.5	1	0.5	Mass per 0.5g				Av mass per 0.5g	Av density g cm-3	Gas phase volume
5	5.9499	5.3025	4.6681	4.0367	3.3961	0.6474	0.6344	0.6314	0.6406	0.6385	1.277	0.018
10	5.9291	5.2598	4.6248	3.9742	3.3246	0.6693	0.6350	0.6506	0.6496	0.6451	1.290	0.008
15	5.9366	5.2936	4.6561	4.0221	3.3893	0.6430	0.6375	0.6340	0.6328	0.6368	1.274	0.020
20	5.9228	5.2795	4.65	4.0123	3.3794	0.6433	0.6295	0.6377	0.6329	0.6339	1.272	0.022
30	5.722	5.1363	4.5195	3.8961	3.2645	0.5857	0.6168	0.6234	0.6316	0.6239	1.248	0.040
41	5.748	5.1405	4.5353	3.9233	3.2998	0.6075	0.6052	0.6120	0.6235	0.6121	1.224	0.058
50	5.7767	5.1492	4.5236	3.9081	3.2738	0.6275	0.6256	0.6155	0.6343	0.6257	1.251	0.037
60	5.7531	5.1445	4.5467	3.9348	3.3144	0.6086	0.5978	0.6119	0.6204	0.6097	1.219	0.062
71	5.7126	5.1078	4.4876	3.8734	3.2688	0.6048	0.6202	0.6142	0.6046	0.6110	1.222	0.060
80	5.6752	5.0662	4.4675	3.8727	3.2705	0.6090	0.5987	0.5948	0.6022	0.6012	1.202	0.075
90	5.6859	5.0925	4.4947	3.9005	3.2979	0.5934	0.5978	0.5942	0.6026	0.5970	1.194	0.082
110	5.6217	5.0239	4.4404	3.8486	3.2718	0.5978	0.5835	0.5918	0.5768	0.5875	1.175	0.096

Table A4 xiv

75% w/w Sweetose 0.3%w/w sucrose ester, S1670 Density of the non-aerated mixture = 1.300 g cm-3

Time (mins)	volume (cm3) 2.5	2	1.5	1	0.5	Mass per 0.5g				Av mass per 0.5g	Av density g cm-3	Gas phase volume
5	5.8565	5.2331	4.6038	3.981	3.3434	0.6234	0.6293	0.6228	0.6376	0.6283	1.257	0.033
10	5.7385	5.1258	4.5057	3.8883	3.2764	0.6127	0.6201	0.6174	0.6119	0.6155	1.231	0.053
15	5.6492	5.0775	4.4841	3.9003	3.3158	0.5717	0.5934	0.5838	0.5845	0.5834	1.167	0.103
20	5.2707	4.7428	4.1809	3.6386	3.1019	0.5279	0.5619	0.5423	0.5367	0.5422	1.084	0.166
30	4.1197	3.8376	3.5398	3.291	3.0306	0.2821	0.2978	0.2488	0.2604	0.2723	0.545	0.581
40	3.7219	3.5333	3.3442	3.1495	2.9561	0.1886	0.1891	0.1947	0.1934	0.1915	0.383	0.705
50	3.7937	3.583	3.3714	3.1647	2.9572	0.2107	0.2116	0.2067	0.2075	0.2091	0.418	0.678
60	3.8138	3.598	3.3767	3.1624	2.959	0.2158	0.2213	0.2143	0.2034	0.2137	0.427	0.671
70	3.832	3.6003	3.3776	3.1536	2.9386	0.2317	0.2227	0.2240	0.2150	0.2234	0.447	0.656
85	3.8786	3.6555	3.4202	3.1934	2.972	0.2231	0.2353	0.2268	0.2214	0.2266	0.453	0.651
100	3.9195	3.6793	3.4426	3.2149	2.9893	0.2402	0.2367	0.2277	0.2256	0.2326	0.465	0.642
120	4.0583	3.7926	3.5286	3.2649	3.0135	0.2657	0.2640	0.2637	0.2514	0.2612	0.522	0.598

Table A4 xv

75% w/w Sweetose 0.2%w/w sucrose ester, S1670 Density of the non-aerated mixture = 1.300 g cm-3

Time (mins)	volume (cm3) 2.5	2	1.5	1	0.5	Mass per 0.5g				Av mass per 0.5g	Av density g cm-3	Gas phase volume
5	5.7438	5.0972	4.4891	3.8777	3.2731	0.6466	0.6081	0.6114	0.6046	0.6177	1.235	0.050
10	5.7565	5.1529	4.4353	3.9138	3.2907	0.6036	0.7176	0.5215	0.6231	0.6165	1.233	0.052
15	5.8361	5.2211	4.61	4.0016	3.3862	0.6150	0.6111	0.6084	0.6154	0.6125	1.225	0.058
20	5.7028	5.0852	4.4724	3.8481	3.2399	0.6176	0.6128	0.6243	0.6082	0.6157	1.231	0.053
30	4.8901	4.4268	3.9812	3.5571	3.1287	0.4633	0.4456	0.4241	0.4284	0.4404	0.881	0.323
40	4.3007	3.9712	3.6574	3.3486	3.0506	0.3295	0.3138	0.3088	0.2980	0.3125	0.625	0.519
50	4.3575	4.0361	3.718	3.397	3.0823	0.3214	0.3181	0.3210	0.3147	0.3188	0.638	0.510
60	4.3418	4.0169	3.6887	3.3742	3.0613	0.3249	0.3282	0.3145	0.3129	0.3201	0.640	0.508
75	4.3741	4.0471	3.7228	3.3973	3.0761	0.3270	0.3243	0.3255	0.3212	0.3245	0.649	0.501
95	4.2821	3.9696	3.6497	3.3355	3.0265	0.3125	0.3199	0.3142	0.3090	0.3139	0.628	0.517
105	4.2775	3.9673	3.6536	3.3511	3.0497	0.3102	0.3137	0.3025	0.3014	0.3070	0.614	0.528
120	4.1935	3.8867	3.5843	3.2905	3.0016	0.3068	0.3024	0.2938	0.2889	0.2980	0.596	0.542

Tables A4 xvi and A4 xvii

Table A4 xvi

75% w/w Sweetose 2%w/w sucrose ester, S1670 Speed 1 Density of the non-aerated mixture = 1.300 g cm-3

Time (mins)	volume (cm3) 2.5	2	1.5	1	0.5	Mass per 0.5g				Av mass per 0.5g	Av density g cm-3	Gas phase volume
5	5.9353	5.2938	4.6617	4.0272	3.3928	0.6415	0.6321	0.6345	0.6344	0.6356	1.271	0.022
10	5.6483	5.0621	4.5068	3.9242	3.35	0.5862	0.5553	0.5826	0.5742	0.5746	1.149	0.116
16	5.5716	5.0282	4.4965	3.9478	3.3973	0.5434	0.5317	0.5487	0.5505	0.5436	1.087	0.164
20	5.365	4.8338	4.3341	3.8236	3.3126	0.5312	0.4997	0.5105	0.5110	0.5131	1.026	0.211
30	4.8321	4.4037	3.9876	3.574	3.1596	0.4284	0.4161	0.4136	0.4144	0.4181	0.836	0.357
40	4.3246	4.0068	3.6977	3.3824	3.0787	0.3178	0.3091	0.3153	0.3037	0.3115	0.623	0.521
50	3.8282	3.6113	3.3837	3.1697	2.9564	0.2169	0.2276	0.2140	0.2133	0.2180	0.436	0.665
	2	*1.6*	*1.2*	*0.8*	*0.4*							
60	3.3343	3.2142	3.1442	3.0231	2.9071	0.1501	0.0875	0.1514	0.1450	0.1488	0.298	0.771
	2	*1.5*	*1.1*	*0.7*	*0.3*							
70	3.2456	3.1141	3.0262	2.9184	2.8105	0.1644	0.1099	0.1348	0.1349	0.1360	0.272	0.791
	2	*1.6*	*1.2*	*0.8*	*0.4*							
82	3.1921	3.0879	3.052	2.9407	2.8373	0.1302	0.0449	0.1391	0.1292	0.1329	0.266	0.796
	2	*1.6*	*1.2*	*0.8*	*0.4*							
95	3.1868	3.0926	3.0282	2.9232	2.8182	0.1177	0.0805	0.1313	0.1313	0.1267	0.253	0.805
	2	*1.5*	*1.1*	*0.7*	*0.3*							
110	3.2517	3.129	3.045	2.937	2.8299	0.1534	0.1050	0.1350	0.1339	0.1318	0.264	0.797
	2	*1.6*	*1.2*	*0.8*	*0.4*							
120	3.2498	3.1421	3.0639	2.9584	2.8456	0.1346	0.0977	0.1319	0.1410	0.1358	0.272	0.791

Table A4 xvii

75% w/w Sweetose 2%w/w sucrose ester, S1670 Speed 3 Density of the non-aerated mixture = 1.300 g cm-3

Time (mins)	volume (cm3) 2.5	2	1.5	1	0.5	Mass per 0.5g				Av mass per 0.5g	Av density g cm-3	Gas phase volume
2	4.2417	3.9461	3.6426	3.3531	3.0702	0.2956	0.3035	0.2895	0.2829	0.2929	0.586	0.549
4	3.5082	3.3482	3.1874	3.0573	2.8971	0.1600	0.1608	0.1301	0.1602	0.1603	0.321	0.753
	2	*1.5*	*1*	*0.5*								
6	3.2771	3.153	3.0238	2.8834		0.1241	0.1292	0.1404		0.1312	0.262	0.798
	2	*1.6*	*1.2*	*0.8*	*0.4*							
10	3.2991	3.1863	3.111	3.0003	2.8878	0.1410	0.0941	0.1384	0.1406	0.1400	0.280	0.785
	2.5	*2*	*1.5*	*1*	*0.5*							
15	3.46	3.3073	3.1626	3.0158	2.864	0.1527	0.1447	0.1468	0.1518	0.1490	0.298	0.771
20	3.5569	3.4022	3.251	3.1027	2.9401	0.1547	0.1512	0.1483	0.1626	0.1542	0.308	0.763
30	3.608	3.414	3.268	3.0908	2.9033	0.1940	0.1460	0.1772	0.1875	0.1762	0.352	0.729
	2	*1.6*	*1.2*	*0.8*	*0.4*							
40	3.5869	3.4127	3.27	3.0968	2.9203	0.2178	0.1784	0.2165	0.2206	0.2183	0.437	0.664
55	3.8745	3.6405	3.4137	3.1817	2.9521	0.2925	0.2835	0.2900	0.2870	0.2883	0.577	0.557
70	4.1787	3.8987	3.6532	3.3785	3.088	0.3500	0.3069	0.3434	0.3631	0.3522	0.704	0.458
90	4.5924	4.2656	3.9237	3.5778	3.1619	0.4085	0.4274	0.4324	0.5199	0.4470	0.894	0.312

APPENDIX A5

Gas microcell concentration after dilution

Table A5 i

Dispersion 1.6 x 10^{-2} g cm^{-3}

Time (mins)	3.75	10	19	41	80	141	230	300
Photo No.	No. cells	No. cells	No. cells	No. cells	No. cells	No. cells	No. cells	No. cells
1	1266	1194	1272	919	748	383	174	170
2	1191	1240	1345	972	710	341	179	174
3	1436	1436	1589	1086	736	434	186	122
4	1486	1398	1525	1072	793	464	238	141
5	1498	1521	1510	1164	731	447	219	204
6	1567		1597	1162	726	544	259	183
7						570	269	205
8						419	322	249
TOTAL No. of cells	8444	6789	8838	6375	4444	3602	1846	1448
Mean No. per photo ± SD	1407 ± 146	1358 ± 137	1473 ± 134	1062 ± 100	740 ± 29	450 ± 76	230 ± 52	181 ± 40
Volume per photo (x10^{-13} m^3)	7.38	7.38	7.38	7.38	7.38	7.38	6.17	6.17
No. per unit Vol. ± SD (x$10^{15}$$m^{-3}$)	1.91 ± 0.20	1.84 ± 0.19	2.00 ± 0.18	1.44 ± 0.14	1.00 ± 0.039	0.610 ± 0.10	0.374 ± 0.084	0.293 ± 0.065

Table A5 ii

Dispersion 1.1 x 10^{-2} g cm^{-3}

Time (mins)	2.83	15	27.5	43	89	177	240
Photo No.	No. cells	No. cells	No. cells	No. cells	No. cells	No. cells	No. cells
1	944	786	583	718	275	185	92
2	1009	975	678	697	340	200	93
3	1093	993	629	608	347	148	90
4	1151	975	718	686	341	171	98
5	1132	1029	824	633	377	183	104
6	1162	1220	742	755	408	191	99
7					371	240	
8					322		
TOTAL No. of cells	6491	5978	4174	4097	2781	1318	576
Mean No. per photo ± SD	1082 ± 87	996 ± 139	696 ± 86	683 ± 54	347 ± 40	188 ± 28	96 ± 5
Volume per photo (x10^{-13} m^3)	7.38	7.38	7.38	7.38	7.38	6.17	6.17
No. per unit Vol. ± SD (x$10^{15}$$m^{-3}$)	1.47 ± 0.12	1.36 ± 0.19	0.943 ± 0.12	0.925 ± 0.073	0.471 ± 0.054	0.305 ± 0.045	0.156 ± 0.0081

APPENDIX A5 Cont'd

Table A5 iii

Dispersion 0.5 x 10^{-2} g cm^{-3}

Time (mins)	3	15	39	71
Photo No.	No. cells	No. cells	No. cells	No. cells
1	508	295	167	184
2	433	311	299	245
TOTAL No. of cells	941	606	466	429
Mean No. per photo ± SD	470 ± 53	303 ± 11	233 ± 93	214 ± 43
Volume per photo ($x10^{-13}$ m^3)	6.17	6.17	6.17	6.17
No. per unit Vol. ± SD ($x10^{15}m^{-3}$)	0.762 ± 0.072	0.491 ± 0.018	0.377 ± 0.151	0.348 ± 0.070

APPENDIX A6

Optical density of gas microcell dispersions

Tables A6 i and A6 ii

Table A6 i

Percentage Transmission of 2.85 micron diameter polystyrene latex at a range of dilutions

	The percentage transmission at each wavelength								
	Percentage transmission at 540nm								
Wavelength	80% trans	60% trans	43% trans	99% trans	90% trans	2% trans	7% trans	27% trans	17% trans
700	79.11	60.67	43.2	99.1	90.77	1.53	4.9	20.74	12.71
680	79.98	61.87	44.63	99.24	91.28	1.61	5.34	22.06	13.73
660	80.33	62.66	45.51	99.13	91.41	1.62	5.6	22.8	14.25
640	80.98	63.96	46.98	99.24	91.66	1.72	6.09	24.11	15.23
620	81.32	64.46	47.83	99.22	91.82	1.81	6.44	24.9	15.91
600	81.6	64.83	48.14	99.29	91.83	1.81	6.55	25.1	16.14
580	81.93	65.42	48.94	99.32	92.1	1.87	6.82	25.74	16.68
560	82.23	65.83	49.43	99.3	92.16	1.97	7.12	26.4	17.18
540	82.33	66.16	49.84	99.41	92.36	2.04	7.33	26.75	17.48
520	82.43	66.31	49.97	99.4	92.39	2.09	7.43	26.94	17.68
500	82.6	66.41	50.05	99.46	92.47	2.1	7.43	26.89	17.64
480	82.29	66.14	49.68	99.43	92.36	2.04	7.23	26.44	17.22
460	82.28	66.06	49.58	99.42	92.43	2.09	7.21	26.31	17.11
440	82.66	66.55	50.2	99.46	92.52	2.29	7.65	27.07	17.75
420	82.38	66.09	49.57	99.44	92.5	2.15	7.34	26.49	17.25
400	82.41	66.13	49.77	99.49	92.47	2.23	7.57	26.82	17.57
At 540 nm;									
%T at T=0 mins =	82.33	66.16	49.84	99.41	92.36	2.0400	7.33	26.75	17.48
Turb. at T=0 mins =	19.443	41.309	69.635	0.592	7.948	389.222	261.319	131.864	174.411

Table A6 ii

Percentage Transmission of polystyrene latices of different diameter

	Percentage Transmission at each wavelength									
	Latex Diameter								Microcell dispersion age	
Wavelength	25 nm	44.8 nm	263 nm	263 nm	490 nm	490 nm	850 nm	850 nm	15 mins	14 hours
700	87.4	87.68	52.56	80.49	49.88	73.93	46.42	80.9	18.1	84.08
680	85.95	86.27	49.95	79.17	47.49	72.31	44.59	79.99	17.52	82.76
660	84.25	84.52	47.09	77.61	45.04	70.66	42.71	78.95	17.19	81.14
640	82.36	82.56	44.1	75.95	42.57	68.93	40.85	78	17.08	80.13
620	80.11	80.27	40.86	74.13	39.97	67.03	39.13	77.01	17.07	79.31
600	77.58	77.99	37.63	72.16	37.24	65.01	37.42	76.16	17.19	78.74
580	74.56	74.9	33.95	69.67	34.25	62.62	35.57	74.92	17.5	78.44
560	70.95	71.42	30.09	66.88	31.13	59.99	33.61	73.57	17.86	78.31
540	66.96	67.55	26.2	63.84	28.07	57.35	31.86	72.49	18.23	78.05
520	62.35	62.9	22.28	60.38	24.99	54.49	30.25	71.31	18.59	77.45
500	57.08	57.6	18.53	56.7	22.05	51.48	28.63	70.09	18.97	76.86
480	51.09	51.76	15.06	52.78	19.23	48.35	27.06	68.9	19.26	75.99
460	44.44	45.18	11.96	48.61	16.41	44.96	25.75	67.78	19.43	74.92
440	37.17	37.97	9.25	44.29	13.72	41.34	24.51	66.74	19.53	73.8
420	29.49	30.29	6.92	39.81	11.29	37.59	23.65	65.96	19.59	72.63
400	21.64	22.34	4.92	34.87	9.16	33.78	23.07	65.37	19.61	71.34
At 540 nm;										
%T at T=0 mins =	66.96	67.55	26.2	63.84	28.07	57.35	31.86	72.49	18.23	78.05
Turb. at T=0 mins =	40.107	39.230	133.941	44.879	127.047	55.600	114.382	32.172	170.210	24.782

Tables A6 iii and A6 iv

Table A6 iii

Turbidity (m-1) of the polystyrene latices in Table A5 i normalised about the turbidity at 540nm

	Turbidity at each wavelength normalised to the turbidity at 540nm (m-1) Percentage transmission at 540nm								
Wavelength	80% trans	60% trans	43% trans	99% trans	90% trans	2% trans	7% trans	27% trans	17% trans
700	1.205	1.210	1.205	1.528	1.218	1.074	1.154	1.193	1.183
680	1.149	1.162	1.159	1.289	1.148	1.061	1.121	1.146	1.138
660	1.126	1.132	1.131	1.477	1.130	1.059	1.103	1.121	1.117
640	1.085	1.082	1.085	1.289	1.096	1.044	1.071	1.079	1.079
620	1.063	1.063	1.059	1.323	1.074	1.031	1.050	1.054	1.054
600	1.046	1.049	1.050	1.204	1.072	1.031	1.043	1.048	1.046
580	1.025	1.027	1.026	1.153	1.035	1.022	1.028	1.029	1.027
560	1.006	1.012	1.012	1.187	1.027	1.009	1.011	1.010	1.010
540	1.000	1.000	1.000	1.000	1.000	1.000	1.000	1.000	1.000
520	0.994	0.995	0.996	1.017	0.996	0.994	0.995	0.995	0.993
500	0.983	0.991	0.994	0.915	0.985	0.993	0.995	0.996	0.995
480	1.002	1.001	1.005	0.966	1.000	1.000	1.005	1.009	1.009
460	1.003	1.004	1.008	0.983	0.990	0.994	1.006	1.013	1.012
440	0.979	0.986	0.990	0.915	0.978	0.970	0.984	0.991	0.991
420	0.997	1.003	1.008	0.949	0.981	0.987	0.999	1.007	1.008
400	0.995	1.001	1.002	0.864	0.985	0.977	0.988	0.998	0.997

Table A6 iv

The turbidity (m-1) of the polystyrene latices in Table A5 ii normalised about the turbidity at 540nm

	Turbidity at each wavelength normalised to the turbidity at 540nm (m-1) Latex diameter								Microcell dispersion age	
Wavelength	25 nm	44.8 nm	263 nm	263 nm	490 nm	490 nm	850 nm	850 nm	15 mins	14 hours
700	0.336	0.335	0.480	0.484	0.547	0.543	0.671	0.659	1.004	0.700
680	0.377	0.376	0.518	0.520	0.586	0.583	0.706	0.694	1.023	0.764
660	0.427	0.429	0.562	0.565	0.628	0.625	0.744	0.735	1.035	0.843
640	0.484	0.489	0.611	0.613	0.672	0.669	0.783	0.772	1.038	0.894
620	0.553	0.560	0.668	0.667	0.722	0.719	0.820	0.812	1.039	0.935
600	0.633	0.634	0.730	0.727	0.777	0.775	0.859	0.846	1.035	0.964
580	0.732	0.737	0.807	0.805	0.843	0.842	0.904	0.898	1.024	0.980
560	0.856	0.858	0.897	0.896	0.919	0.919	0.953	0.954	1.012	0.987
540	1.000	1.000	1.000	1.000	1.000	1.000	1.000	1.000	1.000	1.000
520	1.178	1.182	1.121	1.124	1.091	1.092	1.045	1.051	0.989	1.031
500	1.398	1.406	1.259	1.264	1.190	1.194	1.093	1.105	0.977	1.062
480	1.674	1.679	1.413	1.424	1.298	1.307	1.143	1.158	0.968	1.108
460	2.022	2.025	1.585	1.607	1.423	1.438	1.186	1.209	0.963	1.165
440	2.468	2.468	1.777	1.815	1.563	1.589	1.229	1.257	0.960	1.226
420	3.045	3.044	1.994	2.052	1.717	1.760	1.261	1.293	0.958	1.290
400	3.816	3.821	2.249	2.348	1.881	1.952	1.282	1.321	0.957	1.363

Table A6 v

Percentage Transmission and normalised turbidity of gas microcell dispersions with time

The percentage transmission at 540nm and the normalised turbidity (m-1) in each solvent with time (mins).

Water			0.001% w/w S1670			0.2% w/w S1670			5% w/w Sweetose			10% w/w Sweetose			0.3M NaCl			pH 2.5		
time (mins)	% trans	norm. turbidity	time	% trans	norm. turbidity	time	% trans	norm. turbidity	time	% trans	norm. turbidity	time	% trans	norm. turbidity	time	% trans	norm. turbidity	time	% trans	norm. turbidity
0	22.89	1.000	0	25.03	1.000	0	16.26	1.000	0	16.28	1.000	0	12.42	1.000	0	14.14	1.000	0	5.19	1.000
2	21.77	0.951	1	24.93	0.996	1	16.22	0.997	1	16.08	0.988	1	12.34	0.994	4	12.27	0.868	4	4.71	0.907
5	23.97	0.891	5	27.72	0.920	4	16.31	0.994	4	17.17	0.952	4	12.71	0.980	15	21.37	0.638	7	5.91	0.840
8	26.52	0.828	11	30.44	0.853	7	16.53	0.987	7	17.41	0.945	8	13.34	0.957	24	28.94	0.513	11	7.07	0.786
14	29.67	0.758	14	31.46	0.829	13	16.44	0.990	14	18.09	0.924	11	13.45	0.953	70	58.58	0.221	14	8.50	0.732
18	30.80	0.735	18	36.90	0.715	21	17.11	0.968	20	18.53	0.911	21	14.43	0.919	96	66.78	0.167	17	9.83	0.689
23	31.99	0.711	21	34.97	0.753	29	17.19	0.965	38	19.05	0.896	37	15.35	0.890	153	76.10	0.113	22	11.65	0.638
38	38.47	0.596	35	35.70	0.738	38	17.54	0.954	69	20.21	0.864	62	16.78	0.848	237	82.98	0.077	25	13.47	0.595
69	37.46	0.613	59	41.97	0.622	50	17.63	0.952	116	21.20	0.838	88	17.13	0.838	372	82.03	0.082	28	14.54	0.572
100	38.90	0.589	79	43.85	0.591	81	19.07	0.909	193	23.80	0.776	137	18.13	0.811	424	88.72	0.050	32	16.37	0.537
158	42.51	0.534	103	46.06	0.556	118	19.99	0.883	236	24.48	0.761	172	18.60	0.799	802	93.19	0.029	35	17.68	0.514
217	46.51	0.478	145	50.24	0.494	147	21.06	0.854	320	26.85	0.711	215	19.96	0.765	1402	94.78	0.022	38	18.90	0.495
260	46.15	0.482	209	54.95	0.429	191	23.14	0.803	466	31.22	0.629	299	22.11	0.717	2715	96.59	0.014	41	20.12	0.476
344	50.85	0.422	228	54.86	0.430	292	28.75	0.683	596	35.92	0.553	445	26.72	0.627				45	21.00	0.463
487	56.34	0.358	336	60.42	0.361	339	30.82	0.645	730	41.32	0.478	575	30.87	0.558				49	22.42	0.444
621	67.43	0.246	470	66.41	0.293	452	39.71	0.506	922	54.03	0.333	709	36.57	0.478				53	23.07	0.435
755	65.04	0.268	662	75.31	0.203	527	46.18	0.424	1128	65.22	0.231	901	48.11	0.347				59	26.25	0.397
946	76.13	0.170	868	85.01	0.116	538	47.3	0.411	1319	75.38	0.153	1108	62.67	0.222				68	29.67	0.360
1153	81.69	0.126	1059	88.62	0.087	620	56.87	0.309	1520	87.18	0.074	1298	78.25	0.117				83	34.58	0.315
1343	85.98	0.094	1261	92.73	0.054	687	67.99	0.212	1729	93.68	0.035	1500	86.74	0.068				93	37.02	0.295
1545	89.26	0.071	1470	94.43	0.041	852	85.69	0.085				1708	92.16	0.039				100	38.34	0.285
1754	92.34	0.050				1298	92.9	0.040										116	42.36	0.255
						1524	93.4	0.037										156	49.63	0.208
						1534	93.68	0.036										178	53.19	0.187
																		220	56.87	0.168
																		254	59.21	0.156
																		310	62.44	0.140
																		367	65.58	0.125
																		573	73.62	0.091
																		606	74.71	0.087
																		720	76.70	0.079
																		796	77.87	0.074
																		857	78.77	0.071
																		997	81.01	0.063
																		1052	80.52	0.064
																		1130	81.95	0.059
																		1410	84.46	0.050
																		1607	84.56	0.050